Soil Multi-Meta-Omics: Unraveling microbial regulation at three post-genomic levels

Dissertation

to attain the doctoral degree „Doctor rerum naturalium”

(Dr. rer. Nat.) of the Faculty of Agricultural Sciences

Georg-August University Göttingen

Submitted by

Andreas Breidenbach (M.Sc. Biogeowissenschaften)

born on the 30.07.1989 in Nastätten

Göttingen, 13.10.2023

Reviewer of the thesis:

1. Prof. Dr. Michaela A. Dippold
2. Prof. Dr. Stefan Scholten
3. Prof. Dr. Sandra Spielvogel
4. Prof. Dr. Rolf Daniel

Day of the doctoral defense: 26.01.2024

I. Table of Contents

I. List of Figures

Extended summary figures:

Studies 1 – 4 figures:

List of Figures

independent soil microcosms, except for 1 treatment in each of TAGs and PHB where n = 3). Lowercase letters above the plots show post-hoc differences in total storage with $p < 0.05$ (2-sided pairwise comparison of medians with Benjamini-Hochberg adjustment for multiple comparisons).

S4 Figure 3. **Extractable soil microbial biomass determined by chloroform fumigation-extraction. A** 24 h and **B** 96 h after addition of a readily degradable, ^{13}C-labelled carbon source (glucose at 0, 90, and 400 µg C g^{-1} soil) with or without mineral nutrient supply (ntr.; N, P, K, S). The heights of the bars represent the mean ± standard deviation as black error bars (n = 4 independent soil microcosms except for one treatment with n = 3: zero glucose, no nutrients at 96 h). Contrasting colors reflect the source of the extractable biomass as determined by isotopic composition, with light grey error bars showing mean ± standard deviation of the relative composition. Lowercase letters above the plots show post-hoc differences in mean total storage with $p < 0.05$ (2-sided Tukey HSD test, which adjusts for multiple comparisons). Corresponding C:N ratios are presented in Supplementary Fig. S3.

S4 Figure 4. **Comparison of new storage biosynthesis with DNA-based microbial growth reveals storage as a substantial, overlooked component of biomass growth in soil.** ^{13}C-labelled storage compound synthesis (PHB and TAGs) and DNA-based growth (incorporation of ^{18}O) were measured in soil 24 **A** and 96 h **B** after addition of a readily degradable, ^{13}C-labelled carbon source (glucose at 0, 90, and 400 µg C g^{-1} soil) with or without mineral nutrient supply (ntr.; N, P, K, S). Error bars represent mean ± standard deviation in each component of the stacked bar (n =4 independent soil microcosms). Lowercase letters above the plots show post-hoc differences in total observed growth with $p < 0.05$ (2-sided Tukey HSD test, which adjusts for multiple comparisons).

S4 Figure 5. **Intracellular storage represents an alternative pathway for growth of microbial biomass.** In this conceptual figure the y-coordinates reflect the measured incorporation of added C into storage after 96 h, and the x-axis represents replicative growth measured by ^{18}O incorporation into DNA (see also Fig. 4). According to contemporary assumptions, all growth should follow the stoichiometric growth curve that maintains constant element ratios in the biomass (dashed line to the right). The microbial population is shown schematically by bacterial cells, with yellow lipid inclusion bodies representing storage. Without C supply, only low levels of replicative growth occur **A**. Low C additions (with ample nutrients) stimulate replicative growth and limited C incorporation into storage **B**, with the ratio of new storage to non-storage biomass staying close to that predicted by assuming constant biomass stoichiometry. High C addition with complementary nutrients stimulates both strong replicative growth as well as disproportionately large storage synthesis **C**, moderately violating the stoichiometric assumption. However, nutrient limitation switches growth strongly towards storage **D**, incorporating C into biomass with little replicative growth, closer to the extreme case of pure storage without replication than the assumption of stoichiometric growth.

Supplementary Figures

List of Figures

letters above the plots indicate significant differences in total DOC with $p < 0.05$ (2-sided Tukey HSD test on log-transformed values, which adjusts for multiple comparisons), with n = 4 independent soil microcosms.

S4 Suppl. Fig. 3. **C:N ratio of extractable microbial biomass.** (**A**) 24 h and (**B**) 96 h after glucose and/or nutrient addition to soil microcosms. Error bars show mean ± standard deviation, with n = 4 independent soil microcosms, except for one treatment n = 3 (zero glucose, no nutrients at 96 h).

S4 Suppl. Fig. 4. **Fatty acid profile of glucose-derived TAGs.** (**A**) 24 h and (**B**) 96 h following addition of glucose at 0, 90 and 400 µg C g^{-1} soil (Zero, Low, High) with or without mineral nutrient supply (N, P, K, S). The diagnostic bacterial biomarker 16:1ω6 (highlighted blue on the horizontal axis) and fungal biomarker 18:2ω6 (highlighted in green) showed substantial incorporation of glucose-derived C. Error bars show mean ± standard deviation, with n = 4 independent soil microcosms. Note that the vertical axis scale varies between glucose treatments.

S4 Suppl. Fig. 5. **Total soil content of fungal biomarker TAG 18:2ω6.** (**A**) 24 h and (**B**) 96 h following addition of glucose at 0, 90 and 400 µg C g^{-1} soil (Zero, Low, High) with or without mineral nutrient supply (N, P, K and S). Error bars show mean ± standard deviation, with n = 4 independent soil microcosms. Lowercase letters above the plots show post-hoc differences with $p<0.05$ (2-sided pairwise comparison of medians with Benjamini-Hochberg adjustment for multiple comparisons).

II. List of Tables

S3 Suppl. Table 2. **T-test p-values** from the comparison of the model with and without storage adaptation for phi ratio, br1 and br5 for each treatment.

III. Abbreviations

αKG	α-ketoglutarate
AcCo	Acetyl-CoA
ANOVA	Analysis of variance
ASV	Amplicon sequence variants
BD	Bulk density
bp	Base pair
C	Carbon
CCA	Canonical correspondence analysis
CFE	Chloroform fumigation extraction
CO_2	Carbon dioxide
CUE	Carbon use efficiency
D	value of the corresponding variable in the relevant degradation stage
DMSO	Dimethyl sulfoxide
DN	Dissolved nitrogen
DNA	Desoxyribonucleic acid
DOC	Dissolved organic carbon
E4P	Erythrose-4-phosphate
EDTA	Ethylenediaminetetraacetic acid
EMMEANS	Estimated marginal means
ES	Effect size in %
F6P	Fructose-6-phosphate
G6P	Glucose-6-phosphate
GAP	Glyceraldehyde-3-phosphate
GC-MS	Gas chromatograph mass spectrometer
Glc	Glucose
GOI	Genes of interest
H_2O_{molec}	Molecular biological-grade water
HSD	Honest significant difference

Abbreviations

Icit	Isocitrate
IRMS	Isotope ratio mass spectrometer
LMWOS	Low molecular weight organic substances
MANOVA	Multivariate analysis of variance
MBC	Microbial biomass carbon
mRNA	Messenger ribonucleic acid
N	Nitrogen
NMDS	Non-metric multidimensional scaling
O	Oxygen
OAA	Oxaloacetate
P	Phosphorus
PCR	Polymerase chain reaction
PHB	Polyhydroxybutyrate
PLFA	Phospholipid fatty acid
PPP	Pentose phosphate pathway
Pyr	Pyruvate
R	value of each variable in the non-degraded stage (reference site)
Ru5P	Ribulose-5-phosphate
S7P	Sedoheptulose-7-phosphate
SOC	Soil organic carbon
SOM	Soil organic matter
TAE	Tris base, acetic acid, and EDTA buffer
TAG	Triacylglycerols
TCA	Tricarboxylic acid cycle
TCAA	Trichloroacetic acid
TN	Total nitrogen
TOC	Total organic carbon
TP	Tibetan Plateau
t-RFLP	Terminal restriction fragment length polymorphism
VSC	Sum of Vanillyl, Syringyl and Cinnamyl
WHC	Water holding capacity

IV. Summary

Soil functions are key in all ecosystems globally. Specifically soils play a pivotal role in ecosystem biogeochemical cycles, sequestering but also mineralizing carbon (C), and in this context releasing nutrients from the soil organic matter (SOM). This thesis aims to improve our understanding of key soil microbial functions involved in C and nutrient cycling, starting with a case study from a grassland ecosystem where degradation induces massive C losses and by that shifts in C and nutrient stoichiometry, which induce cascading effects of the interaction of microbes and plants with C and nutrient cycling. This relation of key microbial functions to element stoichiometry is then further deepened in a laboratory study to generate a more holistic understanding on the control of the microbial metabolism by C and nutrient availability.

About 2.5 % of global soil organic carbon (SOC) are stored in Tibetan Plateau's *Kobresia pygmaea* grasslands. Topsoil degradation due to climate change and overgrazing with life stock led to a substantial loss in SOC and nitrogen (N), both vital elements for the flora and fauna. The erosion and depletion of C sources due to decreased C input and increased C mineralization forced a shift of the taxonomic composition of the microbial community and in consequence the enzymatic activities expressed. This led to a change in microbial functions from the utilization of hydrolytic enzymes towards enzymes capable of oxidizing the remaining recalcitrant SOM, being the initial step of the second phase of degradation of the pasture's root mats and thereby removing *Kobresia*'s ability to further grow on the degraded sites. As the key switch towards oxidizing enzymes is controlled by microbial C and nutrient deficiency, further laboratory experiments were needed to elucidate the response of the microbial metabolism on such stoichiometric shifts. Especially deepened insights into the base C metabolism help to understand changes in soil microorganisms' growth modes, the key feature of predicting their C and nutrient demand: (1) Under which conditions is the available soil C sufficient to invest into the formation of new biomass? (2) How does a natural soil microbial community react when C sources are scare or plentiful? (3) Under which conditions do they "merely" invest into the formation of storage compounds and not into growth? (4) How does nutrient availability in this context interact with C availability? To answer these research questions, it is necessary to also understand the regulatory processes from the transcription of base C metabolism genes towards the translation to actual proteins and to trace the C fluxes of the soil microbial metabolism.

The samples from the field experiment in Tibet were analyzed using terminal restriction fragment length polymorphism (t-RFLP) and Illumina MiSeq sequencing to elucidate the microbial community structure. In addition, the enzyme activity of SOM degrading enzymes and N cycling related exoenzymes were measured. The research question regarding regulatory processes in the C

metabolism would have been impossible to be answered in a field experiment, therefore the key questions were targeted by a laboratory experiment with natural agricultural soil. Under controlled laboratory conditions it was possible to manipulate the glucose amounts by adding low and high concentrations of glucose and N and phosphate (P) as nutrients. Over the course of the experiment of 96 h, microcosms were harvested after 24 and 96 hours for the measurements of phospho- (PLFA) and neutral lipid fatty acids (NLFA), polyhydroxybutyrate (PHB), microbial biomass carbon (MBC), the metatranscriptome and metaproteome. For ^{13}C flux modelling, the glucose treatment solutions were also treated with uniformly and position-specifically labelled glucose and $^{13}CO_2$ respiration was measured in time intervals.

The degradation of the *Kobresia* pastures and the loss of the topsoil layer led to a shift in the microbial community structure especially in their mycorrhizal partners. As *Kobresia pygmeae* was first associated with arbuscular mycorrhizal fungi, the increasing severity of the degradation then led to a shift towards an association of *Kobresia* with ectomycorrhizal fungi. Furthermore, the bacterial community shifted towards species capable of degrading complex SOM and nitrifying bacteria further depleting the nutrient stocks on the plateau. The underlying regulatory change in microbial C metabolism of this shift were revealed by the laboratory experiment with reduced C availability in the agricultural soil: Metabolic flux modelling suggests that C fluxes were primarily directed into the catabolic glycolysis rather than the anabolic pentose phosphate pathway (PPP) in low glucose concentrations. After glycolysis, the C fluxes from acetyl-CoA usually enter the strongly catabolic tricarboxylic acid cycle (TCA), where the most energy can be generated. However, flux modelling also detected that from acetyl-CoA the C fluxes were directed towards storage compound formation in low glucose conditions. This hints towards a reserve storage strategy by the microbial community, which was supported by triacylglycerols (TAG) storage compound extraction. In contrast, the direct measurement of the storage compound metabolite PHB revealed a strong contribution to the formation of biomass under glucose excess conditions, a surplus storage strategy. So that both storage compounds fulfill different roles in microbial communities' growth modes. The strong negative relationship between the TCA cycle and storage pathways in the metatranscriptome and metaproteome also underlined the importance of storage compound formation, which is a C resource of intermediate microbial availability, not contributing to the long-term SOC storage of an ecosystem.

In conclusion, environmental changes such as climate change or anthropogenic induced degradation often exert unfavorable consequences on the soil microbial communities by shifting their structural composition and their functioning with implication on various scales. C availability and contents play a major role rather than other nutrients in the regulatory processes on the post-genomic levels, as C is the most restrictive growth factor in soils for bacteria and fungi. The formation of storage compounds

seems to play a much bigger role in soil C cycling than anticipated before. Well-established molecular biology methods on the genome level can give a broad overview of the microbial community structure and – by some extend – of their potential function, but only the combination of metatranscriptomics, metaproteomics and meta-fluxomics in multi-meta-omics approaches will help broaden the insight into the microbial metabolism and deepen the understanding of microbial responses on environmental changes. However, transcription, translation, and the direction of C fluxes towards energy production, replicative growth or storage compound biosynthesis are not always coherent between the post-genomic levels. Therefore, the interpretation of regulatory processes remains a complex and difficult endeavor in natural microbial environments but harbor the possibility of a more profound understanding of the microbial C metabolism if further deepened in comparative, time-resolved approaches. By that, microbial feedbacks within degradation cascades can be revealed and potential mitigation strategies elaborated.

V. Zusammenfassung

Bodenfunktionen haben global eine enorme Wichtigkeit in allen Ökosystemen, insbesondere spielen Böden eine entscheidende Rolle in ökosystemweiten biogeochemischen Stoffkreisläufen, beim Speichern aber auch Mineralisieren von Kohlenstoff (C) und damit zusammenhängend beim Freisetzen von Nährstoffen aus der organischen Bodensubstanz (soil organic matter, SOM). In dieser Dissertation soll unser Verständnis der Schlüsselfunktionen des Bodens im C- und Nährstoffkreislauf verbessert werden. Der Fokus liegt dabei auf einer Feldstudie aus einem Graslandökosystem, wo Veränderungen der Stöchiometrie einem Degradationsprozess unterliegen. Dies hat Konsequenzen für die Interaktionen der Bakterien und Pilze, sowie ihren C- und Nährstoffkreisläufen. Die Beziehung zwischen mikrobiellen Schlüsselfunktionen zur Stöchiometrie wird danach durch ein Laborexperiment, in welchem ein ganzheitliches Verständnis der Regulation des mikrobiellen Metabolismus durch C- und Nährstoffverfügbarkeit generiert werden soll, weiter vertieft.

Das Tibetische Hochland speichert 2,5% des weltweiten bodengebundenen organischen Kohlenstoffs (soil organic carbon, SOC) in seinen *Kobresia pygmaea* Graslandschaften. Die Degradation des Oberbodens, welche durch den Klimawandel und Überweidung mit Nutztieren hervorgerufen wird, führt zu einem substanziellen Verlust des SOC und Stickstoffs (N), beide lebensnotwendige Elemente für Flora und Fauna. Die Erosion und der Schwund der C Quellen durch den verminderten C-Eintrag und erhöhte C-Mineralisierung erzwingt einen Wechsel in der taxonomischen Zusammensetzung der mikrobiellen Gemeinschaft und in der Konsequenz eine Veränderung der Enzymaktivitäten. Dies führt zu einer Verlagerung der mikrobiellen Funktionen von der Verwendung von hydrolytischen Enzymen hin zu Enzymen, die zur Oxidierung von verbleibender persistenter organischen Bodensubstanz in der Lage sind. Dies ist der initiale Schritt der zweiten Phase der Degradation der Wurzelmatten des Graslandes und verhindert, dass *Kobresia* weiterhin auf den degradierten Flächen wachsen kann. Da der Wechsel zu oxidierenden Enzymen durch einen Mangel an C und Nährstoffen in der mikrobiellen Gemeinschaft verursacht wird, waren weitere Laborexperimente, zur Ergründung der Antwort des mikrobiellen Metabolismus erforderlich. Besonders der Kohlenstoffbasismetabolismus hilft dabei das Verständnis von Veränderungen in den Wachstumsmodi der mikrobiellen Gemeinschaften zu vertiefen: Unter welchen Bedingungen reicht der verfügbare Kohlenstoff aus, um in die Erzeugung neuer Biomasse investiert zu werden? Wie reagiert eine natürliche mikrobielle Gemeinschaft im Boden wenn C rar wird oder C im Überfluss vorhanden ist? Unter welchen Bedingungen investiert sie “nur” in die Neubildung von Speicherstoffen und nicht in Wachstum? Wie wirkt sich die Nährstoffverfügbarkeit in diesem Zusammenhang auf die C Verfügbarkeit aus? Es ist daher notwendig die regulativen Prozesse von der Transkription vom C-Basismetabolismusgenen hin zu der Translation

der vorhandenen Proteine zu verstehen und die C-Flüsse des mikrobiellen Metabolismus nachzuverfolgen.

Für das Feldexperiment in Tibet wurde die Struktur der mikrobiellen Gemeinschaft mittels terminalem Restriktionsfragmentlängenpolymorphismus (t-RFLP) und Illumina MiSeq Sequenzierung gemessen. Des Weiteren wurden die Enzymaktivitäten von SOM zersetzenden Enzymen und Enzyme des N-Kreislaufs gemessen. Da es unmöglich ist diese essenziellen Forschungsfragen aus einem Feldexperiment heraus zu beantworten, sie der Fokus eines Laborexperiments mit natürlichem, landwirtschaftlich genutztem Boden. Unter kontrollierten Laborbedingungen war es möglich die Glukosemengen gezielt zu manipulieren indem geringe und hohe Glukosekonzentrationen, sowie Stickstoff- und Phosphatnährstoffe zugesetzt wurden. Während der Experimentdauer von 96 h, wurden nach 24 und 96 h Mikrokosmen geerntet, um Messungen für Phospholipid- (PLFA) und Neutral-Fettsäuren (NLFA), Polyhydroxybuttersäure (PHB), Kohlenstoff in der mikrobiellen Biomasse (microbial biomass carbon, MBC), dem Metatranskriptom und Metaproteom durchzuführen. Für die ^{13}C Fluss-Modellierung wurden die Glukoselösungen zusätzlich mit uniform- und positions-spezifischen ^{13}C Glukose-„Tracer"-Lösungen versetzt und das freigesetzte $^{13}CO_2$ in Zeitintervallen gemessen.

Die Degradation der *Kobresia* Weiden führte zu einer Veränderung der Struktur der mikrobiellen Gemeinschaft, im Besonderen bei deren Mykorrhiza-Partnern. Die Degradation des Graslandes und der Verlust des Oberbodens führte zu einer Verschiebung in der Zusammensetzung der Vegetation und deren assoziierten Mykorrhizapilzen. Zu Anfang ist *Kobresia pygmeae* mit arbuskulärer Mykorrhiza verbunden, aber mit den zunehmenden Folgen der Degradation wechselt *Kobresia* zu einer Partnerschaft mit Ektomykorrhizapilzen. Nach dem Verschwinden von *Kobresia*, verlassen sich die nachfolgenden Sträucher wieder auf arbuskuläre Mykorrhia-Partner. Des Weiteren änderte sich auch die bakterielle Gemeinschaft hin zu Spezies welche komplexe SOM abbauen können und nitrifizierende Bakterien laugen die Nährstoffspeicher des Plateaus weiter aus. Ähnlich ist die reduzierte C Verfügbarkeit im Boden mit der regulativen Veränderung des mikrobiellen C Stoffwechsels aus dem Laborexperiment verbunden: Die C-Flussmodellierung ergab, dass C Flüsse unter niedrigen Glukosekonzentrationen primär eher in die katabole Glykolyse geleitet werden als in den anabolen Pentosephosphatweg. Nach der Glykolyse tritt der C-Fluss aus dem Acetyl-CoA normalerweise in den stark katabolen Tricarbonsäurezyklus (TCA) ein, wo die meiste Energie gewonnen werden kann. Allerdings konnte durch die C-Flussmodellierung festgestellt warden, dass C-Flüsse aus dem Acetyl-CoA in Richtung Speicherstoffbildung gelenkt wurden, wenn niedrige Glukosekonzentrationen vorherrschen. Dies weist auf eine bevorratende Speicherstoffstrategie der mikrobiellen Gemeinschaft hin, welches durch die Messungen von Triglyceriden (TAG) unterstützt wurde. Im Gegensatz dazu, ergab die direkten Messungen des Speicherstoffmetabolites PHB eine starke Beteiligung an der

Bildung von Biomasse unter Glukose C Überschuss, eine Rücklagenspeicherstoffsttrategie. Beide Speicherstoffe erfüllen somit unterschiedliche Rollen in den Wachstumsmodi der mikrobiellen Gemeinschaften. Die starken negativen Wechselwirkungen zwischen dem Tricarbonsäurezyklus- (TCA) und dem Speicherstoff-Pfad im Metatranskriptom und dem Metaproteom untermalen die Wichtigkeit von Speicherstoffbildung, welche eine intermediäre C Quelle für die mikrobielle Gemeinschaft darstellt. Speicherstoffe sind jedoch keine langanhaltenden SOC-Speicher im Ökosystem.

In der Schlussfolgerung sorgen Umweltveränderungen wie der Klimawandel oder anthropogen verursachte Degradation für nachteilige Konsequenzen für die mikrobielle Gemeinschaft im Boden durch einen hervorgerufenen Wechsel in deren struktureller Zusammensetzung und Funktionsweise mit Auswirkungen auf etlichen Ebenen des Ökosystems. C Verfügbarkeit und Gehalt spielen große Rollen in den regulativen Prozessen der post-genomischen Ebenen im Vergleich zu anderen Nährstoffen, da C der limitirendste Faktor für die Bakterien und Pilze des Bodens ist. Die Bildung von Speicherstoffen scheint eine weitaus größere Rolle im C Zyklus des Bodens zu spielen als bisher angenommen. Gut etablierte molekularbiologische Methoden auf der Genomebene können einen groben Überblick über die Strukturen der mikrobiellen Gemeinschaften – und in begrenztem Umfang – auch über deren Funktionen geben, aber Metatranskriptomiks, Metaproteomiks und Meta-Fluxomiks erweitern diese Einsicht in den mikrobiellen Metabolismus und vertiefen das Verständnis über mikrobielle Reaktion auf Umweltveränderungen. Jedoch sind die Richtungen der Regulation in der Transkription, der Translation und der Kohlenstoffflüsse zu Energieproduktion, Replikation oder Speicherstoffbiosynthese nicht immer schlüssig. Daher bleibt die Interpretation der Regulationsprozesse im Besonderen in natürlichen mikrobiellen Umgebungen ein komplexes und schwieriges Unterfangen, welches jedoch bei einer Vertiefung vergleichender und zeitlich aufgelöster Ansätze einen tiefgreifenderen Einblick in den mikrobiellen C Metabolismus erlaubt.

Extended Summary

1.1. Introduction

1.1.1. Factors of carbon loss promoting structural changes of the microbial community.

Soil functions play a pivotal role in global ecosystems, especially in biochemical cycles involving carbon (C) and nutrients such as nitrogen (N) and phosphorus (P) when storing these nutrients in soil organic matter (SOM). Advancing effects of climate change on ecosystems become more important as increasing temperatures, erosion and microbial turn-over rates create a positive feedback loop on C and nutrient loss bringing C sink ecosystems to the brink of climate tipping points (Armstrong McKay et al., 2022; Heimann and Reichstein, 2008). Ecosystems like arctic (Evgrafova et al., 2018) or alpine permafrost soils such as the Tibetan Plateau (TP) (Yao et al., 2012) store vast amounts of carbon and are deeply affected by the advancement of climate change. The TP is capable of storing 2.5% of the world's soil organic carbon (SOC) in its *Kobresia pygmaea* grasslands (Genxu et al., 2002). However, the ecosystem function of the TP as C sink is endangered due to climate change and anthropogenically induced overgrazing with life stock leading to a dramatically increased erosion and degradation of the *Kobresia* pastures (Babel et al., 2014; Qiu, 2016). The *Kobresia* grasslands are essential for water retention, erosion prevention and carbon sequestration due to their root mat properties forming a dense root net allocating vast amounts of C (Hafner et al., 2012; Qiu, 2016). Housing policies transformed the nomad lifestyle of Tibetan inhabitants to being stationary increasing grazing pressure on grasslands surrounding the settlements intensifying their degradation (Qiu, 2016). The degradation of *Kobresia* pastures jeopardizes Tibetan Plateau role as carbon sink, water source for major rivers like the Yangtze and Mekong which provide water for millions of people (Qiu, 2016). Degradation of the *Kobresia* grassland means that the root mats are gradually destroyed by trampling during overgrazing and make the underlying soil prone to water and wind erosion. This affects the N and C cycles in soil which are mainly driven by microbial metabolic activity. Formerly stabilized N is being mineralized to mobile forms of gaseous N_2O or leached in water-soluble form as NH_4^+ and NO_3^- (Zhang et al., 2017). Intact *Kobresia pygmaea* pastures which were moderately grazed increased the C sequestration in its above- and below-ground biomass, so that the combination of plant C input and generation of microbial C necromass in deeper soil depth lead to the stabilization of C and therefore the TP ecosystem's role as C sink (Hafner et al., 2012; He et al., 2021). With the destruction of *Kobresia* root mats, the plant C input is interrupted and already sequestered C in deeper soil layers is then prone for microbial decomposition and released as CO_2 to the atmosphere. Sequestration and decomposition are both driven by the soil microbial community and their metabolic shift from stabilizing to

mineralizing C needs to be understood. It is therefore crucial to understand the regulatory processes of microbial C metabolism.

1.1.2. Base C metabolism as central hub in soil C cycle

Microbes are able to break down a vast variety of C-sources in aerobic and anaerobic conditions to gain energy in form of ATP and reduction equivalents such as NAD^+, $NADP^+$ or FAD^+ (Jurtshuk, 1996; Voet et al., 2008). Their ability to oxidize C structures such as glucose and even rather complex molecules such as hemi-/cellulose and lignin enables soil microbial communities the ability to grow under various environmental conditions (Ottow, 2011; Voet et al., 2008). Under anaerobic conditions bacteria are able to metabolize glucose through fermentation of pyruvate to either lactate or ethanol after the glycolysis pathway (Jurtshuk, 1996; Voet et al., 2008). However, the most energy can be gained through the tricarboxylic acid cycle (TCA) under aerobe conditions. After the cleavage of complex C compounds such as cellulose and lignin, the metabolic products will at some point enter glycolysis or the TCA (Ottow, 2011). Other metabolic products such as galactose, mannose or fructose are able to enter the glycolysis at their specific entry step of the pathway. A glucose molecule can also enter other pathways such as the Entner-Doudroff (ED), an alternative pathway to gain energy, or the pentose phosphate pathway (PPP), a pathway for the biosynthesis of DNA and RNA precursors, reduction equivalents etc. (Voet et al., 2008). The gluconeogenesis is the *de novo* synthesis of glucose from pyruvate, alanine or amino acids over oxalacetate and the reverse reaction path of glycolysis (Fig.1) (Apostel et al., 2018; Voet et al., 2008). At several points during glycolysis, biomass pathways can branch off e.g., those which are responsible for the biosynthesis of cell membrane components such as phospholipid fatty acids (PLFA) or the synthesis of storage compounds like neutral lipid fatty acids (NLFA) and polyhydroxybutyrate (PHB) (br1 – br5, Fig. 1). Finally, the base C metabolism, consistent of the glycolysis, gluconeogenesis PPP and TCA and is an essential hub in soil C cycling (Fig. 1). A vast network of microbial metabolic pathways branch off or lead towards this base C metabolism and it is therefore well-researched and provides vast possibilities to gain information about microbial metabolism and their growth state. Metabolic flux modelling studies try to trace the path of C fluxes throughout the base C metabolism and therefore employ ^{13}C isotopomere tracers in various forms: alanine (Apostel et al., 2018) and pyruvate (Dijkstra et al., 2011a, 2011b; Hagerty et al., 2014) and other low molecular weight organic substances (LMWOS) have been used in the past and also some (but not all) labeled C position in glucose (Apostel et al., 2015; Dijkstra et al., 2011b). The recognition of storage compounds like PHB and triacylglycerols (TAG, component of neutral lipid fatty acids, NLFA) (Harwood and Russell, 1984; López et al., 2015) as growth factor in microbial communities has long been neglected, but recent studies (Manzoni et al., 2021; Mason-Jones et al., 2021) have shown their potential for soil ecology and C flux modelling because of their quantity and the existence of reliable

extraction methods from soils (Mason-Jones et al., 2019). It is therefore crucial to investigate a vast variety of essential basic pathways such as storage compound formation into base C metabolism modelling in order to elucidate and characterize microbial C metabolism in more detail (Dijkstra et al., 2022).

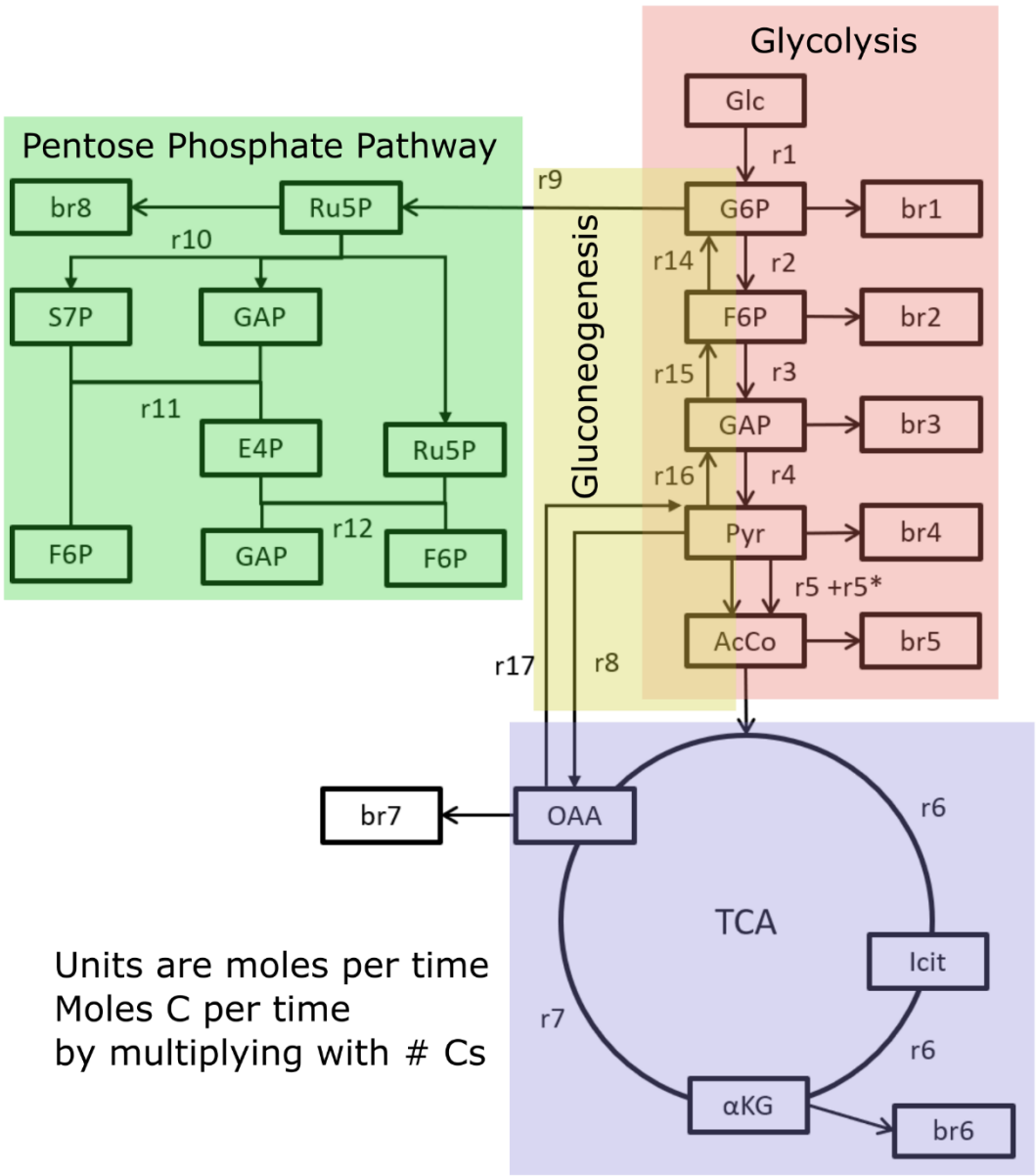

ES Figure 1: **The flux theme of the basic glucose metabolism** divided into glycolysis (r1 to r5), tricarboxylic acid circle (TCA, r6 – r7), gluconeogenesis (r14 – r17) and pentose phosphate pathway (PPP, r9 – r12)

1.1.3. Advances in molecular biology methods

Methods in molecular biology are developing continuously for discovering changes in microbial communities, characterizing their composition and structure. 16S, 18S and ITS rDNA-based methods are well-established: terminal restriction fragment length polymorphism (t-RFLP) is one of the base methods of microbial community structure analysis with the advantage of giving a quick overview of structural changes (Grün et al., 2018). Without the need of extensive bioinformatics t-RFLP has the potential for comparing microbial community structures but on the disadvantage that t-RFLP does not provide any information on the taxonomic composition of a sample. Additionally, t-RFLP requires the use of fluorescence-marked primers and proof-reading polymerase. As taxonomic data is required for a more detailed insight into the microbial community structure Illumina sequencing of 16s rDNA is able to provide this information besides the community structure but requires more bioinformatic analyzes than a t-RFLP analysis (see 2.1.5.9). Both methods have the disadvantage of not providing functional information of the microbial community with the exception that with the taxonomic information from Illumina sequencing it is possible to gain functional information from databases (Aßhauer et al., 2015; Nguyen et al., 2016). A shortcoming of 16S rDNA-based functional databases are microbial phyla which are hard to culture and functionally characterize in single-culture studies so that functional information might not be available or could be falsely linked (Aßhauer et al., 2015). Besides the path over 16S and functional databases, qPCR is a way of quantifying functional genes directly by employing specially designed primer pairs targeting the desired microbial functional genes (Song et al., 2019). There also lies the disadvantage in qPCR, when investigating natural complex microbial communities, some functional genes of metabolic processes are not located in highly conserved regions like the 16S rRNA gene. Therefore, it is sometimes necessary to use more specific primer sets for a functional gene for some bacterial groups, such as hgcA primers for δ-*Proteobacteria*, *Firmicutes* and *Archaea* in Christensen et al. (2016). Furthermore, the numerous proteins and thus gene sequences involved in a metabolic pathway would also need a primer pair for each step of the individual reactions within a pathway. For complex metabolic processes like the base C metabolism, qPCR would be unfeasible and rather applicable on short metabolic processes such as mercury methylation (Christensen et al., 2019)

The development of “omic”-techniques revealed to be one possible solution to the above-mentioned disadvantages of 16S rDNA-based sequencing and qPCR of functional genes: metagenomics, metatranscriptomics and metaproteomics are able to provide taxonomic information, functional information and can be interlinked with each other as gene-, mRNA- and peptide-sequences can be translated into one another (Kohlstedt et al., 2010; Schimel, 2016). Additionally, another advantage to the primer-based sequencing methods is that, meta-omics techniques disentangle the entirety of the microbial metabolism in their respective genome, transcriptome and proteome which can then be

distilled down to the metabolic processes relevant to the research question (Beulig et al., 2016; Schimel, 2016). These genes of interest (GOI) can be universally applied to the analyzed genome, transcriptome, and proteome. *In situ* the degradation of the TP seems to induce complex metabolic responses in the microbial community to which the application of multi-meta-omics would not lead to constructive results. Therefore, an experiment under controlled laboratory conditions on the C metabolism was chosen as the base C metabolism consists of well-researched pathways. C metabolism might help in the understanding of C loss in soil and its metabolic mechanism of microbial growth under scarce C-glucose conditions or when C-glucose is plentiful in soil hotspots (Kuzyakov and Blagodatskaya, 2015).

1.1.4. Objectives

This thesis addresses the role of microbial communities' metabolism in C and nutrient loss in soil on the Tibetan Plateau. For this, it was necessary to deepen the understanding of the microbiota's influence on C cycling in soils through employing a wide range of well-established and state of the art methods to characterize the soil microbiome and its metabolism such as t-RFLP and 16S rDNA sequencing. As microbial community's phylogenetic characterization often only provides indirect information on C cycling functions, this thesis furthermore aimed to develop novel multi-meta-omics approaches for complex soil communities combining three post-genomic levels: metatranscriptomics (level 1), metaproteomics (level 2), and targeted metabolomics (level 3, Fig. 2) in form of biomarker extraction of PHB and NLFA storage compounds. These analyses were combined with application of labeled ^{13}C and ^{14}C glucose (uniformly and ^{13}C position-specifically labeled) for a modified meta-flux modelling approach to uncover the mechanisms of C cycling in microbial metabolism throughout various levels of post-genomic metabolic regulation depending on soil resource availability.

The main objectives of this thesis were:

I) Identifying key microbial players and their functions involved in the C losses during SOM degradation of the globally important pasture ecosystem on the Tibetan Plateau by molecular biological analysis of fungal and bacterial community shifts.

II) Identifying key functional changes in the microbial metabolism under varying C availability utilizing enzyme activity measurements of successively degraded Tibetan root mats and state of the art omics-techniques in controlled laboratory incubations with manipulation of C to nutrient stoichiometry.

III) Assessing the role of storage compounds, a long-term neglected C pool, for soil C cycling by tracing their *de-novo* formation by isotope tracing and metabolic flux modeling of base C metabolism.

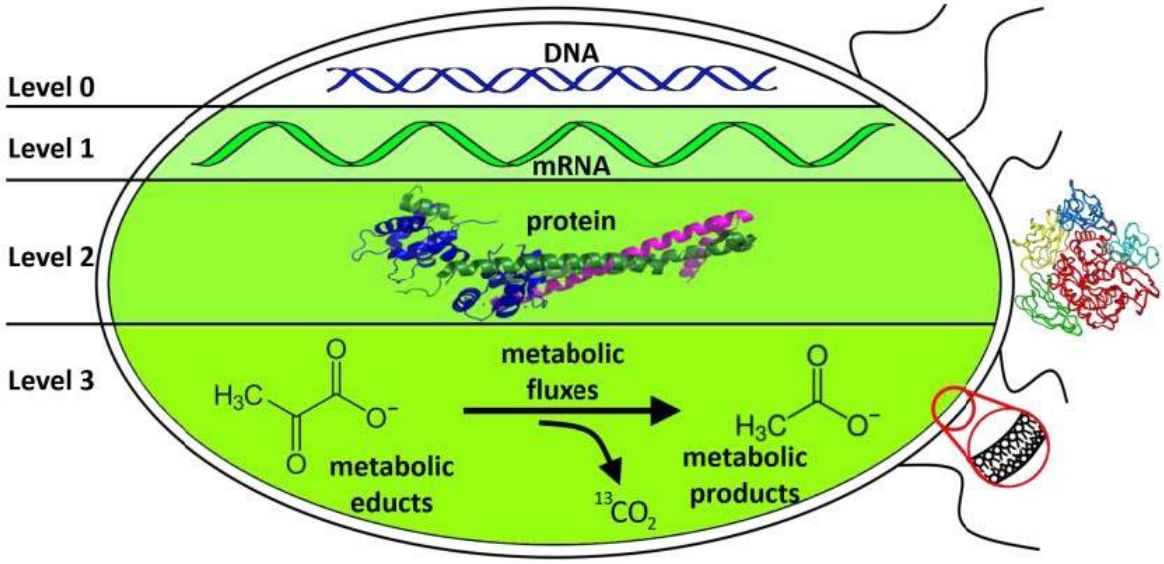

ES Figure 2: **Three levels of post-genomic biochemical regulation:** (**1**) transcriptome, (**2**) proteome and (**3**) metabolome interlinked by its metabolic fluxes.

1.2.Approaches

1.2.1. Field experiment

The severity of *Kobresia* grassland degradation was assessed by a literature study conducted by searching for information about the depletion of SOC, TN, clay content and bulk density (BD) (keywords, see 2.1.5.). The parameters from the chosen studies were then compared to the measured values from our field study of SOC, TN and BD as to assure the representativeness of the study to the degradation of the TP grasslands. The TP *Kobresia* grasslands undergo severe root mat degradation which was classified into 6 stages for this study (ES Fig. 1) and sampled within our sampling site near Nagqu (Tibet, China, (NW: 31.274748°N, 92.108963°E; NE: 31.274995°N, 92.111482°E; SW: 31.273488°N, 92.108906°E; SE: 31.273421°N, 92.112025°E) on an area of 4 ha at 4,484 m a.s.l.: from an intact stage (S0) over increasing degradation and erosion affected stages (S1 – S4) to the most degraded stage (S5). Within the classified stages, SOC loss, potential shifts in the microbial community and their functions are to be identified. The intact soils were classified as Stagnic Eutric Cambisol (Humic) developed on a loess layer and on glacial sediments. The samples were taken in replicates of 4 from the soil horizons at 0 – 5 cm, 5 – 15 cm and 15 – 35 cm. SOC and N characteristics were measured as $\delta^{13}C$ and $\delta^{15}N$ using an isotope ratio mass spectrometer (IRMS, Delta plus, Conflo III, Thermo Electron Cooperation, Bremen Germany) coupled with an elemental analyzer (NA 1500, Fisons

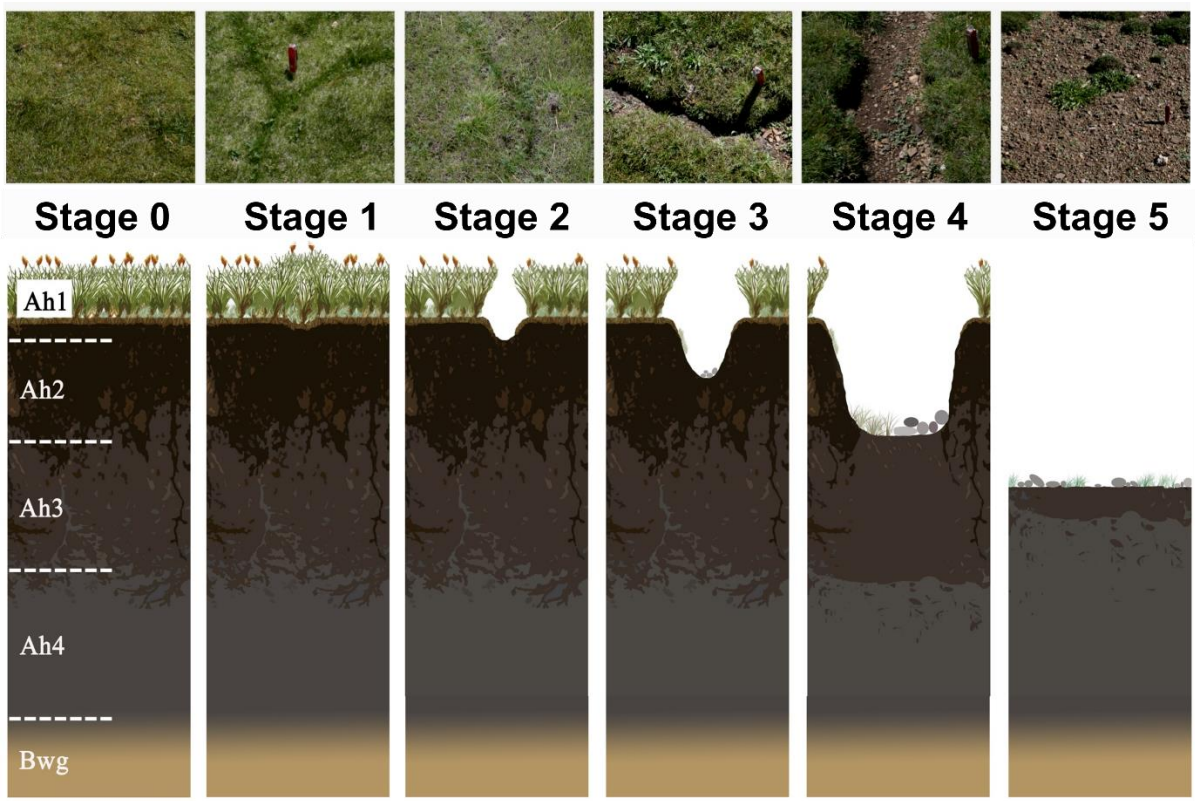

ES Figure 3: **Overview of the degradation sequence from the intact (S0) to severely degraded (S5) stage.**

Instruments, Milano, Italy) at the Centre for Stable Isotope Research and Analysis (KOSI, University of Göttingen, Göttingen, Germany). SOC stock and loss were determined as well as lignin content as sum of vanillyl, syringyl and cinnamyl structural units. For the characterization of the potential functional shifts in the microbial community, enzyme activity of extracellular enzymes was directly measured on site following protocols from Schinner et al. (2012): two hydrolases (β-glucosidase and xylanase), phenol oxidase, urease and alkaline phosphatase to identify C, N and P transformations. Soil samples for the characterization of the microbial community were directly frozen at -20 °C on site. DNA was extracted from soil using the PowerSoil DNA isolation kit (MoBio Laboratories In., Carlsbad, CA, USA) following the manufacturer's manual. DNA concentration was then determined with a NanoDrop 1000 nanophotometer (Thermo Fisher Scientific, Wilmington, DE, USA). For the t-RFLP, DNA was amplified with a fluorescence marked (FAM) primer set while DNA for the Illimina MiSeq sequencing (Illumina Inc., San Diego, USA) was amplified with a primer set with adaptor sequences (forward: 5'-TCG TCG GCA GCG TCA GAT GTG TAT AAG AGA CAG-3'; reverse: 5'-GTC TCG TGG GCT CGG AGA TGT GTA TAA GAG ACA G-3'). Both methods used the same primer pairs for bacterial 16S rDNA V3 (5'-CCT ACG GGN GGC WGC AG-3') and V4 (5'-GAC TAC HVG GGT ATC TAA TCC-3') and ITS primers for fungi: ITS1 (5'-CTT

GGT CAT TTA GAG GAA GTA A-3'), ITS1-F_KYO1 (5'CTH GGT CAT TTA GAG GAA STA A-3'), ITS2 (5'-GCT GCG TTC TTC ATC GAT GC-3') and ITS4 (5'-TCC TCC GCT TAT TGA TAT GC-3'). After PCR (protocol see 2.1.5.7) and agarose gel control, the PCR product was digested with either of two restriction enzymes and then measured in an ABI Prism 3130 Genetic Analyzer (Applied Biosystems, Carlsbad, CA, USA) for t-RFLP analysis or sequenced with Illumina MiSeq (Illumina Inc., San Diego, USA) (details see 2.1.5.8 and 9).

1.2.2. Laboratory experiment

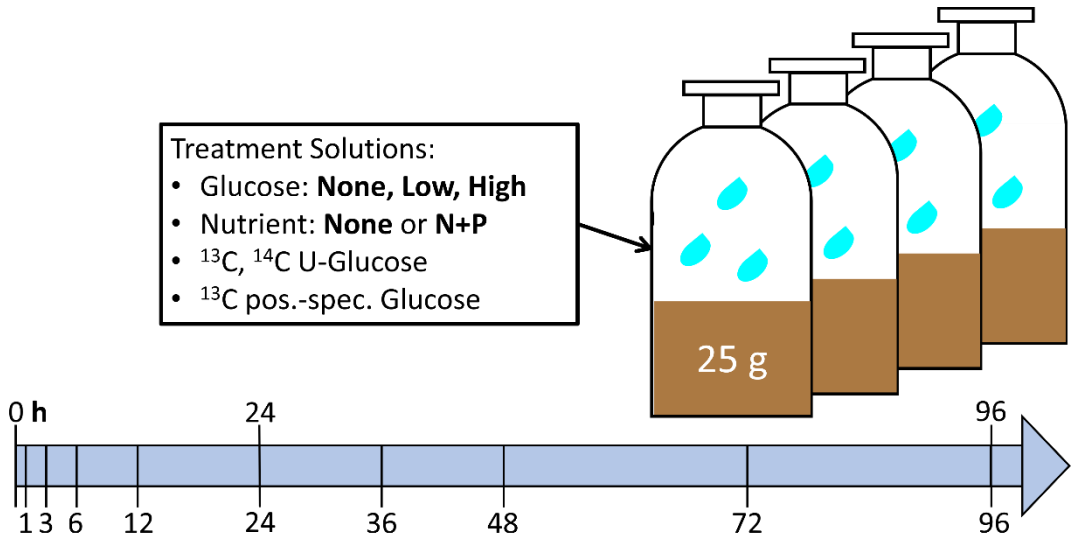

ES Figure 4**: Microcosm lab experiment conducted in air-tight 100 ml glass bottles** with 25 g of agricultural soil incubated with treatment solutions containing glucose (None, Low and High) and nutrients (None and N+P) and labelled with uniformly and position-specific glucose tracers in 4 replicates. Destructive sampling at 0, 24 and 96 h (times marked above the time scale) and $^{13}CO_2$ measurements over the course of the experiment (times marked below the time scale).

The degradation of the TP is a complex ecosystem process with numerous drivers of C and nutrient loss; therefore, it is necessary to transfer the process of C mineralization to a more controlled environment. In a lab experiment with natural soils, we could control any aspect of the environmental conditions such as moisture, aeration and temperature, add treatment solutions with ^{13}C and ^{14}C glucose tracers (uniformly and position-specifically labelled) and manipulate the C amount and nutrients available for the microbial community in soil.

The soil for the lab experiment was a Haplic Luvisol which, like the soil on the TP developed on loess and was sampled at the experimental farm Reinshof near Göttingen, Germany (51°29'51.0'' N, 9°55'59.0'' E). Its low total organic C (TOC) content at 1.4%, and 0.17% total N (TN) at a pH 5.4 would guarantee a microbial reaction when treated with glucose and nutrient solutions. The 100 ml air-tight

microcosm glass bottles were filled with 25 g of soil at 48% water holding capacity (WHC). The treatment solutions consisted of three glucose treatments depending on the microbial biomass carbon (MBC): 0, 90 and 400 µg C g^{-1} soil. Furthermore, the glucose treatments were also divided into a no-nutrient and nutrients in form of ammonium sulfate ($(NH_4)_2SO_4$, 17 µg N g^{-1} soil) and tripotassium phosphate (KH_2PO_4, 3.3 µg P g^{-1} soil) as nitrogen (N) and phosphate (P) sources. With the help of ^{13}C (3at%) and ^{14}C (0.19 kBq) uniformly and position-specifically (1.5at%, all 6 glucose-C positions) labelled glucose tracers added to the treatment solutions the fate of the added glucose could be traced in various ways. Each treatment was conducted in a replicate of 4.

The $^{13}CO_2$ efflux from uniformly- and pos.-spec.-labelled microcosm was measured over the course of the entire 4- day experiment (Fig. 4) with evacuated exetainers (Labco, Ceredigion, U.K.) and measured on an GC-IRMS (GC-Box coupled via a Conflo III interface to a Delta plus XP mass spectrometer, all Thermo Fischer, Bremen, Germany) at the Centre for Stable Isotope Research and Analysis (KOSI, University of Göttingen, Göttingen, Germany). Beside the estimation of glucose-derived respiration from $^{13}CO_2$ efflux, $^{13}CO_2$ from uniformly and pos.-spec. glucose were used to calculate the F values for each U-^{13}C samples and every pos-spec. ^{13}C samples. Ratios from those F values were then calculated ($x^{13}CO_2/U^{13}CO_2$) as input for our unmodified flux model without storage and storage-optimized C flux model (details see 2.3.3.). The model is able to calculate each flux of the base C metabolism (Fig. 1), so that the fate of every glucose-C atom can be traced.

Destructive sampling was done at the beginning of the experiment (t_0), after 24 h and at the end at 96 h and the soil was used for several extractions: MBC was extracted via chloroform fumigation extraction (CFE) to measure the growth in biomass. Radionuclide-labelled ^{14}C glucose enabled the tracing of *de novo* synthesized MBC from glucose and was measured via scintillation counting after CFE. Storage compounds PHB and NLFA, as well as cell membrane component PLFA biomarker were extracted and measured after derivatization on a 7890 A GC-MS and on an IRMS-GC for their ^{13}C incorporation at the KOSI. As an alternative to the $^{13/14}C$ approach, growth was also estimated via ^{18}O incorporation into DNA in a parallelly conducted microcosm experiment with the same parameters and the use of 97at% $H_2{}^{18}O$ water (resulting in 4.2at% ^{18}O in soil) following the protocol of Spohn et al. (2016) and measurement at the KOSI (for details see 2.3.3. or 2.4.4).

Soil samples from the 24 h destructive sampling point were also used for RNA and protein extraction for metatranscriptome and metaproteome analysis. After the RNA extraction with the Qiagen RNeasy PowerSoil kit (Qiagen GmbH, Hilden, Gemany) at the ZALF (Müncheberg, Germany) samples were sent to Macrogen Inc. (Seoul, Republic of Korea) for further preparation and mRNA sequencing. The protein extraction was conducted at the Helmholtz Centre for Environmental Research – UFZ GmbH (Leipzig, Germany) following established protocols by Bastida et al. (2016, 2014). Peptide sequences were

obtained by separating with a Dionex Ultimate RSLC 3000 nano-LC system (Thermo Fisher Scientific, Idstein, Germany) and peptide analysis was performed on a Orbitrap Fusion MS (Thermo Fisher Scientific, Idstein, Germany) coupled with a TriVersa NanoMate source (Advion, Ltd., Harlow, UK). The peptide sequences were then searched against the bacterial NCBInr database for the determination of the contained proteins and their abundances were calculated.

1.3. Results and Discussion

1.3.1. Overview of main results

ES Table 1 gives an overview of the objectives, and conclusions of the studies included in this thesis:

ES Table 1: **Titles, objectives, and conclusions of the individual four studies presented in in this thesis.**

Study	Objectives	Main Conclusions
Study 1: Microbial functional changes mark irreversible course of Tibetan grassland degradation	➢ Identify critical points of microbial functioning and their consequences for SOC and N storage. ➢ Characterization of SOM quality and quantity coupled with feedback loops to microbial community structure and functions.	➢ A highly interrelated process of pasture degradation with freeze-thaw cycles, topsoil erosion and microbial decomposition diminish the SOC and N stock. ➢ SOC decomposition and N loss are accompanied by a shift in microbial functioning as an adaptation to the altered availability of C and N. ➢ *Kobresia's* mycorrhizal partners shifted from arbuscular- to ectomycorrhizal partners with increasing degradation
Study 2: Multi-Meta-Omics in soils: What to learn about the regulation of the basic C metabolism under shifts in habitat element stoichiometry	➢ Disentangle post-genomic responses of the base C metabolism to glucose addition on two post-genomic levels. ➢ Identify whether excess glucose levels are directed towards storage compound biosynthesis on both post-genomic levels. ➢ Characterize the impact of glucose and nutrient addition on the microbial community.	➢ Regulatory processes and time-lag seem to interfere with a coherent response to glucose addition downstream the metatranscriptome and metaproteome. ➢ Storage compound pathways were active throughout both post-genomic levels but decreased with excess glucose. ➢ Glucose and nutrient addition are affecting the microbial community on every metabolic level with a high regulatory response in between the two post-genomic levels.
Study 3: Accounting for storage compounds in soil microbial communities alters carbon flux modelling outcome.	➢ Distinguish between *de novo* synthesis of biomass and storage compound formation via metabolic flux modelling under varying glucose and nutrient amendments.	➢ Excess glucose did not direct modelled fluxes towards surplus storage synthesis, but reserve storage mode was enabled at low glucose condition as an adaptation to limited C in soils.
Study 4: Intracellular carbon storage by microorganisms is	➢ Identify surplus storage formation under C replete and	➢ PHB storage is used as surplus storage under excess glucose

an overlooked pathway of biomass growth.	nutrient-limited conditions in soil. ➢ Analyze the role of storage synthesis in microbial biomass growth. ➢ Disentangle the role of nutrient availability in the formation of storage compounds.	whereas TAG storage is used in reserve storage mode. ➢ Storage compounds harbors substantial amounts of C and increases total microbial biomass aside replicative growth. ➢ Nutrient addition suppresses PHB formation whereas TAG was not affected.

1.3.2. Degradation of Kobresia pastures on the Tibetan plateau induced structural changes in the microbial community.

The degradation of the *Kobresia* root mats had severe consequences to the SOC stock as 42% of it were lost from S0 to S5 due to erosion, overgrazing, freeze-thaw processes in permafrost soils, decreased root litter input and mineralization (Wang et al., 2020). Furthermore, also 33% of N was released from the ecosystem. In consequence, vital structural and functional changes in the soil microbial communities are at play. Soil microbes play an important role in sequestering and mineralizing C and N while C is distributed heterogeneously, it is also sequestered in recalcitrant forms such as vanillyl, syringyl, and cinnamyl (VSC), so that C sources are challenging to break down and C becomes a scarce resource in soils (Kuzyakov and Blagodatskaya, 2015). On the other hand, easily degradable C sources such as glucose-rich root exudates, amino acids, carboxylic acids are available for microbial decomposition in hotspots in the detritus-, drilossphere and rhizosphere (Bååth, 2003; Gunina et al., 2014; Kuzyakov and Blagodatskaya, 2015; Rasse et al., 2005). When *Kobresia* root mats degraded, root litter input is interrupted, and those easily degradable SOC pools are prone for microbial mineralization first. Exoenzyme activity for those C sources declined with the severity of the *Kobresia* pasture degradation. Likewise, the microbial communities' shift towards nitrifying and denitrifying bacteria suggest a major microbial role in N-transformation and N leaching from TP's N-limited ecosystem (Craine et al., 2007; Schleuss et al., 2015). After the disappearance of easily degradable LMWOS, increasing enzyme activity of lignin degrading phenol oxidases and a structural shift towards bacterial and fungal species capable of degrading complex C sources suggest a severe loss of SOC quantity and quality (Fig. 5). Furthermore, with the increasing degradation of *Kobresia* grasslands, its arbuscular mycorrhizal (AMF) partners decline and get replaced by more specialized ectomycorrhizal (EM) partners capable of mineralization of SOM-bound nutrients until the total disappearance of *Kobresia pygmaea*. Then, on the most degraded sites, pioneer plants and their AMF partners are established.

During the increasing degradation of TP's *Kobresia* grasslands the mineralization of easily hydrolysable LMWOS as well as lignin monomers (VSC) were driven by microbials' base C metabolism: When LMWOS, like (hemi-) celluloses, decomposition led into glycolysis delivering the most energy output.

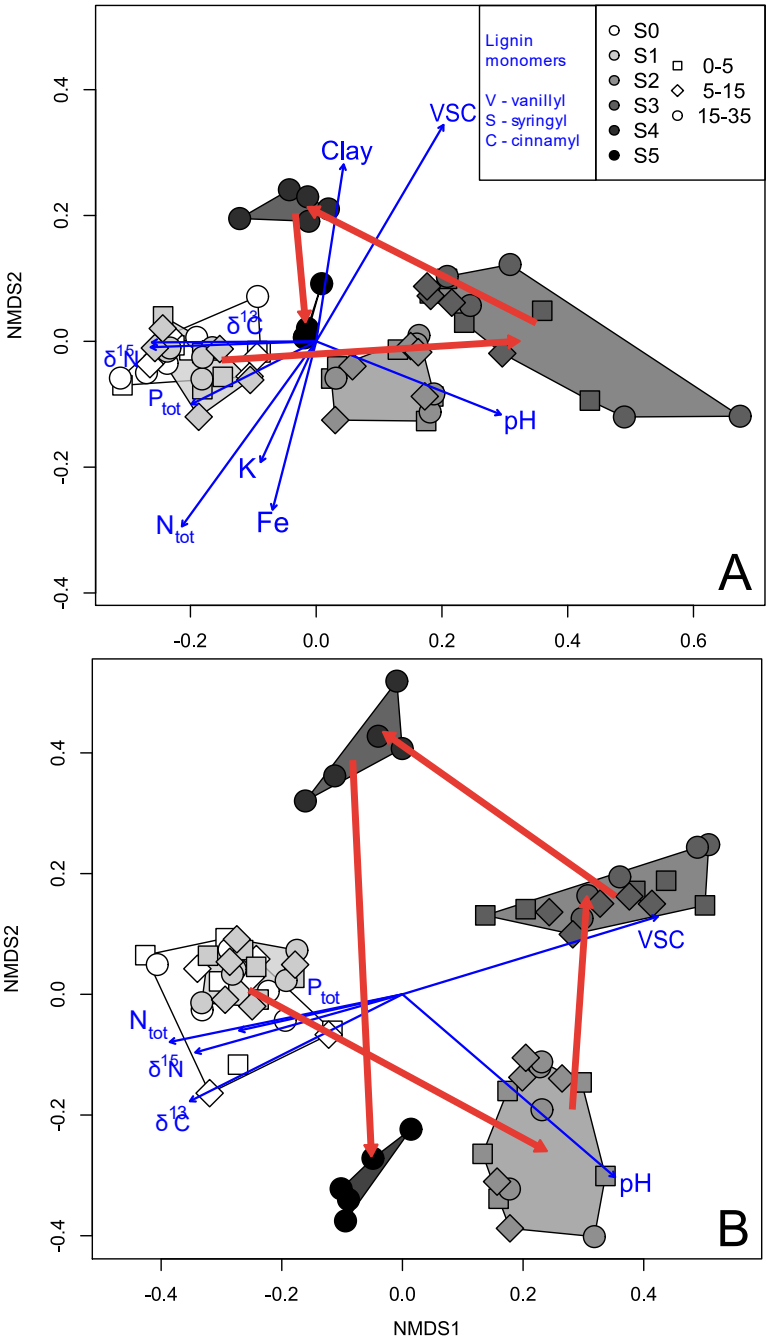

ES Figure 5: **NMDS (non-metric multidimensional scaling) plots derived from Illumina MiSeq sequencing data of the bacterial (A) and fungal (B) communities along degradation stages.** Shaded areas mark each degradation stage, symbols indicate soil depth, and blue arrows show significantly correlated abiotic factors (by CCA, canonical-correlation analysis).

The microbial community can also gain an intermediate level of energy when proteins are decomposed. Protein monomers can enter the base C metabolism at several entry points when being mineralized and release not only CO_2 but also N. For example, the amino acid alanine can enter the glycolysis when transformed into pyruvate and is frequently sorbed to soil particles in the SOM

(Apostel et al., 2017). Finally, complex compounds such as lignin enter the TCA cycle but gain the least energy when decomposed (Ottow, 2011). Therefore, increasing degradation of the TP pastures strongly influences the base C metabolism of the microbial communities as they need to adapt to the ever-changing substrate composition. Analyzing the linkages between substrate composition and base C metabolism will broaden the understanding of microbial contribution to SOM degradation. Measuring enzyme activities of exoenzymes do not give enough insight into the functional shift and metabolic regulatory processes of the TP's microbial community. Additionally, 16S rDNA primer-based sequencing methods only provide information on microbial structural changes and species (Fig. 5). Therefore, the utilization of "omics"-techniques on the base C metabolism is necessary to fully disentangle the microbial processes when an ecosystem such as the TP is facing irreversible changes.

1.3.3. Multi-meta-omics give insight into metabolic regulation under altered C availability and nutrients.

Employing state-of-the-art metatranscriptome and metaproteome analysis on the base C metabolism gave new insights into microbial regulatory processes. Depending on the stoichiometry of C and nutrients, the metaproteome showed deviating patterns in relative abundance in the selected pathways in comparison to the metatranscriptome hinting towards strong regulatory processes in protein translation. The only exception were parts of the glycolysis and TCA. On the one hand glucose amendments greatly affected the metatranscriptome, on the other hand the addition of N and P mainly had an effect on the metaproteome throughout the chosen pathways. While high glucose levels had a reducing effect on the abundance of proteins involved in PHB storage biosynthesis, this reduction was not visible in the abundance of the related genes in the metatranscriptome. Similarly, the abundance of NLFA storage pathway related transcripts and proteins was negatively affected by high glucose concentrations. Nutrient addition seemed to have no regulatory effects on both the metatranscriptome and metaproteome related to the pathways of storage synthesis of PHB and NLFA. These conditions had a similar effect on the extracted PHB and NLFA contents where PHB was also synthesized in low glucose conditions (see 2.4 study 4). Altogether, the two post-genomic levels seem to be strongly influenced by the addition of glucose-C in a C limited agricultural soil rather than by the availability of N and P (Soong et al., 2020). The addition of nutrients solely influenced PPP related genes while disappearing on the translational level as similarly described by Kohlstedt et al. (2010).

Furthermore, the pathways in the metatranscriptome seem to be strongly co-regulated with each other as a correlation analysis revealed: gluconeogenesis was negatively related to both storage pathways and positively related with the TCA. These co-regulatory processes were not represented in the metaproteome. Additionally, PPP was positively correlated with fatty acid biosynthesis and

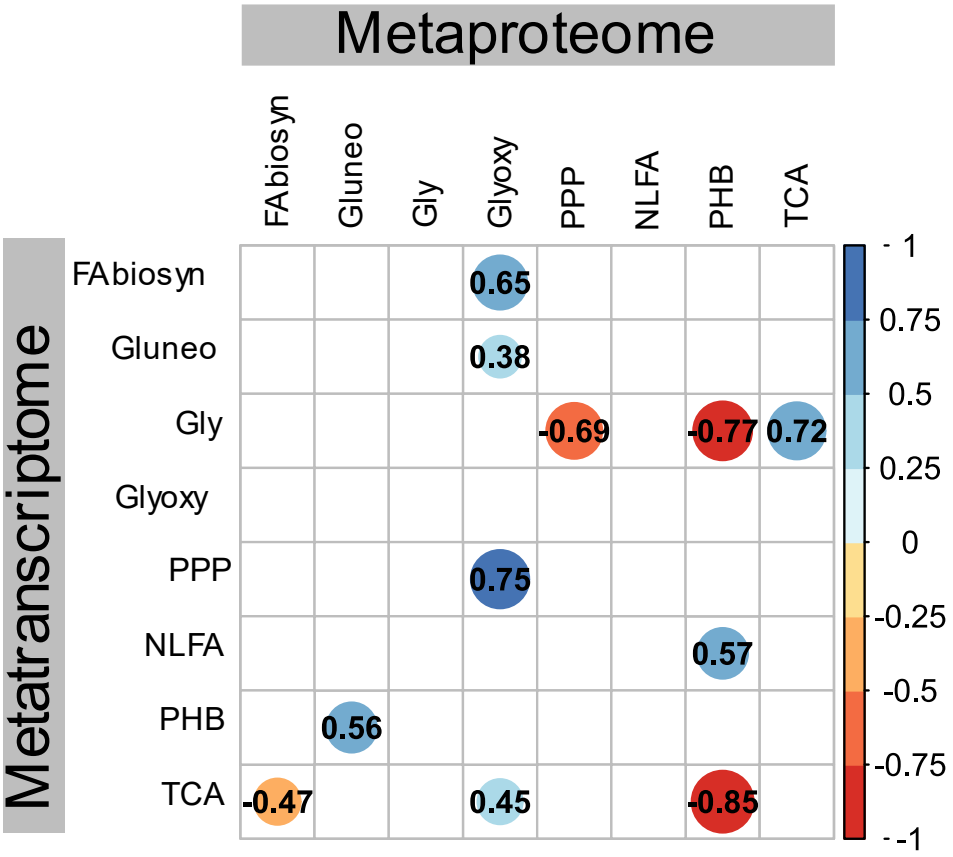

ES Figure 6: **Correlation between the metatranscriptome and metaproteome metabolic processes.** Only significant correlations are displayed, and R values are indicating their positive or negative relationships

negatively correlated with TCA in the proteome. Nevertheless, hinting towards an active pathway towards the *de novo* biosynthesis of biomass. These observations hint towards an inter-regulatory process in between the metatranscriptome and metaproteome (Fig. 6). Several consecutive pathways like glycolysis (mRNA level) and TCA (protein level) were positively correlated suggesting jointly controlled and functional energy producing pathways. Also, storage pathways were positively correlated in both post-genomic levels hinting towards active storage biosynthesis under the underlying glucose conditions. Pathways related to replicative growth (fatty acid biosynthesis, PPP, gluconeogenesis, and TCA) in the metatranscriptome and glyoxylate metabolism in the metaproteome suggest a constant demand of C for anabolism. The excess of glucose in our experiment greatly affected the activation of the transcription and translation of TCA cycle genes related to a strongly catabolic and energy producing pathway (Voet et al., 2008). This hints towards the need of a quick reaction of the microbial community when additional C is available in hotspots in the rhizosphere or detritussphere of an otherwise C-limited (and more strongly SOM-depleted) agricultural soil (Kuzyakov and Blagodatskaya, 2015; Soong et al., 2020). In contrast, glucose amendments led to the inhibition of

the anabolic PPP mRNAs at the translational level as a response to the stoichiometric shifts. This indicates a multi-level regulatory system on all "omic"-levels which can also be interrelated (Kohlstedt et al., 2010). Leading to the suggestion that examining solely one post-genomic level is not sufficient for interpretation of microbial metabolic processes especially in complex communities as genes could be not transcribed, mRNA not translated into proteins or proteins inhibited (Kohlstedt et al., 2010; Schimel, 2016). Therefore, only multi-meta-omic experiments are capable of disentangling the regulatory processes in soil microbiomes (Herold et al., 2020; Kohlstedt et al., 2010; Schimel, 2016). Another factor in regulating metabolic processes is time - while the transcriptome reacts rather fast on altered environmental conditions with mRNA half-lifes of 1 -10 min (Laalami et al., 2014), the translation to proteins takes 10 to 90 min (Takahashi et al., 2011), meaning that the metaproteome has a time-lag response on the past environmental conditions or the metatranscriptome is already reacting to the depletion of the glucose addition at that time. The TCA seems to be a constantly needed process, as it is not affected by the high dynamic response of regulatory processes as much as other pathways and also not affected by the time-lag. This observation is important as the TCA is strongly negatively related to the carbon use efficiency (CUE) (Wu et al., 2022) and can therefore be used to deduce the CUE from transcripts and protein abundance.

1.3.4. Meta-flux modelling and storage compound extraction reveal different growth modes under different glucose and nutrient conditions.

The addition of glucose greatly enhanced CO_2 efflux while nutrient addition only played a role at the high glucose amendments where N and P accelerated glucose mineralization in the first 24 h (see 2.4). The C flux modelling from isotopomere glucose ^{13}C input was done with two modes: one unmodified model and the other with a modelled flux into storage formation which showed an effect on CO_2 respiration when storage formation was enabled. The br5* flux into storage was higher than in the br5 flux in the unmodified model, underlining the importance of storage flux adjustments in modelling approaches. This importance was further highlighted by the direct measurements of storage compounds: PHB and TAG represented one fourth of the MBC pool even in the control soils without glucose or nutrient addition indicating biosynthesis of storage compounds also in C-limited conditions. With increasing glucose levels, a great proportion of new PHB was synthesized (+308% increase over the control). While PHB formation was mainly driven by resource stoichiometry, TAG also depended on the addition of nutrients resembling reserve storage mode (Bååth, 2003; Dijkstra et al., 2022; Mason-Jones et al., 2021) - so that both storage compounds fulfill different roles in a microbial community: On the one hand, PHB is rather responsible for surplus storage when excess C is available (Kourmentza et al., 2017; Sekar et al., 2020). On the other hand, TAG synthesis was not stimulated by surplus stoichiometry and rather resembled a reserve storage strategy where storage compound

formation is active through constant C resource stress (Mason-Jones et al., 2021). Since TAG is not only a storage compound in fungi, but is also produced by some bacterial species (Alvarez, 2003; Kalscheuer et al., 2001), both storage compounds seem to fulfill different roles in a soil microbial community. The modelling results in regard of excess glucose levels triggering surplus storage formation were contradictory to the directly measured storage compounds as the high glucose amendments indicated no flux into storage but rather into the *de novo* formation of biomass through cell devision. While our C flux model relies solely on $^{13}CO_2$ efflux quantified after glucose ^{13}C isotopmere labeling, the directly measured storage pool can also be synthesized from SOM which was seen in the TAG data. Therefore, the flux model neglects metabolic processes from SOM, necromass or sorbed substances, putting an emphasis on rapidly growing and C efficient – glucose utilizing – bacteria (Apostel et al., 2018; Kashi et al., 2022). In the control and low glucose treatments the modelled C flux into storage was playing a more important role than in high glucose hinting towards reserve storage mode preparing for extended periods of C starvation and were comparable to the findings in measured TAG pools (Bååth, 2003; Matin et al., 1979). Our parallel experiment under the same conditions as the main experiment with the incorporation of ^{18}O into DNA to quantify replicative growth is calibrated with MBC from CFE and therefore does not take PHB and TAG into account (Spohn et al., 2016). In comparison with the measured C allocation into storage compounds, ^{18}O-based microbial growth substantially underestimated growth by neglecting storage by 279% (± 72%). Microbial growth is a pivotal factor in C cycle modelling, and storage compound formation needs to be taken into account (Wieder et al., 2018). The assumption of stoichiometric homoeostasis from biomass growth and total biomass under C surplus needs to be adjusted since storage compounds as part of total biomass growth lead to an imbalanced stoichiometry (Mooshammer et al., 2014; Wutzler et al., 2017). Storage compounds are key players in C and nutrient retention in short-term resource pulses by which C can stored in bacterial cells over a long term creating a more resistant and resilient microbial community to ecosystem disruptions (Loreau and de Mazancourt, 2013; Manzoni et al., 2021).

1.4. Conclusions

The degradation of the Tibetan Plateau's *Kobresia* grassland demonstrated the severity of anthropogenically induced soil degradation and erosion due to overgrazing into an irreversible final state. The pasture ecosystem underwent drastic SOC and N losses in proceeding stages of degradation of *Kobresia* root mats, altering the nutrient stoichiometry. The disruption of root litter input for C sequestration into mineralization of remaining C stocks was mainly driven by an ever-adapting microbial community. Well-established primer-based sequencing techniques, measuring exoenzyme activity and the use of 16S-based functional databases aided in revealing a structural and functional

shift in the bacterial and fungal community with the advancing degradation. Until the degradation stage S3, the microbial community seemed to be able to resist the ecosystem disruption in C and N loss, but the exact metabolic response mechanics were only up for debate, as the employed methods have their limitations to investigate the regulative response of the basic C metabolism on successive C depletion of soils. To fully understand the microbial role such a soil degradation, the microbial processes dominating in C scarce soils need to be fully understood.

Therefore, our multi-layered laboratory experiment manipulating C availability and element stoichiometry by addition of easily available glucose-C sources and nutrients could give new and more detailed insights into microbial growth, the regulation of the base C metabolism, and the involvement of storage compounds in environmental stress conditions or excess of glucose-based C availability. With the combination of state-of-the-art metatranscriptome and metaproteome analysis, C flux modelling and extraction of storage compounds, we were able to determine the fate of glucose-C in every step of the base C metabolism in microbial communities. Throughout our experiment we could detect the biosynthesis of storage compounds at all post-genomic levels (i.e from transcriptome until down to targeted metabolite measuring itself) and in our C flux model. We could detect storage compounds even in C depleted soils hinting towards reserve storage as a key strategy under limited C – a processes which might also have been possible in advancing TP degradation stages. The linkages between the metatranscriptome and metaproteome, the measured storage compounds and the outcome of C flux modelling revealed several regulatory steps in microbial metabolism when metabolic processes were not visible in the levels below (e.g., high ϕ ratios in high glucose treatments in the metatranscriptome and partially in the metaproteome while meta flux modelling revealed an inversed pattern with high ϕ ratios in low glucose treatments), hinting towards downregulation (e.g., high abundances of mRNA of PHB biosynthetic process genes across the glucose treatments while being downregulated at high glucose levels in the metaproteome) or protein inhibition. Surplus storage was identified by Mason-Jones et al. (2021) via direct quantification of PHB and by Manzoni et al. (2021) via modeling, but was not visible in the flux model output, which rather suggested a reserve storage mode. TAG storage compounds were identified to be most responsible for a reserve storage mode mostly independent from the usage of glucose but rather surrounding SOM (see 2.4.3.2). In conclusion, the flux model needs to be adjusted towards the different storage modes distinguishing between the two roles of PHB (surplus storage) and TAG (reserve storage). Furthermore, the C flux model's input sources could be broadened with the utilization of more complex ^{13}C input sources such as long-chain dicarboxylic acids (Kashi et al., 2022) instead of easily available glucose-C and therefore representing SOM utilization in the base C metabolism. This might help interpret the role of SOM in building up TAG storage compounds in reserve storage mode. It would therefore be possible to extend the C flux model

to community members utilizing rather complex C sources and take their contributions to overall microbiomes' metabolic fluxes into account (Wu et al., 2020).

Following metabolic processes along the post-genomic levels remains a challenge especially when stepping into regulatory processes in highly complex soil microbial communities. However, by focusing on the base C metabolism and defining highly controlled suitable treatment parameters as here done by altering C and nutrient stoichiometry, it was possible to gain some insight into soil microorganisms' C metabolism. Especially, the investment of C into storage compounds even in C depleted control soils might suggest that microbial communities in degraded *Kobresia* pastures are also directing their C flux into producing storage compounds, which buffers degradation until stage S3, when then towards stage S4 an irreversible stage of degradation is reached. Applying multi-meta-omics to a complex soil ecosystem such as the TP would give new opportunities in revealing the key players and key microbial processes in the degradation of *Kobresia* root mats. While this thesis focused on C metabolic processes, meta-omics techniques retain much more information on other metabolic processes such as N cycle related genes, transcripts, and proteins - another crucial player in nutrient loss and stoichiometric imbalance on the TP. Furthermore, other stress-related genes could also give information when the microbial community has reached its pivoting point in the degrading ecosystem.

On the one hand, the structural and functional analyses based on 16S rDNA sequencing techniques and their (functional) databases of the microbial community on the TP have shown their limitations especially in identifying key players and key functional processes where multi-meta-omics would give potentially more insight. On the other hand, the complexity of analyzing and interpreting the outcome of "-omics" techniques in comparison to the rather quick and more cost-effective 16S rDNA sequencing techniques need to be considered, when conducting a field experiment and sample transport may be a critical issue. This thesis has shown that multi-meta-omics' applications seem to now have reached a step-up form single cultures and mock community studies towards more complex natural microbial communities (in soils) in controlled lab experiments. It is now possible to explore the linkages between several post-genomic levels and even find metabolic processes which can be used as substitute for analyzing microbial metabolic activity like the TCA cycle. The measured TCA process activity can be utilized as a stable proxy for the catabolic activity or help deduce the CUE in the soil microbial communities. Therefore, TCA activity measured on any post-genomic level could reasonably complement taxonomic characterizations of microbial communities. Furthermore, this thesis underlined the importance of storage compounds as a microbial growth factor when it could demonstrate the relevance of storage compound formation on all post-genomic levels.

1.5. References

Alvarez, H.M., 2003. Relationship between β-oxidation pathway and the hydrocarbon-degrading profile in actinomycetes bacteria. International Biodeterioration & Biodegradation 52, 35–42. https://doi.org/10.1016/S0964-8305(02)00120-8

Apostel, C., Dippold, M., Kuzyakov, Y., 2015. Biochemistry of hexose and pentose transformations in soil analyzed by position-specific labeling and 13C-PLFA. Soil Biology and Biochemistry 80, 199–208. https://doi.org/10.1016/j.soilbio.2014.09.005

Apostel, C., Dippold, M.A., Bore, E., Kuzyakov, Y., 2017. Sorption of Alanine changes microbial metabolism in addition to availability. Geoderma 292, 128–134. https://doi.org/10.1016/j.geoderma.2017.01.016

Apostel, C., Herschbach, J., Bore, E.K., Spielvogel, S., Kuzyakov, Y., Dippold, M.A., 2018. Food for microorganisms: Position-specific 13 C labeling and 13 C-PLFA analysis reveals preferences for sorbed or necromass C. Geoderma 312, 86–94. https://doi.org/10.1016/j.geoderma.2017.09.042

Armstrong McKay, D.I., Staal, A., Abrams, J.F., Winkelmann, R., Sakschewski, B., Loriani, S., Fetzer, I., Cornell, S.E., Rockström, J., Lenton, T.M., 2022. Exceeding 1.5°C global warming could trigger multiple climate tipping points. Science 377, eabn7950. https://doi.org/10.1126/science.abn7950

Aßhauer, K.P., Wemheuer, B., Daniel, R., Meinicke, P., 2015. Tax4Fun: predicting functional profiles from metagenomic 16S rRNA data: Fig. 1. Bioinformatics 31, 2882–2884. https://doi.org/10.1093/bioinformatics/btv287

Bååth, E., 2003. The Use of Neutral Lipid Fatty Acids to Indicate the Physiological Conditions of Soil Fungi. Microbial Ecology 45, 373–383.

Babel, W., Biermann, T., Coners, H., Falge, E., Seeber, E., Ingrisch, J., Schleuß, P.-M., Gerken, T., Leonbacher, J., Leipold, T., Willinghöfer, S., Schützenmeister, K., Shibistova, O., Becker, L., Hafner, S., Spielvogel, S., Li, X., Xu, X., Sun, Y., Zhang, L., Yang, Y., Ma, Y., Wesche, K., Graf, H.-F., Leuschner, C., Guggenberger, G., Kuzyakov, Y., Miehe, G., Foken, T., 2014. Pasture degradation modifies the water and carbon cycles of the Tibetan highlands. Biogeosciences 11, 6633–6656. https://doi.org/10.5194/bg-11-6633-2014

Bastida, F., Jehmlich, N., Lima, K., Morris, B.E.L., Richnow, H.H., Hernández, T., von Bergen, M., García, C., 2016. The ecological and physiological responses of the microbial community from a semiarid soil to hydrocarbon contamination and its bioremediation using compost amendment. Journal of Proteomics 135, 162–169. https://doi.org/10.1016/j.jprot.2015.07.023

Bastida, F., Jehmlich, N., Ondoño, S., von Bergen, M., García, C., Moreno, J.L., 2014. Characterization of the microbial community in biological soil crusts dominated by Fulgensia desertorum (Tomin) Poelt and Squamarina cartilaginea (With.) P. James and in the underlying soil. Soil Biology and Biochemistry 76, 70–79. https://doi.org/10.1016/j.soilbio.2014.05.004

Beulig, F., Urich, T., Nowak, M., Trumbore, S.E., Gleixner, G., Gilfillan, G.D., Fjelland, K.E., Küsel, K., 2016. Altered carbon turnover processes and microbiomes in soils under long-term extremely high CO2 exposure. Nat Microbiol 1, 15025. https://doi.org/10.1038/nmicrobiol.2015.25

Christensen, G.A., Gionfriddo, C.M., King, A.J., Moberly, J.G., Miller, C.L., Somenahally, A.C., Callister, S.J., Brewer, H., Podar, M., Brown, S.D., Palumbo, A.V., Brandt, C.C., Wymore, A.M., Brooks, S.C., Hwang, C., Fields, M.W., Wall, J.D., Gilmour, C.C., Elias, D.A., 2019. Determining the Reliability of Measuring Mercury Cycling Gene Abundance with Correlations with Mercury and Methylmercury Concentrations. Environmental Science and Technology 53. https://doi.org/10.1021/acs.est.8b06389

Christensen, G.A., Wymore, A.M., King, A.J., Podar, M., Hurt, R.A., Santillan, E.U., Soren, A., Brandt, C.C., Brown, S.D., Palumbo, A.V., Wall, J.D., Gilmour, C.C., Elias, D.A., 2016. Development and Validation of Broad-Range Qualitative and Clade-Specific Quantitative Molecular Probes for

Assessing Mercury Methylation in the Environment. Applied and Environmental Microbiology 82, 6068–6078. https://doi.org/10.1128/AEM.01271-16

Craine, J.M., Morrow, C., Fierer, N., 2007. MICROBIAL NITROGEN LIMITATION INCREASES DECOMPOSITION. Ecology 88, 2105–2113. https://doi.org/10.1890/06-1847.1

Dijkstra, P., Blankinship, J.C., Selmants, P.C., Hart, S.C., Koch, G.W., Schwartz, E., Hungate, B.A., 2011a. Probing carbon flux patterns through soil microbial metabolic networks using parallel position-specific tracer labeling. Soil Biology and Biochemistry 43, 126–132. https://doi.org/10.1016/j.soilbio.2010.09.022

Dijkstra, P., Dalder, J.J., Selmants, P.C., Hart, S.C., Koch, G.W., Schwartz, E., Hungate, B.A., 2011b. Modeling soil metabolic processes using isotopologue pairs of position-specific 13C-labeled glucose and pyruvate. Soil Biology and Biochemistry 43, 1848–1857. https://doi.org/10.1016/j.soilbio.2011.05.001

Dijkstra, P., Wu, W., Dippold, M., Schwartz, E., Hungate, B., Megonigal, P., Thomas, S., Seymour, C., Martinez, A., 2022. On Maintenance and Metabolisms in Soil Microbial Communities (preprint). In Review. https://doi.org/10.21203/rs.3.rs-1193625/v1

Evgrafova, A., de la Haye, T.R., Haase, I., Shibistova, O., Guggenberger, G., Tananaev, N., Sauheitl, L., Spielvogel, S., 2018. Small-scale spatial patterns of soil organic carbon and nitrogen stocks in permafrost-affected soils of northern Siberia. Geoderma 329, 91–107. https://doi.org/10.1016/j.geoderma.2018.05.014

Genxu, W., Ju, Q., Guodong, C., Yuanmin, L., 2002. Soil organic carbon pool of grassland soils on the Qinghai-Tibetan Plateau and its global implication. Science of The Total Environment 291, 207–217. https://doi.org/10.1016/S0048-9697(01)01100-7

Grün, A.Y., App, C.B., Breidenbach, A., Meier, J., Metreveli, G., Schaumann, G.E., Manz, W., 2018. Effects of low dose silver nanoparticle treatment on the structure and community composition of bacterial freshwater biofilms. PLoS ONE 13, e0199132. https://doi.org/10.1371/journal.pone.0199132

Gunina, A., Dippold, M.A., Glaser, B., Kuzyakov, Y., 2014. Fate of low molecular weight organic substances in an arable soil: From microbial uptake to utilisation and stabilisation. Soil Biology and Biochemistry 77, 304–313. https://doi.org/10.1016/j.soilbio.2014.06.029

Hafner, S., Unteregelsbacher, S., Seeber, E., Lena, B., Xu, X., Li, X., Guggenberger, G., Miehe, G., Kuzyakov, Y., 2012. Effect of grazing on carbon stocks and assimilate partitioning in a Tibetan montane pasture revealed by 13CO2 pulse labeling. Glob Change Biol 18, 528–538. https://doi.org/10.1111/j.1365-2486.2011.02557.x

Hagerty, S.B., van Groenigen, K.J., Allison, S.D., Hungate, B.A., Schwartz, E., Koch, G.W., Kolka, R.K., Dijkstra, P., 2014. Accelerated microbial turnover but constant growth efficiency with warming in soil. Nature Clim Change 4, 903–906. https://doi.org/10.1038/nclimate2361

Harwood, J.L., Russell, N.J., 1984. Lipids in Plants and Microbes. Springer Netherlands, Dordrecht. https://doi.org/10.1007/978-94-011-5989-0

He, M., Fang, K., Chen, L., Feng, X., Qin, S., Kou, D., He, H., Liang, C., Yang, Y., 2021. Depth-dependent drivers of soil microbial necromass carbon across Tibetan alpine grasslands. Glob Change Biol gcb.15969. https://doi.org/10.1111/gcb.15969

Heimann, M., Reichstein, M., 2008. Terrestrial ecosystem carbon dynamics and climate feedbacks. Nature 451, 289–292. https://doi.org/10.1038/nature06591

Herold, M., Martínez Arbas, S., Narayanasamy, S., Sheik, A.R., Kleine-Borgmann, L.A.K., Lebrun, L.A., Kunath, B.J., Roume, H., Bessarab, I., Williams, R.B.H., Gillece, J.D., Schupp, J.M., Keim, P.S., Jäger, C., Hoopmann, M.R., Moritz, R.L., Ye, Y., Li, S., Tang, H., Heintz-Buschart, A., May, P., Muller, E.E.L., Laczny, C.C., Wilmes, P., 2020. Integration of time-series meta-omics data reveals how microbial ecosystems respond to disturbance. Nat Commun 11, 5281. https://doi.org/10.1038/s41467-020-19006-2

Jurtshuk, P., 1996. Bacterial Metabolism, in: Baron, S. (Ed.), Medical Microbiology. University of Texas Medical Branch at Galveston, Galveston (TX).

Kalscheuer, R., Wältermann, M., Alvarez, H., Steinbüchel, A., 2001. Preparative isolation of lipid inclusions from Rhodococcus opacus and Rhodococcus ruber and identification of granule-associated proteins. Arch Microbiol 177, 20–28. https://doi.org/10.1007/s00203-001-0355-5

Kashi, H., Loeppmann, S., Herschbach, J., Schink, C., Imhof, W., Kouchaksaraee, R.M., Dippold, M.A., Spielvogel, S., 2022. Size matters: biochemical mineralization and microbial incorporation of dicarboxylic acids in soil. Biogeochemistry. https://doi.org/10.1007/s10533-022-00990-0

Kohlstedt, M., Becker, J., Wittmann, C., 2010. Metabolic fluxes and beyond—systems biology understanding and engineering of microbial metabolism. Appl Microbiol Biotechnol 88, 1065–1075. https://doi.org/10.1007/s00253-010-2854-2

Kourmentza, C., Plácido, J., Venetsaneas, N., Burniol-Figols, A., Varrone, C., Gavala, H.N., Reis, M.A.M., 2017. Recent Advances and Challenges towards Sustainable Polyhydroxyalkanoate (PHA) Production. Bioengineering 4, 55. https://doi.org/10.3390/bioengineering4020055

Kuzyakov, Y., Blagodatskaya, E., 2015. Microbial hotspots and hot moments in soil: Concept & review. Soil Biology and Biochemistry 83, 184–199. https://doi.org/10.1016/j.soilbio.2015.01.025

Laalami, S., Zig, L., Putzer, H., 2014. Initiation of mRNA decay in bacteria. Cell. Mol. Life Sci. 71, 1799–1828. https://doi.org/10.1007/s00018-013-1472-4

López, N.I., Pettinari, M.J., Nikel, P.I., Méndez, B.S., 2015. Polyhydroxyalkanoates, in: Advances in Applied Microbiology. Elsevier, pp. 73–106. https://doi.org/10.1016/bs.aambs.2015.06.001

Loreau, M., de Mazancourt, C., 2013. Biodiversity and ecosystem stability: a synthesis of underlying mechanisms. Ecology Letters 16, 106–115. https://doi.org/10.1111/ele.12073

Manzoni, S., Ding, Y., Warren, C., Banfield, C.C., Dippold, M.A., Mason-Jones, K., 2021. Intracellular Storage Reduces Stoichiometric Imbalances in Soil Microbial Biomass – A Theoretical Exploration. Front. Ecol. Evol. 9, 714134. https://doi.org/10.3389/fevo.2021.714134

Mason-Jones, K., Banfield, C.C., Dippold, M.A., 2019. Compound-specific ^{13}C stable isotope probing confirms synthesis of polyhydroxybutyrate by soil bacteria. Rapid Commun Mass Spectrom 33, 795–802. https://doi.org/10.1002/rcm.8407

Mason-Jones, K., Breidenbach, A., Dyckmans, J., Banfield, C.C., Dippold, M.A., 2023. Intracellular carbon storage by microorganisms is an overlooked pathway of biomass growth. Nature Communications 14, 2240. https://doi.org/10.1038/s41467-023-37713-4

Mason-Jones, K., Robinson, S.L., Veen, G.F., Manzoni, S., van der Putten, W.H., 2021. Microbial storage and its implications for soil ecology. ISME J. https://doi.org/10.1038/s41396-021-01110-w

Matin, A., Veldhuis, C., Stegeman, V., Veenhuis, M., 1979. Selective Advantage of a Spirillum sp. in a Carbon-limited Environment. Accumulation of Poly- -hydroxybutyric Acid and Its Role in Starvation. Journal of General Microbiology 112, 349–355. https://doi.org/10.1099/00221287-112-2-349

Mooshammer, M., Wanek, W., Zechmeister-Boltenstern, S., Richter, A., 2014. Stoichiometric imbalances between terrestrial decomposer communities and their resources: mechanisms and implications of microbial adaptations to their resources. Frontiers in Microbiology 5.

Nguyen, N.H., Song, Z., Bates, S.T., Branco, S., Tedersoo, L., Menke, J., Schilling, J.S., Kennedy, P.G., 2016. FUNGuild: An open annotation tool for parsing fungal community datasets by ecological guild. Fungal Ecology 20, 241–248. https://doi.org/10.1016/j.funeco.2015.06.006

Ottow, J.C.G., 2011. Mikrobiologie von Böden, Springer-Lehrbuch. Springer Berlin Heidelberg, Berlin, Heidelberg. https://doi.org/10.1007/978-3-642-00824-5

Qiu, J., 2016. Trouble in Tibet. Nature 529, 142–145. https://doi.org/10.1038/529142a

Rasse, D.P., Rumpel, C., Dignac, M.-F., 2005. Is soil carbon mostly root carbon? Mechanisms for a specific stabilisation. Plant Soil 269, 341–356. https://doi.org/10.1007/s11104-004-0907-y

Robinson, C.H., Ritson, J.P., Alderson, D.M., Malik, A.A., Griffiths, R.I., Heinemeyer, A., Gallego-Sala, A.V., Quillet, A., Robroek, B.J.M., Evans, C., Chandler, D.M., Elliott, D.R., Shutttleworth, E.L., Lilleskov, E.A., Kitson, E., Cox, F., Worrall, F., Clay, G.D., Crosher, I., Pratscher, J., Bird, J., Walker, J., Belyea, L.R., Dumont, M.G., Bell, N.G.A., Artz, R.R.E., Bardgett, R.D., Andersen, R., Hutchinson, S.M., Page, S.E., Thom, T.J., Burn, W., Evans, M.G., 2023. Aspects of microbial

communities in peatland carbon cycling under changing climate and land use pressures. Mires and Peat 29, 1–36. https://doi.org/10.19189/MaP.2022.OMB.StA.2404

Schimel, J., 2016. Microbial ecology: Linking omics to biogeochemistry. Nat Microbiol 1, 15028. https://doi.org/10.1038/nmicrobiol.2015.28

Schinner, F., Öhlinger, R., Kandeler, E., Margesin, R., 2012. Methods in Soil Biology. Springer Science & Business Media.

Schleuss, P.-M., Heitkamp, F., Sun, Y., Miehe, G., Xu, X., Kuzyakov, Y., 2015. Nitrogen Uptake in an Alpine Kobresia Pasture on the Tibetan Plateau: Localization by 15N Labeling and Implications for a Vulnerable Ecosystem. Ecosystems 18, 946–957. https://doi.org/10.1007/s10021-015-9874-9

Sekar, K., Linker, S.M., Nguyen, J., Grünhagen, A., Stocker, R., Sauer, U., 2020. Bacterial Glycogen Provides Short-Term Benefits in Changing Environments. Applied and Environmental Microbiology 86, e00049-20. https://doi.org/10.1128/AEM.00049-20

Song, Y., Song, C., Ren, J., Ma, X., Tan, W., Wang, X., Gao, J., Hou, A., 2019. Short-Term Response of the Soil Microbial Abundances and Enzyme Activities to Experimental Warming in a Boreal Peatland in Northeast China. Sustainability 11, 590. https://doi.org/10.3390/su11030590

Soong, J.L., Fuchslueger, L., Marañon-Jimenez, S., Torn, M.S., Janssens, I.A., Penuelas, J., Richter, A., 2020. Microbial carbon limitation: The need for integrating microorganisms into our understanding of ecosystem carbon cycling. Glob Change Biol 26, 1953–1961. https://doi.org/10.1111/gcb.14962

Spohn, M., Klaus, K., Wanek, W., Richter, A., 2016. Microbial carbon use efficiency and biomass turnover times depending on soil depth – Implications for carbon cycling. Soil Biology and Biochemistry 96, 74–81. https://doi.org/10.1016/j.soilbio.2016.01.016

Takahashi, H., Morioka, R., Ito, R., Oshima, T., Altaf-Ul-Amin, Md., Ogasawara, N., Kanaya, S., 2011. Dynamics of Time-Lagged Gene-to-Metabolite Networks of *Escherichia coli* Elucidated by Integrative Omics Approach. OMICS: A Journal of Integrative Biology 15, 15–23. https://doi.org/10.1089/omi.2010.0074

Voet, D., Voet, J.G., Pratt, C.W., 2008. Fundamentals of biochemistry: life at the molecular level, 3rd ed. ed. Wiley, Hoboken, NJ.

Wang, T., Yang, D., Yang, Y., Piao, S., Li, X., Cheng, G., Fu, B., 2020. Permafrost thawing puts the frozen carbon at risk over the Tibetan Plateau. Science Advances 6, eaaz3513. https://doi.org/10.1126/sciadv.aaz3513

Wieder, W.R., Hartman, M.D., Sulman, B.N., Wang, Y.-P., Koven, C.D., Bonan, G.B., 2018. Carbon cycle confidence and uncertainty: Exploring variation among soil biogeochemical models. Global Change Biology 24, 1563–1579. https://doi.org/10.1111/gcb.13979

Wu, W., Dijkstra, P., Dippold, M.A., 2020. 13C analysis of fatty acid fragments by gas chromatography mass spectrometry for metabolic flux analysis. Geochimica et Cosmochimica Acta 284, 92–106. https://doi.org/10.1016/j.gca.2020.05.032

Wu, W., Dijkstra, P., Hungate, B.A., Shi, L., Dippold, M.A., 2022. In situ diversity of metabolism and carbon use efficiency among soil bacteria. Science Advances 8, eabq3958. https://doi.org/10.1126/sciadv.abq3958

Wutzler, T., Zaehle, S., Schrumpf, M., Ahrens, B., Reichstein, M., 2017. Adaptation of microbial resource allocation affects modelled long term soil organic matter and nutrient cycling. Soil Biology and Biochemistry 115, 322–336. https://doi.org/10.1016/j.soilbio.2017.08.031

Yao, T., Thompson, L.G., Mosbrugger, V., Zhang, F., Ma, Y., Luo, T., Xu, B., Yang, X., Joswiak, D.R., Wang, W., Joswiak, M.E., Devkota, L.P., Tayal, S., Jilani, R., Fayziev, R., 2012. Third Pole Environment (TPE). Environmental Development 3, 52–64. https://doi.org/10.1016/j.envdev.2012.04.002

Zhang, L., Unteregelsbacher, S., Hafner, S., Xu, X., Schleuss, P., Miehe, G., Kuzyakov, Y., 2017. Fate of Organic and Inorganic Nitrogen in Crusted and Non-Crusted *Kobresia* Grasslands. Land Degrad. Develop. 28, 166–174. https://doi.org/10.1002/ldr.2582

2. Publications and Manuscripts

2.1.1. Study 1: Microbial functional changes mark irreversible course of Tibetan grassland degradation

Andreas Breidenbach[1,2,#], Per-Marten Schleuss[3,#], Shibin Liu[4], Dominik Schneider[5], Michaela A. Dippold[1,2], Tilman de la Haye[6], Georg Miehe[7], Felix Heitkamp[8], Elke Seeber[9], Kyle Mason-Jones[10], Xingliang Xu[11,12], Yang Huanming[13], Jianchu Xu[14], Tsechoe Dorji[12,15], Matthias Gube[16], Helge Norf[17], Jutta Meier[18], Georg Guggenberger[19], Yakov Kuzyakov[20] & Sandra Spielvogel[6]*

[1] Department for Crop Sciences, Biogeochemistry of Agroecosystems, University of Goettingen, Buesgenweg 2, 37077 Goettingen, Germany.

[2] Department of Geosciences, Geo-Biosphere Interactions, University of Tuebingen, Schnarrenbergstrasse 94-96, 72076 Tuebingen, Germany.

[3] Department of Soil Ecology, University of Bayreuth, Dr. Hans-Frisch Strasse 1-3, 95448 Bayreuth, Germany.

[4] Institute of Ecological Environment, Chengdu University of Technology, 610059 Chengdu, China.

[5] Institute of Microbiology and Genetics and Goettingen Genomics Laboratory, University of Goettingen, Grisebachstrasse. 8, 37077 Goettingen, Germany.

[6] Department of Soil Science, University of Kiel, Hermann-Rodewald-Strasse 2, 24118 Kiel, Germany.

[7] Faculty of Geography, University of Marburg, Deutschhausstrasse 10, 35032 Marburg, Germany.

[8] Environmental Control, Northwest German Forest Research Institute, Graetzelstrasse 2, 37079 Goettingen, Germany.

[9] Department of Botany, Senckenberg Museum of Natural History Goerlitz, 02806 Goerlitz, Germany.

[10] Netherlands Institute of Ecology, Department of Terrestrial Ecology, Postbus 50, 6700 AB Wageningen, the Netherlands.

[11] Key Laboratory Ecosystem Network Observation and Modeling, Institute of Geographic Science and Natural Resources Research, Chinese Academy of Science, 11A Datun Road, 100101 Beijing, China.

[12] CAS Center for Excellence in Tibetan Plateau Earth Sciences, Chinese Academy of Sciences (CAS), 100101 Beijing, China.

[13] Beijing Genomics Institute, BGI Park No. 21 Hongan 3rd Street, Yantian District, 518083 Shenzhen, China.

[14] Center for Mountain Futures, Kunming Institute of Botany, Chinese Academy of Sciences, 650201 Kunming, China.

[15] Institute of Tibetan Plateau Research, Chinese Academy of Sciences, No. 16 Lincui Road, Chaoyang District, 100101 Beijing, China.

[16] Soil Science of Temperate Ecosystems, University of Goettingen, Buesgenweg 2, 37077 Goettingen, Germany.

[17] Department of River Ecology, Department of Aquatic Ecosystems Analysis and Management, Helmholtz Centre for Environmental Research GmbH UFZ, Brueckstrasse 3a, 39114 Magdeburg, Germany.

[18] Institute for Integrated Natural Sciences, University of Koblenz-Landau, Universitätsstrasse. 1, 56070 Koblenz, Germany.

[19] Institute of Soil Science, Leibniz Universität Hannover, Herrenhäuser Strasse 2, 30419 Hannover, Germany.

[20] Agricultural Soil Science, University of Goettingen, Buesgenweg 2, 37077 Goettingen, Germany.

[#]These authors contributed equally: Andreas Breidenbach, Per-Marten Schleuss.

*Corresponding author E-mail address: s.spielvogel@soils.uni-kiel.de

2.1.2. Abstract

The Tibetan Plateau's *Kobresia* pastures store 2.5% of the world's soil organic carbon (SOC). Climate change and overgrazing render their topsoils vulnerable to degradation, with SOC stocks declining by 42% and nitrogen (N) by 33% at severely degraded sites. We resolved these losses into erosion accounting for two-thirds, and decreased carbon (C) input and increased SOC mineralization accounting for the other third and confirmed these results by comparison with a meta-analysis of 594 observations. The microbial community responded to the degradation through altered taxonomic composition and enzymatic activities. Hydrolytic enzyme activities were reduced, while degradation of the remaining recalcitrant soil organic matter by oxidative enzymes was accelerated, demonstrating a severe shift in microbial functioning. This may irreversibly alter the world's largest alpine pastoral ecosystem by diminishing its C sink function and nutrient cycling dynamics, negatively impacting local food security, regional water quality and climate.

2.1.3. Introduction

The Tibetan Plateau (TP) hosts the world's largest high-altitude grasslands, contributing 2.5% to global SOC stocks (Genxu et al., 2002) but covering only 0.3% of the Earth's total terrestrial area. It influences the Asian monsoon climate (Babel et al. 2014), is the water source for one-fifth of the global population (Qui, 2016) and provides grazing grounds for >8 million sheep, yaks, and goats (Zhou et al. 2005). Approximately one-fifth of the TP is covered by Kobresia grasslands (Babel et al., 2014). *Kobresia pygmaea* forms a 2–4 cm high grazing lawn with low shoot biomass but very compact root mats (root-to-shoot ratio >20) (Schleuss et al., 2015), induced by a long history of low-to-moderate grazing intensity, which increases belowground carbon allocation and root biomass (Ingrisch et al., 2015, Wang & Wesche 2016). *Kobresia pygmaea's* dense root network protects it from trampling-induced soil erosion and enables fast regrowth after defoliation (Miehe et al., 2019).

Pasture degradation has increased dramatically in recent decades (Babel et al. 2014, Qui 2016), and about 30% of the Tibetan grasslands are considered to be degraded (Harris, 2010). This has indisputably severe consequences for ecosystem functions, most importantly the major decline in SOC and N storage. Three mechanisms contribute to this—erosion, decreased C and N input, and increased soil organic matter (SOM) mineralization—but their relative importance remains unclear (Wang et al. 2009). We conducted a meta-analysis including 594 single observations from 49 literature studies published between 2002 and 2020 (Supplementary Table 1) to quantify the SOC and N losses for *Kobresia pygmaea's* core area. In a detailed field study, we determined the relative contributions of erosion and net mineralization to SOC losses and identified the underlying changes in microbial community structure and functioning. For this, we categorized six successive stages of degradation,

from intact Kobresia root mats (S0) to stages with increasing extents of surface cracks (S1–S4) to bare soil patches without root mats (S5) (Supplementary Fig. 1).

We hypothesize that substantial parts of the Kobresia pastures are close to a critical point of microbial functioning changes with substantial consequences for SOC and N storage. We further hypothesize that these abrupt shifts are characterized by changes in SOM quality and quantity that are coupled by feedback loops to microbial community structure and functions, which in turn control C and N mineralization.

2.1.4. Results

2.1.4.1. Root-mat cracking and soil erosion.

The formation of polygonal surface cracks is widespread between the Qilian Mountains and the Himalayas (Supplementary Fig. 1). These surface cracks represent the early stages of a degradation process that, in its final stage (S5), is associated with a loss of 42% of SOC compared to non-degraded pastures (Fig. 1A, B; Supplementary Fig. 2). Nitrogen losses were comparably high (33%; Fig. 1C, D; Supplementary Fig. 2). Soil erosion induced preferential loss of the easily erodible fine particles, resulting in a relative accumulation of coarser soil material from S0 to S5 (Fig. 1G, Supplementary Fig. 3), with soil clay content being 60% lower at the most degraded sites compared to intact pastures (Fig. 1G; Supplementary Fig. 3). At the most extreme degradation stage (S5) of our own study site, 81 kg m^{-2} of the most fertile SOC- and N-rich topsoil had been lost to erosion. This corresponds to 5 kg C m^{-2} or 45% of the total soil C stock (Fig. 1A), in agreement with the mean soil C loss found in the literature study (42%). Degradation of the Kobresia turf was furthermore associated with a large decrease in penetration resistance (Fig. 2A) and root density (Fig. 2B) from S1 to S5. Intensified degradation decreased vegetation cover, leaving the soil prone to erosion with extended size and depth of cracks (Supplementary Table 2).

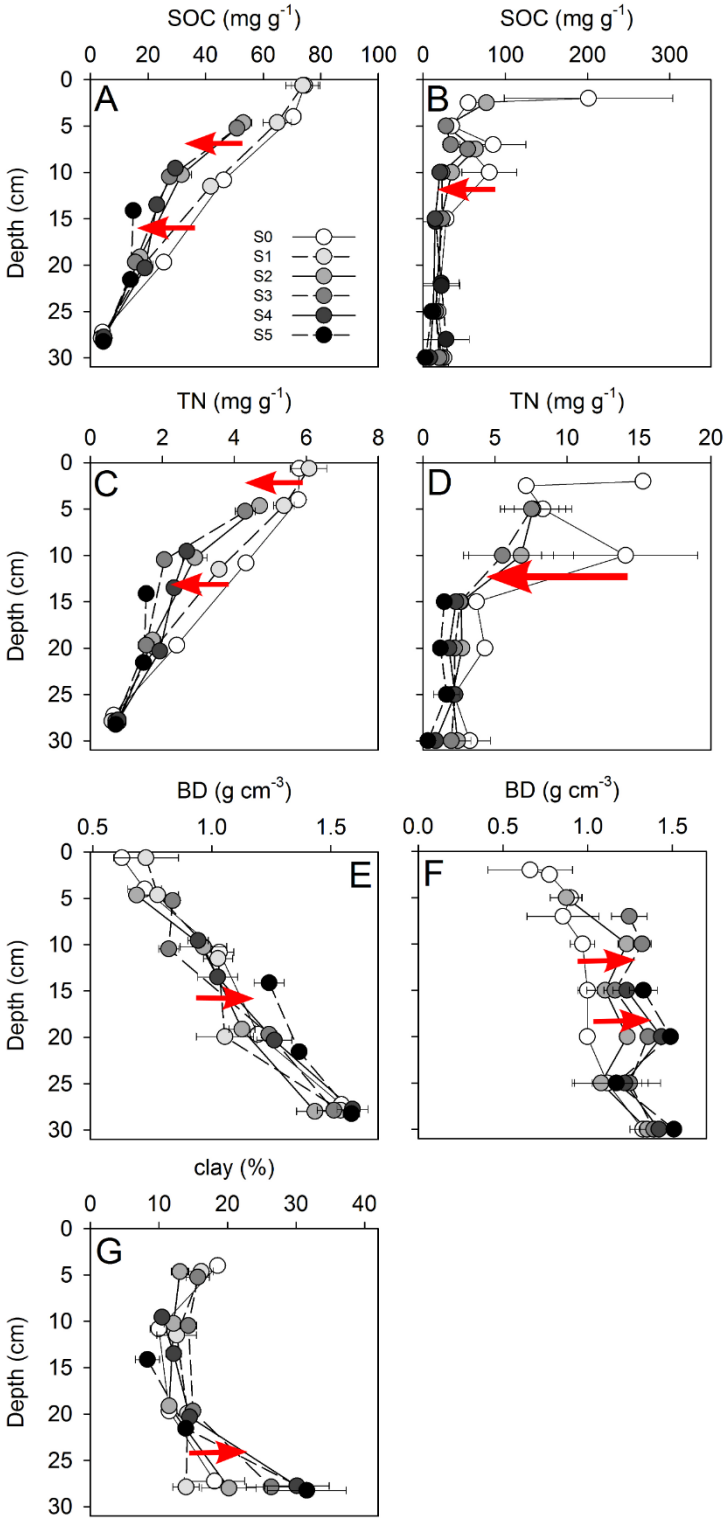

S1 Figure 1: **Changes in soil characteristics with depth according to degradation stage. A** soil organic carbon (SOC) core study site, **B** SOC literature study, **C** total nitrogen (N) core study site, **D** total N literature study, **E** bulk density (BD) core study site, F BD literature study, G clay content core study site. All parameters are presented for each soil horizon at the midpoint of the depth increment. Error bars display standard error. Exact data are provided in Supplementary Table 2.

2.1.4.2. SOC losses through mineralisation and decreased root carbon input.

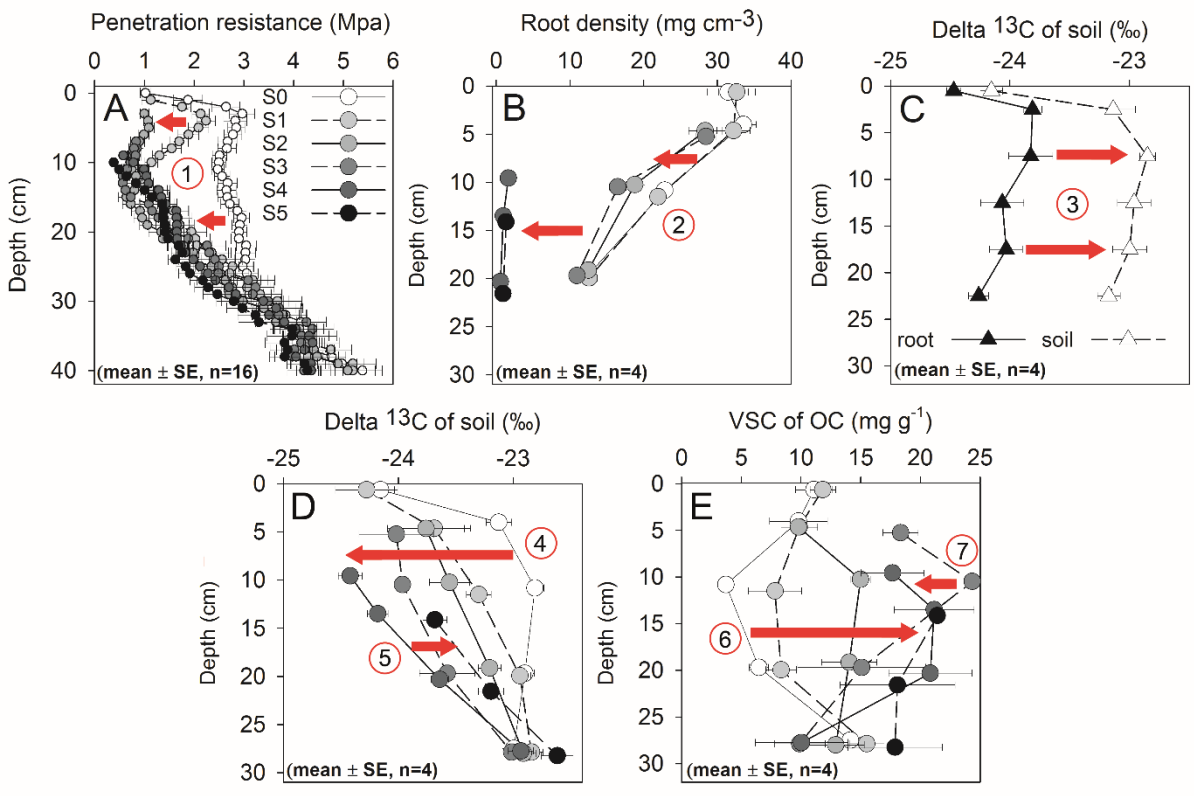

S1 Figure 2: **Changes in soil characteristics with depth according to degradation stage. A** Penetration resistance, **B** root density, **C** $\delta^{13}C$ of soil and roots, **D** $\delta^{13}C$ of soil organic carbon (SOC), **E** content of lignin monomers vanillyl, syringyl, and cinnamyl (VSC). All parameters (means ± SE, n = 4) are presented for each soil horizon at depth midpoint, except for penetration resistance (**A**) and $\delta^{13}C$ values of soil and roots (**C**), which are shown in 1 and 5 cm increments, respectively. Exact data are given in Supplementary Table 2. Progressive changes along the degradation sequence can be explained by the following processes: (a) root-mat cracking by desiccation and frost, (b) root death and decomposition, (c) kinetic ^{13}C fractionation during root decomposition, (d) SOC loss due to reduced root carbon (**C**) input and greater SOC mineralization, (e) relative lignin accumulation and $^{13}C_{SOC}$ depletion (S0–S3), (f) relative lignin accumulation during stages S0–S3, (g) lignin degradation and $^{13}C_{SOC}$ enrichment (S4, S5).

The SOC and N contents were closely positively correlated with root density (Supplementary Fig. 4) and showed a consistent relationship in isotopic composition ($\delta^{13}C$) with the associated roots at each depth (Fig. 2C). This demonstrates the importance of roots as the dominant SOC source for intact Kobresia pastures. An association of increasing $\delta^{13}C$ values with declining SOC content (Fig. 2D) due to kinetic isotope fractionation during decomposition was observed only at the final degradation stage. With degradation from S1 to S4, the SOC content in the upper 20 cm decreased (Fig. 1A, B), while $\delta^{13}C$ values already decreased from S0 to S1 (Fig. 2D). We quantified the sum of lignin monomers vanillyl, syringyl, and cinnamyl as an indicator of complex organic compounds (Kögel-Knabner, 2002)[11]. Vanillyl,

syringyl, and cinnamyl contents increased from S0 to S4 (Fig. 2E), indicating selective lignin preservation during early degradation stages. The close negative correlation between $\delta^{13}C$ and vanillyl, syringyl, and cinnamyl contents in the mineral horizon indicates the selective enrichment of the isotopically light lignin (Supplementary Fig. 5A). However, the decrease of vanillyl, syringyl, and cinnamyl contents from S4 to S5 in the mineral soil (Fig. 2E), accompanied by ^{13}C enrichment (Fig. 2D) and a decrease in SOC content (Supplementary Fig. 5B), indicates a pronounced lignin decomposition at the final degradation stage (S5).

2.1.4.3. Soil microbial community structure and functions

The bacterial (Supplementary Figs. 6A, and 9) and fungal (Supplementary Figs. 6B, and 10) community composition changed significantly ($p < 0.05$, MANOVA) along the degradation sequence. Bacterial groups (Supplementary Table 3) associated with decomposition of low-molecular-weight organic compounds, e.g., Actinobacteria (Supplementary Figs. 7A, and 9), declined with pasture degradation, whereas lignin-degrading groups such as *Rhizobiales* increased (Supplementary Fig. 7D). Nitrifying (*Nitrospirales* and *Nitrosomonadaceae*; Supplementary Fig. 7B, C) and denitrifying (*Pseudomonadales*; Supplementary Fig. 7E) bacteria increased from S0 to S3 and then declined towards S5. These shifts indicate severe changes in N-cycling towards the accelerated microbial transformation of organic N to mineral N in the early stages of degradation. Similarly, fungal groups specialized in efficient lignin degradation increased in relative abundance at later degradation stages, as evidenced by *Agaricomycetes* (Cragg et al., 2015, Andlar et al., 2018) (Supplementary Fig. 7F), which include the brown-rot and white-rot fungi. Correspondingly, groups generally incapable of efficient lignin degradation (Cragg et al., 2015), such as *Ascomycota* (Supplementary Fig. 7G), decreased along the degradation sequence (Supplementary Fig. 10a, b). After a peak at degradation stage S2, *Kobresia pygmaea* successively lost its arbuscular mycorrhizal fungal partners (*Glomeromycota*, Supplementary Fig. 7H), which were replaced by ectomycorrhizal ones (*Thelephoraceae* and *Inocybaceae*, Supplementary Fig. 7I). When *Kobresia pygmaea* largely disappeared (S5), the abundance of its ectomycorrhizal partners also declined and the first arbuscular mycorrhizal partners of the newly establishing pioneer plants appeared (Supplementary Fig. 7H).

Non-metric multidimensional scaling (NMDS), including C/N, $\delta^{13}C$, total N, $\delta^{15}N$, total phosphorus (P), pH, cation exchange capacity, calcium, potassium, iron and aluminum content, clay content and vanillyl, syringyl, and cinnamyl content as explanatory factors revealed a strong correlation between microbial community structure and SOC quality (C/N, $\delta^{13}C$, N, P and vanillyl, syringyl, and cinnamyl) during early degradation stages (Fig. 3). However, changes in microbial community structure during later degradation stages (from S3 to S5) were mainly driven by abiotic soil properties such as increasing pH and decreasing clay content, which had a stronger effect on fungi than on bacterial communities.

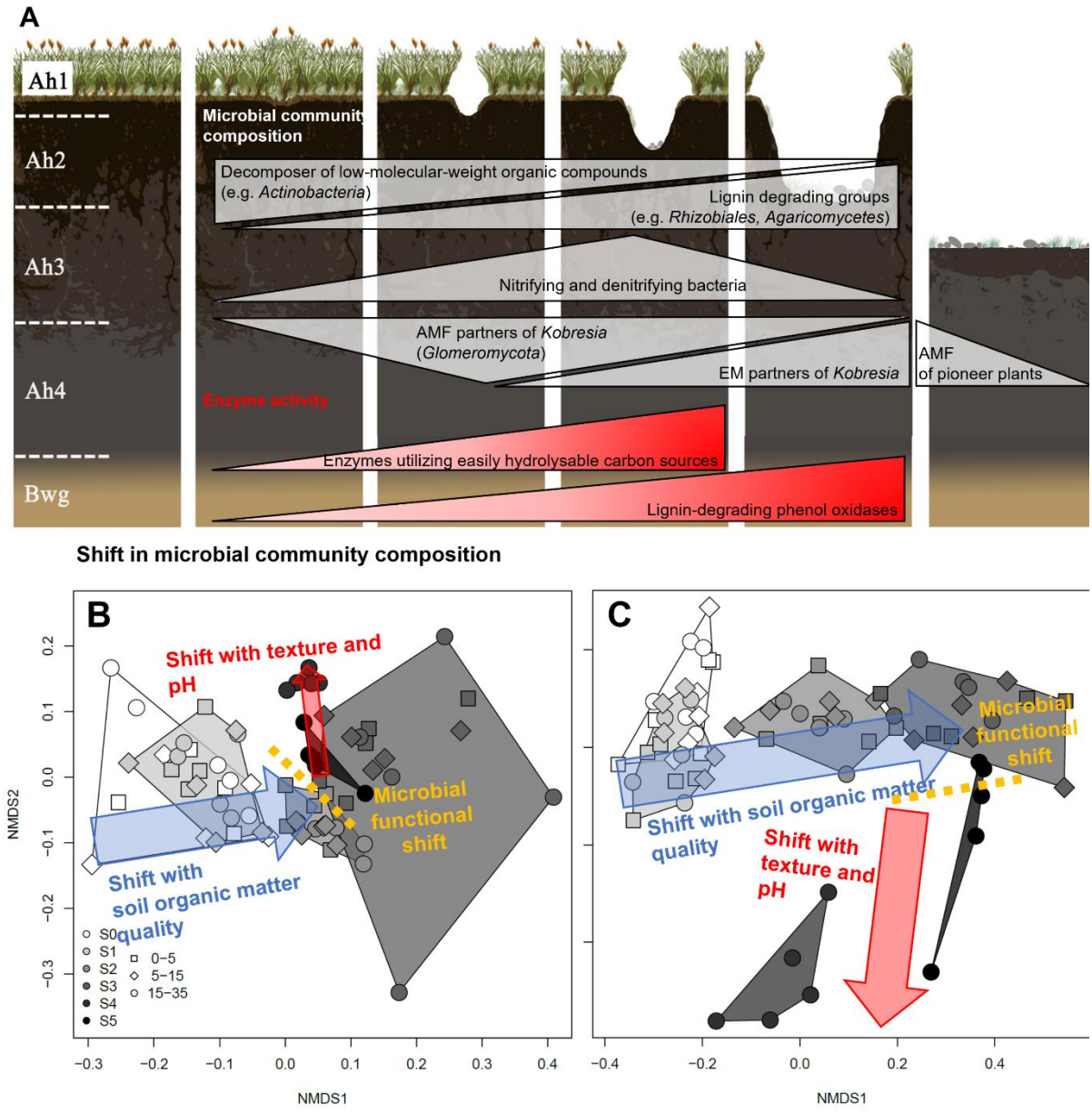

S1 Figure 3: **Overview of generalized changes in microbial community composition and functioning along the degradation sequence from intact (S0) to severely degraded (S5) stage.** Generalized changes in microbial community composition and enzyme activities (**A**). Simplified non-metric multidimensional scaling (NMDS) plots derived from terminal restriction fragment length polymorphism (t-RFLP) data for the bacterial (**B**) and fungal (**C**) communities. Shaded areas mark each degradation stage, symbols indicate soil depth, and arrows show most important driving factors (canonical correspondence analysis, $p < 0.05$). Individual variables underlying the processes described by the blue and red arrows are shown in Supplementary Fig. 6.

Maximal activities of enzymes for utilizing easily hydrolyzable C sources (β-glucosidase and xylanase) significantly increased from S0 to S3 and declined when pasture degradation reached stage S4 (Supplementary Figs. 7J, and 12). Likewise, the activity of N- and P-mobilizing enzymes (urease and alkaline phosphatase) declined from S3 to S4 (Supplementary Figs. 7J, and 12). In contrast, the activity of lignin-degrading phenol oxidases increased steadily with the degradation from S2 to S4 along with the relative increase in vanillyl, syringyl, and cinnamyl monomers (Supplementary Figs. 7J, and 12).

2.1.4.4. Disentangling processes contributing to SOC losses

In the study area, SOC stocks at 0–30 cm depth declined strongly by 7.5 kg C m^{-2} from the stage of intact Kobresia root mats (S0) to that of bare soil patches (S5). This corresponds to a 45% reduction (Fig. 4) and matches well with the mean SOC loss observed for degraded areas across the whole TP (42%). SOC losses were attributed to topsoil erosion, which accounted for two-thirds of the decline (for S5: 5.0 kg C m^{-2}, Fig. 4B), with the combined effects of decreasing root carbon input and accelerated mineralization of root litter and SOC accounting for the remaining one third of the decline (2.5 kg C m^{-2}; Fig. 4B).

2.1.5. Discussion

Above- and belowground linkages of organic matter and energy flux play a central role in the responses of the TP *Kobresia* ecosystem to anthropogenic forcing and climate warming, as reported for mountain ecosystems worldwide (Hagedorn et al., 2019). Severe soil degradation of the Kobresia ecosystem results from complex reinforcing interactions of biotic and abiotic processes, as well as anthropogenic pressure (Fig. 5). Frost events at the beginning of the cold season, when the soil is moist, cause the

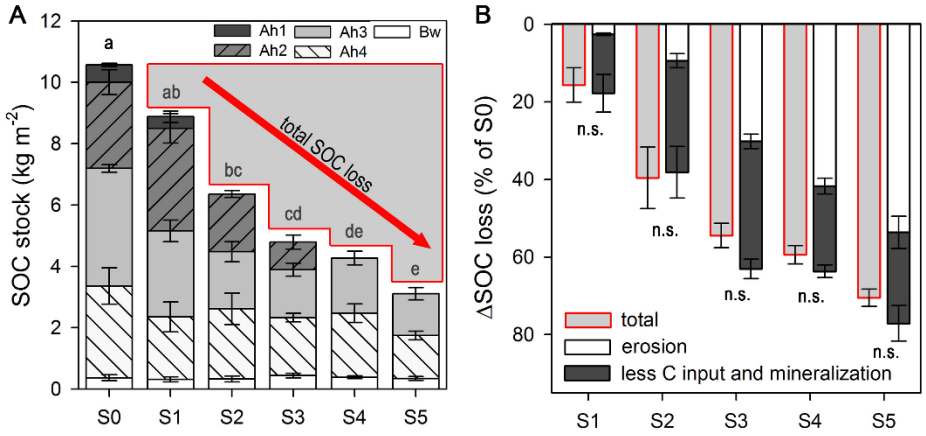

S1 Figure 4: **Soil organic carbon (SOC) stocks and losses with increasing degradation.** Total SOC stocks along the degradation sequence (S0–S5) down to 30 cm for each horizon (**A**). SOC losses by erosion and by reduced C input and increased SOC mineralization (**B**) during degradation (S1–S5). Lowercase letters indicate significant differences in SOC stocks between degradation stages. The absence of significant differences (n.s.) between quantified total SOC losses (red outline) and the calculated sum of erosion- and mineralization-induced SOC losses confirms the validity of the estimations. Error bars display standard error.

formation of polygonal surface cracks, a process severely enhanced by permafrost thaw (Wang et al., 2020). Overgrazing induced trampling, followed by root death and decomposition, expand these surface cracks (S1, S2). Exacerbated polygonal cracking then promotes soil erosion with preferential loss of fine-textured material, containing SOC and nutrients (S3–S4). This implies, among others, a strong reduction in the water holding capacity with as yet unforeseeable consequences for the water supply and quality of one-fifth of the world's population. Moreover, erosion of soil material and the associated loss of SOC carry severe consequences for ecosystem energy, water, and C fluxes, e.g., regionally earlier initiation of convection and cloud generation, affecting the strength and variability of the TP summer monsoon (Babel et al, 2014).

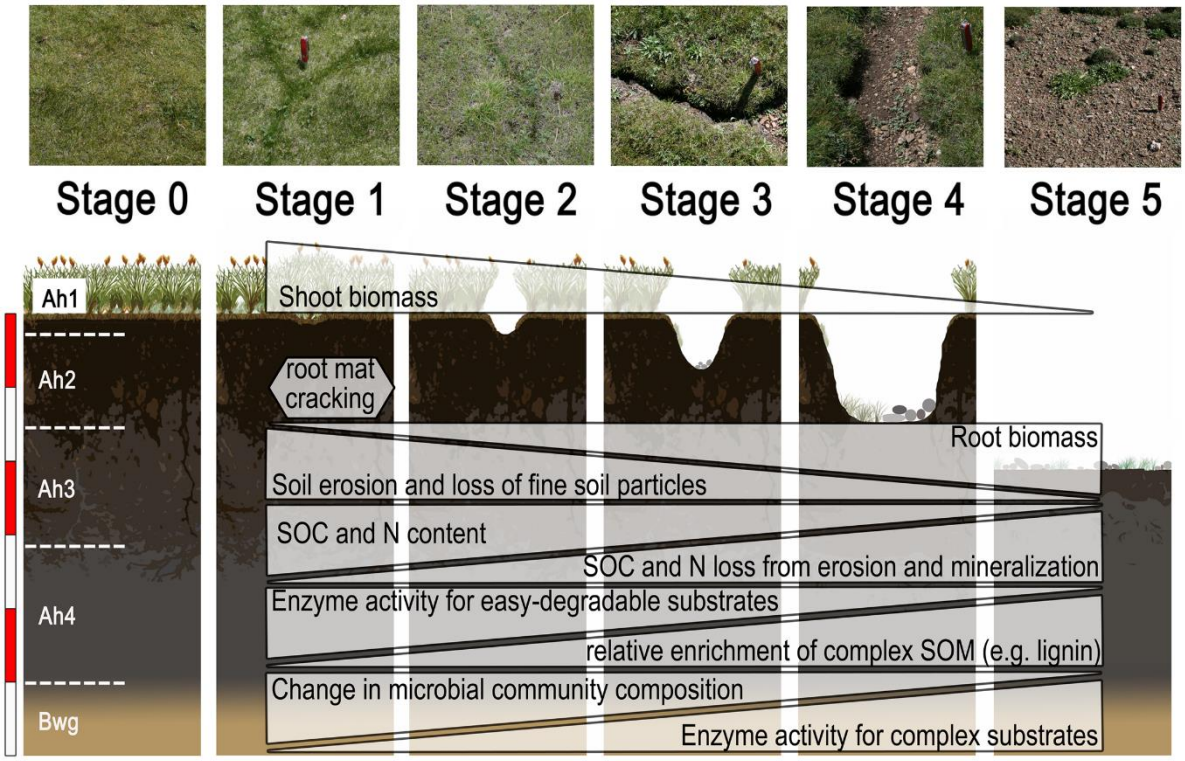

S1 Figure 5: **Overview of the degradation sequence from the intact (S0) to severely degraded (S5) stage, showing the driving forces of degradation.** Polygons describe main biotic and abiotic degradation mechanisms with a focus on soil organic carbon (SOC) pools, in accordance with the hypotheses. The white/red scale on the left shows a soil depth of 30 cm in 5 cm increments.

$\delta^{13}C$ patterns in roots and SOC in undegraded pastures demonstrate that SOC accumulation depends heavily on root biomass input and rhizodeposition. A close correlation between SOC stocks and root density across all degradation stages demonstrates that decreasing C input with degradation is a major driver of decreasing SOC content. Decreasing SOC content along the degradation gradient indicates that root necromass was not stabilized in degraded soils, and consequently labile constituents of root necromass were rapidly mineralized. The large root litter input from dying *Kobresia* stimulated

microorganisms to decompose the old SOC pool (root litter priming). This was confirmed by the increased activity of hydrolyzing enzymes during the early degradation stages. Such priming effects were triggered by the three to four times higher C/N ratio in roots compared to soil, driving microbes in this N-limited ecosystem[5] to decompose SOM to obtain N (N mining) (Craine et al, 2007). Similar effects of N limitation were observed along a thawing permafrost chronosequence in grassland soils of the TP, where N limitation in the late stages of permafrost collapse induced SOC decomposition through priming effects (Chen et al., 2018). In the case of permafrost thawing, a decrease in metabolic efficiency was the major mechanism underlying priming, without a response in hydrolytic enzyme activity. The root litter decomposition observed along our degradation sequence was, however, clearly related to an increase in hydrolytic enzyme activity from S0 to S3. Thus, the successive degradation and subsequent mineralization of the organic N stocks increased the abundance of nitrifying and denitrifying bacteria during the early degradation stages (S0–S3). Using N-cycling gene abundances (*amoA*), Che et al. (2017) identified an up to five-fold increase in nitrifiers associated with a major shift in the N cycle during the degradation of Tibetan pasture meadows. Nitrification produces easily leachable nitrate, a limiting substrate for denitrification in alpine meadows (Xie et al., 2014), which consequently increases in periods of high soil moisture or in moist soil microhabitats. We observed an increase in N-hydrolyzing enzymes, an increase in plant litter decomposers, and an increasing abundance of nitrifier- and denitrifier-hosting bacterial orders and families (*Nitrospirales* and *Nitrosomonadaceae* (Supplementary Fig. 7B, C) and *Pseudomonadales* (Supplementary Fig. 7E), respectively) from degradation state S0–S3. This suggests that all three processes - N mineralization, nitrification, and denitrification—increase along the degradation gradient, which leads to severe nitrogen losses from this ecosystem via leaching, emissions of nitrous oxide and nitrogen gas, and NH_3 volatilization (Liu et al., 2017). Quantification of the net and gross rates of these processes (Gao et al., 2008) as well as corresponding gene abundances (Dong et al., 2020) confirmed that these three key steps of the N cycle accelerate with increased grazing intensity in Tibetan meadows. Concomitant increases in mineral N availability (Gao et al., 2008) induced a change in the mycorrhizal partners of *Kobresia pygmaea*. Arbuscular mycorrhizal fungi, capable of capturing nutrients released by other microorganisms' hydrolytic enzymes, increased along the sequence of increasing hydrolytic organic matter decomposition (S0–S2) and optimized the access to otherwise rapidly leached or consumed ammonia and nitrate. However, toward stage S4, there was a shift in favor of ectomycorrhizal partners of *Kobresia pygmaea*, being specialized for the active mobilization of organic matter-bound nutrients using their own oxidative enzymes. The concurrent decrease in urease activity from S3 to S4, reflecting successive depletion of the easily accessible N in the soil, is evidence of a shift in ecosystem nutrition strategy: mineral nutrient release through AMF-mediated and prokaryote-driven hydrolysis was replaced by fungi-based nutrient scavenging for nutritional elements "locked up" in complex structural

root-mat tissues using oxidative enzymes. Such fundamental shifts in nutritional strategies and biogeochemical cycles suggest that degradation will have large-scale feedback on multiple environmental processes.

As a result of organic matter decomposition, we expected kinetic isotope fractionation to induce a continuous $\delta^{13}C$ increase along the degradation gradient (Schweizer & Cadisch, 1999). However, the opposite was found for early degradation stages. $\delta^{13}C$ values decreased from S0 to S4 within the upper 20 cm, while $\delta^{13}C$ values increased from S4 to S5. We attribute the $\delta^{13}C$ decrease (S0–S4) to a relative accumulation of more complex, ^{13}C-depleted organic compounds such as lignin (Hobbie & Werner, 2004). Assuming a 4.3‰ depletion in lignin $\delta^{13}C$ compared to bulk plant material (Hobbie & Werner, 2004) and a recovery of 38% of the lignin C by the vanillyl, syringyl, cinnamyl method (Pepper et al., 1967), the relative increase of lignin from 0.9 to 4.7% of SOC accounts for nearly 23% of the observed $\delta^{13}C$ shift across the degradation sequence. However, lignin is only one compound class among others (cutins, suberins, etc.) with complex structures and depleted $\delta^{13}C$ values. Lipids have even more depleted $\delta^{13}C$ values than lignin (Hobbie & Werner, 2004). The negative $\delta^{13}C$ shifts observed with soil degradation from S0 to S4 likely reflect the relative accumulation of these rather persistent compounds in addition to lignin. The intact Kobresia root mats at the research site consist of about 6 kg root dry matter m^{-2} (Schleuss et al., 2015), including many woody roots that contain large amounts of lignin and suberin. Root dieback during soil degradation, therefore, provides a substantial source of complex, ^{13}C-depleted compounds. Relative lignin enrichment of the SOC pool was evident not only in the $\delta^{13}C$ decrease but also in the increased abundance of fungal and bacterial specialists decomposing complex SOM (e.g., *Rhizobiales* and *Agaricomycetes*). The elevated abundance of these groups was accompanied by increased phenoloxidase activity, which catalyzes the nonspecific oxidation of complex organic substances, especially lignin. Consequently, after easily available C pools are depleted (S3), complex organic compounds are successively degraded as microbial communities adapt to these distinct carbon sources. While microbial communities changed gradually from S0 to S3, a profound shift in community structure and functions occurred from S3 to S4 (evidenced by a vertical shift in direction in the NMDS plots; Supplementary Figs. 6 and 8). This transition coincided with (a) the exhaustion of easily accessible, hydrolyzable N sources, (b) the complete loss of the topsoil through mineralization and erosion, and (c) the first establishment of pioneer plants on the bare subsoil between Kobresia root-mat remnants. The new fungal symbionts of these pioneer plants explain the particularly pronounced shift in the fungal community from S3 to S4, representing this new ecosystem state. Degradation exceeding S4, therefore, constitutes a severe alteration of microbial community composition and functioning, beyond which biotic and abiotic ecosystem properties have changed so severely that ecosystem recovery is unlikely.

Taken together, overgrazing of *Kobresia* pastures on the TP induces a highly interrelated sequence of abiotic and biotic degradation processes. Polygonal crack extension and root-mat dieback as a result of freeze-thaw cycles and overgrazing induce topsoil erosion and progressive SOC decomposition and N loss. This is accompanied by a shift in microbial community structure and functions to adapt to the altered availability of SOC and N. Studies of the past decade predict an intensification of the degradation of this pastoral ecosystem because of the large population that is dependent on livestock products (Qui, 2016), increasing stocking rates close to settlements (Zhou et al., 2005) and diminishing availability of high-quality grazing grounds following degradation (Harris, 2010). Once the critical point between S3 and S4 has been passed, conventional strategies for mitigating degradation are unlikely to prevent complete loss of the entire C-rich topsoil, with cascading effects on microbial functioning and the related ecosystem services.

The challenges brought about by TP degradation can only be addressed through lowering livestock densities, and perhaps more importantly increasing livestock mobility to maintain important functions of the vulnerable *Kobresia* ecosystem. In 2011, China proposed the Ecological Conservation Redline strategy that protects ecologically fragile zones like the TP (Gao et al., 2020) by prioritizing and prohibiting rangeland degradation. Tibetan pastoralists increasingly manage their rangelands through contracting, assessing limits to livestock holdings based on land availability (Yeh et al.,2017), e.g., by “multi-household management pattern”. This practice has been shown to reduce SOC losses considerably (Cao et al. 2017), more closely resembling pre-settlement grassland management. Further, the reintroduction of seasonal livestock grazing in the framework of community-based villages can protect or even restore vegetation and soil (Zhuang et al., 2019), provided that a certain degradation stage has not been surpassed. Once this critical point is crossed, reseeding has been proposed as a restoration strategy (Liu et al., 2018). However, reseeding of heavily degraded areas generally requires N and P fertilization (Liu et al., 2018), which carries the risk of nutrient leaching and headwater pollution and is nevertheless often unsuccessful (Dong et al., 2012). Dong et al. (2012) studied the restoration potential of TP grasslands and their soil chemical and physical properties in three depth increments (0–4, 4–10, and 10–20 cm). The results show that neither the decreased water holding capacity, nor the SOC and N content could be restored in the reestablished artificial grasslands this was attributed to the loss of the topsoil, changed soil texture, and changes in vegetation composition. This demonstrates the threshold behavior of TP’s pastures, where a complete recovery from highly degraded stages is unlikely, due to slow pedogenic processes and vegetation restoration, as well as continuously increasing global warming.

2.1.6. Methods

2.1.6.1. Literature study

Literature considering the effect of pasture degradation on SOC, N, and clay content, as well as bulk density (BD), was assembled by searching (i) Web of Science V.5.22.1, (ii) ScienceDirect (Elsevier B.V.) (iii) Google Scholar, and (iv) the China Knowledge Resource Integrated Database (CNKI). Search terms were "degradation gradient", "degradation stages", "alpine meadow", "Tibetan Plateau", "soil", "soil organic carbon", and "soil organic matter" in different combinations. The criteria for including a study in the analysis were: (i) a clear and comprehensible classification of degradation stages was presented, (ii) data on SOC, N, and/or BD were reported, (iii) a non-degraded pasture site was included as a reference to enable an effect size analysis and the calculation of SOC and N losses, (iv) sampling depths and study location were clearly presented. (v) Studies were only considered that took samples in 10 cm depth intervals, to maintain comparability to the analyses from our own study site. The degradation stages in the literature studies were regrouped into the six successive stages (S0–S5) according to the respective degradation descriptions. In total, we compiled the results of 49 publications published between 2002 and 2020.

When SOM content was presented, this was converted to SOC content using a conversion factor of 2.0 (Pribyl, 2010). SOC and N stocks were calculated using the following equation:

$$(1)\ Elemental\ stock = 100 * content * BD * depth$$

where elemental stock is SOC or N stock [kg ha^{-1}]; content is SOC or N content [g kg^{-1}]; BD is soil bulk density [g cm^{-3}] and depth is the soil sampling depth [cm].

The effect sizes of individual variables (i.e., SOC and N stocks as well as BD) were quantified as follows:

$$(2)\ ES = \frac{(D-R)}{R*100\%}$$

where ES is the effect size in %, D is the value of the corresponding variable in the relevant degradation stage and R is the value of each variable in the non-degraded stage (reference site). When ES is positive, zero, or negative, this indicates an increase, no change, or decrease, respectively, of the parameter compared to the non-degraded stage.

2.1.6.2. Experimental design of the field study

Large areas in the study region are impacted by grassland degradation. In total, 45% of the surface area of the *Kobresia* pasture ecosystem on the TP is already degraded (Babel et al., 2014). The experiment was designed to differentiate and quantify SOC losses by erosion vs. net decomposition and identify underlying shifts in microbial community composition and link these to changes in key

microbial functions in the soil C cycle. We categorized the range of Kobresia root-mat degradation from non-degraded to bare soils into six successive degradation stages (S0–S5). Stage S0 represented non-degraded root mats, while stages S1–S4 represented increasing degrees of surface cracks, and bare soil patches without root mats defined stage S5 (Supplementary Fig. 1). All six degradation stages were selected within an area of about 4 ha to ensure equal environmental conditions and each stage was sampled in four field replicates. However, the studied degradation patterns are common for the entire *Kobresia* ecosystem (Supplementary Fig. 1).

2.1.6.3. Site description

The field study was conducted near Nagqu (Tibet, China) in the late summer 2013 and 2015. The study site of about 4 ha (NW: 31.274748°N, 92.108963°E; NE: 31.274995°N, 92.111482°E; SW: 31.273488°N, 92.108906°E; SE: 31.273421°N, 92.112025°E) was located on gentle slopes (2–5%) at 4,484 m a.s.l. in the core area of the Kobresia pygmaea ecosystem according to Miehe et al. (2019).The vegetation consists mainly of *K. pygmaea*, which covers up to 61% of the surface. Other grasses, sedges, or dwarf rosette plants (*Carex ivanoviae, Carex spp., Festuca spp., Kobresia pusilla, Poa spp., Stipa purpurea, Trisetum spp.*) rarely cover more than 40%. The growing season is strongly restricted by temperature and water availability. At most, it lasts from mid-May to mid-September, but varies strongly depending on the onset and duration of the summer monsoon. Mean annual precipitation is 431 mm, with roughly 80% falling as summer rains. The mean annual temperature is −1.2 °C, while the mean maximum temperature of the warmest month (July) is +9.0 °C (Babel et al., 2014). A characteristic feature of *Kobresia* pastures is their very compact root mats, with an average thickness of 15 cm at the study site. These consist mainly of living and dead *K. pygmaea* roots and rhizomes, leaf bases, large amounts of plant residue, and mineral particles. Intact soil is a Stagnic Eutric Cambisol (Humic), developed on a loess layer overlying glacial sediments and containing 50% sand, 33% silt, and 17% clay in the topsoil (0–25 cm). The topsoil is free of carbonates and is of neutral pH (pH in H2O: 6.8) (Schleuss et al., 2015). Total soil depth was on average 35 cm. The site is used as a winter pasture for yaks, sheep, and goats from January to April. Besides livestock, large numbers of plateau pikas (*Ochotona*) are found on the sites. These animals have a considerable impact on the plant cover through their burrowing activity, in particular the soil thrown out of their burrows, which can cover and destroy the *Kobresia* turf.

2.1.6.4. Sampling design

The vertical and horizontal extent of the surface cracks was measured for each plot (Supplementary Table 2). Vegetation cover was measured, and the aboveground biomass was collected in the cracks (Supplementary Table 2). In general, intact Kobresia turf (S0) provided high resistance to penetration as measured by a penetrologger (Eijkelkamp Soil and Water, Giesbeek, NL) in 1 cm increments and

four replicates per plot. Soil sampling was conducted using soil pits (30 cm length × 30 cm width × 40 cm depth). Horizons were classified and then soil, and roots were sampled for each horizon directly below the cracks. Bulk density and root biomass were determined in undisturbed soil samples, using soil cores (10 cm height and 10 cm diameter). Living roots were separated from dead roots and root debris by their bright color and soft texture using tweezers under magnification, and the roots were subsequently washed with distilled water to remove the remaining soil. Because over 95% of the roots occurred in the upper 25 cm (Schleuss et al., 2015), we did not sample for root biomass below this depth. Additional soil samples were taken from each horizon for further analysis. Microbial community and functional characterization were performed on samples from the same pits but with a fixed depth classification (0–5cm, 5–15 cm, 15–35 cm) to reduce the number of samples.

2.1.6.5. Plant and soil analyses

Soil and roots were separated by sieving (2 mm) and the roots subsequently washed with distilled water. Bulk density and root density were determined by dividing the dry soil mass (dried at 105 °C for 24 h) and the dry root biomass (60 °C) by the volume of the sampling core. To reflect the root biomass, root density was expressed per soil volume (mg cm^{-3}). Soil and root samples were milled for subsequent analysis.

2.1.6.6. Elemental concentrations and SOC characteristics

Total SOC and total N contents and stable isotope signatures ($\delta^{13}C$ and $\delta^{15}N$) were analyzed using an isotope ratio mass spectrometer (Delta plus, Conflo III, Thermo Electron Cooperation, Bremen, Germany) coupled to an elemental analyzer (NA 1500, Fisons Instruments, Milano, Italy). Measurements were conducted at the Centre for Stable Isotope Research and Analysis (KOSI) of the University of Göttingen. The $\delta^{13}C$ and $\delta^{15}N$ values were calculated by relating the isotope ratio of each sample (Rsample = $^{13}C/^{12}C$ or $^{15}N/^{14}N$) to the international standards (Pee Dee Belemnite $^{13}C/^{12}C$ ratio for $\delta^{13}C$; the atmospheric $^{15}N/^{14}N$ composition for $\delta^{15}N$). Soil pH of air-dried soil was measured potentiometrically at a ratio (v/v) of 1.0:2.5 in distilled water. Lignin phenols were depolymerized using the CuO oxidation method (Pepper et al., 1967) and analyzed with a gas chromatography-mass spectrometry (GC–MS) system (GC 7820 A, MS 5977B, Agilent Technologies, Waldbronn, Germany). Vanillyl and syringyl units were calculated from the corresponding aldehydes, ketones, and carboxylic acids. Cinnamyl units were derived from the sum of p-coumaric acid and ferulic acid. The sum of the three structural units (VSC = V + S + C) was considered to reflect the lignin phenol content in a sample.

2.1.6.7. DNA extraction and PCR

Samples were directly frozen on site at −20 °C and transported to Germany for analysis of microbial community structure. Total DNA was extracted from the soil samples with the PowerSoil DNA isolation kit (MoBio Laboratories Inc., Carlsbad, CA, USA) according to the manufacturer's instructions, and DNA

concentration was determined using a NanoDrop 1000 spectrophotometer (Thermo Fisher Scientific, Wilmington, DE, USA). The extracted DNA was amplified with forward and reverse primer sets suitable for either t-RFLP (fluorescence marked, FAM) or Illumina MiSeq sequencing (Illumina Inc., San Diego, USA): V3 (5'-CCT ACG GGN GGC WGC AG-3') and V4 (5'-GAC TAC HVG GGT ATC TAA TCC-3') primers were used for bacterial 16 S rRNA genes whereas ITS1 (5'-CTT GGT CAT TTA GAG GAA GTA A-3'), ITS1-F_KYO1 (5'CTH GGT CAT TTA GAG GAA STA A-3'), ITS2 (5'-GCT GCG TTC TTC ATC GAT GC-3') and ITS4 (5'-TCC TCC GCT TAT TGA TAT GC-3') were used for fungi (Klindworth et al., 2013, Toju et al., 2012). Primers for Illumina MiSeq sequencing included adaptor sequences (forward: 5'-TCG TCG GCA GCG TCA GAT GTG TAT AAG AGA CAG-3'; reverse: 5'-GTC TCG TGG GCT CGG AGA TGT GTA TAA GAG ACA G-3') (Klindworth et al., 2013). PCR was performed with the Phusion High-Fidelity PCR kit (New England Biolabs Inc., Ipswich, MA, USA) creating a 50 µl master mix with 28.8 µl H_2O_{molec}, 2.5 µl DMSO, 10 µl Phusion GC buffer, 1 µl of forward and reverse primer, 0.2 µl $MgCl_2$, 1 µl dNTPs, 0.5 µl Phusion HF DNA Polymerase, and 5 µl template DNA. PCR temperatures started with initial denaturation at 98 °C for 1 min, followed by denaturation (98 °C, 45 s), annealing (48/60 °C, 45 s), and extension (72 °C, 30 s). These steps were repeated 25 times, finalized again with a final extension (72 °C, 5 min), and cooling to 10 °C. Agarose gel electrophoresis was used to assess the success of the PCR and the amount of amplified DNA (0.8% gel:1.0 g Rotigarose, 5 µl Roti-Safe Gelstain, Carl Roth GmbH & Co. KG, Karlsruhe, Germany; and 100 ml 1× TAE-buffer). PCR product was purified after initial PCR and restriction digestion (t-RFLP) with either NucleoMag 96 PCR (16 S rRNA gene amplicons, Macherey-Nagel GmbH & Co. KG, Düren, Germany) or a modified clean-up protocol after Moreau (2014) (t-RFLP): 3× the volume of the reaction solution as 100% ethanol and ¼x vol. 125 mM EDTA was added and mixed by inversion or vortex. After incubation at room temperature for 15 min, the product was centrifuged at 25,000 × g for 30 min at 4 °C. Afterwards the supernatant was removed, and the inverted 96-well plate was centrifuged shortly for 2 min. Seventy microliters ethanol (70%) were added and centrifuged at 25,000 × g for 30 min at 4 °C. Again, the supernatant was removed, and the pallet was dried at room temperature for 30 min. Finally, the ethanol-free pallet was resuspended in H_2O_{molec}.

2.1.6.8. T-RFLP fingerprinting

The purified fluorescence-labeled PCR products were digested with three different restriction enzymes (*MspI and BstUI, HaeIII*) according to the manufacturer's guidelines (New England Biolabs Inc., Ipswich, MA, USA) with a 20 µl master mix: 16.75 µl H_2O_{molec}, 2 µl CutSmart buffer, 0.25 or 0.5 µl restriction enzyme, and 1 µl PCR product for 15 min at 37 °C (*MspI*) and 60 °C (*BstUI, HaeIII*), respectively. The digested PCR product was purified a second time (Moreau, 2014), dissolved in Super-DI Formamide (MCLAB, San Francisco, CA, USA) and, along with Red DNA size standard (MCLAB, San Francisco, USA), analyzed in an ABI Prism 3130 Genetic Analyzer (Applied Biosystems, Carlsbad, CA, USA). Terminal

restriction fragments shorter than 50 bp and longer than 800 bp were removed from the t-RFLP fingerprints.

2.1.6.9. 16S rRNA gene and internal transcribed spacer (ITS) sequencing and sequence processing

The 16 S rRNA gene and ITS paired-end raw reads for the bacterial and fungal community analyses were deposited in the National Center for Biotechnology Information (NCBI) Sequence Read Archive (SRA) and can be found under the BioProject accession number PRJNA626504. This BioProject contains 70 samples and 139 SRA experiments (SRR11570615–SRR11570753) which were processed using CASAVA software (Illumina, San Diego, CA, USA) for demultiplexing of MiSeq raw sequences (2 × 300 bp, MiSeq Reagent Kit v3). Paired-end sequences were quality-filtered with fastp (version 0.19.4) (Chen et al., 2018) using default settings with the addition of an increased per base phred score of 20, basepair corrections by overlap (-c), as well as 5'- and 3'-end read trimming with a sliding window of 4, a mean quality of 20 and minimum sequence size of 50 bp. Paired-end sequences were merged using PEAR v0.9.11 (Zhang et al., 2014) with default parameters. Subsequently, unclipped reverse and forward primer sequences were removed with cutadapt v1.18 (Martin, 2011) with default settings. Sequences were then processed using VSEARCH (v2.9.1) (Rognes et al., 2016). This included sorting and size-filtering (—sortbylength, minseqlength) of the paired reads to ≥300 bp for bacteria and ≥140 bp for ITS1, dereplication (—derep_fulllength). Dereplicated sequences were denoised with UNOISE3 (Edgar, 2016) using default settings (—cluster_unoise—minsize 8) and chimeras were removed (—uchime3_denovo). An additional reference-based chimera removal was performed (—uchime_ref) against the SILVA (Quast et al., 2013) SSU NR database (v132) and UNITE (Abarenkov et al., 2010) database (v7.2) resulting in the final set of amplicon sequence variants (ASVs) (Callahan et al., 2017). Quality-filtered and merged reads were mapped to ASVs (usearch_global–id 0.97). Classification of ASVs was performed with BLAST 2.7.1+ against the SILVA SSU NR (v132) and UNITE (v7.2) database with an identity of at least 90%. The ITS sequences contained unidentified fungal ASVs after UNITE classification, these sequences were checked (blastn) (Altschult et al.,1990) against the "nt" database (Nov 2018) to remove non-fungal ASVs and only as fungi classified reads were kept. Sample comparisons were performed at the same surveying effort, utilizing the lowest number of sequences by random selection (total 15,800 bacteria, 20,500 fungi). Species richness, alpha and beta diversity estimates, and rarefaction curves were determined using the QIIME 1.9.1 (Caporaso et al., 2010) script alpha_rarefaction.py. The final ASV tables were used to compute heatmaps showing the effect of degradation on the community using R (Version 3.6.1, R Foundation for Statistical Computing, Vienna, Austria) and R packages "gplots", "vegan", "permute" and "RColorBrewer". Fungal community functions were obtained from the FunGuild database (Nguyen et al., 2016). Plant mycorrhizal

association types were compiled from the literature (Gai et al., 2006, Shi et al., 2006, Tian et al.,2009, Wang & Qiu, 2006). If no direct species match was available, the mycorrhizal association was assumed to remain constant within the same genus.

2.1.6.10. Enzyme activity

Enzyme activity was measured to characterize the functional activity of the soil microorganisms. The following extracellular enzymes, involved in C, N, and P transformations, were considered: two hydrolases (β-glucosidase and xylanase), phenoloxidase, urease, and alkaline phosphatase. Enzyme activities were measured directly at the sampling site according to protocols after Schinner et al. (1996). Beta-glucosidase was incubated with saligenin for 3 h at 37 °C, xylanase with glucose for 24 h at 50 °C, phenoloxidase with L-3,4-dihydroxy phenylalanine (DOPA) for 1 h at 25 °C, urease with urea for 2 h at 37 °C and alkaline phosphatase on P-nitrophenyl phosphate for 1 h at 37 °C. Reaction products were measured photometrically at recommended wavelengths (578, 690, 475, 660, and 400 nm, respectively).

2.1.6.11. SOC stocks and SOC loss

The SOC stocks (in kg C m^{-2}) for the upper 30 cm were determined by multiplying the SOC content (g C kg^{-1}) by the BD (g cm^{-3}) and the thickness of the soil horizons (m). SOC losses (%) were calculated for each degradation stage and horizon and were related to the mean C stock of the reference stage (S0). The erosion-induced SOC loss of the upper horizon was estimated by considering the topsoil removal (extent of vertical soil cracks) of all degraded soil profiles (S1–S5) and the SOC content and BD of the reference (S0). To calculate the mineralization-derived SOC loss, we accounted for the effects of SOC and root mineralization on both SOC content and BD. Thus, we used the SOC content and BD from each degradation stage (S1–S5) and multiplied it by the mean thickness of each horizon (down to 30 cm) from the reference site (S0). The disentanglement of erosion-derived SOC loss from mineralization-derived SOC loss was based on explicit assumptions that (i) erosion-derived SOC losses are mainly associated with losses from the topsoil, and (ii) the decreasing SOC contents in the erosion-unaffected horizons were mainly driven by mineralization and decreasing root C input.

2.1.6.12. Statistical analysis

Statistical analyses were performed using PASW Statistics (IBM SPSS Statistics) and R software (Version 3.6.1). Soil and plant characteristics are presented as means and standard errors (means ± SE). The significance of treatment effects (S0–S5) and depth was tested by one-way ANOVA at $p < 0.05$. Prior to this, we checked for normality and homogeneity of variance using the Shapiro–Wilk test and Levene's test, respectively. Post-hoc multiple comparisons were carried out using the LSD or Tukey HSD ANOVA, if normality was indicated. In cases of non-normal distribution, the nonparametric Kruskal–Wallis test was implemented coupled with a Bonferroni correction. To detect relationships

between various plant and soil characteristics, we used linear and nonlinear regressions. Correlations were deemed significant for single regressions at $p < 0.05$. Before testing for significant differences, three outliers were detected by Grubbs outlier test ($p < 0.05$) in the bacterial t-RFLP and MiSeq datasets: MspI: S0_B_0-5, S1_E_0-5; BstuI: S5_A_15-35; MiSeq: S3_E_5-15 and were excluded from the analysis. T-RFLP and MiSeq data of all degradation stages were compared for significant differences with MANOVA, based on the Bray–Curtis index for dissimilarity. For pairwise multilevel comparisons, "pairwiseAdonis" was used (Martinez, 2020). Differences in microbial community data from t-RFLP and MiSeq were displayed in non-metric multidimensional scaling (NMDS) plots and environmental factors were correlated by canonical correspondence analysis (CCA). Statistics on community data were carried out with R statistical software (Version 3.6.1).

2.1.6.13. Reporting summary

Further information on research design is available in the Nature Research Reporting Summary linked to this article.

2.1.7. Data availability

The data generated in this study have been deposited in the PANGAEA Open Access library under accession code https://doi.org/10.1594/PANGAEA.918249. The 16 S rRNA and ITS gene paired-end raw reads for the bacterial and fungal community analyses have been deposited in the National Center for Biotechnology In-formation (NCBI) Sequence Read Archive (SRA) under the accession code PRJNA626504; BioProject: Tibetan plateau microbiome.

2.1.8. Acknowledgements

We thank our colleagues T. Biermann, W. Babel, U. Bange, L. Becker, C. Blaser, H. Coners, I. Hoeft, P. Jannack, K. Krüger, K. Schützenmeister, L. Steingräber, Y. Sun, and S. Willinghöfer for helping in the field and the laboratory. The German Research Council (Priority Program 1372) and the Centre for Stable Isotope Research and Analysis (KOSI) of Göttingen supported this project. This research was funded by the German Research Foundation (DFG) in the frame of the Priority Program SPP 1372 "Tibetan Plateau: Formation—Climate—Ecosystems",DFG.2009–2015; KU 1184/14-2, GU 406/22-2. We acknowledge financial support by DFG within the funding programme Open Access-Publikationskosten.

2.1.9. Author contributions

P.-M.S., G.G., Y.K., and S.S. designed the study. P.-M.S. and X.X. performed SOC, N, P CEC, and stable isotope signature ($\delta^{13}C$ and $\delta^{15}N$) measurements. S.S. performed measurements of enzyme activity and lignin phenol content. S.L. conducted the literature study and meta-analysis. J.X., D.S., A.B., C.B.,

M.G., H.N., Y.H., and J.M. contributed to molecular biological analyses and biostatistics. P.-M.S., G.M., E.S., X.X., and S.S. performed soil and vegetation sampling, field measurements, and vegetation description. P.M.S., F.H., A.B., T.d.l.H., S.L., T.D., and K.M.-J. performed statistical data analyses and interpretation. G.G., Y.K., M.A.D., and S.S. conceptualized and supervised the research. All authors were involved in the data interpretation, writing, and editing of the manuscript.

2.1.10. Funding

Open Access funding enabled and organized by Projekt DEAL.

2.1.11. Competing interests

The authors declare no competing interests.

2.1.12. References

Abarenkov, K., Nilsson, R.H., Larsson, K.-H., Alexander, I.J., Eberhardt, U., Erland, S., Høiland, K., Kjøller, R., Larsson, E., Pennanen, T., Sen, R., Taylor, A.F.S., Tedersoo, L., Ursing, B.M., Vrålstad, T., Liimatainen, K., Peintner, U., Kõljalg, U., 2010. The UNITE database for molecular identification of fungi – recent updates and future perspectives. The New Phytologist 186, 281–285.

Altschul, S.F., Gish, W., Miller, W., Myers, E.W., Lipman, D.J., 1990. Basic local alignment search tool. Journal of Molecular Biology 215, 403–410. https://doi.org/10.1016/S0022-2836(05)80360-2

Andlar, M., Rezić, T., Marđetko, N., Kracher, D., Ludwig, R., Šantek, B., 2018. Lignocellulose degradation: An overview of fungi and fungal enzymes involved in lignocellulose degradation. Engineering in Life Sciences 18, 768–778. https://doi.org/10.1002/elsc.201800039

Babel, W., Biermann, T., Coners, H., Falge, E., Seeber, E., Ingrisch, J., Schleuß, P.-M., Gerken, T., Leonbacher, J., Leipold, T., Willinghöfer, S., Schützenmeister, K., Shibistova, O., Becker, L., Hafner, S., Spielvogel, S., Li, X., Xu, X., Sun, Y., Zhang, L., Yang, Y., Ma, Y., Wesche, K., Graf, H.-F., Leuschner, C., Guggenberger, G., Kuzyakov, Y., Miehe, G., Foken, T., 2014. Pasture degradation modifies the water and carbon cycles of the Tibetan highlands. Biogeosciences 11, 6633–6656. https://doi.org/10.5194/bg-11-6633-2014

Callahan, B.J., McMurdie, P.J., Holmes, S.P., 2017. Exact sequence variants should replace operational taxonomic units in marker-gene data analysis. ISME J 11, 2639–2643. https://doi.org/10.1038/ismej.2017.119

Cao, J., Gong, Y., Yeh, E.T., Holden, N.M., Adamowski, J.F., Deo, R.C., Liu, M., Zhou, J., Zhang, J., Zhang, W., Zhang, S., Sheng, D., Yang, S., Xu, X., Li, M., Feng, Q., 2017. Impact of grassland contract policy on soil organic carbon losses from alpine grassland on the Qinghai–Tibetan Plateau. Soil Use and Management 33, 663–671. https://doi.org/10.1111/sum.12387

Caporaso, J.G., Kuczynski, J., Stombaugh, J., Bittinger, K., Bushman, F.D., Costello, E.K., Fierer, N., Peña, A.G., Goodrich, J.K., Gordon, J.I., Huttley, G.A., Kelley, S.T., Knights, D., Koenig, J.E., Ley, R.E., Lozupone, C.A., McDonald, D., Muegge, B.D., Pirrung, M., Reeder, J., Sevinsky, J.R., Turnbaugh, P.J., Walters, W.A., Widmann, J., Yatsunenko, T., Zaneveld, J., Knight, R., 2010. QIIME allows analysis of high-throughput community sequencing data. Nat Methods 7, 335–336. https://doi.org/10.1038/nmeth.f.303

Che, R., Wang, F., Wang, W., Zhang, J., Zhao, X., Rui, Y., Xu, Z., Wang, Y., Hao, Y., Cui, X., 2017. Increase in ammonia-oxidizing microbe abundance during degradation of alpine meadows may lead to greater soil nitrogen loss. Biogeochemistry 136, 341–352. https://doi.org/10.1007/s10533-017-0399-5

Chen, L., Liu, L., Mao, C., Qin, S., Wang, J., Liu, F., Blagodatsky, S., Yang, G., Zhang, Q., Zhang, D., Yu, J., Yang, Y., 2018. Nitrogen availability regulates topsoil carbon dynamics after permafrost thaw by altering microbial metabolic efficiency. Nat Commun 9, 3951. https://doi.org/10.1038/s41467-018-06232-y

Chen, S., Zhou, Y., Chen, Y., Gu, J., 2018. fastp: an ultra-fast all-in-one FASTQ preprocessor. Bioinformatics 34, i884–i890. https://doi.org/10.1093/bioinformatics/bty560

Cragg, S.M., Beckham, G.T., Bruce, N.C., Bugg, T.D., Distel, D.L., Dupree, P., Etxabe, A.G., Goodell, B.S., Jellison, J., McGeehan, J.E., McQueen-Mason, S.J., Schnorr, K., Walton, P.H., Watts, J.E., Zimmer, M., 2015. Lignocellulose degradation mechanisms across the Tree of Life. Current Opinion in Chemical Biology, Energy • Mechanistic biology 29, 108–119. https://doi.org/10.1016/j.cbpa.2015.10.018

Craine, J.M., Morrow, C., Fierer, N., 2007. MICROBIAL NITROGEN LIMITATION INCREASES DECOMPOSITION. Ecology 88, 2105–2113. https://doi.org/10.1890/06-1847.1

Dong, S., Li, Y., Ganjurjav, H., Gao, Q., Gao, X., Zhang, J., Yan, Y., Zhang, Y., Liu, S., Hu, G., Wang, X., Wu, H., Li, S., 2020. Grazing promoted soil microbial functional genes for regulating C and N cycling in alpine meadow of the Qinghai-Tibetan Plateau. Agriculture, Ecosystems & Environment 303, 107111. https://doi.org/10.1016/j.agee.2020.107111

Dong, S.K., Wen, L., Li, Y.Y., Wang, X.X., Zhu, L., Li, X.Y., 2012. Soil-Quality Effects of Grassland Degradation and Restoration on the Qinghai-Tibetan Plateau. Soil Science Society of America Journal 76, 2256–2264. https://doi.org/10.2136/sssaj2012.0092

Edgar, R.C., 2016. UNOISE2: improved error-correction for Illumina 16S and ITS amplicon sequencing. https://doi.org/10.1101/081257

Gai, J.P., Feng, G., Cai, X.B., Christie, P., Li, X.L., 2006. A preliminary survey of the arbuscular mycorrhizal status of grassland plants in southern Tibet. Mycorrhiza 16, 191–196. https://doi.org/10.1007/s00572-005-0032-7

Gao, J., Zou, C., Zhang, K., Xu, M., Wang, Y., 2020. The establishment of Chinese ecological conservation redline and insights into improving international protected areas. Journal of Environmental Management 264, 110505. https://doi.org/10.1016/j.jenvman.2020.110505

Gao, Y.H., Luo, P., Wu, N., Chen, H., Wang, G.X., 2008. Impacts of grazing intensity on nitrogen pools and nitrogen cycle in an alpine meadow on the eastern Tibetan Plateau. Applied Ecology and Environmental Research 6, 69–79.

Genxu, W., Ju, Q., Guodong, C., Yuanmin, L., 2002. Soil organic carbon pool of grassland soils on the Qinghai-Tibetan Plateau and its global implication. Science of The Total Environment 291, 207–217. https://doi.org/10.1016/S0048-9697(01)01100-7

Hagedorn, F., Gavazov, K., Alexander, J.M., 2019. Above- and belowground linkages shape responses of mountain vegetation to climate change. Science 365, 1119–1123. https://doi.org/10.1126/science.aax4737

Harris, R.B., 2010. Rangeland degradation on the Qinghai-Tibetan plateau: A review of the evidence of its magnitude and causes. Journal of Arid Environments 74, 1–12. https://doi.org/10.1016/j.jaridenv.2009.06.014

Hobbie, E.A., Werner, R.A., 2004. Intramolecular, compound-specific, and bulk carbon isotope patterns in C3 and C4 plants: a review and synthesis. New Phytologist 161, 371–385. https://doi.org/10.1111/j.1469-8137.2004.00970.x

Ingrisch, J., Biermann, T., Seeber, E., Leipold, T., Li, M., Ma, Y., Xu, X., Miehe, G., Guggenberger, G., Foken, T., Kuzyakov, Y., 2015. Carbon pools and fluxes in a Tibetan alpine Kobresia pygmaea pasture partitioned by coupled eddy-covariance measurements and 13CO2 pulse labeling. Science of The Total Environment 505, 1213–1224. https://doi.org/10.1016/j.scitotenv.2014.10.082

Klindworth, A., Pruesse, E., Schweer, T., Peplies, J., Quast, C., Horn, M., Glöckner, F.O., 2013. Evaluation of general 16S ribosomal RNA gene PCR primers for classical and next-generation sequencing-based diversity studies. Nucleic Acids Research 41, e1–e1. https://doi.org/10.1093/nar/gks808

Kögel-Knabner, I., 2002. The macromolecular organic composition of plant and microbial residues as inputs to soil organic matter. Soil Biology and Biochemistry 34, 139–162. https://doi.org/10.1016/S0038-0717(01)00158-4

Liu, S., Schleuss, P., Kuzyakov, Y., 2017. Carbon and Nitrogen Losses from Soil Depend on Degradation of Tibetan *Kobresia* Pastures. Land Degrad. Develop. 28, 1253–1262. https://doi.org/10.1002/ldr.2522

Liu, S., Zamanian, K., Schleuss, P.-M., Zarebanadkouki, M., Kuzyakov, Y., 2018. Degradation of Tibetan grasslands: Consequences for carbon and nutrient cycles. Agriculture, Ecosystems & Environment 252, 93–104. https://doi.org/10.1016/j.agee.2017.10.011

Martin, M., 2011. Cutadapt removes adapter sequences from high-throughput sequencing reads. EMBnet.journal 17, 10–12. https://doi.org/10.14806/ej.17.1.200

Martinez Arbizu, P., 2020. pairwiseAdonis: Pairwise multilevel comparison using adonis. R package version 0.4 1.

Miehe, G., Schleuss, P.-M., Seeber, E., Babel, W., Biermann, T., Braendle, M., Chen, F., Coners, H., Foken, T., Gerken, T., Graf, H.-F., Guggenberger, G., Hafner, S., Holzapfel, M., Ingrisch, J., Kuzyakov, Y., Lai, Z., Lehnert, L., Leuschner, C., Li, X., Liu, J., Liu, S., Ma, Y., Miehe, S., Mosbrugger, V., Noltie, H.J., Schmidt, J., Spielvogel, S., Unteregelsbacher, S., Wang, Y., Willinghöfer, S., Xu, X., Yang, Y., Zhang, S., Opgenoorth, L., Wesche, K., 2019. The Kobresia

pygmaea ecosystem of the Tibetan highlands – Origin, functioning and degradation of the world's largest pastoral alpine ecosystem: Kobresia pastures of Tibet. Science of The Total Environment 648, 754–771. https://doi.org/10.1016/j.scitotenv.2018.08.164

Moreau, C.S., 2014. A practical guide to DNA extraction, PCR, and gene-based DNA sequencing in insects. Halteres 5, 32–42.

Nguyen, N.H., Song, Z., Bates, S.T., Branco, S., Tedersoo, L., Menke, J., Schilling, J.S., Kennedy, P.G., 2016. FUNGuild: An open annotation tool for parsing fungal community datasets by ecological guild. Fungal Ecology 20, 241–248. https://doi.org/10.1016/j.funeco.2015.06.006

Pepper, J.M., Casselman, B.W., Karapally, J.C., 1967. Lignin oxidation. Preferential use of cupric oxide. Canadian Journal of Chemistry 45, 3009–3012.

Pribyl, D.W., 2010. A critical review of the conventional SOC to SOM conversion factor. Geoderma 156, 75–83. https://doi.org/10.1016/j.geoderma.2010.02.003

Qiu, J., 2016. Trouble in Tibet. Nature 529, 142–145. https://doi.org/10.1038/529142a

Quast, C., Pruesse, E., Yilmaz, P., Gerken, J., Schweer, T., Yarza, P., Peplies, J., Glöckner, F.O., 2013. The SILVA ribosomal RNA gene database project: improved data processing and web-based tools. Nucleic Acids Research 41, D590–D596. https://doi.org/10.1093/nar/gks1219

Rognes, T., Flouri, T., Nichols, B., Quince, C., Mahé, F., 2016. VSEARCH: a versatile open source tool for metagenomics. PeerJ 4, e2584. https://doi.org/10.7717/peerj.2584

Schinner, F., Öhlinger, R., Kandeler, E., Margesin, R., 2012. Methods in Soil Biology. Springer Science & Business Media.

Schleuss, P.-M., Heitkamp, F., Sun, Y., Miehe, G., Xu, X., Kuzyakov, Y., 2015. Nitrogen Uptake in an Alpine Kobresia Pasture on the Tibetan Plateau: Localization by 15N Labeling and Implications for a Vulnerable Ecosystem. Ecosystems 18, 946–957. https://doi.org/10.1007/s10021-015-9874-9

Schweizer, M., Fear, J., Cadisch, G., 1999. Isotopic (13C) fractionation during plant residue decomposition and its implications for soil organic matter studies. Rapid Communications in Mass Spectrometry 13, 1284–1290. https://doi.org/10.1002/(SICI)1097-0231(19990715)13:13<1284::AID-RCM578>3.0.CO;2-0

Shi, Z.Y., Feng, G., Christie, P., Li, X.L., 2006. Arbuscular mycorrhizal status of spring ephemerals in the desert ecosystem of Junggar Basin, China. Mycorrhiza 16, 269–275. https://doi.org/10.1007/s00572-006-0041-1

Tian, H., Gai, J.P., Zhang, J.L., Christie, P., Li, X.L., 2009. Arbuscular mycorrhizal fungi associated with wild forage plants in typical steppe of eastern Inner Mongolia. European Journal of Soil Biology 45, 321–327. https://doi.org/10.1016/j.ejsobi.2009.05.003

Toju, H., Tanabe, A.S., Yamamoto, S., Sato, H., 2012. High-Coverage ITS Primers for the DNA-Based Identification of Ascomycetes and Basidiomycetes in Environmental Samples. PLoS ONE 7, e40863. https://doi.org/10.1371/journal.pone.0040863

Wang, B., Qiu, Y.-L., 2006. Phylogenetic distribution and evolution of mycorrhizas in land plants. Mycorrhiza 16, 299–363. https://doi.org/10.1007/s00572-005-0033-6

Wang, C.T., Long, R.J., Wang, Q.L., Jing, Z.C., Shi, J.J., 2009. Changes in plant diversity, biomass and soil C, in alpine meadows at different degradation stages in the headwater region of three rivers, China. Land Degradation & Development 20, 187–198. https://doi.org/10.1002/ldr.879

Wang, T., Yang, D., Yang, Y., Piao, S., Li, X., Cheng, G., Fu, B., 2020. Permafrost thawing puts the frozen carbon at risk over the Tibetan Plateau. Science Advances 6, eaaz3513. https://doi.org/10.1126/sciadv.aaz3513

Wang, Y., Wesche, K., 2016. Vegetation and soil responses to livestock grazing in Central Asian grasslands: a review of Chinese literature. Biodivers Conserv 25, 2401–2420. https://doi.org/10.1007/s10531-015-1034-1

Xie, Z., Le Roux, X., Wang, C., Gu, Z., An, M., Nan, H., Chen, B., Li, F., Liu, Y., Du, G., Feng, H., Ma, X., 2014. Identifying response groups of soil nitrifiers and denitrifiers to grazing and associated soil environmental drivers in Tibetan alpine meadows. Soil Biology and Biochemistry 77, 89–99. https://doi.org/10.1016/j.soilbio.2014.06.024

Yeh, E.T., Samberg, L.H., Gaerrang, Volkmar, E., Harris, R.B., 2017. Pastoralist Decision-Making on the Tibetan Plateau. Hum Ecol 45, 333–343. https://doi.org/10.1007/s10745-017-9891-8

Zhang, J., Kobert, K., Flouri, T., Stamatakis, A., 2014. PEAR: a fast and accurate Illumina Paired-End reAd mergeR. Bioinformatics 30, 614–620. https://doi.org/10.1093/bioinformatics/btt593

Zhou, H., Zhao, X., Tang, Y., Gu, S., Zhou, L., 2005. Alpine grassland degradation and its control in the source region of the Yangtze and Yellow Rivers, China. Grassland Science 51, 191–203. https://doi.org/10.1111/j.1744-697X.2005.00028.x

Zhuang, M., Gongbuzeren, Zhang, J., Li, W., 2019. Community-based seasonal movement grazing maintains lower greenhouse gas emission intensity on Qinghai-Tibet Plateau of China. Land Use Policy 85, 155–160. https://doi.org/10.1016/j.landusepol.2019.03.032

2.2. Study 2: Multi-Meta-Omics in soils: What to learn about the regulation of the basic C metabolism under shifts in habitat element stoichiometry.

Andreas Breidenbach[1,2]*, Kyle Mason-Jones[3], Sonja Wende[4], Callum Banfield[1,2], Yakov Kuzyakov[2], Sandra Spielvogel[5], Nico Jehmlich[6], Steffen Kolb[4], Michaela A. Dippold[1,2]*

[1] Department of Geosciences, Geo-Biosphere Interactions, University of Tuebingen, Schnarrenbergstrasse 94-96, 72076 Tuebingen, Germany.

[2] Division of Biogeochemistry of Agroecosystems, Georg-August University of Göttingen, Buesgenweg 2, 37073 Göttingen, Germany

[3] Department of Terrestrial Ecology, Netherlands Institute of Ecology (NIOO-KNAW), 6708 PB Wageningen, the Netherlands

[4] Research Area 1 Landscape Functioning, Leibniz Centre for Agricultural Landscape Research (ZALF), Eberswalder Straße 84, 15374 Müncheberg

[5] Department of Soil Science, University of Kiel, Hermann-Rodewald-Strasse 2, 24118 Kiel, Germany.

[6] Department of Molekular Systems Biology, Helmholtz-Centre for Environmental Research – UFZ, Permoserstr. 15, 04318 Leipzig, Germany.

*Corresponding author E-mail address: abreide@gwdg.de, michaela.dippold@uni-tuebingen.de

2.2.1. Abstract

Soil microbial communities play a key role in mineralizing carbon (C) while building up biomass, the basis of C sequestration, by replicative and storage growth. Understanding the regulatory processes of the microbial base C metabolism, i.e. the channeling of C between cata- and anabolism, is therefore essential. Shifts in microbial functions due to changes in environmental conditions were usually deduced from CO_2 efflux changes, enzymatic activity, indirect growth measurements or the quantification of metabolites. Whereas traditionally molecular biological methods were mainly used to gain a phylogenetic fingerprint of microbial communities, they meanwhile increasingly get also employed to acquire detailed information on microbial functions. Therefore, the utilization of state-of-the-art "omics"-techniques provide new insight in microbial functioning. In our study we aim to elucidate the regulatory processes of the base C metabolism in soil microbial communities by employing and linking metatranscriptomics and metaprotemomics. In a laboratory microcosm experiment using natural agricultural soil we treated the soil with ascending glucose concentrations with or without nutrient addition and extracted and purified total mRNA and proteins for a multi-meta-omics study. The metatranscriptome and metaproteome revealed complex regulatory processes from the expression of genes to the actual translation of proteins where transcribed genes were not necessarily also translated. The tricarboxylic acid cycle (TCA) was an exception to this finding, showing a positive correlation between the metatranscriptome and metaproteome suggesting a stable response across all post-genomic levels with lower temporal dynamic than many other reactions. The process of storages compound biosynthesis was highly depended on the glucose concentration in soil. The linkage of both "omics-techniques revealed strong regulatory responses in the base C metabolism in consequence of an altered resource stoichiometry in soils, but temporal shifts between formation of a transcript and the respective protein need to be taken into account for interpretation. It looks promising to exploit TCA cycle gene transcripts or proteins as indicator for shifts in carbon use efficiency (CUE) – an observation to be further confirmed by comparison with metaflux modeling to finally decipher the actual C partitioning between cata- and anabolism in soils.

2.2.2. Introduction

Microbial communities play an important role in soil as they mobilize and transform carbon (C) and nutrient sources to gain energy, invest into cell growth or build-up storage (Malik et al., 2018; Mason-Jones et al., 2021; Robinson et al., 2023). Therefore, a fundamental understanding of the microbial metabolism is essential to understand the regulatory principles underlying soil C and nutrient fluxes. Microbial turnover and functional changes in microbial communities were deduced from CO_2 respiration, shifts in nutrient contents or the profile of metabolic products (Blagodatskaya et al., 2011; Bonkowski and Roy, 2005; de Graaff et al., 2014). For many years, understanding functions of microbial

communities was limited due to their complex composition with different metabolic roles and capabilities. Usually, functions such as storage compound synthesis were deducted from single culture studies of bacteria in an artificial environment in laboratory experiments and such experiments feed majorly into our databases about bacterial and fungal functions (Carter and Bull, 1969; Gasser et al., 2009; Hansen, 1993). Through 16S rDNA sequencing and functional databases like "Tax4Fun" or "FUNGuild" *in-situ* microbial communities can be assigned to their functions (Aßhauer et al., 2015; Breidenbach et al., 2022; Nguyen et al., 2016), but only known and tested functions are part of these databases. However, if the responsible gene for a metabolic function is known, qPCR can be utilized to quantify the amount of the genes of interest (GoI) in the microbial community and after reverse transcription of the respective rRNA even the gene expression. But this is also limited to functions where the corresponding proteins and their gene sequences are already identified and a suitable set of soil-applicable primers exist. A major challenge remains untouched by these well-established methods: linking the metabolic potential from microbial communities' complex and highly divers genomic inventory and structure to their actual present proteins and active pathways represented by their metabolites to reveal their functional potential in the environment (Robinson et al., 2023).

Metagenomics tell the potential metabolic capabilities of microbial communities down to the species level, but this is not yet a function, but only a theoretical functional capacity. Metatranscriptomics disentangle the actively transcribed genes in the microbial community, but they are not able to distinguish if the mRNA gets translated into a protein or if it gets down-regulated in between (Herold et al., 2020; Kohlstedt et al., 2010). Therefore, metaproteome analyzes is additionally needed to illustrate the actual protein inventory of a microbial community (Bastida et al., 2009). Several studies employed either metatranscriptomics (Nacke et al., 2014) or metraproteomics (Malik et al., 2018), but attempts in combining both on complex native microbial communities in ecosystems are yet rare to find. It is predicted, that only when post-genomic levels such as metatranscriptomics and metaproteomics are combined, it is possible to elucidate the regulatory controls of the microbial metabolism (Malik et al., 2016). Protein- and mRNA-sequences can be inter-linked with each other so that regulatory processes and responses of the microbial community to changing environmental conditions can be interpreted easier than with other established methods.

Combining "-omics"-techniques from the metagenome, -transcriptome, -proteome and -metabolome is a key to fully unravel microbial communities' responses to changes in environmental conditions (Zhang et al., 2010). It is especially challenging when employed on samples from natural systems such as soils, but as Robinson et al. (2023) states, structural and functional changes of a microbial community are still desperately needed in understanding the impact on whole environmental systems. Therefore, utilizing well-known and well-researched metabolic pathways of the base C metabolism as

key examples for our understanding of regulatory principles in microbial growth, catabolism, and storage formation is a first step in disentangling the role of microbial communities' regulatory responses in the ecosystem. Multi-omics single culture studies about the base C metabolism aid in understanding the mechanisms of metabolic regulation but are not near the complexity of interactions and regulatory processes in a complex natural microbial community (Kohlstedt et al., 2014; Kukurugya et al., 2019). For that, our study chose to incubate natural agricultural soil in a controlled laboratory experiment with maximal contrasting stoichiometric conditions, i.e. with increasing C availability and nutrient addition in form of nitrogen (N) and phosphate (P). As soils are generally C limited habitats , this setup was hypothesized to enforce a maximum metabolic response of the microbial communities in the base C metabolism (Kuzyakov and Blagodatskaya, 2015; Soong et al., 2020). Extremely elevated C and nutrient content might also trigger an extreme response in the C storage metabolism as storage formation of microbial communities is controlled by the stoichiometry of available nutrients to convert into energy or biomass (Manzoni et al., 2021). Such a response in storage and base C metabolism is expected to be measurable in both metatranscriptome and metaproteome leading towards our study's hypotheses: (1) Glucose addition will trigger a cascade of post-genomic response of genes responsible for the base C metabolism detectable throughout the metatranscriptome and the metaproteome. (2) The soil microbial community will direct its metabolism toward storage compound biosynthesis when excess glucose levels are available which will be visible in both post-genomic levels. (3) The addition of glucose will have a stronger effect on the regulation of the base C metabolism than the addition of nutrients in form of N and P, as C is the most limited element restricting replicative growth. With our experimental design with an agricultural soil and its natural microbial community in a controlled laboratory environment, we analyzed key processes in the microbial base C metabolism. We unravel the regulatory checks and balances controlling the microbial metabolism where between the metatranscriptome and metaproteome can only be revealed by a multi-meta-omic approach covering metatranscriptome and metaproteome.

2.2.3. Material and methods

2.2.3.1. Experimental setup

The soil for the microcosm experiment was sampled from the Ap horizon (0 - 25 cm) at the experimental farm "Reinshof" (51°29'51.0"N, 9°55'59.0"E) of the faculty of agricultural sciences at the University of Goettingen in November 2017. The organically managed fields had been harvested two months prior to sampling. The soil was a haplic luvisol, developed from aeolian loess and had a pH 5.4, 1.4% TOC, 0.17% TN and a C/N ratio of 8.2 These low TOC and TN amounts ensure that the addition of glucose and nutrients would result in a strong response of the microbial base C metabolism.

Soil was sieved (2 mm) and stored at 4 °C before the start of the experiment. Then, 25 g of this soil was transferred airtight 125 ml glass bottle and adjusted to a 70% WHC. After applying the treatment solutions (glucose and/or nutrient addition), the further incubation was conducted in a dark climate chamber at 15 °C for a period of 4 days. The treatment solutions consisted of a "Low" glucose concentration (90 µg C g-1 soil, 45% of extractable MBC), a "High" glucose concentration (400 µg C g-1 soil, 200%) and a control without glucose addition (Zero). Besides Glucose, also nitrogen (N) and phosphate (P) nutrients were added as ammonium sulfate (17 µg N g^{-1} soil) and tripotassium phosphate (3.3 µg P g^{-1} soil). Soil microcosms were replicated four times and destructively sampled at 0, 24 and 96 h after the addition of the solutions.

2.2.3.2. Protein extraction and mass spectrometry

Soil samples from the 24 h sampling point were transported to the Helmholtz Centre for Environmental Research – UFZ GmbH (Leipzig, Germany) and proteins extracted according to Bastida et al. (2016): 5 g of each sample were treated with 10 ml of SDS lysis buffer (including 50 mM dithiothreitol) and vortexed for 2 min, followed by cell lysis in a boiling water bath for 10 min. Adding trichloroacetic acid (TCAA) achieved protein precipitation followed by three acetone washes of the pellet afterwards. Samples were then dissolved in 10 ml deionized water in an ultrasonic bath for 5 min and then mixed with 2x SDS loading buffer (consisting of 1.25 ml 1 M Tris-HCl pH 6.8, 4.0 ml 10% (w/v) SDS, 2.0 ml glycerol, 0.5 ml 0.5 M EDTA, 4 mg bromophenol blue, 0.2 ml β-mercaptoethanol 14.3 M) (Laemmli, 1970). This mixture was then incubated for 5 min at 90 °C and loaded on a 4% stacking gel and 12% separating gel. The SDS-gel was only run short for about 10 min. Colloidal Coomassie brilliant blue was used to stain the protein band. The protein band was cut into three pieces, washed and proteolytically cleaved into peptides using trypsin (Sigma, Munich, Germany) at 37 °C overnight, followed by two acetonitrile extractions and vacuum concentration for 15 min. Peptide lysates were dissolved in 20 µL 0.1% formic acid before injection into the mass spectrometer. In total, 5 µl of peptide lysates were loaded to a Dionex Ultimate RSLC 3000 nano-LC system (Thermo Fisher Scientific, Idstein, Germany) to separate the peptides according Bastida et al. (2014). Peptide analysis was performed on a Orbitrap Fusion MS (Thermo Fisher Scientific, Idstein, Germany) coupled with a TriVersa NanoMate source (Advion, Ltd., Harlow, UK) as described in Bastida et al. (2016). The Proteome Discoverer software (v1.4.0288, Thermo Scientific) was used to search the acquired MS/MS data with the SEQUEST HT algorithm against the bacterial NCBInr database with the following settings by Bastida et al. (2016). To assign the proteins to their phylogeny and calculating their abundances, the software PROPHANE (Schneider et al., 2011) and NSAF (Zybailov et al., 2006) was used.

2.2.3.3. Nucleic acid extraction

RNA was extracted from the 24 h soil samples with the Qiagen RNeasy PowerSoil kit (Qiagen GmbH, Hilden, Germany). RNA was sent to Macrogen Inc. (Seoul, Republic of Korea) for further processing for metatranscriptome analysis. After quality control on a TapeStation D1000 (Agilent Technologies, Santa Clara, CA, USA), the samples were prepared with the TruSeq Stranded Total RNA LT Sample Prep Kit (Illumina, San Diego, CA, USA) This included rRNA depletion and mRNA purification (Ribo-Zero), the reverse transcribtion of the mRNA to double stranded cDNA. A single adenine is ligated to the 3'-end of the cDNA to prevent ligation to each other. Adapters were ligated to the cDNA ends and enriched with PCR targeting cDNA that have adapters attached. Success of the adapter ligation, amplification and quality of the cDNA with adapters was then again controlled with a TapeStation D1000. Raw RNA reads were then provided by Macrogen for further bioinformatic processing.

2.2.3.4. Data processing for metatranscriptome data

Quality control (QC) for the reads of 14 metatranscriptomes was performed using kneaddata version 0.8.0 with default options for trimmomatic and added trimming of repetitive sequences *(--run-trim-repetitive*). Reads were then filtered for remaining rRNA using SortMeRNA 4.2.0 (Kopylova et al., 2012), which lead to a removal of an average of 12% of reads.

The taxonomic composition of samples checked by running "kraken2" (Wood and Salzberg, 2014) followed by "bracken" on quality controlled reads with a custom microbial database built from National Center for Biotechnologie Information (NCBI) refseq genomes for archaea, bacteria, fungi, protozoa, viral and Univex_Core sequences (access date 08-2020). Results were visualized with "Krona" (Ondov et al., 2011).

To quantify genes, GoI forward and reverse reads were combined and screened against a custom reference database using "diamond" version 2.0.9 (Buchfink et al., 2015) with parameter setting -k 1. For the reference database we gathered the IDs from KEGG Orthologues (KO) involved in pathways of interest from the KEGG website (Kanehisa and Goto, 2000) and downloaded the set of connected protein reference sequences from Uniprot using in-house python scripts. The counts (number or reads mapped on each reference gene) were extracted from "diamond" result files and normalized by gene length.

2.2.3.5. Statistics

Protein and RNA data were normalized by the total amount of found proteins to achieve a comparable relative abundance for the targeted metabolism processes. Alongside our research questions, we chose to filter all proteins, and protein sequences for specific processes related to C metabolism (glycolysis, gluconeogenesis, tricarboxylic acid cycle, pentose phosphate pathway and glyoxylate

metabolism), storage compound formation (PHB and NLFA) and fatty acid biosynthesis. The ratio ϕ (phi) expresses the partitioning of glycolysis compared to PPP as the main glucose consuming pathways, considering the influence of gluconeogenesis:

(1)

$$\varphi = \frac{Glycolysis - Gluconeogenesis}{Glycolysis - Gluconeogenesis + PPP}$$

Furthermore, ρ (rho) is calculated to emphasize energy-generating versus energy-demanding metabolic modes of the microbial communities, and to assess whether the microbial community are breaking down glucose to gain energy or build up glucose molecules from proteins due to a lack of monosaccharide C sources:

(2)

$$\rho = \frac{Glycolysis}{Gluconeogenesis}$$

All mRNA- and proteins sequences belonging to these pathways were summarized. Sequences present in more than one pathway were accounted for every pathway these sequences were listed. Pathways from metaproteome data were tested for significant differences with a two-way ANOVA and a post-hoc TukeyHSD which were performed for single comparisons of the treatments (R 4.2.2). Due to poor mRNA quality and/or quantity, replicates of soil samples dedicated for RNA extraction were lost. Fortunately, all treatments had at least one replicate left. Statistical tests had to be chosen who took these circumstances into account for the metatranscriptome, so that we chose an ANOVA type 3 (“emmeans” package, R 4.2.2).

2.2.4. Results

2.2.4.1. Effects of C and nutrient amendment on mRNA and protein abundance of the base C metabolism

The relative protein abundances for the selected pathways of the base carbon metabolism showed a strongly deviating pattern from the relative transcript abundance depending on stoichiometry, except for the TCA and partially for the glycolysis (Fig. 1). The addition of high amounts of glucose induced the transcription of glycolysis genes which got also translated into glycolysis proteins, but this effect solely exists for high glucose and high nutrient additions (Fig. 1, Table 1). Glucose and nutrient addition had

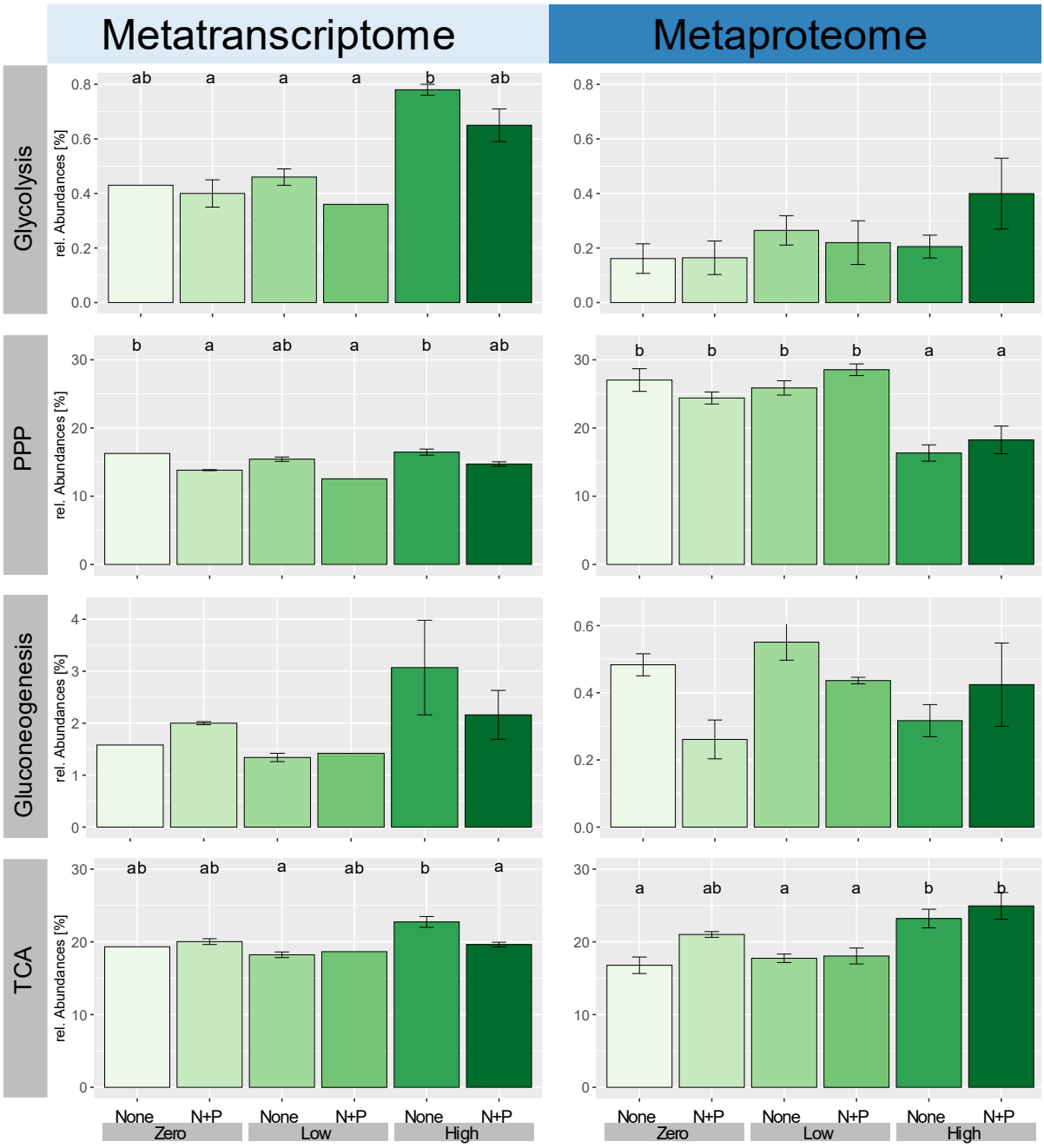

S2 Figure 1: **Relative abundances of metabolic processes related to glycolysis, pentose phosphate pathway (PPP), gluconeogenesis and tricarboxylic acid cycle (TCA) in the metatranscriptome and metaproteome.** Significant differences of the posthoc Tukey HSD are indicated with small letters (emmeans ANOVA, $p < 0,05$)

a significant effect on inducing the transcription of PPP genes (Table 1). Unexpectedly, gluconeogenesis genes relative abundance were about 5 times higher than the relative abundances in the metaproteome and seemed to be expressed at the high glucose amendments. In contrast, gluconeogenesis related proteins displayed a pattern where nutrient addition hindered the translation to proteins in the zero and low treatments. Whereas PPP genes were largely unaffected by glucose

addition, its proteins experience a downregulation at the metaproteome level under high glucose amendment. In contrast to this often with anabolic demand linked pathway the merely catabolic TCA enzymes increased in abundance on high glucose availability, which is only weakly visible in the metatranscriptome.

S2 Table 1: p values (marked in bolt) of ANOVA from metranscriptome and metaproteome demonstrating single effects of glucose, nutrients, and the combination of both.

	Metatranscriptome			**Metaproteome**		
Pathway	**p value glucose**	**p value nutrient**	**p value glucose: nutrient**	**p value glucose**	**p value nutrient**	**p value glucose: nutrient**
Glycolysis	**0.0008**	0.1485	0.7280	0.2102	0.4234	0.2751
PPP	**0.0332**	**0.0006**	0.4941	**<0.0001**	0.5615	0.1339
Gluconeogenesis	0.3678	0.8701	0.7132	0.1208	0.1634	**0.0568**
TCA	**0.0128**	0.3324	**0,0352**	**0.0001**	**0.0392**	0.2549
Storage PHB	0.3582	0.2509	**0.0217**	**<0.0001**	0.4504	**0.0353**
Storage NLFA	**0.0162**	**0.0167**	0.6030	**0.0425**	0.8347	0.1367

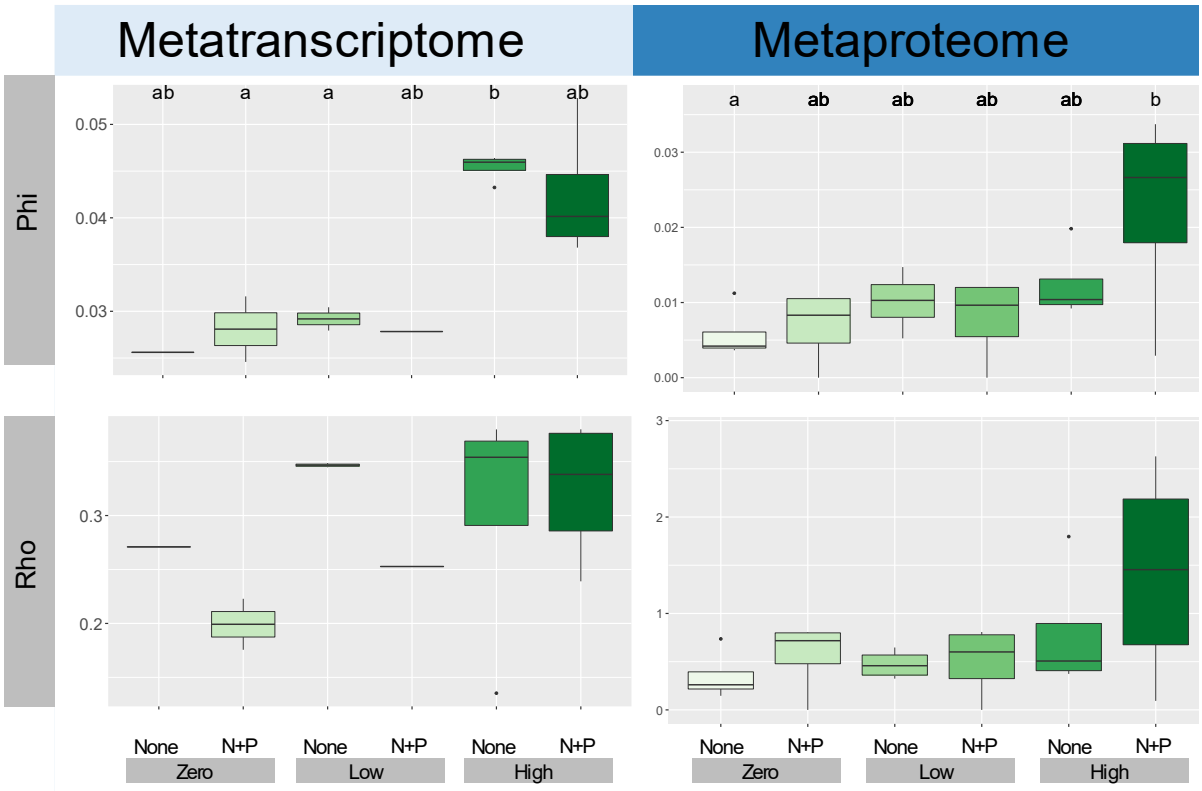

S2 Figure 2: **Ratios of Phi (ϕ) and Rho (ρ).** Significant differences of the posthoc Tukey HSD are indicated with small letters (emmeans ANOVA, p < 0,05)

The ϕ ratio showed a clear allocation towards energy metabolism under high glucose amendments in the metatranscriptome, which was also visible in the metaproteome but only when additional nutrients were provided (Fig. 2). The ρ ratio revealed that nutrient addition without strongly increasing C availability led to an increase in the anabolic, energy-demanding gluconeogenesis pathway in relation to catabolic glycolysis in the metatranscriptome, which was not imprinted in the metaproteome (Fig. 2).

The glucose and nutrient amendment had significant effects on NLFA but not on the PHB gene expression, whereas only the glucose treatment had significant effects on both storage compounds (Table 1). The abundance of proteins involved in the synthesis of PHB got reduced upon high C supply supposedly a regulatory effect which is not reflected in the relative abundances of the underlying genes in the metatranscriptome (Fig. 3). Similarly, NLFA metabolism also showed a tendency in reducing the abundance of NLFA synthesis related transcripts and proteins with increasing C availability, but this effect is much less pronounced than for PHB (Fig. 3). No significant effect of nutrient amendment on the regulation of storage-producing enzymes in either the metatranscriptome or the metaproteome was observed.

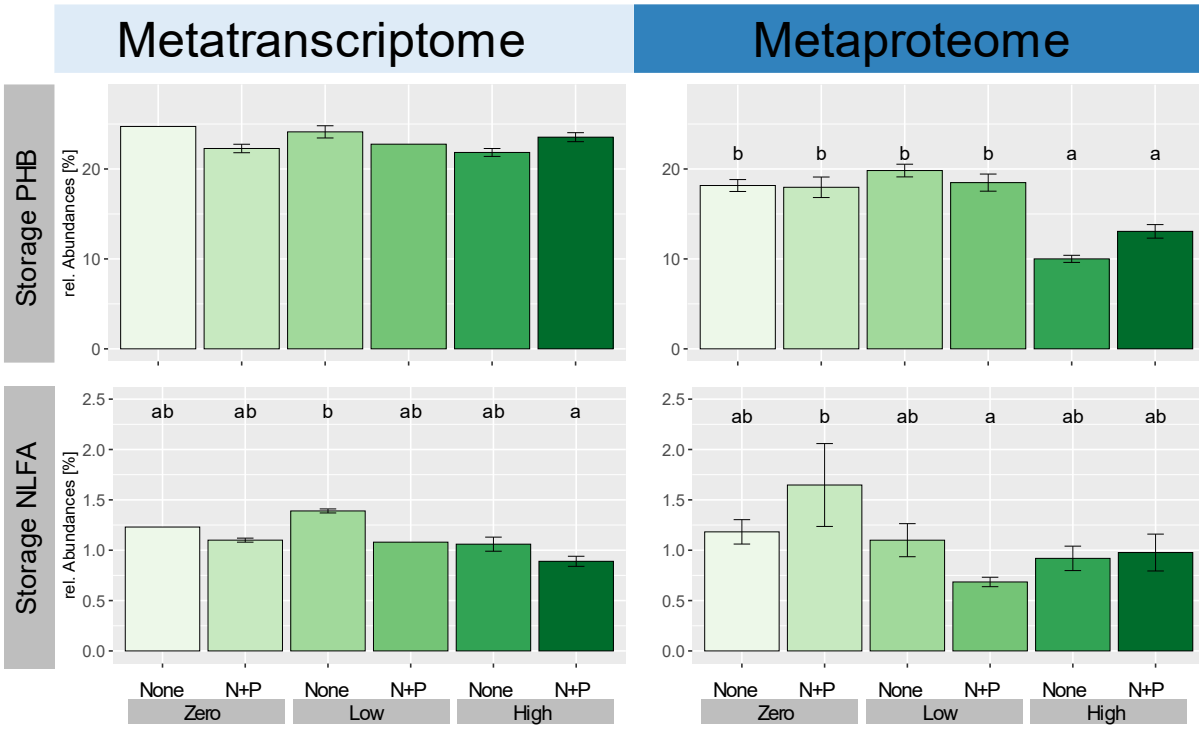

S2 Figure 3: **Relative abundances of metabolic processes related to storage compounds PHB and NLFA.** Significant differences of the posthoc Tukey HSD are indicated with small letters (emmeans ANOVA, p < 0,05)

2.2.4.2. Interrelations of protein- and mRNA abundances within and between pathways

Across the major glucose-related pathways, solely the TCA cycle displayed a significant correlation between mRNA and the respective protein abundance (Fig. 4). Most notable, PPP and Gluconeogenesis even showed a negative relation between the mRNA abundance and the number of proteins of the respective pathway (Fig. 4). There was no indication for a specific effect or a responsibility of either C or nutrient amendment on regression between the metatranscriptome and the respective metaproteome.

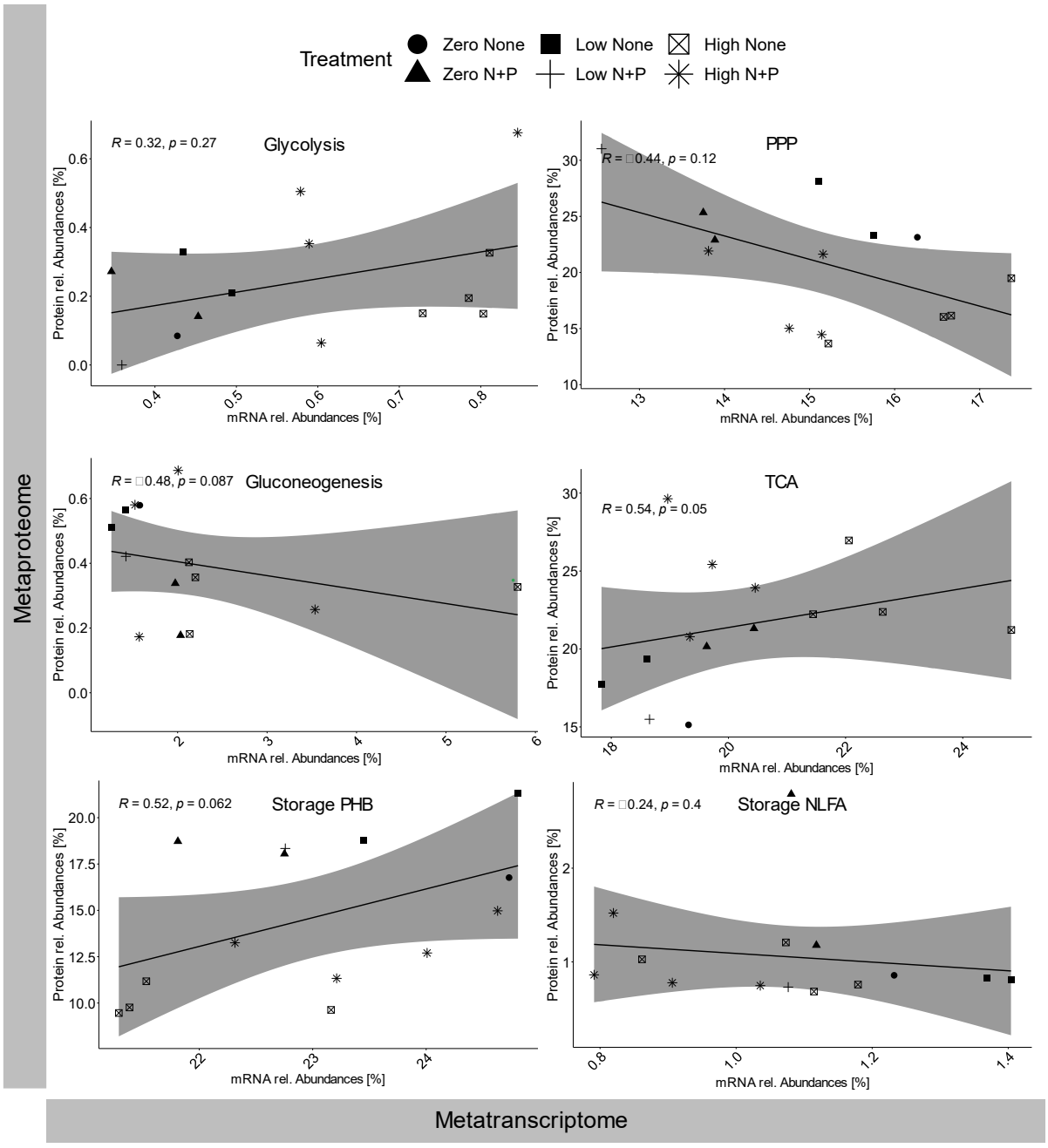

S2 Figure 4: **Correlations between relative abundances of the metatranscriptome and metaproteome** of the metabolic processes glycolysis, pentose phosphate pathway (PPP), gluconeogenesis and tricarboxylic acid cycle (TCA).

We furthermore tested for potential relations within the metatranscriptome, indicating that various metabolic pathways are co-regulated. The correlation analysis revealed that gluconeogenesis had a negative relation with the synthesis of PHB (R = -0.78) and also slightly with NLFA (R = -0.46) build-up (Fig. 5A). The corresponding correlation of gluconeogenesis and storage compound synthesis pathways was not significant in the metaproteome (Fig. 5B). The positive co-regulation of gluconeogenesis and TCA (R = 0.97) on the mRNA level is highly significant but was not represented on the metaproteome level. When TCA is upregulated PHB storage was downregulated in both the metatranscriptome (R = -0.8) and metaproteome (R = -0.6). While PPP and the biosynthesis of fatty acids correlated positively (R = 0.79) hinting towards a co-regulation of pathways forming new biomass during replicative growth on the metatranscriptome level, the PPP was negatively correlated with TCA in the metaproteome (R = -0.79) indicating a reduction of energy production during de novo biomass formation (Fig. 5).

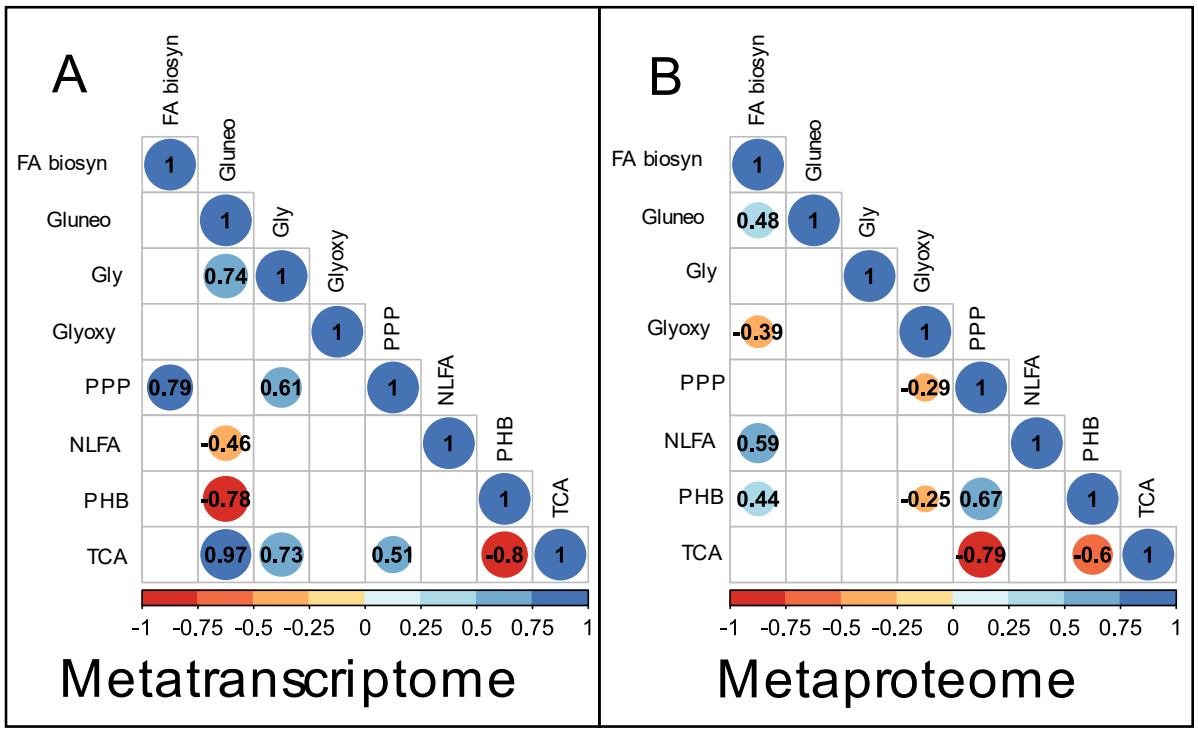

S2 Figure 5: **Correlation between the metabolic processes** in the metatranscriptome (**A**) and metaproteome (**B**). Only significant correlations are displayed, and R values are indicating their positive or negative relationships.

This observation suggests potential cross-regulatory effects between the regulation of transcription and translation of different pathways and motivated us to examine the correlation between the metatranscriptome and metaproteome of the base C metabolism (Fig. 6). We observed a noteworthy positive correlation (R = 0.72) between glycolysis at the mRNA level and the tricarboxylic acid cycle (TCA) at the metaproteome level suggesting the two successive energy producing pathways to be jointly controlled, i.e., no downregulation of proteins of the TCA when glycolysis is enhanced by mRNA formation. Additionally, also NLFA storage related gene sequences are transcribed and positively correlated with the PHB storage in the proteome (R = 0.56), which hints towards similar soil conditions inducing storage compound formation, even if the key regulatory step might be located on different post-genomic levels. Fatty acid biosynthesis (R = 0.65), gluconeogenesis (R = 0.38), PPP (R = 0.75) and TCA (R = 0.45) gene transcriptions were positively correlated with glyoxylate metabolism enzyme abundance suggesting a potential demand of replicative growth building blocks is ensured by their co-regulation, i.e., the anaplerotic glyoxylate pathway providing C for anabolism and gluconeogenesis within the TCA. This is also supported by the negative correlation between proteins for PHB synthesis and glycolysis (R = -0.77), and TCA (R = -0.85) transcripts, all known to be enhanced under high energy demand.

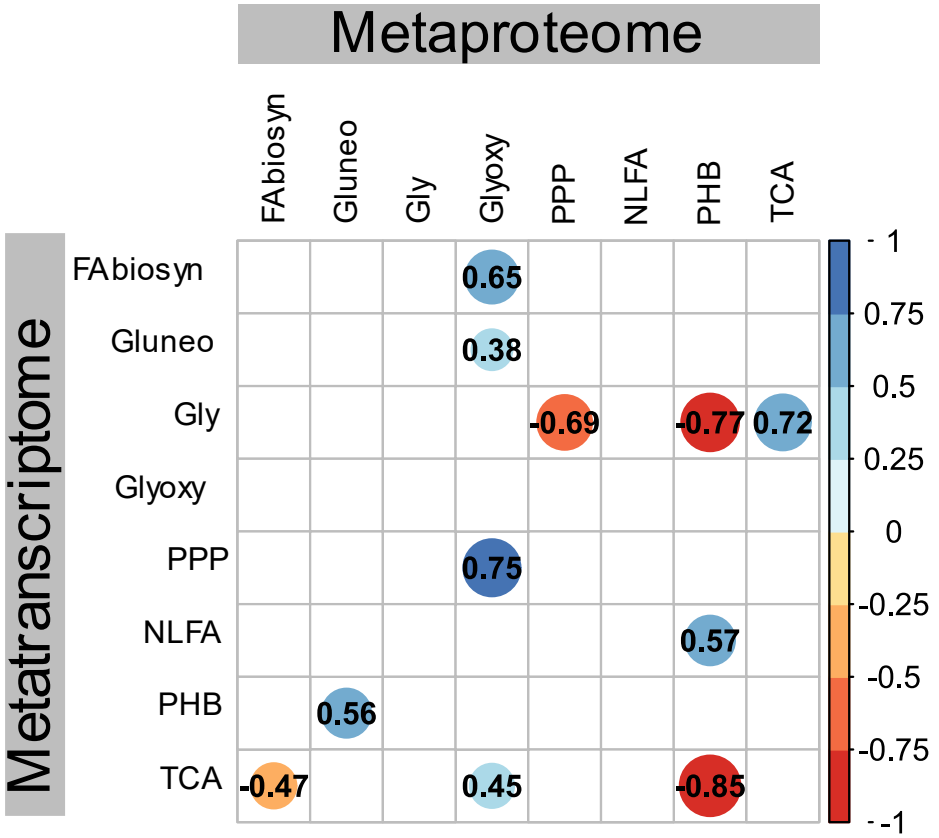

S2 Figure 6: **Correlation between the metatranscriptome and metaproteome metabolic processes.** Only significant correlations are displayed, and R values are indicating their positive or negative relationships.

2.2.5. Discussion

2.2.5.1. Effects of C and nutrient availability on the regulation of the base C metabolism

The metatranscriptome and metaproteome of the base metabolism were more strongly influenced by C than by nutrient availability in soil. Even in the rather low-fertilized soil of this study, the N- and P-sources seemed to be sufficient and microbial dynamics and metabolism were rather controlled by C limitation (Soong et al., 2020). Nutrient addition solely influenced the transcription of PPP related genes, but this effect disappeared on the translational level as similarly described by Kohlstedt et al. (2010).

Generally, soils (and more strongly SOM-depleted agricultural soils) are usually C limited and thus the microbial community needs to react quickly on sudden additional C supply, the underlying principle of the formation of hotspots such as the rhizosphere or detritusphere (Kuzyakov and Blagodatskaya, 2015; Soong et al., 2020). When the soil microbial community is faced with an excess of glucose, like in our experiment, the bacteria react by activating transcripts and translation of proteins of the TCA cycle, a strongly catabolic, energy producing pathway (Voet et al., 2008). Additionally, high glucose amendment induced transcription of glycolysis and unexpectedly also gluconeogenesis genes, but only the corresponding TCA and glycolysis proteins were also visible in the metaproteome. As glycolysis and gluconeogenesis share largely the same genes, a generic upregulation and interruption at a later post-genomic regulatory level, i.e. during translation, seems probable and 5x lower relative abundances in the metaproteome are hinting towards such downregulatory process. The increase in energy metabolism by glucose amendment were accompanied by a downregulation of the anabolic precursor producing PPP on the level of the metaproteome. As this was not visible in the metatranscriptome, this very likely occurred by an inhibition of the translation of the PPP mRNAs. This indicates that regulatory processes in response to stoichiometric shifts can occur on both levels, metatranscriptome or metaproteome, and that even regulatory processes on the translational level blocking an altered transcription process or that altered translation rates without altered transcript abundances can occur within the regulation of the base C metabolism. This observation suggests that conclusions from altered transcript or protein profiles are not easy to convert to conclusions about the final process rates. The regulatory processes specifically in complex communities where individual members may have different sensitivities, thresholds and response behaviors seem to be highly complex with many potential regulatory responses on the various post-genomic levels, strongly aggravating interpretations of mere mRNA or protein abundances.

2.2.5.2. Time-lag response to changing environmental conditions.

The correlation results between metatranscriptome and metaproteome revealed that the altered C and nutrient conditions had not the anticipated coherent downstream effect on the targeted

metabolic processes from genome over mRNA to protein. This can be explained by regulatory processes at the level of mRNA translation to proteins that interrupt or counteract a metatranscriptomes' response. Additionally, the weak correlations of metatranscriptome and -proteome (Fig. 4) could also be explained by a time-lag response of the metaproteome on past environmental conditions or *vice versa* an already modified response of transcription regulation on altered conditions such as a depletion of a glucose level. As Takahashi et al. (2011) pointed out, the time of transcription of a gene to mRNA over the translation to its corresponding proteins can take 60 min until it's measurable in the metabolome in a single culture study. Additionally, mRNA has different half-lives in bacteria ranging from 1 – 10 min depending on the bacteria's turn-over times (Laalami et al., 2014) Given that a soil microbial community is much more complex than a single culture, the time-lag and mRNA half-lives in a microbial community may play an even more important role than for single cultures. It is known that glucose is consumed very rapidly in soil e.g. (Jones and Murphy, 2007) demonstrated an instantaneous uptake of glucose by the microbial community and (Gunina and Kuzyakov, 2015) reported glucose decomposition rates of 1.1% min^{-1} of the added glucose. Considering the short half-life time of mRNA and the rapid *de novo* production of new mRNA responding to the already strongly reduced amount of glucose in the soil solution after 24 h, our measurement may have lost most of the mRNAs specifically expressed as response to high C availability. This indicates that the simultaneous measurement of mRNA and proteins is critical and may not represent a corresponding response of metatranscriptome and metaproteome on the addition of glucose and nutrients. As the transcription of mRNA is induced much faster in response to changing environmental conditions as the translation of the metaproteome, a considerably earlier sampling of mRNA is required and may have resulted in an improved match of the two omics datasets.

The TCA seems to be partially exceptional to that, as there is similar response at least on C addition (Fig. 1) and a correlation between mRNA and protein abundance (Fig. 4). Counterregulatory effects and smoothing down of mRNA regulation on the level of translation or vice versa induction of protein production on the level of mRNA translation seems to be not as strong for this major energy producing pathway as for the other pathways, producing or consuming the pyruvate precursor. This result alone without further time resolved analysis and higher treatment diversity is hardly to explain, as the ongoing ATP demand even if precursor demand changes or the final regulation of activity by absence or presence of acetyl-CoA (which is metabolically cheaper than removing existing proteins) may be explanatory here. Irrespective of the potential underlying reason, this observation is important, as Wu et al. (2022) have shown, that it's the TCA activity which is ultimately negatively linked with the carbon use efficiency (CUE). In consequence, if finally, the linkage of protein abundance (which correlates with mRNA abundance) with TCA activity can be confirmed, the metaproteome but also metatranscriptome

data can be used for deducing CUEs of soil samples, even if potentially the ideal timepoint of maximal transcript or protein abundance are not met by the sampling event.

2.2.5.3. Regulation of metabolic processes of the base C metabolism

The multi-meta-omic approach of this study reveals a complex network of strongly cross-regulated processes in the base C metabolism of soil microbiomes. Only these multi-meta-omic experiments are capable of revealing these regulatory interactions in soil microbiomes (Herold et al., 2020; Kohlstedt et al., 2010; Schimel, 2016), which can even with further analysis be attributed to individual groups of microorganisms. Especially the regulatory relationship between the TCA and PHB storage pathways were apparent not only in the metatranscriptome but also in the metaproteome and clearly demonstrate that either energy for immediate consumption is produced as ATP or that C and energy are stored in PHBs. Mason-Jones et al. (2023) demonstrated that soil microbiomes respond on conditions as simulated in this study by strong response in enhanced or reduced C storage in PHBs, reflected here in a response of both, PHB gene transcription and mRNA translation but also that of TCA genes. As the strongly negative relationship between TCA and PHB could be observed in the metatranscriptome and the metaproteome, this hints towards a strong, long lasting regulatory process with low dynamics along the 24 h of this experiment. As TCA is clearly linked to CUE, a close interdependency of CUE and C storage in the soil microbiome is likely (Manzoni et al., 2012) and waits upon confirmation in further experimental studies.

2.2.6. Conclusion

Our study managed to show that a controlled laboratory microcosm experiment with natural soils is a suitable framework to study the linkage of metatranscriptome and metaproteome in complex environmental microbiomes e.g., found in soils. We focused on the base C metabolism as our main interest was related to implications of stoichiometric resource shifts in C metabolizing pathways with implications for soil C cycling. The correlations between mRNA and proteins hint towards a time-lag between transcript and protein level, with regulatory processes modulating responses on the translational level and leading to differences in metatranscriptome and -proteome among the treatments, when sampled at a single time point. Short half-life of mRNA and the much longer time span required for protein biosynthesis suggest that sampling at the same time point should be adjusted towards time shift sampling where samples for metatranscriptomics are taken at least 60 min before sampling for metaproteomics. As to complete the understanding the regulatory processes on all post-genomic levels in natural soil microbiomes, it would be necessary to extend the studies parameters for the meta-metabolome and the metafluxome to cover all potential regulatory stages of the base C

metabolism down to the endpoints of the pathways and their C fluxes. This would finally allow us to conclude, which processes relevant for soil C cycling can be covered by high-throughput metatrancriptome studies versus more complex mass-spectrometric analysis of metaproteoms or meta-metabolomes and which processes can only be adequately studied, if really a process rate itself by quantifying the respective C flux (i.e., the metafluxome) via isotope labeling approaches is necessary.

2.2.7. References

Aßhauer, K.P., Wemheuer, B., Daniel, R., Meinicke, P., 2015. Tax4Fun: predicting functional profiles from metagenomic 16S rRNA data: Fig. 1. Bioinformatics 31, 2882–2884. https://doi.org/10.1093/bioinformatics/btv287

Bastida, F., Moreno, J.L., Nicolás, C., Hernández, T., García, C., 2009. Soil metaproteomics: a review of an emerging environmental science. Significance, methodology and perspectives. European Journal of Soil Science 60, 845–859. https://doi.org/10.1111/j.1365-2389.2009.01184.x

Blagodatskaya, E., Yuyukina, T., Blagodatsky, S., Kuzyakov, Y., 2011. Three-source-partitioning of microbial biomass and of CO2 efflux from soil to evaluate mechanisms of priming effects. Soil Biology and Biochemistry 43, 778–786. https://doi.org/10.1016/j.soilbio.2010.12.011

Bonkowski, M., Roy, J., 2005. Soil microbial diversity and soil functioning affect competition among grasses in experimental microcosms. Oecologia 143, 232–240. https://doi.org/10.1007/s00442-004-1790-1

Breidenbach, A., Schleuss, P.-M., Liu, S., Schneider, D., Dippold, M.A., de la Haye, T., Miehe, G., Heitkamp, F., Seeber, E., Mason-Jones, K., Xu, X., Huanming, Y., Xu, J., Dorji, T., Gube, M., Norf, H., Meier, J., Guggenberger, G., Kuzyakov, Y., Spielvogel, S., 2022. Microbial functional changes mark irreversible course of Tibetan grassland degradation. Nat Commun 13, 2681. https://doi.org/10.1038/s41467-022-30047-7

Buchfink, B., Xie, C., Huson, D.H., 2015. Fast and sensitive protein alignment using DIAMOND. Nat Methods 12, 59–60. https://doi.org/10.1038/nmeth.3176

Carter, B.L.A., Bull, A.T., 1969. Studies of fungal growth and intermediary carbon metabolism under steady and non-steady state conditions. Biotechnol. Bioeng. 11, 785–804. https://doi.org/10.1002/bit.260110508

de Graaff, M.-A., Jastrow, J.D., Gillette, S., Johns, A., Wullschleger, S.D., 2014. Differential priming of soil carbon driven by soil depth and root impacts on carbon availability. Soil Biology and Biochemistry 69, 147–156. https://doi.org/10.1016/j.soilbio.2013.10.047

Gasser, I., MÃ¼ller, H., Berg, G., 2009. Ecology and characterization of polyhydroxyalkanoate-producing microorganisms on and in plants: PHA producers on and in plants. FEMS Microbiology Ecology 70, 142–150. https://doi.org/10.1111/j.1574-6941.2009.00734.x

Gunina, A., Kuzyakov, Y., 2015. Sugars in soil and sweets for microorganisms: Review of origin, content, composition and fate. Soil Biology and Biochemistry 90, 87–100. https://doi.org/10.1016/j.soilbio.2015.07.021

Hansen, T.A., 1993. Carbon Metabolism of Sulfate-Reducing Bacteria, in: Odom, J.M., Singleton, R. (Eds.), The Sulfate-Reducing Bacteria: Contemporary Perspectives, Brock/Springer Series in Contemporary Bioscience. Springer New York, New York, NY, pp. 21–40. https://doi.org/10.1007/978-1-4613-9263-7_2

Herold, M., Martínez Arbas, S., Narayanasamy, S., Sheik, A.R., Kleine-Borgmann, L.A.K., Lebrun, L.A., Kunath, B.J., Roume, H., Bessarab, I., Williams, R.B.H., Gillece, J.D., Schupp, J.M., Keim, P.S., Jäger, C., Hoopmann, M.R., Moritz, R.L., Ye, Y., Li, S., Tang, H., Heintz-Buschart, A., May, P.,

Muller, E.E.L., Laczny, C.C., Wilmes, P., 2020. Integration of time-series meta-omics data reveals how microbial ecosystems respond to disturbance. Nat Commun 11, 5281. https://doi.org/10.1038/s41467-020-19006-2

Jones, D.L., Murphy, D.V., 2007. Microbial response time to sugar and amino acid additions to soil. Soil Biology and Biochemistry 39, 2178–2182. https://doi.org/10.1016/j.soilbio.2007.03.017

Kanehisa, M., Goto, S., 2000. KEGG: Kyoto Encyclopedia of Genes and Genomes. Nucleic Acids Research 28, 27–30. https://doi.org/10.1093/nar/28.1.27

Kohlstedt, M., Becker, J., Wittmann, C., 2010. Metabolic fluxes and beyond—systems biology understanding and engineering of microbial metabolism. Appl Microbiol Biotechnol 88, 1065–1075. https://doi.org/10.1007/s00253-010-2854-2

Kohlstedt, M., Sappa, P.K., Meyer, H., Maaß, S., Zaprasis, A., Hoffmann, T., Becker, J., Steil, L., Hecker, M., van Dijl, J.M., Lalk, M., Mäder, U., Stülke, J., Bremer, E., Völker, U., Wittmann, C., 2014. Adaptation of *B acillus subtilis* carbon core metabolism to simultaneous nutrient limitation and osmotic challenge: a multi-omics perspective: Multi-omics perspective on *B. subtilis*. Environ Microbiol 16, 1898–1917. https://doi.org/10.1111/1462-2920.12438

Kopylova, E., Noé, L., Touzet, H., 2012. SortMeRNA: fast and accurate filtering of ribosomal RNAs in metatranscriptomic data. Bioinformatics 28, 3211–3217. https://doi.org/10.1093/bioinformatics/bts611

Kukurugya, M.A., Mendonca, C.M., Solhtalab, M., Wilkes, R.A., Thannhauser, T.W., Aristilde, L., 2019. Multi-omics analysis unravels a segregated metabolic flux network that tunes co-utilization of sugar and aromatic carbons in Pseudomonas putida. Journal of Biological Chemistry 294, 8464–8479. https://doi.org/10.1074/jbc.RA119.007885

Kuzyakov, Y., Blagodatskaya, E., 2015. Microbial hotspots and hot moments in soil: Concept & review. Soil Biology and Biochemistry 83, 184–199. https://doi.org/10.1016/j.soilbio.2015.01.025

Laalami, S., Zig, L., Putzer, H., 2014. Initiation of mRNA decay in bacteria. Cell. Mol. Life Sci. 71, 1799–1828. https://doi.org/10.1007/s00018-013-1472-4

Laemmli, U.K., 1970. Cleavage of Structural Proteins during the Assembly of the Head of Bacteriophage T4. Nature 227, 680–685. https://doi.org/10.1038/227680a0

Malik, A.A., Chowdhury, S., Schlager, V., Oliver, A., Puissant, J., Vazquez, P.G.M., Jehmlich, N., Von Bergen, M., Griffiths, R.I., Gleixner, G., 2016. Soil Fungal:Bacterial Ratios Are Linked to Altered Carbon Cycling. Front. Microbiol. 7. https://doi.org/10.3389/fmicb.2016.01247

Malik, A.A., Puissant, J., Buckeridge, K.M., Goodall, T., Jehmlich, N., Chowdhury, S., Gweon, H.S., Peyton, J.M., Mason, K.E., Van Agtmaal, M., Blaud, A., Clark, I.M., Whitaker, J., Pywell, R.F., Ostle, N., Gleixner, G., Griffiths, R.I., 2018. Land use driven change in soil pH affects microbial carbon cycling processes. Nat Commun 9, 3591. https://doi.org/10.1038/s41467-018-05980-1

Manzoni, S., Ding, Y., Warren, C., Banfield, C.C., Dippold, M.A., Mason-Jones, K., 2021. Intracellular Storage Reduces Stoichiometric Imbalances in Soil Microbial Biomass – A Theoretical Exploration. Front. Ecol. Evol. 9, 714134. https://doi.org/10.3389/fevo.2021.714134

Manzoni, S., Taylor, P., Richter, A., Porporato, A., Ågren, G.I., 2012. Environmental and stoichiometric controls on microbial carbon-use efficiency in soils. New Phytologist 196, 79–91. https://doi.org/10.1111/j.1469-8137.2012.04225.x

Mason-Jones, K., Robinson, S.L., Veen, G.F., Manzoni, S., van der Putten, W.H., 2021. Microbial storage and its implications for soil ecology. ISME J. https://doi.org/10.1038/s41396-021-01110-w

Nacke, H., Fischer, C., Thürmer, A., Meinicke, P., Daniel, R., 2014. Land Use Type Significantly Affects Microbial Gene Transcription in Soil. Microb Ecol 67, 919–930. https://doi.org/10.1007/s00248-014-0377-6

Nguyen, N.H., Song, Z., Bates, S.T., Branco, S., Tedersoo, L., Menke, J., Schilling, J.S., Kennedy, P.G., 2016. FUNGuild: An open annotation tool for parsing fungal community datasets by ecological guild. Fungal Ecology 20, 241–248. https://doi.org/10.1016/j.funeco.2015.06.006

Ondov, B.D., Bergman, N.H., Phillippy, A.M., 2011. Interactive metagenomic visualization in a Web browser. BMC Bioinformatics 12, 385. https://doi.org/10.1186/1471-2105-12-385

Robinson, C.H., Ritson, J.P., Alderson, D.M., Malik, A.A., Griffiths, R.I., Heinemeyer, A., Gallego-Sala, A.V., Quillet, A., Robroek, B.J.M., Evans, C., Chandler, D.M., Elliott, D.R., Shutttleworth, E.L., Lilleskov, E.A., Kitson, E., Cox, F., Worrall, F., Clay, G.D., Crosher, I., Pratscher, J., Bird, J., Walker, J., Belyea, L.R., Dumont, M.G., Bell, N.G.A., Artz, R.R.E., Bardgett, R.D., Andersen, R., Hutchinson, S.M., Page, S.E., Thom, T.J., Burn, W., Evans, M.G., 2023. Aspects of microbial communities in peatland carbon cycling under changing climate and land use pressures. Mires and Peat 29, 1–36. https://doi.org/10.19189/MaP.2022.OMB.StA.2404

Schimel, J., 2016. Microbial ecology: Linking omics to biogeochemistry. Nat Microbiol 1, 15028. https://doi.org/10.1038/nmicrobiol.2015.28

Schneider, T., Schmid, E., de Castro, J.V., Cardinale, M., Eberl, L., Grube, M., Berg, G., Riedel, K., 2011. Structure and function of the symbiosis partners of the lung lichen (*Lobaria pulmonaria* L. Hoffm.) analyzed by metaproteomics. Proteomics 11, 2752–2756. https://doi.org/10.1002/pmic.201000679

Soong, J.L., Fuchslueger, L., Marañon-Jimenez, S., Torn, M.S., Janssens, I.A., Penuelas, J., Richter, A., 2020. Microbial carbon limitation: The need for integrating microorganisms into our understanding of ecosystem carbon cycling. Glob Change Biol 26, 1953–1961. https://doi.org/10.1111/gcb.14962

Voet, D., Voet, J.G., Pratt, C.W., 2008. Fundamentals of biochemistry: life at the molecular level, 3rd ed. ed. Wiley, Hoboken, NJ.

Wood, D.E., Salzberg, S.L., 2014. Kraken: ultrafast metagenomic sequence classification using exact alignments. Genome Biol 15, R46. https://doi.org/10.1186/gb-2014-15-3-r46

Zhang, W., Li, F., Nie, L., 2010. Integrating multiple 'omics' analysis for microbial biology: application and methodologies. Microbiology 156, 287–301. https://doi.org/10.1099/mic.0.034793-0

Zybailov, B., Mosley, A.L., Sardiu, M.E., Coleman, M.K., Florens, L., Washburn, M.P., 2006. Statistical Analysis of Membrane Proteome Expression Changes in *Saccharomyces c erevisiae*. J. Proteome Res. 5, 2339–2347. https://doi.org/10.1021/pr060161n

2.3. Study 3: Accounting for storage compounds in soil microbial communities alters carbon flux modelling outcome.

Andreas Breidenach[1,2]*, Kyle Mason-Jones[3], Callum C. Banfield[1,2], Sandra Spielvogel[4], Michaela A. Dippold[1,2]*

[1] Biogeochemistry of Agroecosystems, Department of Crop Sciences, Georg-August University of Göttingen, Göttingen, Germany.

[2] Geo-Biosphere Interactions, Department of Geosciences, University of Tübingen, Tübingen, Germany.

[3] Department of Terrestrial Ecology, Netherlands Institute of Ecology (NIOO-KNAW), Wageningen, the Netherlands.

[6] Department of Soil Science, University of Kiel, Hermann-Rodewald-Strasse 2, 24118 Kiel, Germany.

*Corresponding author E-mail address: k.masonjones@nioo.knaw.nl; michaela.dippold@uni-tuebingen.de

2.3.1. Abstract

Carbon (C) sources in soils are consumed by microbial communities to be metabolized into energy, new biomass, while respiring CO_2. Microbes utilize easily available glucose-C in nutrient hotspots in soil to replicate or synthesize storage compounds. C flux modelling with ^{13}C position specifically labelled glucose enables us to decipher the fate of each C atom through microbial metabolic pathways. Therefore, it can be determined whether the microbial community is investing soil C into energy through glycolysis, replicative growth from pentose phosphate pathway or redirecting C flux into storage compounds. These storage compounds are usually neglected in metabolic modelling but play an important role in microbial growth and stress resistance. We modified a C flux model to additionally fit for storage synthesis under altering glucose-C levels and nutrient availability in a lab controlled natural soil microbial community. Microbial communities especially invest into storage compounds in conditions with low glucose concentrations and available nutrients hinting towards a reserve storage strategy. Contradictory to widespread understanding, high glucose concentration had not initiated surplus storage formation. Overall, the implementation of storage compound formation into C flux models will broaden the understanding of soil microbial metabolism.

2.3.2. Introduction

Soil microbial communities utilize various carbon (C) sources of soil organic matter (SOM) to generate biomass and drive their metabolism. Due to its heterogeneously distributed C and nutrient sources, soils harbor bacteria and fungi in nutrient hotspots in the detritus-, drilossphere and rhizosphere where they can utilize, root exudates, such as carbohydrates, amino acids, and carboxylic acids for their microbial growth (Apostel et al., 2015; Bååth, 2003; Gunina et al., 2014; Kuzyakov and Blagodatskaya, 2015; Rasse et al., 2005). As of the labile structure of these low molecular weight organic substances (LMWOS), they are mainly stabilized in soil by microbial uptake and incorporated into newly formed, more stable biomass compounds (Gunina et al., 2014). Usually, it is thought that the soil C and nutrient sources are used for cellular replication, including DNA replication and the extension of cell membranes, both prerequisites enabling cell division and thus growth of the microbial populations. Therefore, an increase of microbial biomass carbon (MBC) is often perceived as sufficient method to calculate microbial growth However, many soil microorganisms are capable of incorporating C into intracellular storage compounds, which constitutes an alternative mechanism for biomass growth (Mason-Jones et al., 2021). Conventional biomass methods, however, commonly neglect storage compound formation or underestimated as a growth factor while storage compounds can make up a large proportion of C allocation in microbial communities (Mason-Jones et al., 2022; Mason-Jones et al., 2019; Rinnan and Bååth, 2009). As storage compounds are usually not extractable via established chloroform fumigation extraction (CFE) protocols, Mason-Jones et al. (2019) suggested

that storage compound formation and additional extraction of storage compounds need to be taken into account when discussing biomass growth. This is especially important considering their quantitative relevance, e.g., 68% of glucose C was allocated to the bacterial storage compound polyhydroxybutyrate (PHB) relative to C allocated to extractable MBC (Mason-Jones et al., 2019). However, besides their quantitative measurement, which requires compound-specific elaborated laboratory techniques, they can and should also be considered in modeling approaches as of with this study. In contrast to (Manzoni et al., 2021) theoretical approach on a laboratory experiment, we chose to execute such endeavor and performed a microcosm experiment with isotopomerically ^{13}C-labelled glucose to gain actual measured position-specific $^{13}CO_2$ efflux as input for our storage compound-optimized model.

When bacteria and fungi redirect their C metabolism towards the biosynthesis of storage compounds in an environment where resources such as C are available in excess, the storage mode is defined as surplus storage (Mason-Jones et al., 2021). As previous data suggests, that can often happen when other nutrients such as nitrogen (N) or phosphor (P) are lacking (Bååth, 2003; Mason-Jones et al., 2019). However, ecological theories also suggest that reserve storage irrespective of surplus may be an advantageous strategy for soil microbes (Manzoni et al. 2021). When organisms divert their nutrient fluxes towards the formation of storage compounds instead of their other functions in normal environmental conditions, they can ensure survival during future food scarcity events or warrant reproductive success among their competitors in the future (Mason-Jones et al., 2021).

PHB and triacylglycerols (TAG, constituent of neutral lipid fatty acids, NLFA) (Harwood and Russell, 1984; López et al., 2015) are especially relevant for soil ecology and C flux modelling as they are quantitatively significant and the only lipid storage compounds with existing methods for their measurement in soil (Mason-Jones et al., 2019). Both, PHB and TAG are widespread intracellular storage compounds in bacteria and fungi and their synthesis are a common metabolic trait found in soil microbial communities (Mason-Jones et al., 2021). For the formation of storage compounds, the C flux from glucose is therefore redirected from glycolysis at the acetyl-CoA step towards storage compound synthesis instead of TCA for producing reducing equivalents and generating ATP. PHB is derived from an acetyl-CoA branch when entry into the tricarboxylic acid cycle (TCA) is inhibited and is subsequently synthesized via an acetoacetyl-CoA reductase, a beta-ketothiolase and a PHB synthase (López et al., 2015). Similarly to PHB, TAG are also directly derived from acetyl-CoA and compete with each other for their precursor and are closely related in their synthesis as inhibition of PHB synthesis can trigger the biosynthesis of TAG in mutant *Rhodococcus ruber* cultures (Alvarez and Steinbüchel, 2002; Pieper, 1993).

The reactions of the major metabolic pathways have been highly characterized, such that the fate of each atom in a degraded molecule is known, if a particular pathway is followed. Metabolic flux modelling turns this around by using position-specifically labelled substrates to determine the fate of each substrate atom in particular products (e.g., CO_2), thereby allowing qualitative and quantitative reconstruction of metabolic C fluxes through different pathways (Apostel et al., 2015). Position-specific labelling of key metabolic precursors is widely established in biochemistry and enables tracing of ^{13}C from specific molecular positions throughout the metabolism. In the past, isotopomers from different LMWOS like alanine (Apostel et al., 2018) and pyruvate (Dijkstra et al., 2011b, 2011a; Hagerty et al., 2014) as well as some (but often not all) labeled C positions in glucose (Apostel et al., 2015; Dijkstra et al., 2011b) were used in soil studies for qualitative metabolism analysis. However, for robust quantitative metabolic flux modelling of heterotrophic metabolism the use of glucose, separately labelled at each of the six C positions, is established as an ideal standard, whenever this number of parallel assays can be performed experimentally (Dijkstra et al., 2015; Klingner et al., 2015; Wu et al., 2020; Zamboni et al., 2009). However, as these experiments require a large number of microcosms, this approach is rather time consuming and systematic applications are still rather rare. Here we applied this comprehensive position-specific glucose labeling for a robust reconstruction of glucose metabolism covering glycolysis, pentose phosphate pathway (PPP), gluconeogenesis and tricarboxylic acid cycle (TCA). As storage is a significant microbial biomass pool, we additionally aimed to take this flux into account within the applied metabolic flux model, considering a flexible flux from acetyl-CoA towards a quantitatively non-restricted biomass pool in contrast to the unmodified flux model where the flux into storage compound formation was a fixed ratio dependent on other fluxes into biomass formation.

With our experiment, we aimed to shed a light on the various growth and storage modes in a soil microbial community using metabolic flux modelling and decipher the switch between growth by *de novo* synthesis of biomass and the creation of storage compounds. Therefore, we conducted a microcosm experiment with agricultural soil adding low and high amounts of glucose and accompanied them with trace amounts of position-specifically ^{13}C-labelled glucose. Additionally, to the variating glucose concentrations, treatment solutions were treated with or without nutrients (N and P). The respective $^{13}CO_2$ effluxes were used to predict metabolic fluxes in a model with and without the option for storage. We hypothesized that: (1) The addition of excess glucose without nutrients will result in the redirection of C fluxes towards storage compound synthesis (surplus storage). (2) In contrast, the microbial community will utilize excess glucose and nutrients for the *de novo* synthesis of biomass through cell division when both, glucose and nutrients are provided. With our study, we try to apply

metabolic flux models that account for storage compound formation on experimental data and prove the importance to consider storage for accessing C fluxes in natural soil microbial communities.

2.3.3. Material and Methods

2.3.3.1. Experimental setup

The soil for the microcosm experiment was sampled from the Ap horizon (0-25 cm) at the experimental farm "Reinshof" (51°29'51.0"N, 9°55'59.0"E) of the Faculty of Agricultural Sciences of the University of Goettingen in November 2017. The fields are organically farmed consecutively with red clover and summer wheat and were harvested two months before sampling. The soil is characterized as haplic Luvisol developed from aeolian loess with pH 5.4, 1.4% TOC, 0.17% TN and a C/N ratio of 8.2. These low amounts of available carbon and nitrogen were intended to ensure that the glucose and nutrient treatments resulted in an adequate metabolic reaction of the microbial community. Until the start of the experiment, the soil was sieved with 2 mm and stored at 4 °C. For the microcosm experiment, air-tight 100 ml glass bottles were filled with 25 g of soil which was adjusted to 70% WHC. The experiment took place in a darkened climate chamber at 15°C over 4 days. The treatment solutions were applied, consisting of a low glucose concentration (90 µg C g-1 soil, 45% of extractable MBC), a high glucose concentration (400 µg C g-1 soil, 200%) and a control without glucose addition. In Addition, nutrients in form of ammonium sulfate (17 µg N g^{-1} soil) and tripotassium phosphate (3.3 µg P g^{-1} soil) were added as nitrogen (N) and phosphate (P) sources. All treatment solutions were split up for labeling with ^{13}C: uniformly labelled glucose (3 at%, U-^{13}C) and position-specifically labelled glucose (1.5 at%) for each C position (1^{13}C to 6^{13}C) in glucose in 4 replicates, resulting in 96 uniformly labeled microcosms and 192 position specifically labelled microcosms. CO_2 was sampled with an air-tight gas syringe from the microcosms' headspace, transferred to exetainers (Labco, Ceredigion, UK), where we measured their CO_2 concentration and at% ^{13}C /^{12}C a 0, 1, 3, 6, 12, 24, 33, 48, 72 and 96 h after adding glucose and/or nutrients. After every CO_2 sampling, the headspace of each microcosm was flushed with CO_2-free synthetic air. $^{13}CO_2$ and CO_2 concentrations were measured on a Trace-GC coupled via GC Isolink and ConFlo IV to a MAT 253 IRMS (Thermo Scientific, Bremen, Germany) at the KOSI (Centre for Staple Isotope Research and Analysis, Goettingen, Germany).

2.3.3.2. Flux model and its modification for storage compound formation

As input for the flux model, the F values (fraction of glucose-derived C) of the $^{13}CO_2$ at% values of the at% ^{13}C emitted from labelled C, background at% ^{13}C from controls and originally added at% ^{13}C from labelled glucose from the 24 and 96 h time points were calculated using the following equation:

(1)

$$F = \frac{at\%_{13C} - at\%_{Background}}{at\%_{Glucose} - at\%_{Background}}$$

These F values from position-specific and uniformly labelled microcosms were then used to calculate ratios for the model input as follows: As microcosms of uniformly and position-specific samples are independent from each other, every possible $^{13}CO_2$ combination of uniformly and position-specifically labelled microcosm replicates were used for calculating $x^{13}CO_2/U^{13}CO_2$ ratios (x = position of labelled ^{13}C in glucose 1-6, U =uniformly labelled glucose), resulting more than 130,000 combinations. Form these combinations, 128 CO_2 ratios (4 combinations for each 4 uniformly labelled replicates) were randomly chosen. As an example for pairing uniformly labeled microcosms with isotopomeric ones: uniformly labelled replicate "a" from the "Low N+P" glucose amendment was paired with the same treatment of position-specific replicates in a random combination: "ccddbb" (Supple. Table 1). Those combinations were then used in a modified flux model by (Dijkstra et al., 2011b) where the flux rates are calculated throughout the base C metabolism until they match the observed $^{13}CO_2$ ratios from isotopomere glucose-C: The model calculated each carbon flux from each metabolic transformation of glucose (Fig. 1A) into glycolysis (r1 – r5), tricarboxylic acid circle (TCA, r6 – r7), gluconeogenesis (r14 – r17) and pentose phosphate pathway (PPP, r9 – r12). Additionally, to the values of flux entry points into PPP (r9), gluconeogenesis (r17) and biomass formation (br1), we used one model version where the flux into biomass (br5) got now extended for an additional storage term that sum up to br5*. The br5 flux was formerly a fixed fraction of br1 and could therefore not account a shift in microbial metabolism to storage compound formation. In consequence, br5* of the storage-adjusted model is now variable and br5*was constrained by being equal or higher than the biomass-associated br5 derived from the fixed precursor ration for biomass production. The partitioning of C to glycolysis (r2) compared to PPP (r9) as one of the two glucose C consuming pathways was expressed as φ (phi), considering the gluconeogenesis-related fluxes:

(2)

$$\varphi = \frac{r2 - r14}{r2 - r14 + r9}$$

Total storage production is then calculated by subtracting the flux of stoichiometric biomass demand using acetyl-CoA (br5) from the newly generated br5* flux, containing this biomass demand plus storage to calculate the C flux into the Acetyl-CoA derived storage pool.

(3)

$$Storage = br5^* - 7.065 * br1 = br5^* - br5$$

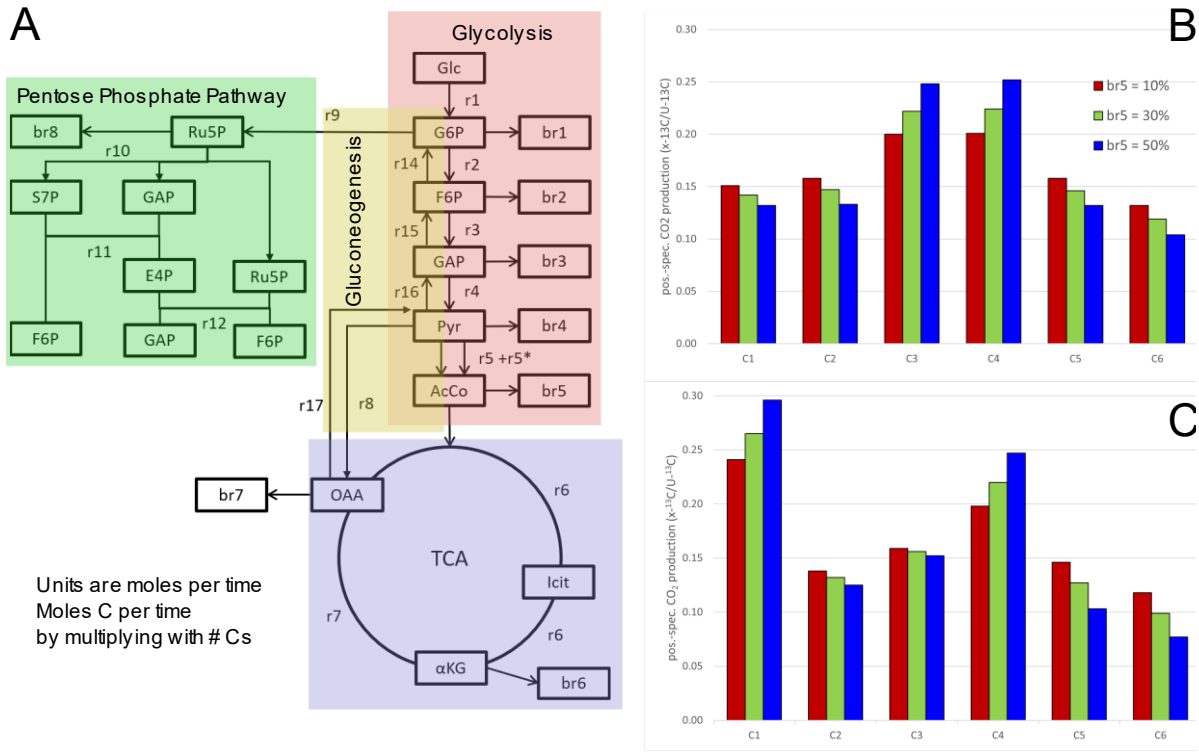

S3 Figure 1: **A:** The flux scheme of the basic glucose metabolism divided into glycolysis (r1 to r5), tricarboxylic acid circle (TCA, r6 – r7), gluconeogenesis (r14 – r17) and pentose phosphate pathway (PPP, r9 – r12); **B** and **C**: flux model sensitivity for storage compound formation represented in three levels of flux into br5 (10, 30, 50%) and set parameters for a mean br1 flux at 2.2 and two levels of fluxes into PPP at 10% (**B**) and 90% (**C**).

2.3.3.3. Model sensitivity for flux into storage formation

Our approach using position-specific isotopomeres of glucose for metabolic flux tracing was tested for its sensitivity to be able to identify C allocation towards storage compound formation form Acetyl-CoA. Therefore, we tested whether an increase in storage formation would result in considerable (i.e. detectable) changes of the CO_2 respiration from the glucose isotopomeres. Therefore, two scenarios were set-up: i) a 10% (Fig. 1B) and 90% flux (Fig. 1C) into PPP as $^{13}CO_2$ efflux patterns are severely influenced by the PPP similar to (Dijkstra et al., 2015). ii) We used a fixed 2.2% flux into br1 derived from the mean value of this dataset resulting from model runs without the option for storage compound formation. iii) Three levels of relative fluxes into br5, which comprises the flux into storage compound synthesis were tested to proof the sensitivity and influence of the br5 flux: 10, 30 and 50% of glucose C input.

2.3.3.4. Statistics

Data was checked for normality with the Shapiro-Wilk test and variance homogeneity was inspected using R statistical software (version 4.1.1). Possible outliers were removed when they exceeded a 1.5x interquartile range (Tukey fence). Beta regression was used to inspect x $^{13}CO_2$/U $^{13}CO_2$ ratios for

significant differences (Suppl. Fig. 3). The CO_2 fluxes were then checked for significant differences between the treatments by testing them with Kruskal-Wallis test. Comparisons between each treatment were determined by a post hoc Dunn test. Furthermore, the φ (phi) ratio, br1 and br5 fluxes of each treatment from the model without storage adaptation was compared with its counterpart from the storage-adjusted model via using either t-test.

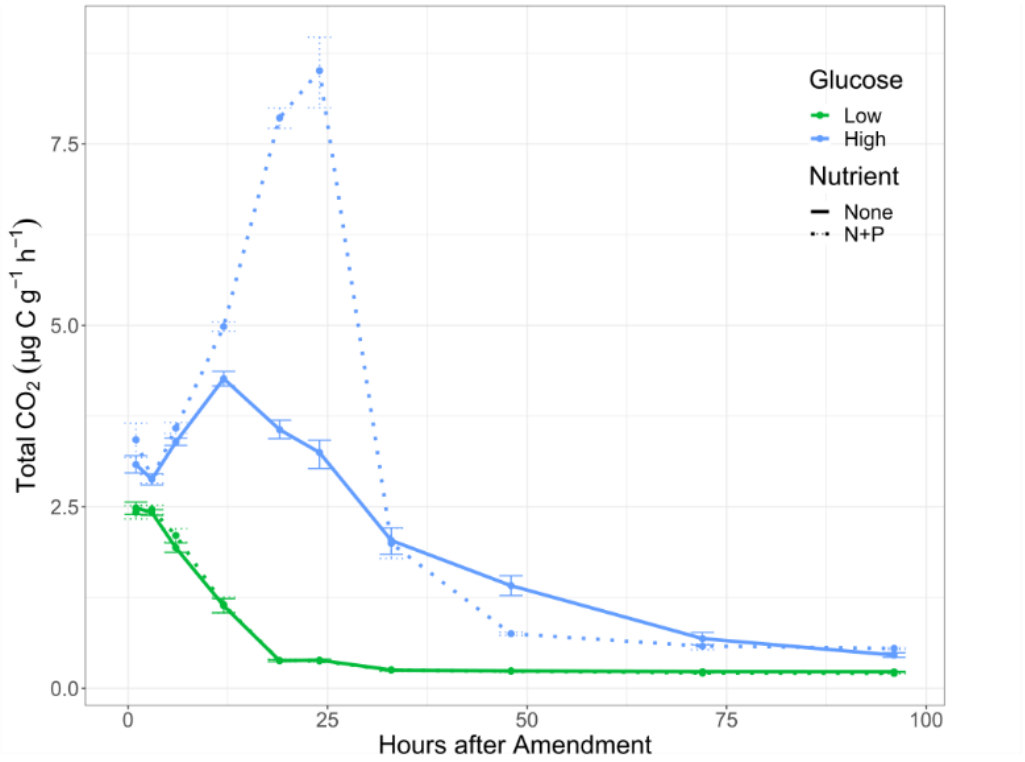

S3 Figure 2: **Labelled CO_2 efflux** depending on glucose and nutrient amendment over the curse of the experiment. Data points represent arithmetic means and error bars standard error of the mean.

2.3.4. Results

2.3.4.1. Microbial respiration

Labelled CO_2 efflux over the course of the incubation experiment were determined by considering the individual positions as replicates (Fig. 2). CO_2 respiration showed an identical pattern for both treatments with low glucose addition, "Low none" and "Low N+P" with maximum CO_2 efflux of 2.93 µg C g^{-1} h^{-1}after 1 h and a steady decline to a steady respiration of 0.3 µg C g^{-1} h^{-1} after 20 h. The high glucose treatments showed overall higher CO_2 respiration rates than the low treatments, but in contrast to them exhibited different respiration curves between the two nutrient treatments with a higher CO_2 rate for N+P. Furthermore, high glucose treatments reached their peak CO_2 efflux later than low treatments at 4.8 µg C g^{-1} h^{-1} ("High none") after 12 h and 10.14 µg C g^{-1} h^{-1} ("High N+P") after 24 h,

respectively. After its peak, the CO_2 rate "High none" declined steadily towards 0.46 µg C g^{-1} h^{-1} at the end of the experiment after 96 h. In contrast, "High N+P" experienced a steep decline after its peak to 2.0 µg C g^{-1} h^{-1} 33 h into the experiment, reaching a similar respiration rate to "High none" and higher than the low treatments at 0.5 µg C g^{-1} h^{-1} after 48 h.

2.3.4.2. Response of glucose isotopomere composition to storage formation

Our chosen predefined model conditions of 2.2 % mean br1 flux, 10% or 90% flux into PPP and an increasing br5 flux from 10, 30 to 50% influenced the $^{13}CO_2$ production of the glucose-C positions. Increasing the C flux into PPP up to 90%, influenced the proportion of CO_2 released from different C positions: where at 10% flux into PPP (Fig. 1B) the highest proportion of CO_2 from glucose-C was respired from positions C3 and C4 from glycolysis, at 90% PPP mostly positions C1 and C4 of glucose-C played a role in CO_2 production (Fig. 1C). While these patterns of CO_2 production are expected, the model sensitivity to the adjustment of br5 was more important. We could show that the increasing flux into br5 had an effect on CO_2 production at various C positions: Under high glycolysis (PPP 10%), most pronounced difference occurs in positions C3 and C4 respiration, by an increase of released CO_2 from 20 to 25% when br5 flux was increased from 10 to 50%. For the remaining C positions, raising br5 led to a decrease in CO_2 production (Fig. 1B). A similar pattern was visible for positions C1 and C4 in the model for 90% C flux into PPP (Fig. 1C), it also expressed a sensitivity towards a br5 flux increase as those C positions experienced a relative increase in levels of CO_2 production. Besides these important C positions, the remaining C positions in both model outcomes were respirated less and rather showed a decrease in CO_2 release with increased br5 flux.

2.3.4.3. Prediction of C fluxes through basic metabolism with and without storage

The results from both models (with and without storage flux model fit) were significantly different from each other (Fig. 3, * t- test, $p < 0.05$). However, the relative C fluxes of φ, br1 and br5 or br5*, respectively, showed higher variability in the model with storage. The φ values for low glucose treatments were significantly higher than those of the high glucose treatments regardless of nutrient treatment (Kruskal-Wallis, $p < 0.05$) in both model runs showing a shift from glucose allocation via glycolysis towards PPP with increasing glucose addition. For the br1 flux, representing biomass formation, the model result without storage consideration had significantly lower C flux into br1 in the lower glucose treatments than under high glucose amendment. Nutrient addition caused a significantly lower influx into br1 under "High" glucose amendment in comparison to the treatment

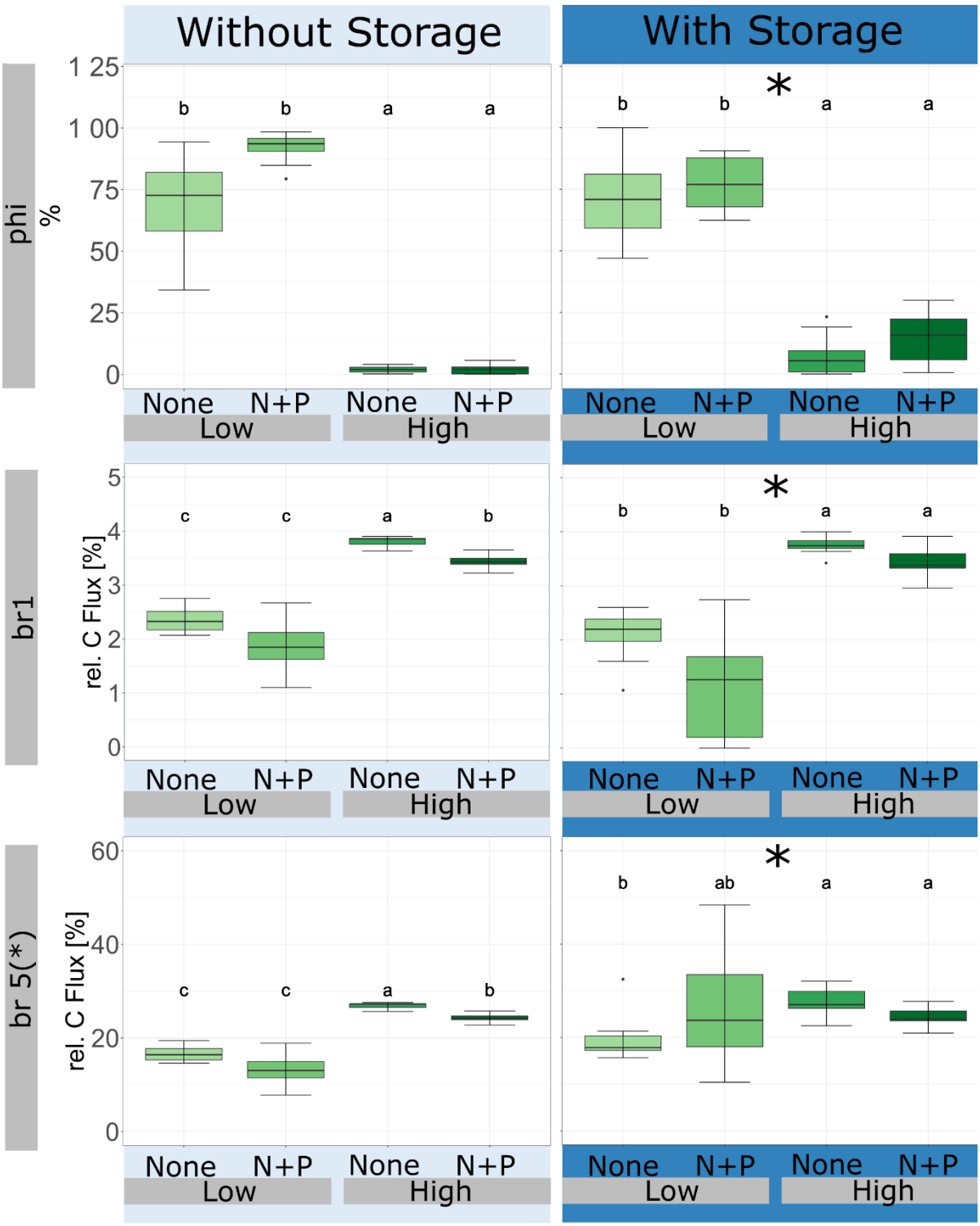

S3 Figure 3: **Comparison of both flux model outcomes** excluding (left) and allowing for (right) storage compound formation. Relative C fluxes into representative metabolic processes: φ (phi) representing the C flux partitioning between glycolysis and PPP towards PPP, br1 as representative flux for biomass formation (letters indicate significant differences $p < 0.05$, Kruskal-Wallis) and br5 as sum of the biomass formation and storage compound formation starting from Acetyl-CoA (Kruskal- Wallis test). Significant differences between models with and without storage compound formation (t-test, see suppl. table 2) are indicated with *.

without addition of nutrients (Fig. 3). Overall, the model result with storage for br1 showed the same pattern with significant differences between the glucose treatments, but without a nutrient effect. The flux br5*, a flux into all biomass products of acetyl-CoA including phospholipid fatty acid (PLFA) and storage compounds (PHB and TAG) formation had significantly lower rates in the “Low” treatments than the “High” ones without a nutrient effect in the model results without consideration of storage compound formation. In the “High” glucose treatments br5 was significantly lower in the treatment with nutrient addition. Flux into br5* was overall higher in the model with storage fit than in the model without storage formation br5 ($p < 0.05$, t-test, Fig. 3, suppl. table 1). Only br5* in “Low None” was significantly lower than br5* in “High” treatments in the storage model.

Correcting the C flow into br5* for the flux that is needed for biomass production (br5), following the stoichiometric precursor ratio approach, yielded finally the flux into storage compound formation represented in figure 4. This revealed that the high biomass flux in the high glucose treatments was nearly solely used for biomass formation irrespective of nutrient addition and no storage compounds were synthesized. Low treatments showed storage production but without a significant nutrient effect although the variety in the “Low N+P” treatment was higher than in the “Low None” treatment.

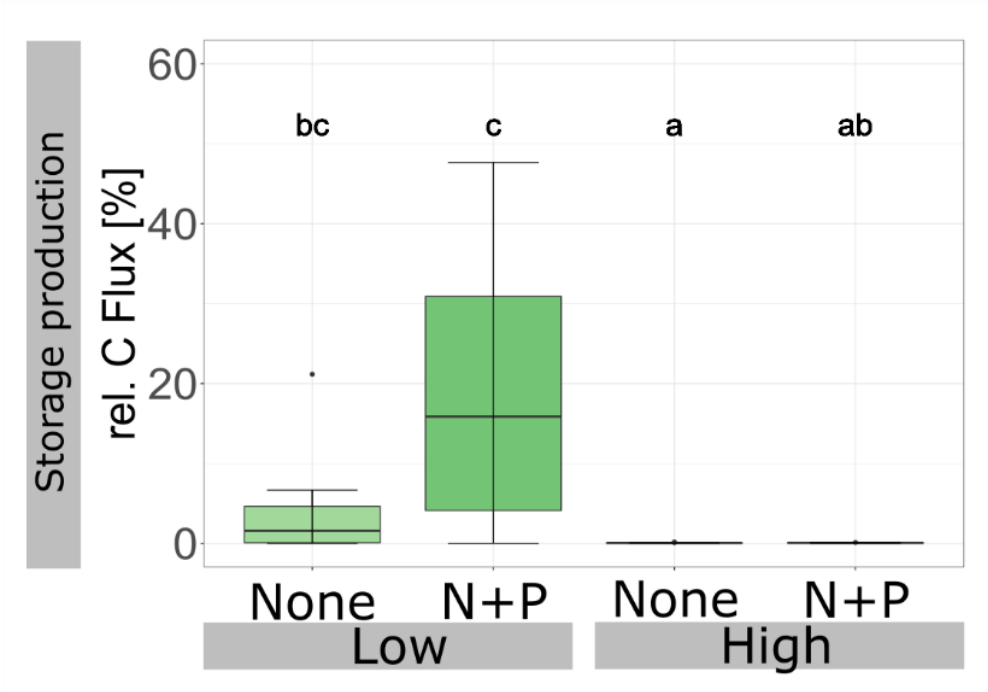

S3 Figure 4: Relative C flux into storage compound synthesis (see equation 3). Letters a-c indicate significant differences determined by Kruskal-Wallis test.

2.3.5. Discussion

2.3.5.1. Metabolism of glucose-induced microbial growth

The glucose and nutrient treatments triggered a significant response of the soil microbial community visible in the overall CO_2 production. CO_2 data demonstrated that in high glucose treatments nutrient addition led to a rapid and most pronounced CO_2 release in the first 24 h of the experiment in contrast to the same "High" treatment without nutrient addition. A clear nutrient effect in high glucose treatments in the overall respiratory CO_2 efflux was not as expressed in the individual metabolic pathways from the flux model results. However, flux modelling offered a more detailed look into the fate of glucose-C into various pathways of the basic C metabolism: Low values of ϕ in both high glucose treatments show a high flux into PPP suggesting an elevated synthesis of compounds required for biomass synthesis such as new DNA. This is backed up by a high flux into the *de novo* formation of biomass (br1) under high glucose amendment.

For both low treatments, slightly elevated C3 and C4 CO_2 production leading to high ϕ values point towards higher glycolysis in these treatments (Suppl. Fig. 1A, B) (Dijkstra et al., 2022). Currently, the flux models do not include the Entner-Doudoroff (ED) pathway, a pathway that yields smaller amounts of ATP and reduction equivalents than glycolysis but starts from glucose-6-phosphate like PPP (Dijkstra et al., 2022; Voet et al., 2008). Dijkstra et al. (2022) have recently shown, that high rates of r9 in models without ED can be misinterpreted as high fluxes into PPP associate to biomass production although it could alternatively represent an increased C allocation through the ED pathway. Dijkstra et al. (2022) suggested a quick qualitative check for quantitatively relevant C fluxes directed into ED versus PPP by the relation of CO_2 production from C positions C2 and C3 from glucose: ED dominance is indicated by a higher proportion of C2 in comparison to C3, *vice versa* flux into PPP is determined by a higher C3 respiration than that of C2. Following this interpretation of CO_2 patterns ED pathway seemed only to be relevant in the high glucose treatment with nutrient addition (Suppl. Fig. 1D), which could be proposedly assigned to a high relative C allocation through gram negative bacteria, which are known for utilizing the ED pathway (Kersters and De Ley, 1968). They are also known as copiotrophs, dealing well with optimum conditions in a high C environment (Fierer et al., 2007). Future modelling efforts should therefore implement the ED into their flux models especially when contrasting C availability scenarios shall be studied. Furthermore, it seems necessary to combine flux models of soil microbial communities with state-of-the-art metagenomic and metatranscriptomic methods to identify ED enzyme sequences and the community members responsible for their expression.

Treatments without nutrient addition showed a trend towards a higher br1 flux i.e., formation of new biomass. Besides biomass formation, this could also point towards the synthesis of nutrient mining enzymes to gain nutrients from SOM and therefore ensure cellular maintenance without growth. The

model is not able to distinguish the production of exoenzymes from the production of structural or functional proteins involved in cellular replicative growth and both scenarios may lead to such a slightly enhanced br1 flux. The model's underestimation of those exoenzyme therefore might have led to an underrepresentation of fungi and other bacteria with the metabolic preferences for e.g. complex polymeric compounds like microbial necromass or sorbed substrates, thus showing a microbial response to glucose addition be dominated by microorganisms with capabilities for rapid and efficient glucose metabolism, predominantly gram negative bacteria (Apostel et al., 2018; Kashi et al., 2022). This suggest future environmentally applicable metabolic flux models to be extended for the vast variety of substrates included in the highly diverse organic matter in ecosystems. (Dijkstra et al., 2022, 2011c).

2.3.5.2. Glucose induces reserve storage but no surplus storage.

It is most likely that the microbial community in high glucose treatments is growing by cell division rather than building up a surplus storage supply as suggested by Mason-Jones et al. (2021) and Manzoni et al. (2021). We rather observed the contrasting scenario, i.e., that storage compound synthesis in both high glucose treatments was completely shut down in our model (Fig. 4). In contrast to the high glucose treatments, in both low treatments the microbial community shifted its basic C metabolism to glycolysis, maintaining their existence but also directing their C flux into the synthesis of storage compounds rather than investing into growth through cell division like the community with excess glucose. The addition of the option for storage compound formation into the flux model proofed itself to have a significant effect on the C fluxes of the basic glucose metabolism of the soil microbial community. However, *de novo* synthesis of biomass was of higher relevance for high glucose treatments, whereas storage compound synthesis appeared to play an important role in low glucose treatments. There, the soil microbial community relied on cell maintenance with a high C flux rate into glycolysis, represented via a high ϕ, from which a high proportion with up to 50 % of C is directing towards storage formation. This creates a reserve storage pool to save resources for a later use while competing with the rest of microbial metabolism. Reserve storage is considered as a resource deposit for future needs, e.g. insurance against environmental changes (Manzoni et al., 2021). Declining CO_2 efflux (Fig. 2) in the low glucose treatments before the 24 h mark suggest that reserve storage has already been synthesized, therefore the measured $^{13}CO_2$ for low glucose treatments as model input had already depleted glucose isotopomere tracer sources so that the effect of low glucose concentrations could be underestimated at the 24 h. An earlier time point for modelling low glucose treatments would therefore be necessary. Most likely, microbiomes of rather C poor soils, as intentionally selected for this experiment, exhibit a rather high threshold of C addition required to induce replicative growth, whereas a moderate increase in C availability may rather be used for storage

formation preventing for frequent and extended periods of C starvation they are used to (Bååth, 2003; Matin et al., 1979).

The addition of nutrients did not have a significant effect on the microbial communities' investment into biomass. Nutrient addition in C limited conditions had a favorable effect on storage formation when soil microbial communities built up reserve storage (Bååth, 2003; Dijkstra et al., 2022). The here applied flux models with and without storage compound adjustment were unable to differentiate between bacterial or fungal groups and their different ecological roles in a soil microbial community so that different ecological niches such as C nutrient sources were not considered. Thus, it cannot be finally stated whether the whole community profited from the added glucose as C source or only single bacterial groups which profited most from the addition of glucose (Dijkstra et al., 2011c). Others, e.g. *Actinobacteria* are known to gain energy from necromass and would rather display ^{13}C labelled compound uptake from dead bacteria previously fed on the added glucose (Apostel et al., 2018). However, we chose our experimental period with 96 h rather short to avoid such secondary, food-web C utilization in the observed position specific patterns, as e.g. Apostel et al. (2018) demonstrated necromass C incorporation to occur only after 10 days approximately. Nevertheless, it is necessary to identify key role players in the soil microbial community and advance with metabolic tracing techniques towards a resolution of individual community members contribution to the overall microbiomes' metabolic fluxes (Wu et al., 2020). Additionally, it is essential to couple the storage compound adjusted flux model with high-throughput molecular biological metagenomics and metatranscriptomics techniques to reveal their composition and active enzyme repertoire carrying out the here quantified functions of the basic C metabolism. Furthermore, interpreting modelled C fluxes should not solely rely on measured $^{13}CO_2$ data, but also be accompanied by measuring key metabolites such as storage compounds (PHB, TAG) (Bååth, 2003; Mason-Jones et al., 2019) or phospholipid fatty acids (PLFA) and ^{18}O DNA for differencing between replicative or storage growth in microbial communities (Spohn et al., 2016).

2.3.6. Conclusion

Like any microbial communities, soil microbes have various methods in gaining (and storing) energy from SOM where glycolysis and pentose-phosphate pathway are not the only pathways how monomers enter basic C metabolism. The Entner-Doudoroff pathway appears to be a frequently used metabolism mode in microorganisms under certainly high C concentrations and therefore needs be included into flux models (Dijkstra et al., 2015). Furthermore, Mason-Jones et al. (2021) proclaimed to

also take extracellular polymeric substances (EPS) as significant sink of microbial C into account – a compound class with many functional roles but which could also serve as microbial storage.

The recent proofs of high relevance of reserve and surplus storage as quantitative biomass compound, makes it essential to implement the process of storage compound formation into metabolic flux modelling. Our flux model could demonstrate that C is directed towards storage synthesis depending on the stoichiometric conditions.

Contradicting the rather widespread understanding that high C input will result in build-up of surplus storage and that surplus storage is the dominant storage mode of microbes, our model could not confirm storage synthesis from excess glucose addition. On the other hand, reserve storage formation in low glucose treatments was clearly predicted by our metabolic flux model and could be an ecological adaptation to strongly C limited soils with long bare-soil periods without C input throughout the cropping season.

2.3.7. References

Alvarez, H.M., Steinbüchel, A., 2002. Triacylglycerols in prokaryotic microorganisms. Applied Microbiology and Biotechnology 60, 367–376. https://doi.org/10.1007/s00253-002-1135-0

Apostel, C., Dippold, M., Kuzyakov, Y., 2015. Biochemistry of hexose and pentose transformations in soil analyzed by position-specific labeling and 13C-PLFA. Soil Biology and Biochemistry 80, 199–208. https://doi.org/10.1016/j.soilbio.2014.09.005

Apostel, C., Herschbach, J., Bore, E.K., Spielvogel, S., Kuzyakov, Y., Dippold, M.A., 2018. Food for microorganisms: Position-specific 13 C labeling and 13 C-PLFA analysis reveals preferences for sorbed or necromass C. Geoderma 312, 86–94. https://doi.org/10.1016/j.geoderma.2017.09.042

Bååth, E., 2003. The Use of Neutral Lipid Fatty Acids to Indicate the Physiological Conditions of Soil Fungi. Microbial Ecology 45, 373–383.

Dijkstra, P., Blankinship, J.C., Selmants, P.C., Hart, S.C., Koch, G.W., Schwartz, E., Hungate, B.A., 2011a. Probing carbon flux patterns through soil microbial metabolic networks using parallel position-specific tracer labeling. Soil Biology and Biochemistry 43, 126–132. https://doi.org/10.1016/j.soilbio.2010.09.022

Dijkstra, P., Dalder, J.J., Selmants, P.C., Hart, S.C., Koch, G.W., Schwartz, E., Hungate, B.A., 2011b. Modeling soil metabolic processes using isotopologue pairs of position-specific 13C-labeled glucose and pyruvate. Soil Biology and Biochemistry 43, 1848–1857. https://doi.org/10.1016/j.soilbio.2011.05.001

Dijkstra, P., Salpas, E., Fairbanks, D., Miller, E.B., Hagerty, S.B., van Groenigen, K.J., Hungate, B.A., Marks, J.C., Koch, G.W., Schwartz, E., 2015. High carbon use efficiency in soil microbial communities is related to balanced growth, not storage compound synthesis. Soil Biology and Biochemistry 89, 35–43. https://doi.org/10.1016/j.soilbio.2015.06.021

Dijkstra, P., Thomas, S.C., Heinrich, P.L., Koch, G.W., Schwartz, E., Hungate, B.A., 2011c. Effect of temperature on metabolic activity of intact microbial communities: Evidence for altered metabolic pathway activity but not for increased maintenance respiration and reduced carbon use efficiency. Soil Biology and Biochemistry 43, 2023–2031. https://doi.org/10.1016/j.soilbio.2011.05.018

Dijkstra, P., Wu, W., Dippold, M., Schwartz, E., Hungate, B., Megonigal, P., Thomas, S., Seymour, C., Martinez, A., 2022. On Maintenance and Metabolisms in Soil Microbial Communities (preprint). In Review. https://doi.org/10.21203/rs.3.rs-1193625/v1

Fierer, N., Bradford, M.A., Jackson, R.B., 2007. Toward an Ecological Classification of Soil Bacteria. Ecology 88, 1354–1364.

Gunina, A., Dippold, M.A., Glaser, B., Kuzyakov, Y., 2014. Fate of low molecular weight organic substances in an arable soil: From microbial uptake to utilisation and stabilisation. Soil Biology and Biochemistry 77, 304–313. https://doi.org/10.1016/j.soilbio.2014.06.029

Hagerty, S.B., van Groenigen, K.J., Allison, S.D., Hungate, B.A., Schwartz, E., Koch, G.W., Kolka, R.K., Dijkstra, P., 2014. Accelerated microbial turnover but constant growth efficiency with warming in soil. Nature Clim Change 4, 903–906. https://doi.org/10.1038/nclimate2361

Harwood, J.L., Russell, N.J., 1984. Lipids in Plants and Microbes. Springer Netherlands, Dordrecht. https://doi.org/10.1007/978-94-011-5989-0

Kashi, H., Loeppmann, S., Herschbach, J., Schink, C., Imhof, W., Kouchaksaraee, R.M., Dippold, M.A., Spielvogel, S., 2022. Size matters: biochemical mineralization and microbial incorporation of dicarboxylic acids in soil. Biogeochemistry. https://doi.org/10.1007/s10533-022-00990-0

Kersters, K., De Ley, J., 1968. The occurrence of the Entner-Doudoroff pathway in bacteria. Antonie van Leeuwenhoek 34, 393–408. https://doi.org/10.1007/BF02046462

Klingner, A., Bartsch, A., Dogs, M., Wagner-Döbler, I., Jahn, D., Simon, M., Brinkhoff, T., Becker, J., Wittmann, C., 2015. Large-Scale ^{13} C Flux Profiling Reveals Conservation of the Entner-Doudoroff Pathway as a Glycolytic Strategy among Marine Bacteria That Use Glucose. Appl. Environ. Microbiol. 81, 2408–2422. https://doi.org/10.1128/AEM.03157-14

Kuzyakov, Y., Blagodatskaya, E., 2015. Microbial hotspots and hot moments in soil: Concept & review. Soil Biology and Biochemistry 83, 184–199. https://doi.org/10.1016/j.soilbio.2015.01.025

López, N.I., Pettinari, M.J., Nikel, P.I., Méndez, B.S., 2015. Polyhydroxyalkanoates, in: Advances in Applied Microbiology. Elsevier, pp. 73–106. https://doi.org/10.1016/bs.aambs.2015.06.001

Manzoni, S., Ding, Y., Warren, C., Banfield, C.C., Dippold, M.A., Mason-Jones, K., 2021. Intracellular Storage Reduces Stoichiometric Imbalances in Soil Microbial Biomass – A Theoretical Exploration. Front. Ecol. Evol. 9, 714134. https://doi.org/10.3389/fevo.2021.714134

Mason-Jones, K., Banfield, C.C., Dippold, M.A., 2019. Compound-specific ^{13} C stable isotope probing confirms synthesis of polyhydroxybutyrate by soil bacteria. Rapid Commun Mass Spectrom 33, 795–802. https://doi.org/10.1002/rcm.8407

Mason-Jones, K., Breidenbach, A., Dyckmans, J., Banfield, C.C., Dippold, M.A., 2022. Intracellular carbon storage by microorganisms is an overlooked pathway of biomass growth (preprint). Ecology. https://doi.org/10.1101/2022.06.28.497677

Mason-Jones, K., Robinson, S.L., Veen, G.F., Manzoni, S., van der Putten, W.H., 2021. Microbial storage and its implications for soil ecology. ISME J. https://doi.org/10.1038/s41396-021-01110-w

Matin, A., Veldhuis, C., Stegeman, V., Veenhuis, M., 1979. Selective Advantage of a Spirillum sp. in a Carbon-limited Environment. Accumulation of Poly- -hydroxybutyric Acid and Its Role in Starvation. Journal of General Microbiology 112, 349–355. https://doi.org/10.1099/00221287-112-2-349

Pieper, U., 1993. Biosynthesis of a copolymer from 3-hydroxybutyric acid and 3-hydroxyvalerianic acid in Rhodococcus ruber NCIMB 40126. Unitext.

Rasse, D.P., Rumpel, C., Dignac, M.-F., 2005. Is soil carbon mostly root carbon? Mechanisms for a specific stabilisation. Plant Soil 269, 341–356. https://doi.org/10.1007/s11104-004-0907-y

Rinnan, R., Bååth, E., 2009. Differential Utilization of Carbon Substrates by Bacteria and Fungi in Tundra Soil. Appl Environ Microbiol 75, 3611–3620. https://doi.org/10.1128/AEM.02865-08

Spohn, M., Klaus, K., Wanek, W., Richter, A., 2016. Microbial carbon use efficiency and biomass turnover times depending on soil depth – Implications for carbon cycling. Soil Biology and Biochemistry 96, 74–81. https://doi.org/10.1016/j.soilbio.2016.01.016

Voet, D., Voet, J.G., Pratt, C.W., 2008. Fundamentals of biochemistry: life at the molecular level, 3rd ed. ed. Wiley, Hoboken, NJ.

Wu, W., Dijkstra, P., Dippold, M.A., 2020. 13C analysis of fatty acid fragments by gas chromatography mass spectrometry for metabolic flux analysis. Geochimica et Cosmochimica Acta 284, 92–106. https://doi.org/10.1016/j.gca.2020.05.032

Zamboni, N., Fendt, S.-M., Rühl, M., Sauer, U., 2009. 13C-based metabolic flux analysis. Nat Protoc 4, 878–892. https://doi.org/10.1038/nprot.2009.58

2.4. Study 4: Intracellular carbon storage by microorganisms is an overlooked pathway of biomass growth.

Kyle Mason-Jones[1,2]*, Andreas Breidenach[2,3], Jens Dyckmans[4], Callum C. Banfield[2,3], Michaela A. Dippold[2,3]*

[1] Department of Terrestrial Ecology, Netherlands Institute of Ecology (NIOO-KNAW), Wageningen, the Netherlands.

[2] Biogeochemistry of Agroecosystems, Department of Crop Sciences, Georg-August University of Göttingen, Göttingen, Germany.

[3] Geo-Biosphere Interactions, Department of Geosciences, University of Tübingen, Tübingen, Germany.

[4] Centre for Stable Isotope Research and Analysis, Georg-August University of Göttingen, Göttingen, Germany.

*Corresponding author E-mail address: k.masonjones@nioo.knaw.nl; michaela.dippold@uni-tuebingen.de

2.4.1. Abstract

The concept of biomass growth is central to microbial carbon (C) cycling and ecosystem nutrient turnover. Microbial biomass is usually assumed to grow by cellular replication, despite microorganisms' capacity to increase biomass by synthesizing storage compounds. Resource investment in storage allows microbes to decouple their metabolic activity from immediate resource supply, supporting more diverse microbial responses to environmental changes. Here we show that microbial C storage in the form of triacylglycerides (TAGs) and polyhydroxybutyrate (PHB) contributes significantly to the formation of new biomass, i.e., growth, under contrasting conditions of C availability and complementary nutrient supply in soil. Together these compounds can comprise a C pool 0.19 ± 0.03 to 0.46 ± 0.08 times as large as extractable soil microbial biomass and reveal up to 279 ± 72% more biomass growth than observed by a DNA-based method alone. Even under C limitation, storage represented an additional 16–96% incorporation of added C into microbial biomass. These findings encourage greater recognition of storage synthesis as a key pathway of biomass growth and an underlying mechanism for resistance and resilience of microbial communities facing environmental change.

2.4.2. Introduction

Microbial assimilation of organic resources is crucial to the flow of C and other nutrients through ecosystems. Soil heterotrophs perform key steps in terrestrial carbon (C) and nutrient cycles, yet how microorganisms use the available organic resources and regulate their allocation to competing metabolic demands remains a subject of research and debate (Dijktra et al., 2015, Geyer et al., 2019, Sokol et al, 2022). Microbial assimilation of organic C into an organism is conceptualized as biomass growth. This is frequently understood as synonymous with an increase in individuals, in other words, the replicative growth of microbial populations. However, many microorganisms are capable of storage, defined as the accumulation of chemical resources in particular forms or compartments to secure their availability for future use by the storing organism (Mason-Jones et al., 2021). Various microbial storage compounds are known, among them polyhydroxybutyrate (PHB) and triacylglycerides (TAGs) (López et al., 2015, Murphy, 2012). These two C-rich storage compounds are of particular interest as they are accumulated by diverse microbial taxa (Mason-Jones et al., 2021) and methods are available for their measurement in soil (Banfield et al., 2017, Mason-Jones et al., 2019). These are both hydrophobic lipids that are stored as inclusion bodies in the cytosol (i.e., intracellular lipid droplets) (Murphy, 2012). PHB is a high-molecular-weight polyester of β-hydroxybutyrate, while TAGs consist of three fatty acids (of diverse structures) esterified to a glycerol backbone (Mason-Jones et al., 2021). PHB storage is only known among bacteria, while TAGs are accumulated by both bacteria

and fungi (Mason-Jones et al., 2021). Biosynthesis of PHB has been demonstrated by compound-specific measurement in soil (Mason-Jones et al., 2019) and TAGs in marine and soil systems show responsiveness to resource supply consistent with a C-storage function (Bååth et al., 2003, Becker et al., 2018). Microbial storage could substantially influence microbial fluxes of C and other nutrients (Manzoni et al., 2021), changing our understanding of soil biogeochemical fluxes and their response to environmental changes. Biomass growth is a cornerstone concept at scales from the ecological stoichiometry of individual cells to microbially-explicit models of the C cycle (Manzoni & Poporato, 2009, Wieder et al., 2015), and for defining the nutrient demands of organisms and their productivity (Manzoni & Poporato, 2009). Accumulation of storage compounds corresponds to an increase in microbial biomass without replication, and therefore represents an alternative pathway for growth that is not usually considered in the C cycle. There is therefore a need to assess how severely the omission of storage may bias our understanding of C assimilation and utilization (Mason-Jones et al., 2021). Conventional measurement of soil microbial biomass uses fumigation with chloroform to lyse cells, followed by extraction of the released biomass into an aqueous solution for measurement (chloroform fumigation-extraction, CFE) (Vance et al., 1987). This method assumes a proportionality between extractable and non-extractable biomass (Jenkinson et al., 2004). Other measures in widespread use are proxies such as cell membrane lipids or substrate-induced respiration (Anderson & Domsch, 1978, Baily et al., 2002, Zelles et al. 1995). Only CFE provides biomass in units of C, however, and these other methods are typically calibrated against it. However, hydrophobic storage compounds like PHB and TAGs are not extractable in aqueous solution and are therefore overlooked by CFE. Furthermore, there is no biological reason to expect proportionality between these storage compounds and any of the conventional biomass proxies. DNA-based measures of microbial abundance and replication also do not capture storage (Blaszewicz & Schwartz, 2011, Spohn et al., 2016), since it is not expected to form a constant proportion of each cell's biomass. Interpretation of microbial storage patterns is facilitated by distinguishing two storage modes, which represent the end-members on a gradient of storage strategies (Chapin et al., 1990, Mason-Jones et al., 2021). Surplus storage is the accumulation of resources that are available in excess of immediate needs, at little to no opportunity cost, while reserve storage accumulates limited resources at the cost of other metabolic functions. Surplus storage of C would be predicted under conditions of C oversupply, when replicative growth is constrained by other factors such as nutrient limitation. Reserve storage, on the other hand, indicates that storage may also occur under C-limited conditions. The evidence assembled from pure culture studies confirms the operation of both storage modes among microorganisms (Kourmentza et al., 2017, Mason-Jones et al., 2021, Matin et al., 1979, Poblete-Castro et al., 2012). Here we experimentally investigate the importance of microbial storage in soil, and show how storage

responses to resource supply and stoichiometry can advance our understanding of resource allocation and microbial biomass growth. We hypothesized as follows:

1. Microbial storage compounds are a quantitatively important pool of soil microbial biomass under C-replete, nutrient-limited conditions.

2. Microbial biomass growth is substantially underestimated by neglecting intracellular storage synthesis.

3. Due to low opportunity costs, surplus storage is likely to be quantitatively more important than reserve storage when measured across an entire soil community. Therefore, nutrient supplementation (N, P, K, and S) will suppress storage compound accumulation in favour of replicative growth.

Soil microcosms were incubated under controlled conditions, with C availability manipulated through additions of isotopically labelled (^{13}C and ^{14}C) glucose, which is common in soil, including as a component of plant root exudates and the most abundant product of plant-derived organic matter decomposition (Gunina & Kuzyakov, 2015). A combined nutrient treatment (N, P, K, and S) provided inorganic fertilizers common in agriculture. A fully crossed design included three levels of C addition (zero-C, low-C and high-C; 0, 90 and 400 μg C g^{-1} soil) and two levels of nutrient supply (no-nutrient and nutrient-supplemented) with nutrients added at a level predicted to enable full C assimilation under the high-C treatment, based on microbial biomass C:N:P ratios typical of agricultural soil (Xu et al., 2013) and an assumed C-use efficiency of 50%. CO_2 efflux and its isotopic composition was monitored at regular intervals. Microcosms were harvested after 24 and 96 h, with these incubation times selected to balance the synthesis of storage (previously observed over a timeframe of days, Mason-Jones et al., 2019) with the risk of artefacts induced by recycling of labelled biomass (Blazewicz & Schwartz, 2011). Harvested soil was analyzed for microbial biomass (by CFE), dissolved organic carbon (DOC), dissolved nitrogen (DN) and the storage compounds PHB and TAGs. In parallel, a set of smaller microcosms (0.5 g soil) was incubated under otherwise identical conditions to measure microbial growth as the incorporation of ^{18}O from $H_2{}^{18}O$ into DNA (Spohn et al., 2016). This method captures replicative growth better than tracing specific C substrates. Together these provide integrated observations of heterotrophic microbial biomass, growth, and storage in a natural microbiome, examining the importance of storage as a resource-use strategy in response to environmental resource supply and changes in element stoichiometry.

2.4.3. Results and Discussion*Microbial nutrient limitations and CO2 efflux*

We first describe observed patterns of soil respiration and dissolved nutrients that aid interpretation of the prevailing resource limitations during storage compound synthesis and degradation. Glucose

addition stimulated large increases in CO_2 efflux (Fig. 1), primarily derived from glucose mineralization (Fig. 1B). Nutrient supplementation barely affected CO_2 efflux rates from the zero- or low-C additions and for none of the zero- or low-C treatments was N availability (measured as DN) significantly reduced relative to the control at 24 h (Supplementary Fig. S1A, B). Thus, C limitation dominated in the zero- and low-C treatments throughout the experimental period, irrespective of nutrient additions.

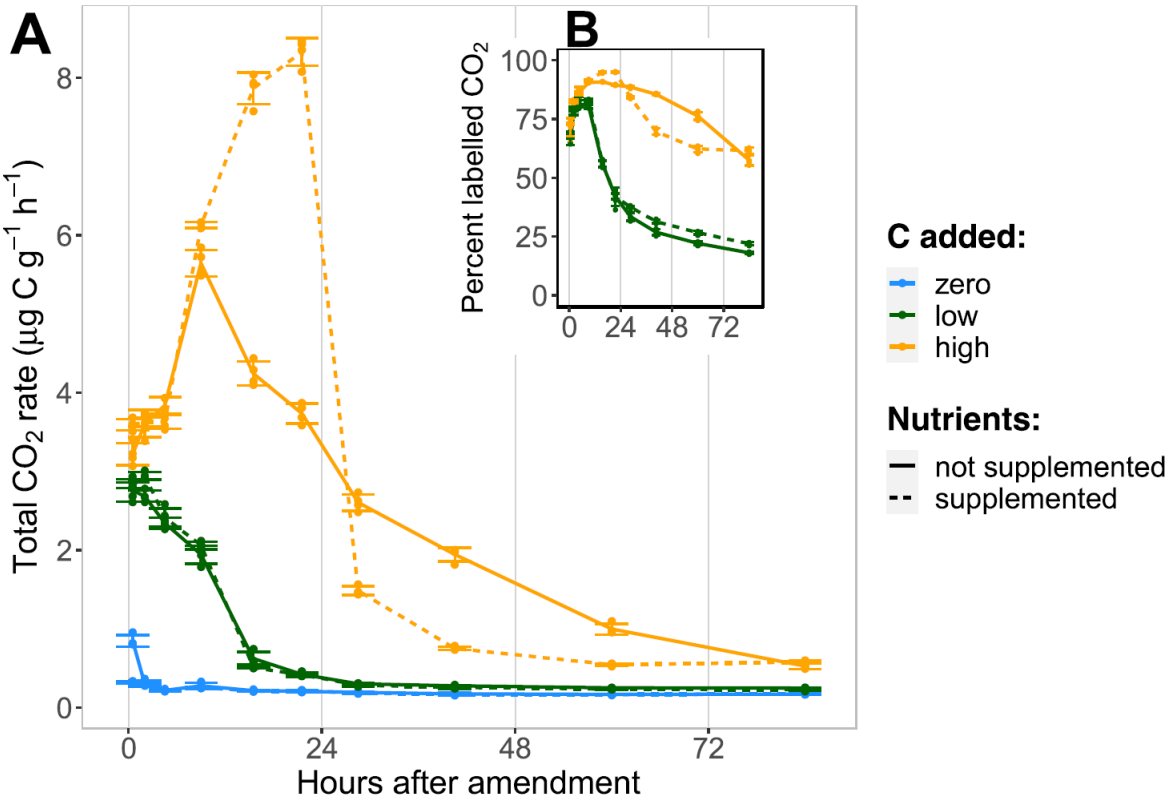

S4 Figure 1: **Time-series of the CO_2 efflux from soil microcosms. A** Total CO_2 efflux following addition of a readily degradable ^{13}C-labelled carbon source (glucose at 0, 90, and 400 µg C g^{-1} soil) with or without mineral nutrient supply (N, P, K, S). Each point reflects the average rate of CO_2 efflux at the mid-point of the sampling interval. **B** Percent of total CO_2 derived from the added glucose. Error bars show standard deviation (n = 4 independent soil microcosms).

With high-C addition, CO_2 efflux rates under the two nutrient levels diverged strongly after 12 h, with the no-nutrient treatment declining steadily from 12 h until the end of the experiment. This early decline in mineralization was consistent with the onset of nutrient limitation, after microbial growth on the added glucose had depleted easily available soil nitrogen and driven up the C:N ratio of dissolved resources (Supplementary Fig. S1). This depletion in the high-C, no-nutrient treatment was reflected in suppressed DN after 24 h, with only 35.8 – 62.5% of the zero-C, no-nutrient control (family-wise 95% confidence interval; Supplementary Fig. S1). Nutrient limitation was accompanied by an accumulation of highly labelled DOC at 24 h in the soil solution, reflecting unused glucose or soluble

by-products in an amount 19.6 ± 2.1% (mean ± standard deviation) of the original C addition (Supplementary Fig. S2). Therefore, high C addition without supplementary nutrients resulted in rapid mineralization at first, but nutrient limitation set in within 12 h and continued for the remaining experimental period.

Nutrient addition had a strong effect in combination with high-C supply: it accelerated glucose mineralization until 24 h after addition (Fig. 1), after which CO_2 efflux dropped precipitously to below that of the high-C, no-nutrient treatment. For this high-C, nutrient supplemented treatment, dissolved N decreased only moderately over 24 h (56.2 – 97.9% relative to the zero-C, no-nutrient treatment). With high-C addition after 24 h, DOC was far lower with nutrient supplementation than without (Cohen's d >> 1, family-wise $p < 0.001$), and DOC level for this treatment did not change further to 96 h, despite having higher N availability at 24 h than the no-nutrient treatment (Cohen'sd»1, family-wise $p < 0.001$). This indicates that the microbial community had depleted the added C and re-entered C-limited conditions. Therefore, high C addition with supplementary nutrients maintained rapid C mineralization through the first 24 h, but glucose depletion then reasserted C-limitation for the rest of the experimental period.

2.4.3.2. Presence and synthesis of microbial compounds

PHB and TAGs were both found in the control soil (zero-C, no nutrients after 24 h; Fig. 2A, C), together representing a C pool 0.25 ± 0.03 (mean ± standard deviation) times as large as the extractable microbial biomass C (MBC, by CFE; Fig. 3). This ratio of stored C (PHB + TAG) to extractable MBC ranged from 0.19 ± 0.02 to 0.46 ± 0.08 over all treatments, indicating that storage is a significant pool of biomass not only under C-replete conditions, as hypothesized, but even when C availability is limited. Furthermore, the common measures of soil microbial biomass rely on extraction of water-soluble C after chloroform fumigation, which does not capture these highly hydrophobic storage compounds. This suggests that microbial biomass C may be widely underestimated in soil and calls for methodological advancements to more systematically capture these (and possibly other) storage compounds in assessments of microbial growth.

The two storage compounds were both responsive to the supply of C and complementary nutrients ($p < 0.01$), but with very different behaviors. At both timepoints, the low input of C stimulated only a moderate increase in total PHB, irrespective of nutrient supply. In contrast, high C input stimulated a large increase in PHB, particularly when not supplemented with nutrients (a 308% increase over the zero-glucose, no-nutrient treatment at 96 h, with Hodges-Lehmann median difference of 36.0–42.9 µg C g^{-1}). In comparison, extractable biomass reflected a non-significant mean difference of only 33% between these treatments. Nutrient supply significantly suppressed PHB storage, even in the absence

of added C (nutrient main effect, robust ANOVA of medians 24 h: $F_{(1,\infty)}$ =35, p <0.001; 96h: $F_{(1,\infty)}$ =275, p < 0.001). Isotopic composition (^{13}C) indicated that assimilation of glucose C into new PHB continued

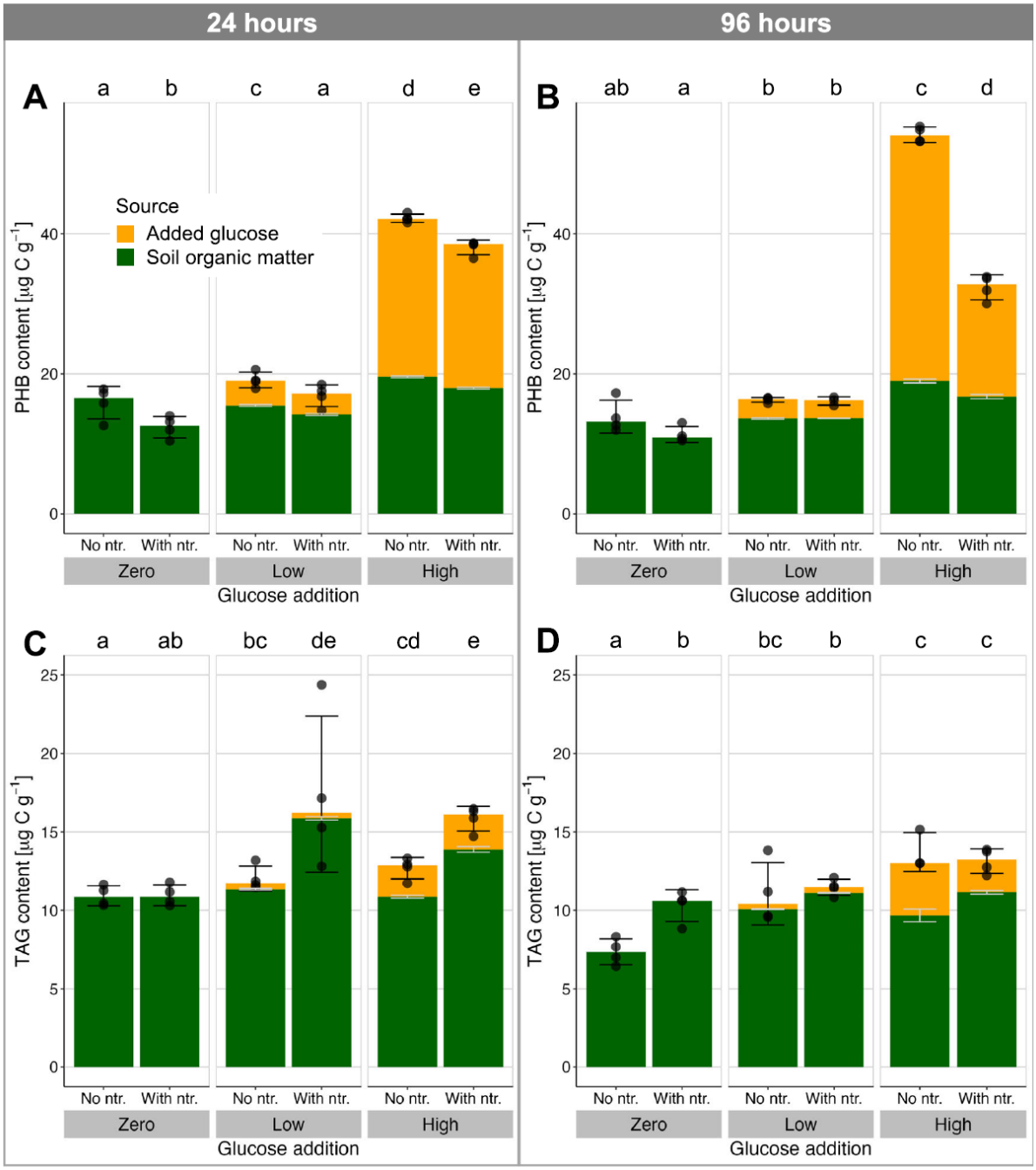

S4 Figure 2: **Response of soil microbial storage to organic carbon and nutrient supply.** Storage compounds PHB **A**, **B** and TAGs **C**, **D** in soil 24 h **A**, **C**, and 96h **B**, **D** after addition of a readily degradable, ^{13}C-labelled carbon source (glucose at 0, 90 and 400 µg C g^{-1} soil) with or without mineral nutrient supply (ntr.; N, P, K, S). The source of the stored C is shown in contrasting colors as determined by isotopic composition, with light grey error bars reflecting mean ± standard deviation of the relative composition. Black error bars show mean ± standard deviation of the total storage compound pools, while color bar heights show medians, as used in the robust analysis of medians (n = 4 independent soil microcosms, except for 1 treatment in each of TAGs and

PHB where n = 3). Lowercase letters above the plots show post-hoc differences in total storage with $p < 0.05$ (2-sided pairwise comparison of medians with Benjamini-Hochberg adjustment for multiple comparisons).

between 24 and 96 h under the nutrient-limited conditions of the high-C, no-nutrient treatment (Hodges-Lehmann median difference of 10.2–13.3 µg C g^{-1}, 95% confidence interval), while extractable microbial biomass C showed no significant change. For the high-C, nutrient-supplemented treatment, the increased C limitation after 24 h induced degradation of PHB during this later incubation period (median reduction of 2.7–8.6 µg C g^{-1}). The PHB storage pool therefore responded dynamically to shifts in resource stoichiometry on a timescale of hours to days, with changes as expected from a surplus storage strategy. These observations are consistent with PHB biosynthesis in pure culture (Sekar et al., 2020), which is stimulated by excess C availability in diverse bacterial taxa (Kourmentza et al., 2017). This study demonstrates such microbial storage dynamics in a terrestrial ecosystem. At the end of the incubation, stored C across the various treatments was sufficient to support 109 – 347 h of microbial respiration at the CO_2 efflux rate of the zero-C, no-nutrient treatment (i.e., basal respiration). Much longer periods would be envisaged if accompanied by strong downregulation of energy use in response to the stress (Dijkstra et al., 2022). Storage could thus be a crucial resource for withstanding starvation or other stress. A surplus storage strategy is particularly effective at buffering microbial activity by levelling out fluctuations in resource availability and stoichiometry (Manzoni et al., 2021). Furthermore, storage representing a substantial proportion of biomass offers a resource for regrowth following disturbance, indicating a potential role of storage in supporting resilience of this soil microbial community. In these ways, the resources stored in PHB could support the resistance and resilience of this soil microbial community against environmental disturbance (Mason-Jones et al., 2021).

Storage of TAGs was enhanced by C input (Fig. 2C, D), but its response to resource stoichiometry differed greatly from PHB. Over 24 h, nutrient supplementation stimulated more TAG accumulation, rather than suppressing it (main nutrient effect $F_{(1,\infty)} = 10.8$, $p = 0.001$ and nutrient:glucose interactions between zero-C and the two C-supplemented treatments, both $p < 0.01$), while over 96 h, nutrient supply had little effect with C addition and increased TAGs when C was not added (95% confidence interval for Hodges-Lehmann median difference 0.5 – 4.7 µg C g^{-1}). The TAG response to C and nutrient supply over 96 h resembled changes in extractable microbial biomass (Fig. 3), which was increased by C supply but not significantly enhanced by nutrients (ANOVA main effect of C supply at 96 h: $F_{(2,17)} = 7.1$, $p = 0.006$). Therefore, unlike PHB, TAG synthesis was not stimulated by a stoichiometric surplus of available C, suggesting a reserve storage function for this compound. Notably, the relative allocation of glucose C between PHB and TAG remained relatively constant (PHB:TAG ratio of glucose-derived C ranged between 7.0 and 11.5 across all treatments) because the C source used for TAG biosynthesis

varied more strongly than total TAG levels in response to C supply. This corroborates a reserve storage function of TAG, with total storage synthesis regulated independently of C supply and drawing on

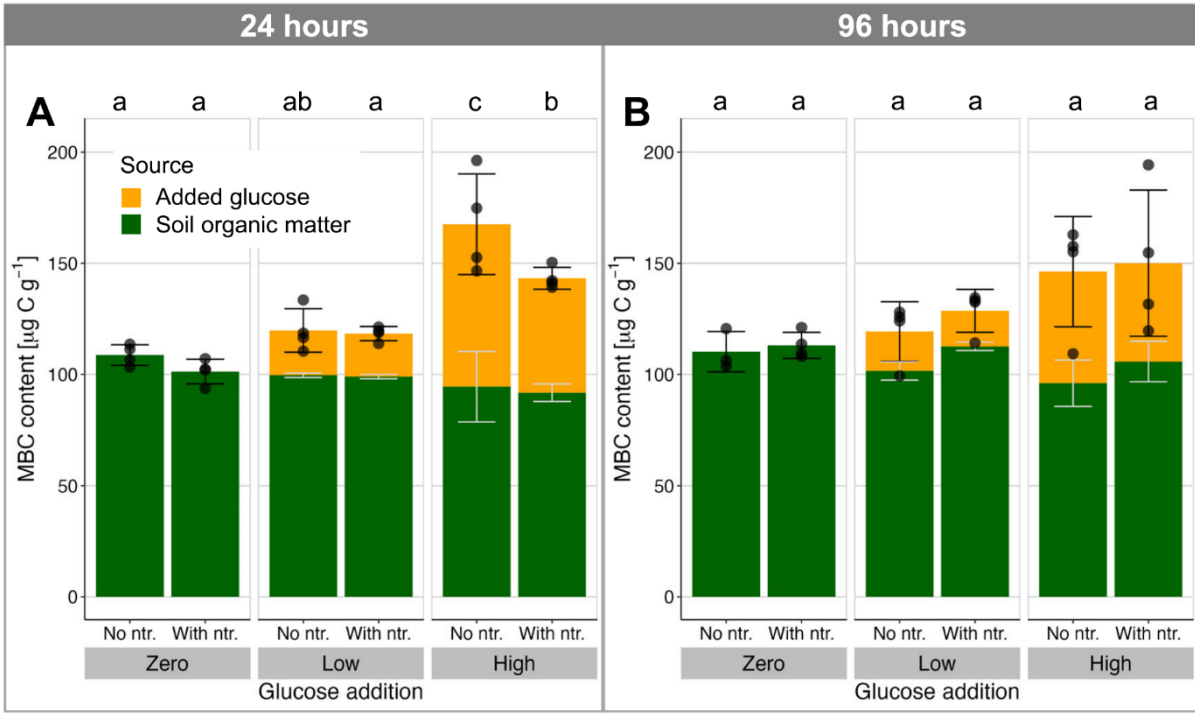

S4 Figure 3: **Extractable soil microbial biomass determined by chloroform fumigation-extraction. A** 24 h and **B** 96 h after addition of a readily degradable, ^{13}C-labelled carbon source (glucose at 0, 90, and 400 µg C g^{-1} soil) with or without mineral nutrient supply (ntr.; N, P, K, S). The heights of the bars represent the mean ± standard deviation as black error bars (n = 4 independent soil microcosms except for one treatment with n = 3: zero glucose, no nutrients at 96 h). Contrasting colors reflect the source of the extractable biomass as determined by isotopic composition, with light grey error bars showing mean ± standard deviation of the relative composition. Lowercase letters above the plots show post-hoc differences in mean total storage with $p < 0.05$ (2-sided Tukey HSD test, which adjusts for multiple comparisons). Corresponding C:N ratios are presented in Supplementary Fig. S3.

whichever C resources are available, whether glucose- or soil-derived. One advantage of a reserve storage strategy is that strategic stores are assembled even under conditions of chronic resource shortage. This allows for bursts of activity to support, for example, reproduction or transition to a resilient starvation state (Mason-Jones et al., 2021). Therefore, while reserve storage may be quantitatively smaller than surplus storage (reflected here in the lower amounts and changes in TAG relative to PHB; Fig. 2), it can help communities to persist under conditions of sustained stress, and even exhibit resilience against additional disturbances.

A reserve storage function for TAG contrasts with most observations of TAG accumulation in pure culture in response to excess C (Ratledge, 2004). Our observations also contrast with an earlier report

that fungal TAG accumulation in a forest soil was largely eliminated by complementary nutrient supply (Bååth et al., 2003), but much larger amounts of C were provided in that experiment (16 mg glucose-C g^{-1}). The observed patterns of TAG storage are however consistent with abundant evidence of reserve storage among microorganisms, in particular that C storage occurs despite or in response to declining or limiting C availability (Mason-Jones et al.,2021). For example, *Rhodococcus opacus* accumulated 21% of cell dry weight as TAG in the presence of excess N (Alvarez et al., 1996). In our experiment C was traced into both bacterial (16:1ω7) and fungal (18:2ω6) TAGs (Supplementary material Figs. S4 and S5). The fungal biomarker 18:2ω6 was only a minor contributor to TAG incorporation in the current experiment, yet even this fungal TAG was not suppressed by nutrient addition. Our results suggest that both fungi and bacteria employed TAGs as a reserve storage form, with overall levels of TAG storage more closely linked to replicative growth than to resource stoichiometry.

In summary, the response of PHB storage to different C and nutrient conditions was largely consistent with the hypothesized surplus storage mode. In contrast, patterns of TAG storage were better characterized by the reserve storage mode. There is no a priori reason to expect distinct storage strategies to correspond to different compounds, since both PHB and TAG can in principle provide C storage and mobilization under comparable conditions. Since some bacterial taxa can synthesize both PHB and TAGs (Alvarez et al., 2003, Kalscheuer et al., 2001), the question arises whether these compounds fulfil different storage functions in individual organisms, or whether the different responses emerge at a community scale, with each compound used by a different set of microbial taxa following divergent storage strategies. The first possibility would suggest as-yet unidentified differences in the metabolism of these compounds that distinguish them for different storage purposes. On the other hand, if storage strategy and preferred storage forms are correlated across taxa, then storage traits could prove useful as proxies of resource allocation strategy in microbial trait-based frameworks.

2.4.3.3. Microbial storage as a component of biomass growth

The incorporation of C into soil microbial biomass is an essential step in the terrestrial C cycle (Sokol et al., 2022), and appropriate estimates of these flows are required for understanding and managing ecosystem C balances (Kallenbach et al., 2019). We simultaneously performed a parallel experiment using identical treatments and temperature and moisture conditions to measure microbial growth using ^{18}O incorporation into DNA (Spohn et al., 2016). This method is calibrated to units of C based on extractable biomass from the CFE method, and therefore does not capture hydrophobic PHB or TAG storage. We compared the ^{18}O-DNA-based measure of growth with the incorporation of isotopically labelled glucose C into storage compounds (Fig. 4). This provides a comparison of magnitude using a lower bound for storage synthesis by neglecting the biosynthesis of storage from other C sources and

any degradation of labelled storage during the incubation. Furthermore, only two storage forms were measured here, whereas other microbial storage compounds are also known (Mason-Jones et al., 2021). Storage comprised up to 279 ± 72% more biomass growth than observed by the DNA-based method (for the high-C, no-nutrient treatment at 24 h, Fig. 4A). Even under conditions of C limitation (zero and low-C treatments), biomass growth through allocation to storage represented an additional 16–96% incorporation of C into biomass. Intracellular storage evidently plays a quantitatively significant role in microbial assimilation of C under a broad range of stoichiometric conditions, and biomass growth would be substantially underestimated by neglecting storage. Microbial growth is a central variable in microbially-explicit models of the C cycle (Wieder et al., 2018), so the substantial scale of storage also encourages a reassessment of model inputs and interpretation of results wherever short-term measurements or dynamic changes are involved. The important model parameter of carbon-use efficiency is typically measured over 24-h periods (Geyer et al., 2016), but over this timeframe we observed storage changes that constituted a substantial component of the microbial C balance. This suggests that more nuanced representations of microbial metabolism and C allocation may be required to accurately account for microbial C use.

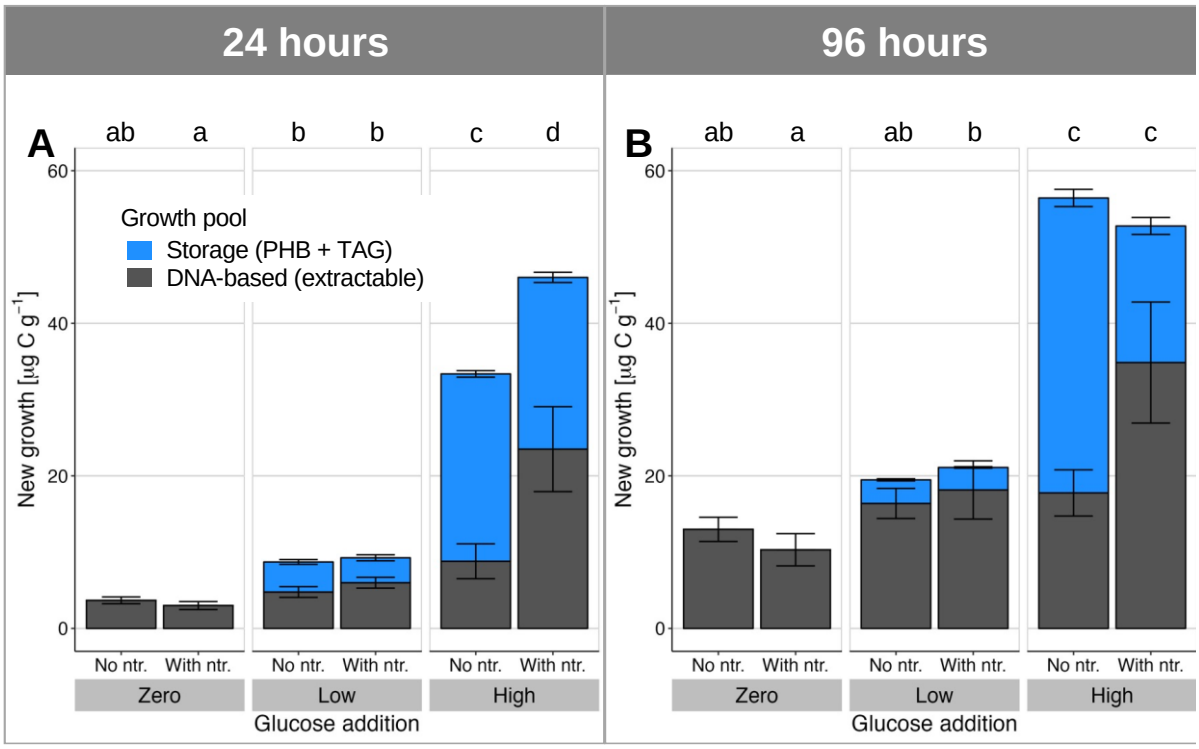

S4 Figure 4: **Comparison of new storage biosynthesis with DNA-based microbial growth reveals storage as a substantial, overlooked component of biomass growth in soil.** ^{13}C-labelled storage compound synthesis (PHB and TAGs) and DNA-based growth (incorporation of ^{18}O) were measured in soil 24 **A** and 96 h **B** after addition of a readily degradable, ^{13}C-labelled carbon source (glucose at 0, 90, and 400 µg C g^{-1} soil) with or without mineral nutrient supply (ntr.; N, P, K, S). Error bars represent mean ± standard deviation in each component

of the stacked bar (n =4 independent soil microcosms). Lowercase letters above the plots show post-hoc differences in total observed growth with $p < 0.05$ (2-sided Tukey HSD test, which adjusts for multiple comparisons).

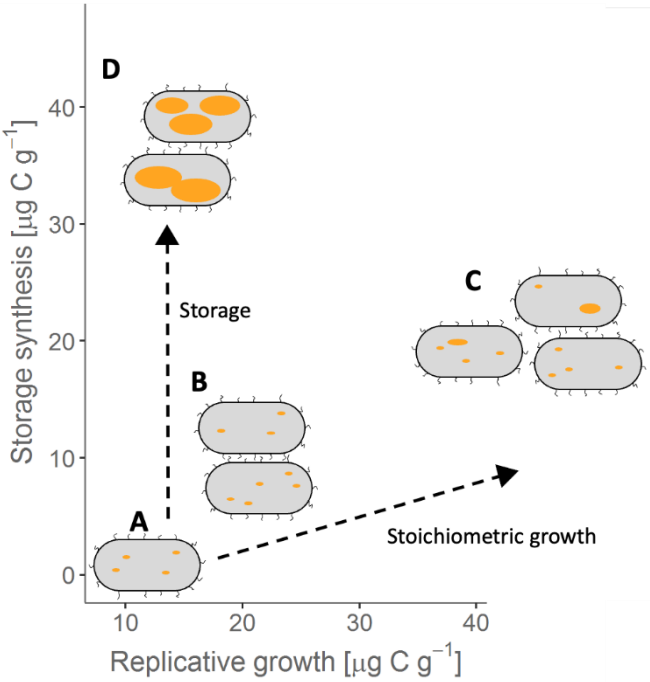

S4 Figure 5: **Intracellular storage represents an alternative pathway for growth of microbial biomass.** In this conceptual figure the y-coordinates reflect the measured incorporation of added C into storage after 96 h, and the x-axis represents replicative growth measured by ^{18}O incorporation into DNA (see also Fig. 4). According to contemporary assumptions, all growth should follow the stoichiometric growth curve that maintains constant element ratios in the biomass (dashed line to the right). The microbial population is shown schematically by bacterial cells, with yellow lipid inclusion bodies representing storage. Without C supply, only low levels of replicative growth occur **A**. Low C additions (with ample nutrients) stimulate replicative growth and limited C incorporation into storage **B**, with the ratio of new storage to non-storage biomass staying close to that predicted by assuming constant biomass stoichiometry. High C addition with complementary nutrients stimulates both strong replicative growth as well as disproportionately large storage synthesis **C**, moderately violating the stoichiometric assumption. However, nutrient limitation switches growth strongly towards storage **D**, incorporating C into biomass with little replicative growth, closer to the extreme case of pure storage without replication than the assumption of stoichiometric growth.

Microbial biomass growth is frequently understood as synonymous with the replicative growth of microbial populations. However, the incorporation of C into storage compounds represents an alternative growth pathway (Fig. 5), which differs from replicative growth in crucial ways. Models of microbial growth typically assume that increases in biomass match the elemental stoichiometry of the total biomass (the assumption of stoichiometric homoeostasis, Mooshammer et al., 2014), and therefore implement overflow respiration of excess C under conditions of C surplus (Wutzler et al.,

2017). However, substantial incorporation of C into otherwise nutrient-free PHB and TAG clearly does not follow whole-organism stoichiometry. Growth in storage therefore increases total biomass in a stoichiometrically unbalanced manner. The short experimental timeframe here is representative of environmental resource pulse and depletion processes, such as the arrival of a root tip in a particular soil volume or death and decay of a nearby organism. Storage provides stoichiometric buffering during such transient resource pulses, which is predicted to increase C and N retention over the longer term (Manzoni et al., 2021). By enhancing the efficiency with which microbes incorporate transient resource pulses and supporting metabolic activity through periods of resource scarcity, storage can contribute to the survival of microbes facing stressful habitat changes. Resource availability in natural and agroecosystems changes over various time-scales, and we hypothesize that microbial storage may also be responsive to, for example, seasonal changes in belowground C inputs, supporting microbial activity through resource-poor winter periods or dry summers. Moreover, storage enables a diversification of resource-use strategies, reflected here in the contrasting responses of PHB and TAG. Ecosystem stability is promoted by diverse strategies within the community (Loreau & Mazancourt, 2013), suggesting that storage can contribute to resistance and resilience of microbial communities facing environmental disturbances.

These findings encourage greater recognition of storage synthesis and degradation as pathways of microbial biomass change, in addition to cellular replication. Accounting for microbial storage as a key ecophysiological strategy can enrich our understanding of microbial resource use and its contributions to biogeochemical cycles and ecosystem responses under global change.

2.4.4. Methods

2.4.4.2. Experimental design

Topsoil (0–25 cm) was collected in November 2017 from the Reinshof experimental farm near Göttingen, Germany (51°29’51.0’’ N, 9°55’59.0’’ E) following an oat crop. Five samples along a 50 m field transect were mixed to provide a single homogenized soil sample. The soil was a Haplic Luvisol, pH 5.4 ($CaCl_2$), C_{org} 1.4% (Ehlers et al., 2000). Soil was stored at 4 °C for one week prior to sieving (2 mm) and then distributed into airtight 100 mL microcosms in laboratory bottles with the equivalent of 25 g dry soil at 48% of water holding capacity (WHC). Four replicates were prepared for each treatment and sampling timepoint. Microcosms were placed in a climate-controlled room at 15 °C and preincubated for one week before adding treatment solutions.

Treatment solutions provided glucose as a C source (0, 90 or 400 µg C g^{-1} soil) in a fully crossed design with added nutrients or a no-nutrient control (combined $(NH_4)_2SO_4$ and KH_2PO_4, respectively 0.613 and 0.106 µmol g^{-1} soil). Glucose levels were selected to probe the effects of C supply on storage, with

additions above and below the magnitude of MBC having potentially contrasting effects on microbial growth (Blagodatskaya & Kuzyakov, 2008). Glucose treatments contained uniformly isotopically labelled glucose (3 at% ^{13}C and 0.19 kBq ^{14}C per microcosm, respectively from Sigma-Aldrich, Munich, Germany and from American Radiolabelled Chemicals, Saint Louis, U.S.A.). The ^{14}C label in the added glucose enabled rapid and accurate measurement of glucose-derived C in liquid extracts by scintillation counting, while ^{13}C was traced in all other pools. The same amount of nutrients was used in all nutrient-addition treatments, with this set to be sufficient for the complete utilisation of all C added in the high glucose treatment, assuming a C:N:P ratio of 38:5:1 for an agricultural microbial community (Xu et al., 2013) and a C-use efficiency of 50% (Manzoni et al., 2012). Addition of the treatment solutions raised the soil moisture to 70% of WHC, after which the microcosms were sealed with air-tight butyl rubber septa and their headspace flushed with CO_2-free synthetic air. Headspace gas was sampled with a 30 mL gas syringe at regular intervals and collected in evacuated exetainers (Labco, Ceredigion, U.K.) for measurement by gas chromatography—isotope ratio mass spectrometry (GC-IRMS, GC-Box coupled via a Conflo III interface to a Delta plus XP mass spectrometer, all Thermo Fischer, Bremen, Germany). After gas sampling, the headspace in each microcosm was again flushed with CO_2-free air. Microcosms were harvested 24 and 96 h after application of the treatment solutions. The soil in each microcosm was thoroughly mixed by hand for 30 sec and subsampled for chemical analysis.

2.4.4.3. Chemical analysis

Extractable microbial biomass was measured by CFE (Gunina et al., 2014, Vance et al., 1987). A total of two 5 g subsamples of moist soil were taken from each microcosm. One was immediately extracted by shaking in 20 mL of 0.05 M K_2SO_4 for 1 h at room temperature, then centrifuged and the supernatant filtered. The other was exposed to a chloroform-saturated atmosphere for 24 h, after which residual chloroform was removed by repeated evacuation and the fumigated soil was extracted in the same manner as the nonfumigated subsample. Extractable MBC was calculated as the difference in DOC between the fumigated and non-fumigated samples, measured on a Multi N/C 2100 S analyser (Analytik Jena, Jena, Germany). CFE biomass is reported here as extractable biomass, without conversion with uncertain extraction efficiencies. Glucose-derived MBC was similarly calculated from the difference in radioactivity (^{14}C) of the extracts as measured on a Hidex 300 SL scintillation counter (TDCR efficiency correction, Hidex, Turku, Finland) using Rotiszint Eco Plus scintillation cocktail (Carl Roth, Karlsruhe, Germany). DOC and DN were determined respectively as organic carbon and total nitrogen in the extracts of the unfumigated soil.

PHB was determined by Soxhlet extraction of 4 g freeze-dried soil into chloroform, followed by acid-catalysed transesterification in ethanol and GC-MS quantification of the resulting ethyl hydroxybutyrate on a 7890 A gas chromatograph (DB1-MS column, 100% dimethyl polysiloxane, 15 m

long, inner diameter 0.25 mm, film thickness 0.25 µm), with helium (5.0) as the mobile phase at a flow rate of 1mL min^{-1}, coupled to a 7000 A triple quadrupole mass spectrometer (all Agilent, Waldbronn, Germany) (Mason-Jones et al., 2019).Injection volume was 1 µL at an inlet temperature of 270 °C and split ratio of 25:1. The GC temperature was: 42 °C isothermal for 7 min; ramped to 77 °C at 5 °C min^{-1}; then to 155 °C at 15 °C min^{-1}; held for 15 min; and then ramped to 200 °C at 10 °C min^{-1}. The transfer line temperature was 280 °C, with electron ionization at 70 eV. Quantification was based on ions at m/z 43, 60, and 87 for the ethyl 3-hydroxybutyrate analyte, and at m/z 57, 71, and 85 for the undecane internal standard. Identity and purity of peaks was confirmed by scan measurement across the range m/z 40 to 300. The same chromatographic conditions were used for determination of the PHB isotopic composition on a Thermo GC Isolink coupled with a Conflo IV interface to a MAT 253 isotope ratio mass spectrometer (all Thermo Fisher, Bremen, Germany), but with splitless injection. The measured isotopic compositions were corrected for C added in derivatization (Glaser & Amelung, 2002).

TAGs were quantified as neutral lipid fatty acids as follows (Banfield et al., 2017): Lipids were first extracted from 5 g frozen soil into a single-phase chloroform–methanol–water solution, purified by solvent extraction, and neutral lipids separated from more polar lipids on a silica solid-phase extraction column. Following removal of the solvent by evaporation, the purified TAGs were hydrolyzed (0.5 M NaOH in MeOH, 10 min at 100 °C) and methylated (12.5 M BF_3 in MeOH, 15 min at 85 °C), followed by extraction into hexane, drying and redissolution in toluene. The resulting fatty acid methyl esters were quantified by GC-MS on a 7890 A gas chromatograph (DB-5 MS column, 5%-phenyl methylpolysiloxane, 30 m coupled to a DB1-MS 15 m long, both with an inner diameter 0.25 mm and film thickness 0.25 µm) with an injection volume of 1 µl into the splitless inlet heated to 270 °C, and at a constant flow of helium (4.6) of 1.2 mL min^{-1}, coupled to a 5977B series mass spectrometer (Agilent, Waldbronn, Germany), set to 70 eV electron impact energy, with the GC oven programme as follows: initial temperature 80 °C isothermal for 1 min, ramped at 10 °C min^{-1} to 171 °C, ramped at 0.7 °C min^{-1} to 196 °C, isothermal for 4 min, ramped at 0.5 °C min^{-1} to 206°C,and ramped at 10°C min^{-1} to the final temperature of 300 °C, isothermal for 10 min for column reconditioning. Isotopic composition was determined in triplicate using a Trace GC 2000 (CE Instruments ThermoQuest Italia, S.p.A), coupled with a Combustion Interface III to a DeltaPlus isotope-ratio mass spectrometer (Thermo Finnigan, Bremen, Germany) using the same GC parameters.

Growth was estimated by ^{18}O incorporation into DNA (Blazewicz & Schwartz, 2011, Spohn et al., 2016). Parallel microcosms were prepared with 0.50 g soil in 2 mL Eppendorf tubes (Eppendorf, Hamburg, Germany) and incubated alongside the larger microcosms. This smaller scale was necessitated by the cost of ^{18}O-water. This is nevertheless larger than the soil amounts typically used for DNA extraction, which achieve consistent measures of bacterial and fungal community composition. This is also orders

of magnitude larger than the scale of microbial interactions (Nunan, 2017). These considerations, alongside the care taken to ensure identical conditions of temperature, moisture and handling, give confidence that this incubation was representative of the same processes occurring in the larger microcosms. Treatment solutions were prepared at the same concentrations as for the larger microcosms but enriched with 97 at% $H_2{}^{18}O$ so that addition provided a final soil solution of 4.2 at% ^{18}O. Tubes were withdrawn from incubation 24 h and 96 h after addition and immediately frozen at −80 °C. DNA was subsequently extracted using MP Bio FastDNA Spin Kit for Soil (MP Biomedicals, Solon, OH, USA). DNA concentration in the extract was measured on an Implen MP80 nanophotometer (Implen, Munich, Germany) at 260 nm, with A260/280 and A260/A230 to confirm quality, and 50 µL was pipetted into silver capsules, freeze dried, and measured by TC/EA (Thermo Finnigan, Bremen, Germany) coupled with a Conflo III interface to a Delta V Plus isotope ratio mass spectrometer (all Thermo Finnigan, Bremen, Germany). The total measured O content of the sample, the O content of the DNA (31% by mass), and the ^{18}O natural abundance of unlabeled control samples were used to calculate the background ^{18}O from the kit. This background ^{18}O was deducted to obtain ^{18}O abundance of the DNA, which was applied in a 2-pool mixing model with 70% of O in new DNA derived from water (Pold et al., 2020) (model detailed in Supplementary B). This provided the fraction of extracted DNA that had been newly synthesized during the incubation period. This fraction was multiplied by extractable microbial biomass to arrive at gross biomass growth in units of µg C g^{-1} soil.

2.4.4.4. Statistical analysis

Statistical analysis was performed in R (R Core Team, 2020) with preliminary calculations in Microsoft Excel (version 16.67). Results for CO_2, MBC, DOC, DN, TAG, PHB, and isotopic compositions were calculated for each independent sample and reported as mean ± standard deviation for each treatment group, unless otherwise noted. Comparisons between these pools were similarly calculated at the sample level before expressing as mean ± standard deviation.

DN and DOC data were log-transformed to satisfy assumptions for ANOVA (Shapiro-Wilk's test of normality and Levene's test for homogeneity of variance), followed by Tukey's HSD test for pairwise comparisons of treatment effects. The same analyses were performed on untransformed extractable microbial biomass data. Ranges for treatment effects on DN, DOC and MBC reported in the text reflect 95% family-wise confidence intervals from pair-wise Tukey's HSDtests. Where relevant, effect sizes were computed as Cohen's d, using the effsize package (Torchiano, 2020).

Levels of labelled storage compounds showed considerable heteroskedasticity that could not be consistently corrected by transformation, particularly due to very high levels of unsaturated fatty acids in one of the 24 h samples. This conceivably reflected a hotspot of fungal activity in the soil. This datapoint was therefore conservatively retained since this would comprise relevant variability in the

soil. Analysis of storage compounds (PHB and TAG) proceeded by robust ANOVA of medians for each timepoint separately using the R package WRS2 (Mair & Wilcox, 2020). Consistent with the median-based robust ANOVA, storage differences between treatments reported in the text are median differences, with uncertainty given as 95% confidence intervals calculated by the Hodges-Lehmann estimator (R package DescTools, Signorell et al., 2021). Comprehensive pairwise post-hoc comparisons of medians was performed using medpb to provide significance indicators in figures (Fig. 2) (R package WRS, Wilcox, 2016), with Benjamini-Hochberg adjustment of p values for multiple comparisons.

Growth estimation by ^{18}O incorporation used DNA concentration and its ^{18}O enrichment to determine mean gross microbial growth for each treatment in relative terms, and the associated standard deviation. The corresponding mean extractable microbial biomass values were applied to convert to absolute units of µg C, using standard rules of error propagation (Meyer, 1975), to provide the DNA-based measure of mean microbial biomass growth for each treatment. These DNA-based growth estimates were combined with the mean production of labelled storage compounds (sum of C in glucose-derived PHB and TAG), again using rules of error propagation, to obtain estimates of total (DNA-based and storage) mean biomass growth and associated standard deviations. These were subjected to 2-way ANOVA and Tukey HSD to test the significance and size of treatment effects (Fig. 3). Arithmetic comparisons between MBC, growth, and storage pools (for example, the relative scales of DNA-based growth and storage growth) were calculated using mean values with error propagation.

2.4.5. Reporting Summary

Further information on research design is available in the Nature Portfolio Reporting Summary linked to this article.

2.4.6. Data availability

All source data generated in this study has been deposited in the Zenodo open data repository (Mason-Jones et al., 2023) under https://doi.org/10.5281/zenodo. 6386047. This data is publicly available.

2.4.7. Code availability

R scripts used for data analysis are publicly available on the Zenodo open data repository under https://doi.org/10.5281/zenodo.6386047.

2.4.8. References

Alvarez, H.M., 2003. Relationship between β-oxidation pathway and the hydrocarbon-degrading profile in actinomycetes bacteria. International Biodeterioration & Biodegradation 52, 35–42. https://doi.org/10.1016/S0964-8305(02)00120-8

Alvarez, H.M., Mayer, F., Fabritius, D., Steinbüchel, A., 1996. Formation of intracytoplasmic lipid inclusions by Rhodococcus opacus strain PD630. Arch Microbiol 165, 377–386. https://doi.org/10.1007/s002030050341

Anderson, J.P.E., Domsch, K.H., 1978. A physiological method for the quantitative measurement of microbial biomass in soils. Soil Biology and Biochemistry 10, 215–221. https://doi.org/10.1016/0038-0717(78)90099-8

Bååth, E., 2003. The Use of Neutral Lipid Fatty Acids to Indicate the Physiological Conditions of Soil Fungi. Microbial Ecology 45, 373–383.

Bailey, V.L., Peacock, A.D., Smith, J.L., Bolton, H., 2002. Relationships between soil microbial biomass determined by chloroform fumigation–extraction, substrate-induced respiration, and phospholipid fatty acid analysis. Soil Biology and Biochemistry 34, 1385–1389. https://doi.org/10.1016/S0038-0717(02)00070-6

Banfield, C.C., Dippold, M.A., Pausch, J., Hoang, D.T.T., Kuzyakov, Y., 2017. Biopore history determines the microbial community composition in subsoil hotspots. Biol Fertil Soils 53, 573–588. https://doi.org/10.1007/s00374-017-1201-5

Becker, K.W., Collins, J.R., Durham, B.P., Groussman, R.D., White, A.E., Fredricks, H.F., Ossolinski, J.E., Repeta, D.J., Carini, P., Armbrust, E.V., Van Mooy, B.A.S., 2018. Daily changes in phytoplankton lipidomes reveal mechanisms of energy storage in the open ocean. Nat Commun 9, 5179. https://doi.org/10.1038/s41467-018-07346-z

Blagodatskaya, E., Kuzyakov, Y., 2008. Mechanisms of real and apparent priming effects and their dependence on soil microbial biomass and community structure: critical review. Biol Fertil Soils 45, 115–131. https://doi.org/10.1007/s00374-008-0334-y

Blazewicz, S.J., Schwartz, E., 2011. Dynamics of 18O Incorporation from H218O into Soil Microbial DNA. Microb Ecol 61, 911–916. https://doi.org/10.1007/s00248-011-9826-7

Chapin, F.S., Schulze, E., Mooney, H.A., 1990. The Ecology and Economics of Storage in Plants. Annu. Rev. Ecol. Syst. 21, 423–447. https://doi.org/10.1146/annurev.es.21.110190.002231

Dijkstra, P., Salpas, E., Fairbanks, D., Miller, E.B., Hagerty, S.B., van Groenigen, K.J., Hungate, B.A., Marks, J.C., Koch, G.W., Schwartz, E., 2015. High carbon use efficiency in soil microbial communities is related to balanced growth, not storage compound synthesis. Soil Biology and Biochemistry 89, 35–43. https://doi.org/10.1016/j.soilbio.2015.06.021

Dijkstra, P., Wu, W., Dippold, M., Schwartz, E., Hungate, B., Megonigal, P., Thomas, S., Seymour, C., Martinez, A., 2022. On Maintenance and Metabolisms in Soil Microbial Communities (preprint). In Review. https://doi.org/10.21203/rs.3.rs-1193625/v1

Ehlers, W., Werner, D., Mähner, T., 2000. Wirkung mechanischer Belastung auf Gefüge und Ertragsleistung einer Löss-Parabraunerde mit zwei Bearbeitungssystemen. Journal of Plant Nutrition and Soil Science 163, 321–333. https://doi.org/10.1002/1522-2624(200006)163:3<321::AID-JPLN321>3.0.CO;2-Y

Geyer, K.M., Dijkstra, P., Sinsabaugh, R., Frey, S.D., 2019. Clarifying the interpretation of carbon use efficiency in soil through methods comparison. Soil Biology and Biochemistry 128, 79–88. https://doi.org/10.1016/j.soilbio.2018.09.036

Geyer, K.M., Kyker-Snowman, E., Grandy, A.S., Frey, S.D., 2016. Microbial carbon use efficiency: accounting for population, community, and ecosystem-scale controls over the fate of metabolized organic matter. Biogeochemistry 127, 173–188. https://doi.org/10.1007/s10533-016-0191-y

Glaser, B., Amelung, W., 2002. Determination of 13C natural abundance of amino acid enantiomers in soil: methodological considerations and first results. Rapid Commun. Mass Spectrom. 16, 891–898. https://doi.org/10.1002/rcm.650

Gunina, A., Dippold, M.A., Glaser, B., Kuzyakov, Y., 2014. Fate of low molecular weight organic substances in an arable soil: From microbial uptake to utilisation and stabilisation. Soil Biology and Biochemistry 77, 304–313. https://doi.org/10.1016/j.soilbio.2014.06.029

Gunina, A., Kuzyakov, Y., 2015. Sugars in soil and sweets for microorganisms: Review of origin, content, composition and fate. Soil Biology and Biochemistry 90, 87–100. https://doi.org/10.1016/j.soilbio.2015.07.021

Jenkinson, D.S., Brookes, P.C., Powlson, D.S., 2004. Measuring soil microbial biomass. Soil Biology & Biochemistry 36, 5–7.

Kallenbach, C.M., Wallenstein, M.D., Schipanksi, M.E., Grandy, A.S., 2019. Managing Agroecosystems for Soil Microbial Carbon Use Efficiency: Ecological Unknowns, Potential Outcomes, and a Path Forward. Frontiers in Microbiology 10.

Kalscheuer, R., Wältermann, M., Alvarez, H., Steinbüchel, A., 2001. Preparative isolation of lipid inclusions from Rhodococcus opacus and Rhodococcus ruber and identification of granule-associated proteins. Arch Microbiol 177, 20–28. https://doi.org/10.1007/s00203-001-0355-5

Kourmentza, C., Plácido, J., Venetsaneas, N., Burniol-Figols, A., Varrone, C., Gavala, H.N., Reis, M.A.M., 2017. Recent Advances and Challenges towards Sustainable Polyhydroxyalkanoate (PHA) Production. Bioengineering 4, 55. https://doi.org/10.3390/bioengineering4020055

López, N.I., Pettinari, M.J., Nikel, P.I., Méndez, B.S., 2015. Chapter Three - Polyhydroxyalkanoates: Much More than Biodegradable Plastics, in: Sariaslani, S., Gadd, G.M. (Eds.), Advances in Applied Microbiology. Academic Press, pp. 73–106. https://doi.org/10.1016/bs.aambs.2015.06.001

Loreau, M., de Mazancourt, C., 2013. Biodiversity and ecosystem stability: a synthesis of underlying mechanisms. Ecology Letters 16, 106–115. https://doi.org/10.1111/ele.12073

Mair, P., Wilcox, R., 2020. Robust statistical methods in R using the WRS2 package. Behav Res 52, 464–488. https://doi.org/10.3758/s13428-019-01246-w

Manzoni, S., Ding, Y., Warren, C., Banfield, C.C., Dippold, M.A., Mason-Jones, K., 2021. Intracellular Storage Reduces Stoichiometric Imbalances in Soil Microbial Biomass – A Theoretical Exploration. Front. Ecol. Evol. 9, 714134. https://doi.org/10.3389/fevo.2021.714134

Manzoni, S., Porporato, A., 2009. Soil carbon and nitrogen mineralization: Theory and models across scales. Soil Biology and Biochemistry 41, 1355–1379. https://doi.org/10.1016/j.soilbio.2009.02.031

Manzoni, S., Taylor, P., Richter, A., Porporato, A., Ågren, G.I., 2012. Environmental and stoichiometric controls on microbial carbon-use efficiency in soils. New Phytologist 196, 79–91. https://doi.org/10.1111/j.1469-8137.2012.04225.x

Mason-Jones, K., Banfield, C.C., Dippold, M.A., 2019. Compound-specific 13C stable isotope probing confirms synthesis of polyhydroxybutyrate by soil bacteria. Rapid Communications in Mass Spectrometry 33, 795–802. https://doi.org/10.1002/rcm.8407

Mason-Jones, K., Breidenbach, A., Dyckmans, J., Banfield, C.C., Dippold, M.A., 2023. Dataset for: Intracellular carbon storage by microorganisms is an overlooked pathway of biomass growth. https://doi.org/10.5281/zenodo.6386047

Mason-Jones, K., Robinson, S.L., Veen, G.F., Manzoni, S., van der Putten, W.H., 2021. Microbial storage and its implications for soil ecology. ISME J. https://doi.org/10.1038/s41396-021-01110-w

Matin, A., Veldhuis, C., Stegeman, V., Veenhuis, M., 1979. Selective Advantage of a Spirillum sp. in a Carbon-limited Environment. Accumulation of Poly- -hydroxybutyric Acid and Its Role in Starvation. Journal of General Microbiology 112, 349–355. https://doi.org/10.1099/00221287-112-2-349

Meyer, S.L., 1975. Data analysis for scientists and engineers. New York: Wiley.

Mooshammer, M., Wanek, W., Zechmeister-Boltenstern, S., Richter, A., 2014. Stoichiometric imbalances between terrestrial decomposer communities and their resources: mechanisms and implications of microbial adaptations to their resources. Frontiers in Microbiology 5.

Murphy, D.J., 2012. The dynamic roles of intracellular lipid droplets: from archaea to mammals. Protoplasma 249, 541–585. https://doi.org/10.1007/s00709-011-0329-7

Nunan, N., 2017. The microbial habitat in soil: Scale, heterogeneity and functional consequences. Journal of Plant Nutrition and Soil Science 180, 425–429. https://doi.org/10.1002/jpln.201700184

Poblete-Castro, I., Escapa, I.F., Jäger, C., Puchalka, J., Chi Lam, C.M., Schomburg, D., Prieto, M.A., Martins dos Santos, V.A., 2012. The metabolic response of P. putida KT2442 producing high levels of polyhydroxyalkanoate under single- and multiple-nutrient-limited growth: Highlights from a multi-level omics approach. Microb Cell Fact 11, 34. https://doi.org/10.1186/1475-2859-11-34

Pold, G., Domeignoz-Horta, L.A., DeAngelis, K.M., 2020. Heavy and wet: The consequences of violating assumptions of measuring soil microbial growth efficiency using the 18O water method. Elem Sci Anth 8, 069.

R Core Team, R., 2013. R: A language and environment for statistical computing.

Ratledge, C., 2004. Fatty acid biosynthesis in microorganisms being used for Single Cell Oil production. Biochimie, Recent advances in lipid metabolism and related disorders 86, 807–815. https://doi.org/10.1016/j.biochi.2004.09.017

Sekar, K., Linker, S.M., Nguyen, J., Grünhagen, A., Stocker, R., Sauer, U., 2020. Bacterial Glycogen Provides Short-Term Benefits in Changing Environments. Applied and Environmental Microbiology 86, e00049-20. https://doi.org/10.1128/AEM.00049-20

Signorell, A., Aho, K., Alfons, A., Anderegg, N., Aragon, T., Arppe, A., Baddeley, A., Barton, K., Bolker, B., Borchers, H.W., 2019. DescTools: Tools for descriptive statistics. R package version 0.99 28, 17.

Sokol, N.W., Slessarev, E., Marschmann, G.L., Nicolas, A., Blazewicz, S.J., Brodie, E.L., Firestone, M.K., Foley, M.M., Hestrin, R., Hungate, B.A., Koch, B.J., Stone, B.W., Sullivan, M.B., Zablocki, O., Pett-Ridge, J., 2022. Life and death in the soil microbiome: how ecological processes influence biogeochemistry. Nat Rev Microbiol 20, 415–430. https://doi.org/10.1038/s41579-022-00695-z

Spohn, M., Klaus, K., Wanek, W., Richter, A., 2016. Microbial carbon use efficiency and biomass turnover times depending on soil depth – Implications for carbon cycling. Soil Biology and Biochemistry 96, 74–81. https://doi.org/10.1016/j.soilbio.2016.01.016

Torchiano, M., 2016. Effsize - a package for efficient effect size computation. https://doi.org/10.5281/zenodo.1480624

Vance, E.D., Brookes, P.C., Jenkinson, D.S., 1987. An extraction method for measuring soil microbial biomass C. Soil Biology and Biochemistry 19, 703–707. https://doi.org/10.1016/0038-0717(87)90052-6

Wieder, W.R., Allison, S.D., Davidson, E.A., Georgiou, K., Hararuk, O., He, Y., Hopkins, F., Luo, Y., Smith, M.J., Sulman, B., Todd-Brown, K., Wang, Y.-P., Xia, J., Xu, X., 2015. Explicitly representing soil microbial processes in Earth system models. Global Biogeochemical Cycles 29, 1782–1800. https://doi.org/10.1002/2015GB005188

Wieder, W.R., Hartman, M.D., Sulman, B.N., Wang, Y.-P., Koven, C.D., Bonan, G.B., 2018. Carbon cycle confidence and uncertainty: Exploring variation among soil biogeochemical models. Global Change Biology 24, 1563–1579. https://doi.org/10.1111/gcb.13979

Wilcox, R.R., 2011. Introduction to robust estimation and hypothesis testing. Academic press.

Wutzler, T., Zaehle, S., Schrumpf, M., Ahrens, B., Reichstein, M., 2017. Adaptation of microbial resource allocation affects modelled long term soil organic matter and nutrient cycling. Soil Biology and Biochemistry 115, 322–336. https://doi.org/10.1016/j.soilbio.2017.08.031

Xu, X., Thornton, P.E., Post, W.M., 2013. A global analysis of soil microbial biomass carbon, nitrogen and phosphorus in terrestrial ecosystems. Global Ecology and Biogeography 22, 737–749. https://doi.org/10.1111/geb.12029

Zelles, L., Bai, Q.Y., Rackwitz, R., Chadwick, D., Beese, F., 1995. Determination of phospholipid- and lipopolysaccharide-derived fatty acids as an estimate of microbial biomass and community structures in soils. Biol Fertil Soils 19, 115–123. https://doi.org/10.1007/BF00336146

2.4.9. Acknowledgements

We gratefully acknowledge the laboratory assistance provided by Kali Middleby, Andrew Gall, Lydia Köbele and Karin Schmidt. We gratefully acknowledge the financial support of the Deutscher Akademischer Austauschdienst (DAAD; 91525994) for a fellowship supporting the experimental work (K.M.J.), the Dutch Research Council (N.W.O.) for funding of the Veni project VI.Veni.202.086 (K.M.J.), and the Open Access Publication Fund of the University of Tübingen (M.A.D.). This work is associated to the DFG Priority Program 2322 SoilSystems, project EcoEnergeticS (DFG DI 2136/17−1; M.A.D.). We thank the staff of the core projects of the SPP and the scientific committee for establishing the SPP project.

2.4.10. Author Contributions

K.M.J., A.B., C.C.B., and M.A.D. jointly initiated and designed the experiment; K.M.J., A.B., and J.D. conducted the experiment and analyses; K.M.J. and A.B. undertook data analysis; K.M.J. wrote the manuscript with assistance and comments of all co-authors.

2.4.11. Funding

Open Access funding enabled and organized by Projekt DEAL.

2.4.12. Competing interests

The authors declare no competing interests.

2.4.13. Abstract of additional Manuscripts: Organic Nutrients Induced Coupled C- and P-Cycling Enzyme Activities During Microbial Growth in Forest Soils

Besides environmental and soil physical drivers, the functional properties of microbial populations, i. e., growth rate, enzyme production, and maintenance requirements are dependent on the microbes' environment. The soil nutrition status and the quantity and quality of the substrate input, both infer different growth strategies of microorganisms. It is uncertain, how enzyme systems respond during the different phases of microbial growth and retardation in soil. The objective of this study was to uncover the changes of microbial functioning and their related enzyme systems in nutrient-poor and nutrient-rich beech forest soil during the phases of microbial growth. We determined microbial growth via kinetic approach by substrate-induced respiratory response of microorganisms, enabling the estimation of total, and growing biomass of the microbial community. To induce microbial growth we used glucose, while yeast extract simulated additional input of nutrients and factors indicating microbial residues (i.e., necromass compounds). Microbial growth on glucose showed a 12 – 18 h delay in associated enzyme activity increase or the absence of distinct activity responses (V_{max}). β-glucosidase and chitinase (NAG) demonstrated clear differences of V_{max} in time and between P-rich and P-poor soils. However, during microbial growth on glucose + yeast extract, the exponential increase in enzymatic activity was clearly stimulated accompanied by a delay of 8 – 12 h, smoothing the differences in nutrient-acquisition dynamics between the two soils. Furthermore, cross-correlation of β-glucosidase and acid phosphatase between the two sites demonstrated harmonized time constraints, which reflected the establishment of comparable and balanced enzymatic systems within the decomposition network. The network accelerated nutrient acquisition to maintain microbial growth, irrespective of the contrasting soil properties and initial nutrient stocks, indicating similar tradeoffs of C- and P- cycling enzymes in both soils. This reflects comparable temporal dynamics of activities in nutrient-poor and nutrient-rich soil when the glucose + yeast extract was added. During lag phase and phase of exponential microbial growth, substrate turnover time of all enzymes was shortened in nutrient-poor forest soil exclusively, reflecting that the quality of the added substrate strongly matters during all stages of microbial growth in soil.

3. Appendix

3.1.1. Supplement

3.1.2. Study 1: Microbial functional changes mark irreversible course of Tibetan grassland degradation

Andreas Breidenbach[1,2,#], Per-Marten Schleuss[3,#], Shibin Liu[4], Dominik Schneider[5], Michaela A. Dippold[1,2], Tilman de la Haye[6], Georg Miehe[7], Felix Heitkamp[8], Elke Seeber[9], Kyle Mason-Jones[10], Xingliang Xu[11,12], Yang Huanming[13], Jianchu Xu[14], Tsechoe Dorji[12,15], Matthias Gube[16], Helge Norf[17], Jutta Meier[18], Georg Guggenberger[19], Yakov Kuzyakov[20] & Sandra Spielvogel[6]*

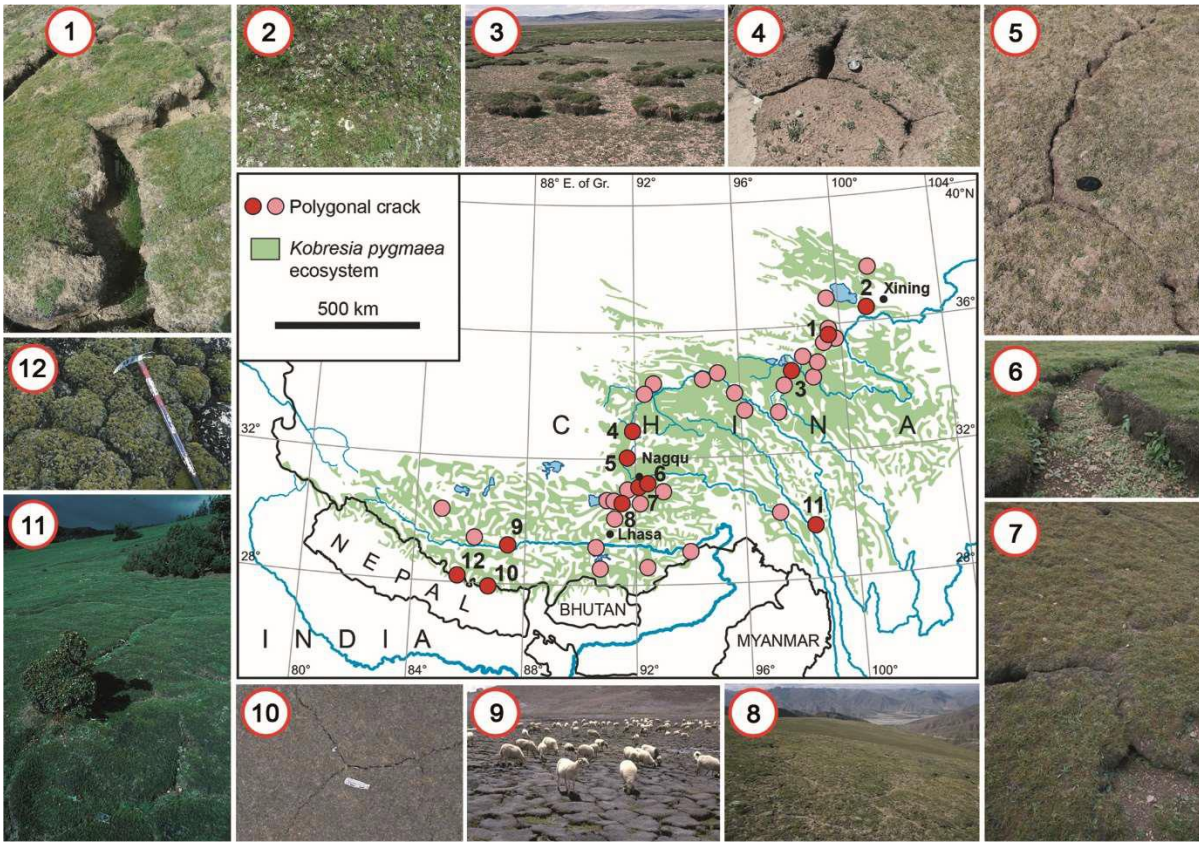

S1 Suppl. Fig. 1: **Selected examples of polygonal cracking and extension on the Tibetan Plateau (TP).** Red dots show locations of polygonal cracks based on observations during field trips on the TP and the Himalayas between 1982 and 2015. The map reflects the widespread distribution of this specific degradation phenomenon, but not its actual distribution or intensity. Photo credits: E. Seeber (1, 2), G. Miehe (3–5, 9, 11, 12), P.-M. Schleuss (6–8) and R. Bäumler (10). Cartography: C. Enderle.

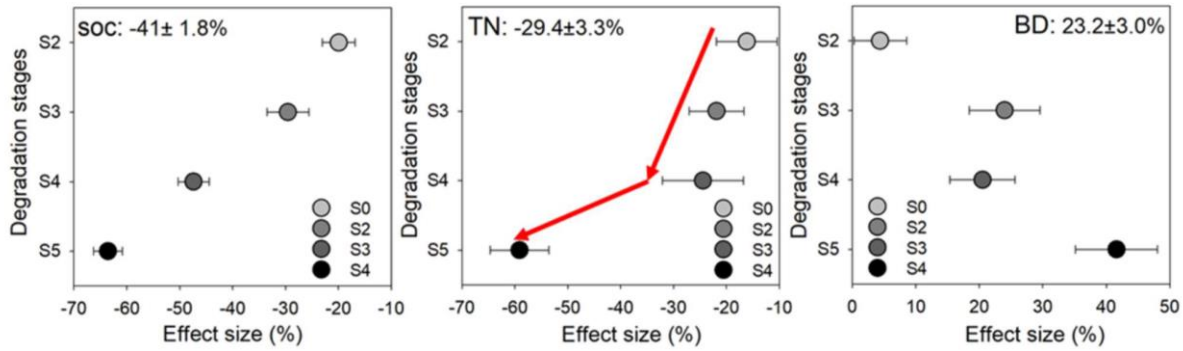

S1 Suppl. Fig. 2: **Effect sizes of SOC (soil organic carbon) content, total nitrogen (TN) content and soil bulk density (BD) for degradation stages S1 to S4 compared to non-degraded pastures (S0).** The percentage value at the top shows the average effect size of the four degradation stages (meta-analysis including 594 single observations from literature studies published between 2002 and 2020, error bars display standard error).

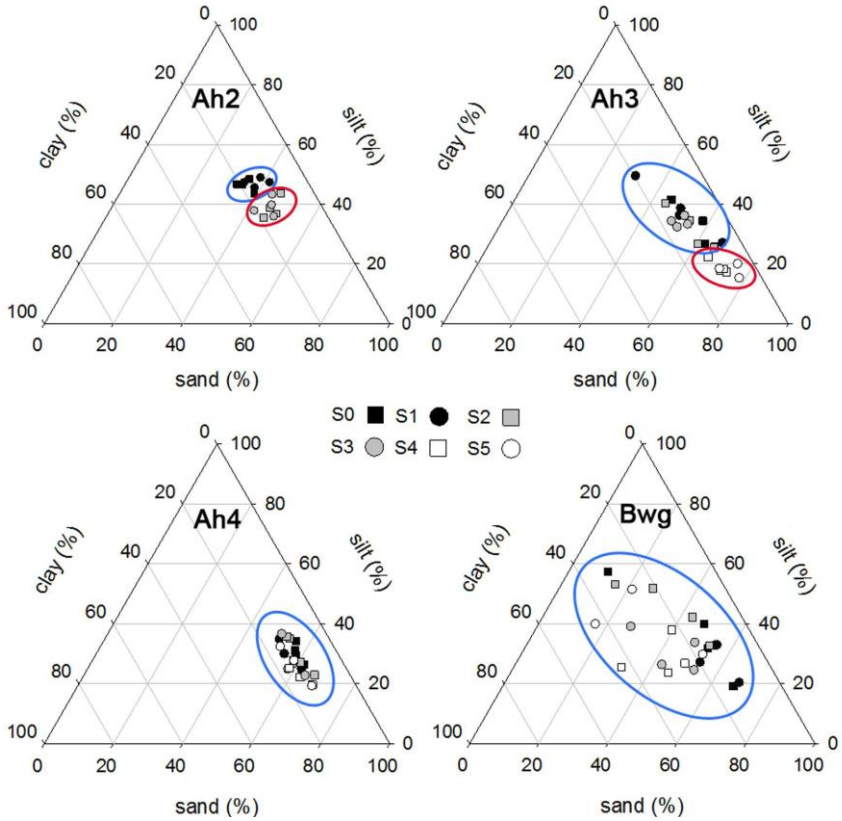

S1 Suppl. Fig. 3: **Changes in particle size distribution for each soil horizon at each degradation stage.** The soil texture was measured for each soil horizon (Ah2, Ah3, Ah4, Bwg), except for the densely rooted and thin Ah1 horizon, with low amounts of mineral soil. Circled in blue are the "protected horizons" having an overlying horizon. Circled in red are the upper soil horizons, which are prone to erosion processes and shift toward a coarser soil texture.

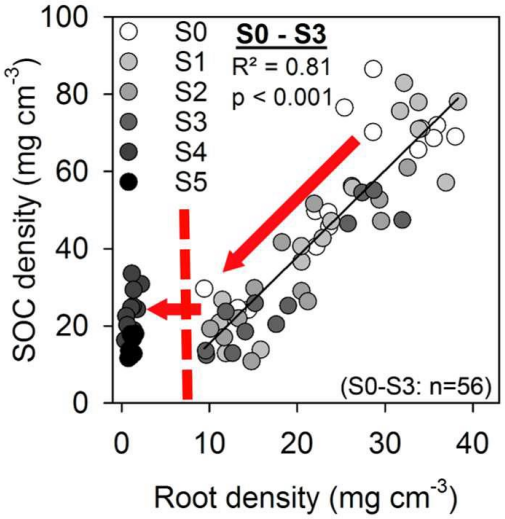

S1 Suppl. Fig. 4: **Relationship between soil organic carbon (SOC) density and root density for all soil horizons at each degradation stage.** Linear regression covers degradation stages S0 to S3. At degradation stages S4 and S5, SOC density is independent of root density and represents remnant SOC.

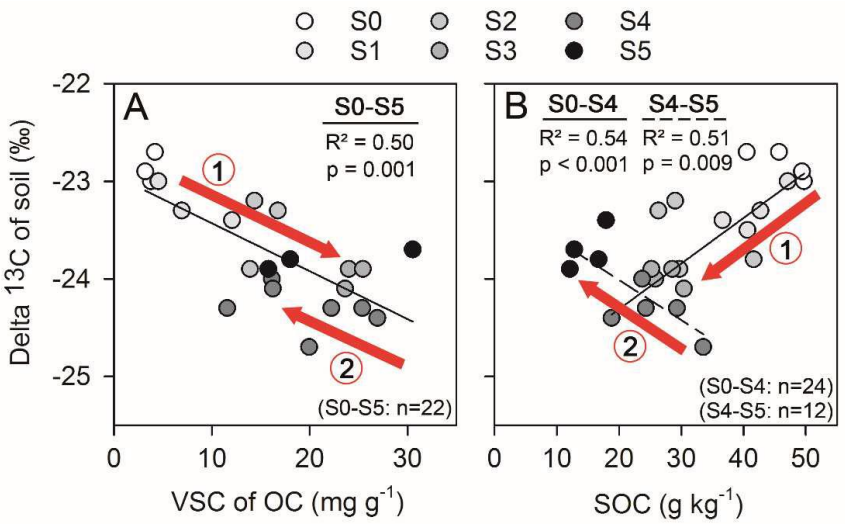

S1 Suppl. Fig. 5: **Relationship between $\delta^{13}C$ values and (A) content of lignin monomers vanillyl, syringyl, and cinnamyl (VSC) or (B) soil organic carbon (SOC) content in the Ah3 horizon for each degradation stage.** The pattern along the degradation sequence can be explained by the following processes: (1) decreasing SOC concentrations associated with a relative accumulation of lignin and an associated decrease in $\delta^{13}CS_{OC}$ values (S0–S3) and (2) decreasing SOC concentrations associated with lignin degradation and $^{13}C_{SOC}$ enrichment (S4, S5).

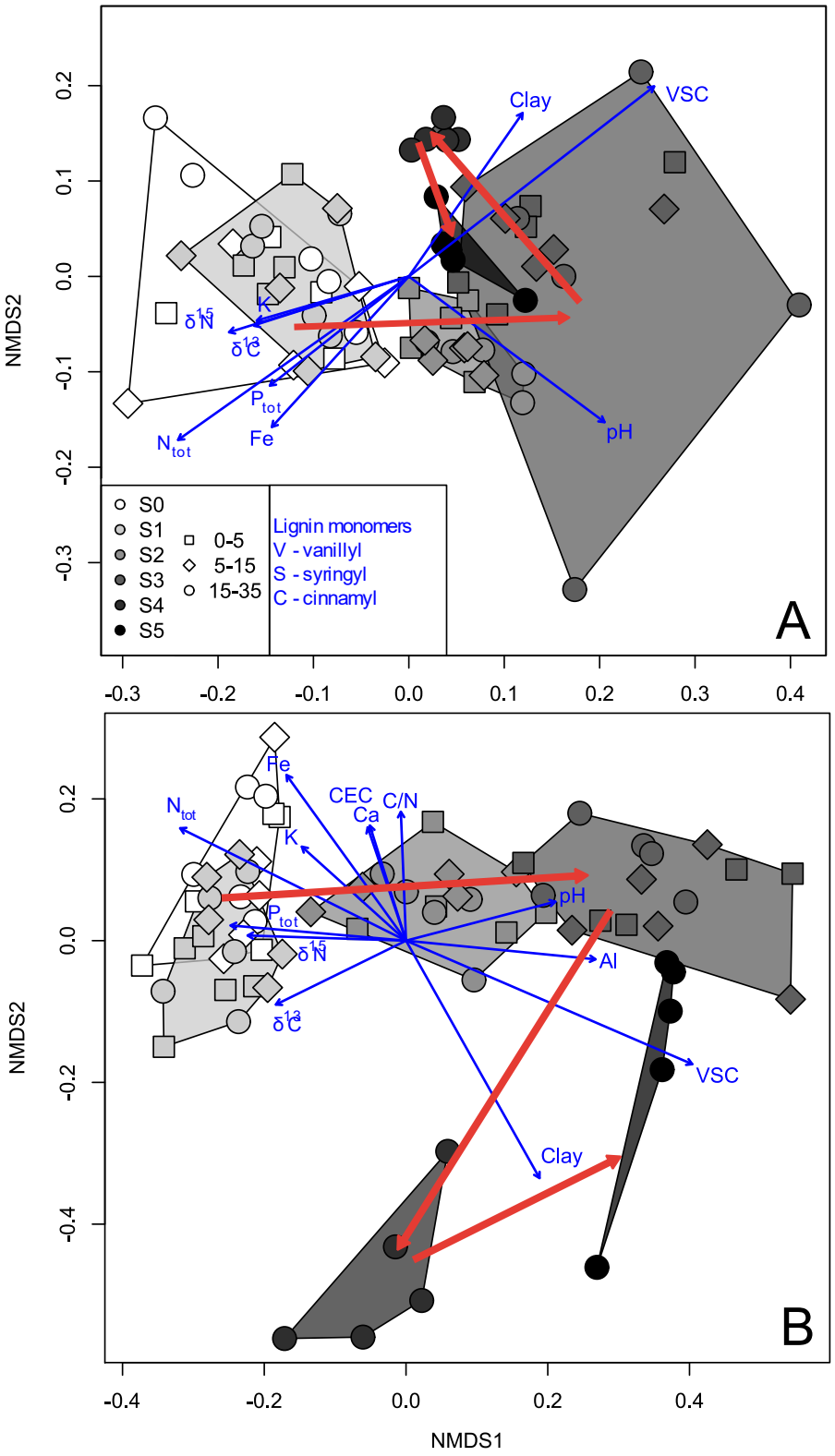

S1 Suppl. Fig. 6: **NMDS (non-metric multidimensional scaling) plots derived from t-RFLP data for the bacterial (A) and fungal (B) communities.** Shaded areas mark each degradation stage, symbols indicate soil depth, and blue arrows show significantly correlated abiotic factors (canonical correspondence analysis, $p < 0.05$). Red arrows mark key structural shifts of the microbial community.

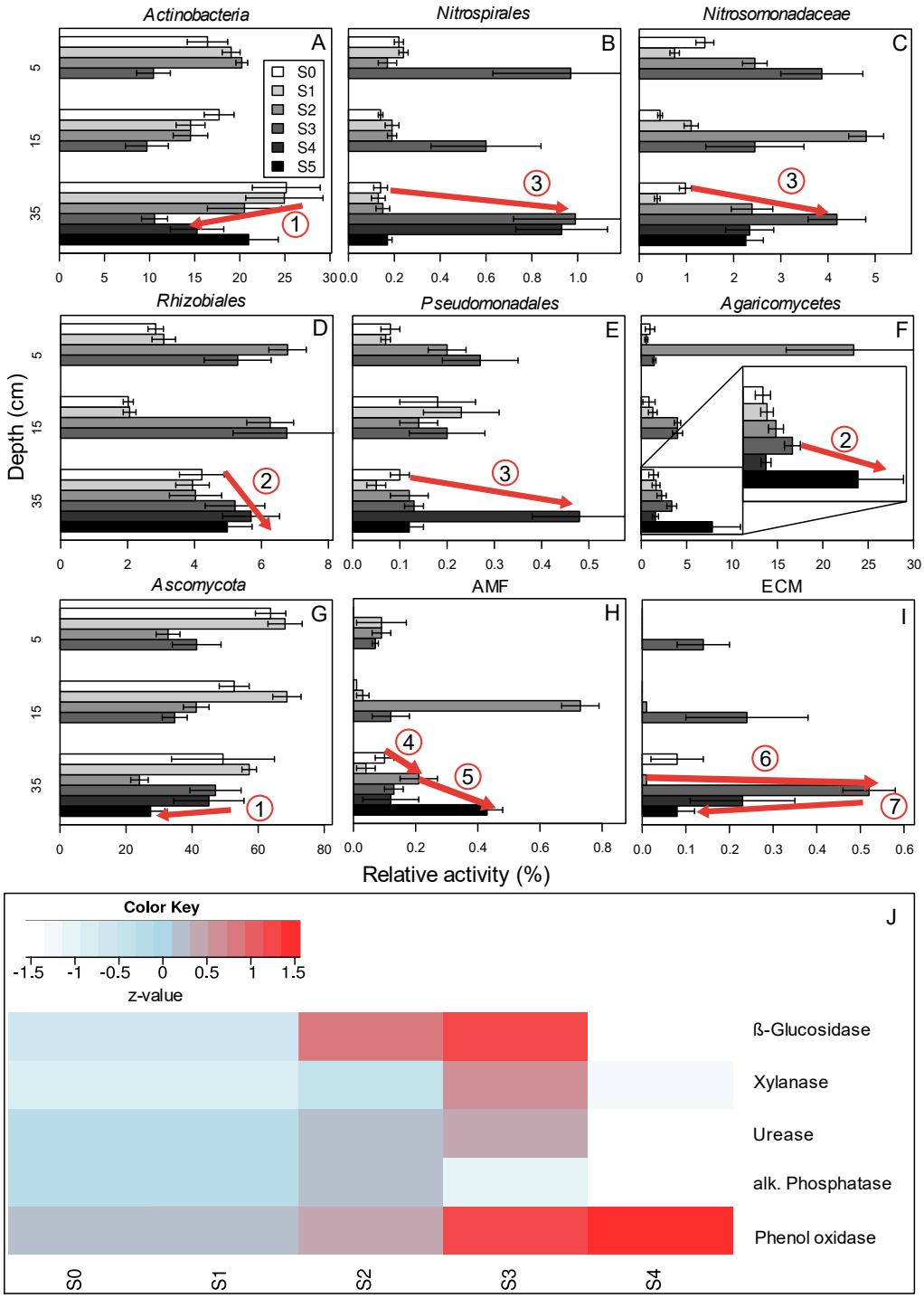

S1 Suppl. Fig. 7: **Relative abundance of key microbial functional groups.** Shifts are indicated by red arrows for the lowest depth, representing the complete range of degradation stages (S0–S5): (1) decline of bacterial (**A**) and fungal (**G**) litter degraders, (2) increase in bacterial (**D**) and fungal (F**)** litter degraders, (3) increase in nitrifying (**B, C**) and denitrifying (**E**) bacteria, (4) increase in arbuscular mycorrhizal fungi (AMF) until S2 (**H**), (6) which are then replaced by ectomycorrhizal fungi (ECM) (**I**); (7) ECM decline toward S5 (**I**) as new plants with new AMF (5) become established after *Kobresia pygmaea disappears* (**H**). Key enzyme activities (**J**) reflect shifts in microbial community functions from hydrolytic to oxidative soil organic carbon (SOC) decomposition.

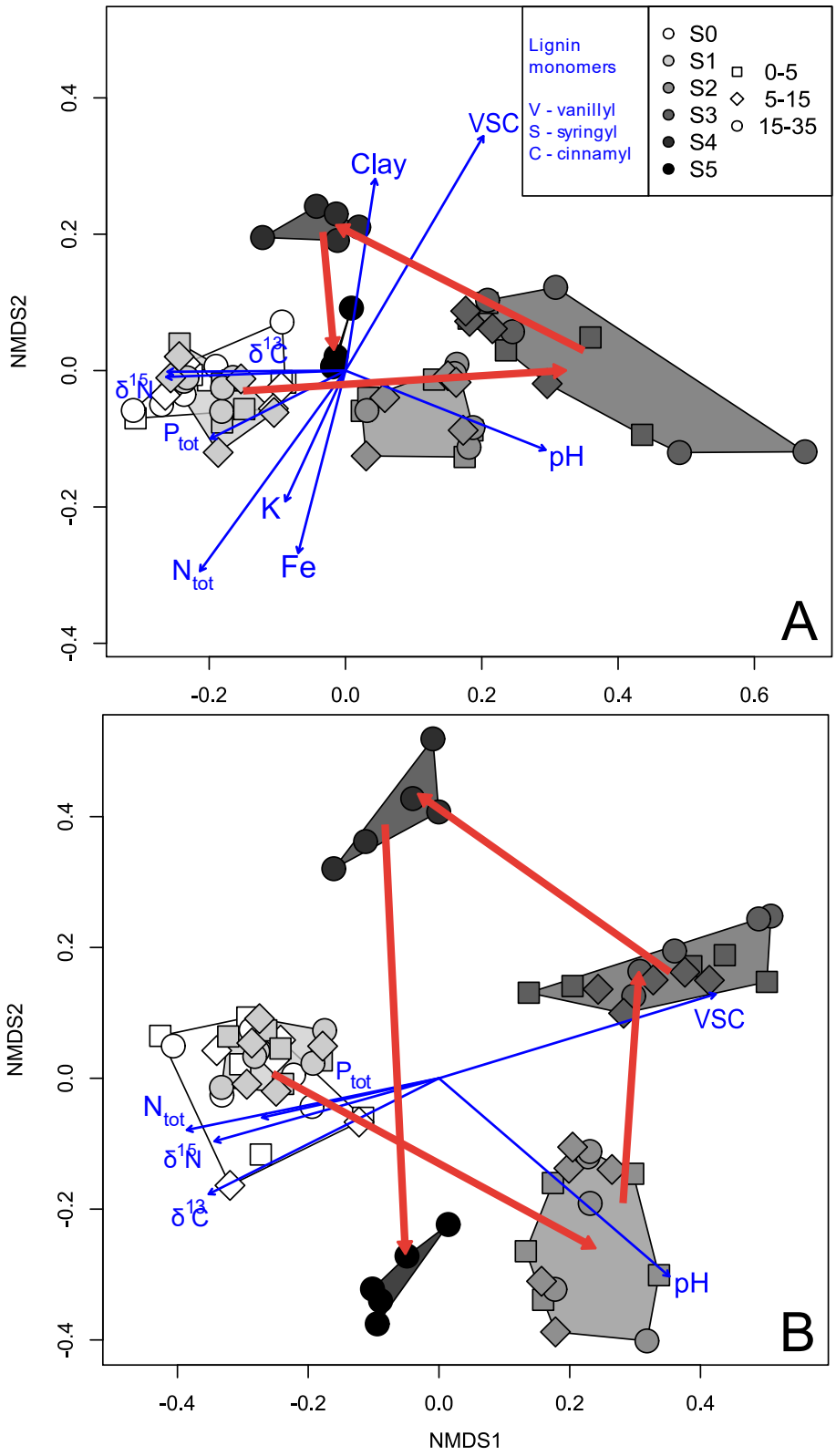

S1 Suppl. Fig. 8: **NMDS (non-metric multidimensional scaling) plots derived from Illumina MiSeq sequencing data of the bacterial (A) and fungal (B) communities along degradation stages.** Shaded areas mark each degradation stage, symbols indicate soil depth, and blue arrows show significantly correlated abiotic factors (by CCA, canonical-correlation analysis).

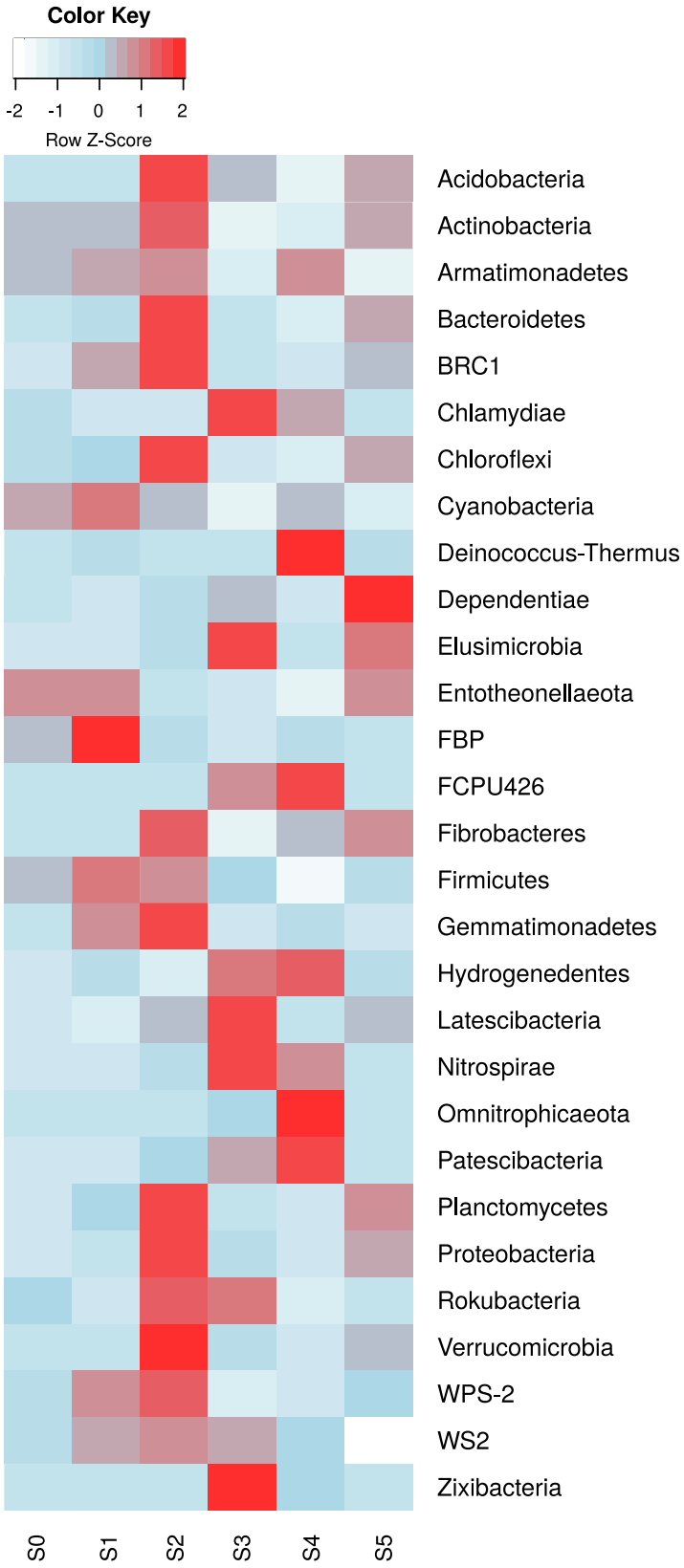

S1 Suppl. Fig. 9: **Heat map of the bacterial community along degradation stages (soil depth 15–35 cm).** Shades of color indicate abundance of bacterial phyla as z-values.

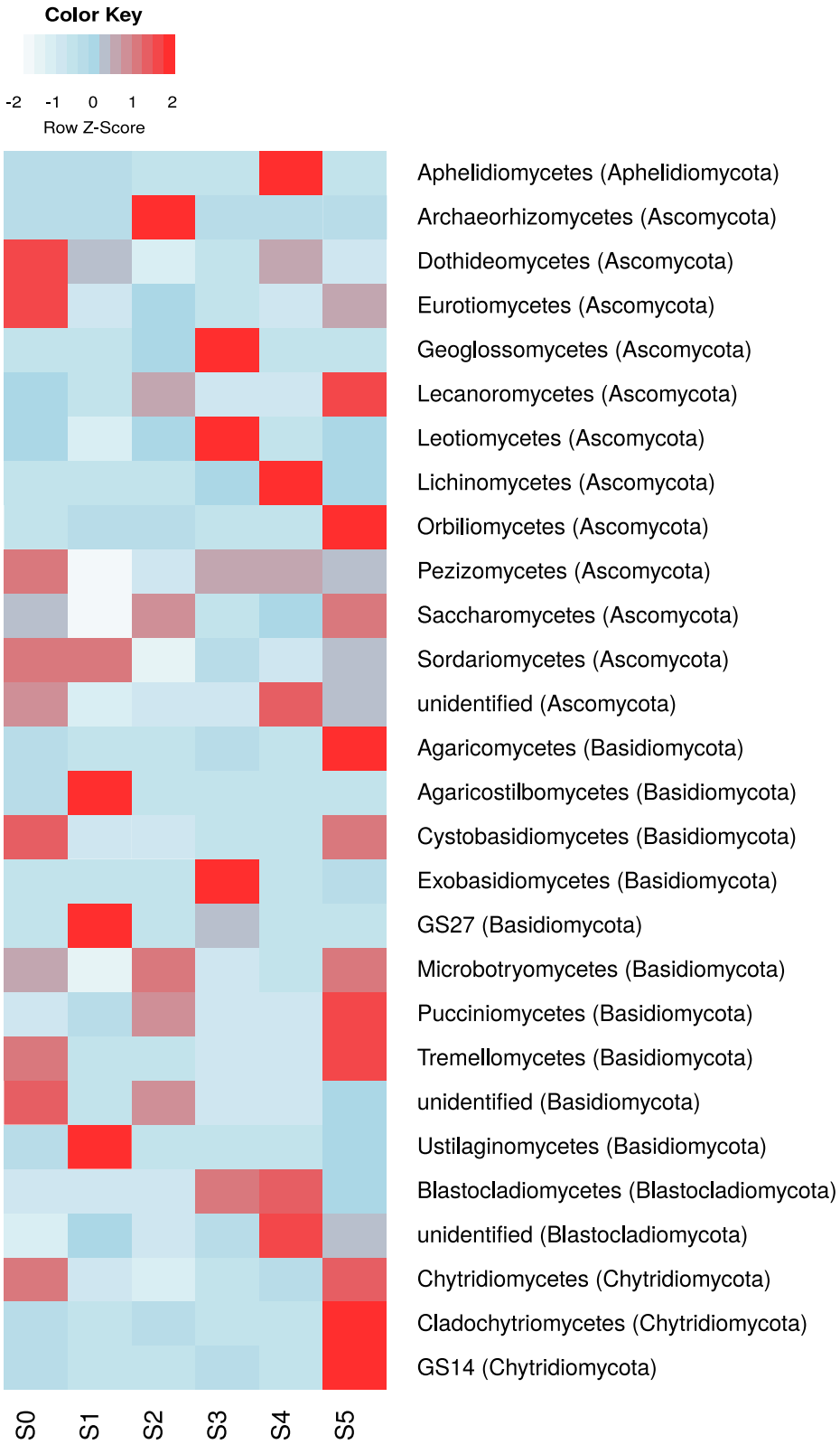

S1 Suppl. Fig. 10a: **Heat map of the fungal community along degradation stages (soil depth 15–35 cm).** Shades of color indicate abundance of fungal phyla as z-values.

S1 Suppl. Fig. 10b: **Heat map of the fungal community along degradation stages (soil depth 15–35 cm).** Shades of color indicate abundance of fungal phyla as z-values (continuation from S10a).

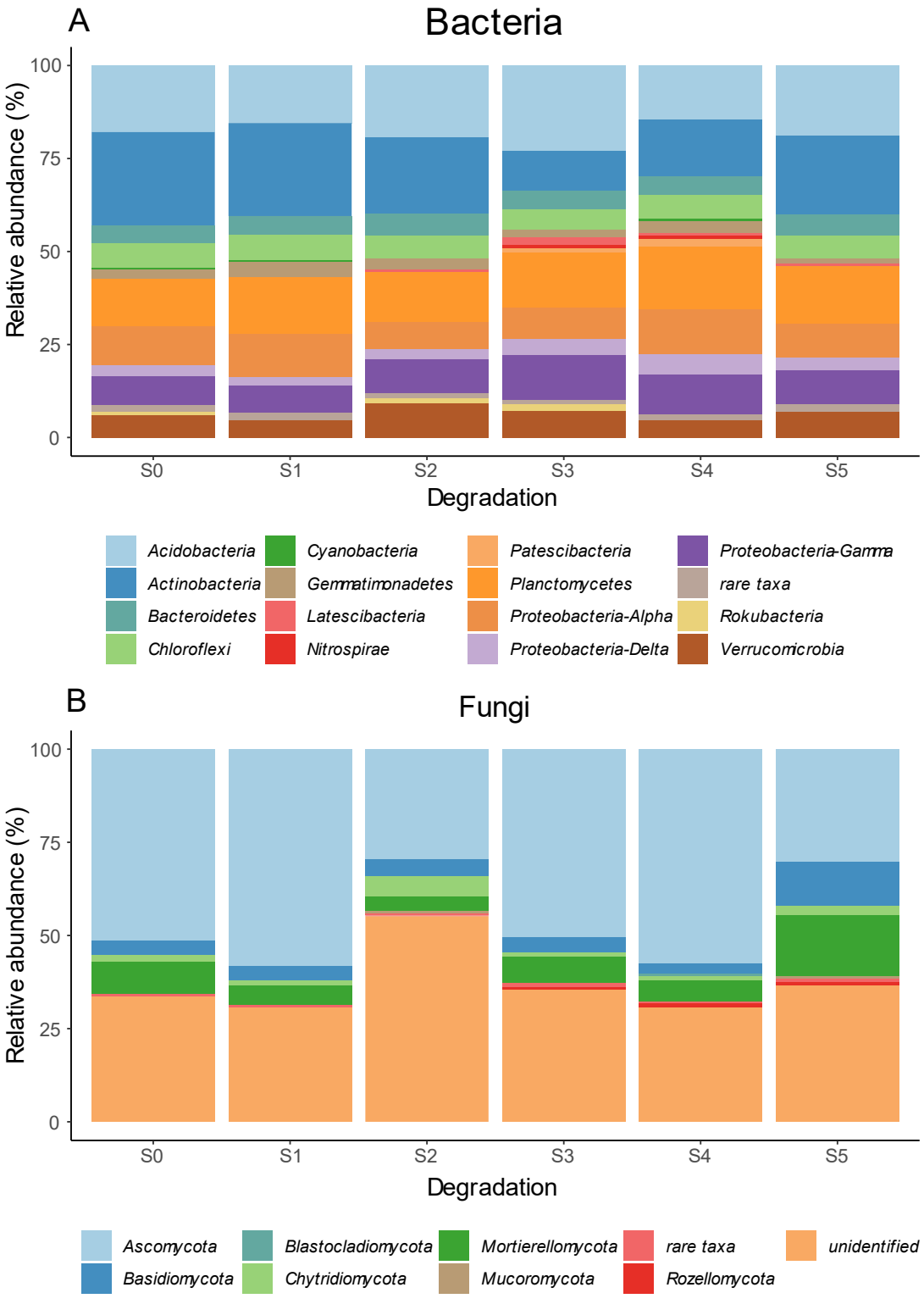

S1 Suppl. Fig. 11: **Relative abundance of bacterial (A) and fungal (B) phyla found along the degradation sequence (soil depth 15–35 cm).** Phyla amounting to less than 0.5% were grouped as 'rare taxa'.

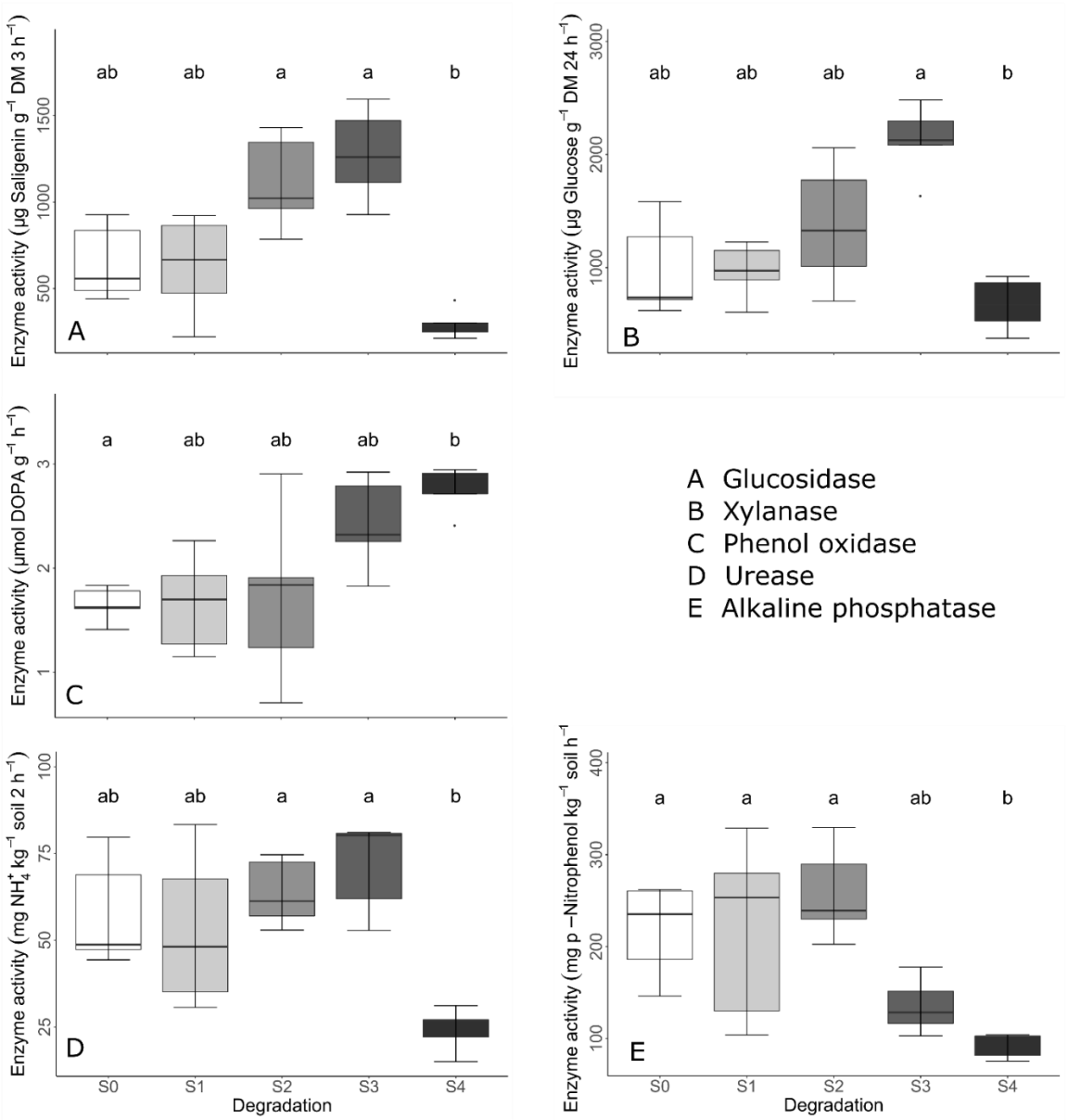

S1 Suppl. Fig. 12: **Enzyme activities of carbon-hydrolyzing enzymes (A, B), ligninoxidizing enzyme (C), and enzymes hydrolyzing nitrogen (D) and phosphorus (E) compounds.** Significant differences ($p < 0.05$) from Kruskal–Wallis and Dunn's tests (Holm's p adjustment) indicated with lowercase letters (a, b). Error bars display standard error.

S1 Suppl. Table 1: **List of publications included in the meta-analysis to quantify the SOC and N losses for *Kobresia pygmaea's* core area.**

Authors	Year	Journal	Title	Pages
Ma Y, et al.	2002	Pratacultural Science	Study on rehabilitating and rebuilding technologies for degenerated alpine meadow in the Changjiang and Yellow river source region	1-5
Zhou H, et al.	2005	Acta Prataculturae Sinica	A study on correlations between vegetation degradation and soil degradation in the 'alpine meadow' of the Qinghai-Tibetan Plateau	31-40
Wang W, et al.	2006	Ecology and Environment	Effects of land degradation and rehabilitation on soil carbon and nitrogen content on alpine Kobresia meadow	362-366
Wang J, et al.	2007	Chinese Science Bulletin	Effects of swamp and alpine meadow degradation on CO_2 emission during growing season in Qinghai-Tibetan Plateau	1554-1560
Wang JF, et al.	2007	Chinese Science Bulletin	Influences of the degradation of swamp and alpine meadows on CO_2 emission during growing season on the Qinghai-Tibet Plateau	2565-2574
Wang W, et al.	2007	Journal of Plant Ecology (Chinese Version)	Effects of land degradation and rehabilitation on vegetation carbon and nitrogen content of alpine meadow in China	1073-1078
Zhao D & Xu Z	2007	Prataculture & Animal Husbandry	Research on the effect of degradation degree of subalpine meadow on soil nutrient in Laji Mountain Area	4-7
Li Y, et al.	2008	Chinese Journal of Grassland	Effect of typical alpine meadow degradation on soil enzyme and soil nutrient in source region of three rivers	51-58
Liu X, et al.	2008	Acta Prataculturae Sinica	Community structure and plant diversity of alpine meadow under different degrees of degradation in the Eastern Qilian Mountains	1-11
Wang C, et al.	2008	Chinese Journal of Applied and Environmental Biology	Changes in soil organic carbon and microbial biomass carbon at different degradation successional stages of alpine meadows in the headwater region of three rivers in China	225-230
Liu Y, et al.	2009	Journal of Agro-Environment Science	Vegetation decline and reduction of soil organic carbon stock in high-altitude meadow grasslands in the source area of Three Major Rivers of China	2559-2567

Wang CT, et al.	2009	Land Degradation & Development	Changes in plant diversity, biomass and soil C, in alpine meadows at different degradation stages in the headwater region of three rivers, China	187-198
Wang J, et al.	2009	China Environmental Science	Influence of degradation of the swamp and alpine meadows on CH_4 and CO_2 fluxes on the Qinghai-Tibetan Plateau	474-480
Xing X	2009	Journal of Anhui Agricultural Sciences	Different stages of degradation characteristics of alpine meadow in the Yellow River Source Area	10578-10580
Sheng L & Wang Y	2010	Chinese Qinghai Journal of Animal and Veterinary Sciences	Characteristics variation of soil nutrition in different degraded degree alpine meadow in Dawu Region of Guoluo Prefecture	4-6
Wang J, et al.	2010	Environmental Earth Sciences	The influence of degradation of the swamp and alpine meadows on CH_4 and CO_2 fluxes on the Qinghai-Tibetan Plateau	537-548
Cao L, et al.	2011	Pratacultural Science	Distribution of soil organic carbon and its relationship with soil physical and chemical properties on degraded alpine meadows	1411-1415
Yu J & Shi H	2011	Acta Agroculturae Boreali-occidentalis Sinica	Changes of microbes' population in the different degraded alpine meadows on the Qinghai-Tibetan Plateau	77-81
Luo Y, et al.	2012	Chinese Journal of Ecology	Soil stoichiometry characteristics of alpine meadow at its different degradation stages	254-260
Wang Y, et al.	2012	Environmental Earth Sciences	Correlation of alpine vegetation degradation and soil nutrient status of permafrost in the source regions of the Yangtze River, China	1215-1223
Yi XS, et al.	2012	Procedia Environmental Sciences	The impacts of grassland vegetation degradation on soil hydrological and ecological effects in the source region of the Yellow River-A case study in Junmuchang region of Maqin Country	967-981
Yu X, et al.	2012	Journal of Geo-Information Science	Spectral analysis of different degradation level alpine meadow in 'Three-River headwater' region	398-404

Zhang S, et al.	2012	Pratacultural Science	Soil nutrient characteristics of alpine meadow at different degradation degrees in Eastern Qilian Mountains	1028-1032
Zhang Z	2012	Heilongjiang Animal Science and Veterinary Medicine	Vegetation community structure and productivity of different degraded alpine meadow	83-85
Li Y, et al.	2013	Journal of Environmental Management	The effects of fencing on carbon stocks in the degraded alpine grasslands of the Qinghai-Tibetan Plateau	393-399
Wen L, et al.	2013	Plosone	Effect of degradation intensity on grassland ecosystem services in the alpine region of Qinghai-Tibetan Plateau, China	e58432
Wen L, et al.	2013	Plant and Soil	The impact of land degradation on the C pools in alpine grasslands of the Qinghai-Tibet Plateau	329-340
Zeng C, et al.	2013	Journal of Hydrology	Impact of alpine meadow degradation on soil hydraulic properties over the Qinghai-Tibetan Plateau	148-156
Li Y, et al.	2014	Geoderma	Soil carbon and nitrogen pools and their relationship to plant and soil dynamics of degraded and artificially restored grasslands of the Qinghai-Tibetan Plateau	178-184
Lu J, et al.	2014	Environmental Earth Sciences	The effect of desertification on carbon and nitrogen status in the northeastern margin of the Qinghai-Tibetan Plateau	807-815
Wang X, et al.	2014	Environmental Monitoring and Assessment	The effects of grassland degradation on plant diversity primary productivity, and soil fertility in the alpine region of Asian's headwaters	6903-6917
Wu GL, et al.	2014	Clean Soil Air Water	Above- and belowground response along degradation gradient in an alpine grassland of the Qinghai-Tibetan Plateau	319-323
Li J, et al.	2015	Ecological Research	Response of the plant community and soil water status to alpine Kobresia meadow degradation gradients on the Qinghai–Tibetan Plateau, China	589-596
Li Y, et al.	2015	Soil Biology &Biochemistry	Seasonal changes of CO_2, CH_4 and N_2O fluxes in different types of alpine grassland in the Qinghai-Tibetan Plateau of China	306-314

Lin L, et al.	2015	Solid Earth	Predicting parameters of degradation succession processes of Tibetan Kobresia grasslands	1237-1246
Liu Y, et al.	2015	Acta Agriculturae Boreali-occidentalis Sinica	Characteristics of soil organic carbon fractions in alpine meadow with different degradation	168-174
Liu Y, et al.	2015	Hubei Agricultural Sciences	Distribution characteristics of soil carbon on different degraded degree alpine meadow in the source area of Three Major Rivers in China	308-312
Shang ZH, et al.	2015	Plant Ecology & Diversity	Recruitment of seedlings versus ramets as affected by pasture degradation in alpine meadows and the implications for ecological restoration	547-557
Su X, et al.	2015	Journal of Mountain Sciences	Effects of grassland degradation and re-vegetation on carbon and nitrogen storage in the soils of the headwater area nature reserve on the Qinghai-Tibetan Plateau, China	582-591
Wu P, et al.	2015	Applied Soil Ecology	The response of soil macroinvertebrates to alpine meadow degradation in the Qinghai-Tibetan Plateau, China	60-67
Yu H, et al.	2015	Acta Agrestia Sinica	Distribution patterns of ratio of root to soil and soil physical chemical characteristics at the different degraded successional stages in an alpine meadow	1151-1160
Li Y, et al.	2016	Agriculture, Ecosystems & Environment	Changes of soil microbial community under different degraded gradients of alpine meadow	213-222
Liu SL, et al.	2016	Pratacultural Science	Effects of grazing season and degradation degree on the soil organic carbon in alpine meadow	11-18
Shang Z, et al.	2016	Ecological Engineering	Soil seed bank and its relation with above-ground vegetation along the degraded gradients of alpine meadow	268-277
Li W, et al.	2018	Ecological Engineering	Effect of degradation and rebuilding of artificial grasslands on soil respiration and carbon and nitrogen pools on an alpine meadow of the Qinghai-Tibetan Plateau	134-142
Lai ZM, et al.	2019	Pratacultural Science	Alpine meadows at different levels of degradation in the Beiluhe Basin of Tibetan Plateau Characteristics of soil respiration	952-959

Yang J, et al.	2020	Chinese Journal of Applied Ecology	Plant community and soil nutrient of alpine meadow in different degradation stages on the Tibetan Plateau, China	4067-4072
Yuan ZQ, et al.	2020	Journal of Soils and Sediments	Pasture degradation impact on soil carbon and nitrogen fractions of alpine meadow in a Tibetan permafrost region	2330-2342
Zhang ZH, et al.	2020	Journal of Arid Land	Degradation leads to dramatic decrease in topsoil but not subsoil root biomass in an alpine meadow on the Tibetan Plateau, China	806-818

S1 Suppl. Table 2: **Soil and plant characteristics with successive degradation (own field study).** Values are means ± SE. Lowercase letters indicate significant differences between degradation stages ($p < 0.05$). Missing values with increasing degradation result from erosion removing the upper soil horizons.

	Degradation stage					
	S0	**S1**	**S2**	**S3**	**S4**	**S5**
Horizontal crack (cm)						
	-	4.0 (0.9)^{c}	6.6 (0.6)^{bc}	10.3 (1.9)^{ab}	17 (1.2)^{a}	-
Vertical crack (cm)						
	-	0.6 (0.1)^{e}	2.0 (0.3)^{d}	5.8 (0.3)^{c}	8.0 (0.4)^{b}	10.4 (0.8)^{a}
Vegetation cover (%)						
	95 (0.6)^{a}	92 (1.0)^{ab}	79 (3.5)^{b}	30 (3.0)^{c}	24 (2.9)^{c}	9 (0.9)^{d}
Shoot biomass (g m^{-2})						
	179 (11)^{ab}	210 (8)^{a}	70 (4)^{bc}	41 (5)^{c}	48 (11)^{cd}	22 (1)^{d}
Root biomass in 0–25 cm (kg m^{-2})						
	5.2 (0.12)^{a}	5.4 (0.06)^{a}	4.1 (0.33)^{b}	3.2 (0.42)^{b}	0.15 (0.02)^{c}	0.17 (0.01)^{c}
Root density (mg cm^{-3})						
Ah1	31 (2.8)^{a}	33 (2.5)^{a}				
Ah2	34 (1.7)^{ab}	32 (2.2)^{a}	28 (2.3)^{b}	28 (1.3)^{c}		
Ah3	23 (0.4)^{a}	22 (0.9)^{ab}	19 (1.4)^{bc}	16 (1.1)^{ab}	1.5 (0.2)^{d}	1.3 (0.1)^{cd}
Ah4	12 (1.1)^{a}	13 (1.1)^{ab}	12 (1.0)^{ab}	11 (0.8)^{ab}	0.6 (0.1)^{bc}	0.9 (0.1)^{c}
Bulk density (mg cm^{-3})						
Ah1	0.62 (0.01)^{a}	0.72 (0.14)^{a}				
Ah2	0.72 (0.07)^{a}	0.77 (0.09)^{a}	0.68 (0.01)^{a}	0.84 (0.00)^{a}		
Ah3	1.03 (0.06)^{a}	1.03 (0.06)^{a}	0.96 (0.01)^{ab}	0.82 (0.10)^{b}	0.98 (0.07)^{a}	1.24 (0.06)^{c}
Ah4	1.19 (0.02)^{ab}	1.06 (0.12)^{b}	1.13 (0.01)^{b}	1.24 (0.05)^{ab}	1.26 (0.07)^{ab}	1.37 (0.02)^{a}
Bwg	1.54 (0.02)^{a}	1.54 (0.04)^{a}	1.43 (0.01)^{a}	1.51 (0.08)^{a}	1.59 (0.06)^{a}	1.59 (0.03)^{a}
SOC (g C kg^{-1})						
Ah1	74 (4.6)^{a}	74 (6.0)^{a}				
Ah2	70 (0.7)^{a}	65 (5.0)^{ab}	53 (2.9)^{bc}	51 (4.6)^{c}		
Ah3	46 (2.1)^{a}	42 (2.2)^{a}	32 (3.4)^{b}	27 (4.6)^{b}	26 (2.3)^{b}	15 (1.4)^{c}
Ah4	25 (1.4)^{a}	19 (3.2)^{ab}	17 (2.4)^{ab}	13 (4.6)^{b}	19 (1.5)^{ab}	14 (1.4)^{b}
Bwg	4 (0.4)^{a}	4 (0.4)^{a}	5 (4.6)^{a}	5 (1.0)^{a}	5 (0.3)^{a}	4 (0.5)^{a}
δ^{13}C of SOC (‰)						
Ah1	-24.16 (0.12)^{a}	-24.28 (0.27)^{a}				
Ah2	-23.13 (0.11)^{a}	-23.69 (0.31)^{a}	-23.76 (0.34)^{a}	-24.02 (0.32)^{a}		
Ah3	-22.81 (0.08)^{a}	-23.30 (0.11)^{bc}	-23.56 (0.18)^{c}	-23.97 (0.18)^{d}	-24.30 (0.11)^{e}	-23.68 (0.10)^{cd}
Ah4	-22.90 (0.08)^{a}	-22.94 (0.09)^{a}	-23.21 (0.10)^{ab}	-23.58 (0.10)^{b}	-23.64 (0.08)^{b}	-23.19 (0.11)^{ab}
Bwg	-23.00 (0.10)^{a}	-22.84 (0.10)^{ab}	-22.91 (0.11)^{ab}	-23.01 (0.11)^{a}	-22.93 (0.11)^{a}	-22.62 (0.14)^{b}
VSC of OC (mg g^{-1})						
Ah1	11.1 (1.6)^{a}	11.8 (1.1)^{a}				
Ah2	9.8 (2.4)^{b}	9.9 (1.5)^{b}	9.8 (0.6)^{b}	18.3 (1.5)^{a}		
Ah3	3.7 (0.3)^{c}	6.4 (0.9)^{bc}	15.0 (0.9)^{abc}	24.3 (0.6)^{a}	19.4 (3.0)^{a}	21.4 (4.6)^{ab}
Ah4	6.5 (0.8)^{c}	8.3 (1.3)^{bc}	14.0 (2.3)^{abc}	15.1 (5.4)^{abc}	20.8 (3.5)^{a}	18.1 (4.8)^{ab}
Bwg	14.1 (1.6)^{a}	15.5 (1.5)^{a}	12.9 (2.4)^{a}	9.9 (2.1)^{a}	10.1 (3.9)^{a}	17.9 (3.9)^{a}

SOC, soil organic carbon; VSC, vanillyl, syringyl and cinnamyl units

S1 Suppl. Table 3: **Important microbial taxonomic groups described for the *Kobresia* ecosystem.**

Taxonomic group	**Function**	**Literature**
Actinobacteria	Degrading low-molecular-mass compounds	Šnajdr et al. (44)
Agaricomycetes	Lignin degrader	Ahmad et al. (45)
Ascomycota	Litter degrader	Rajala et al. (46)
Glomeromycota	AMF/VAM	Brundrett (47)
Inocybaceae	ECM partner of *Kobresia sp.*	Gao and Yang (48)
Nitrosomonadaceae	Nitrifier	Jetten et al. (49)
Nitrospirales	Nitrifier	Jetten et al. (49)
Pseudomonadales	Denitrifier, lignin degrader	Ahmad et al. (45)
Rhizobiales	Lignin degrader	Nacke et al. (50)
Thelephoraceae	ECM partner of *Kobresia* sp.	Gao and Yang (48)

3.1.3. Study 3: Accounting for storage compounds in soil microbial communities alters carbon flux modelling outcome.

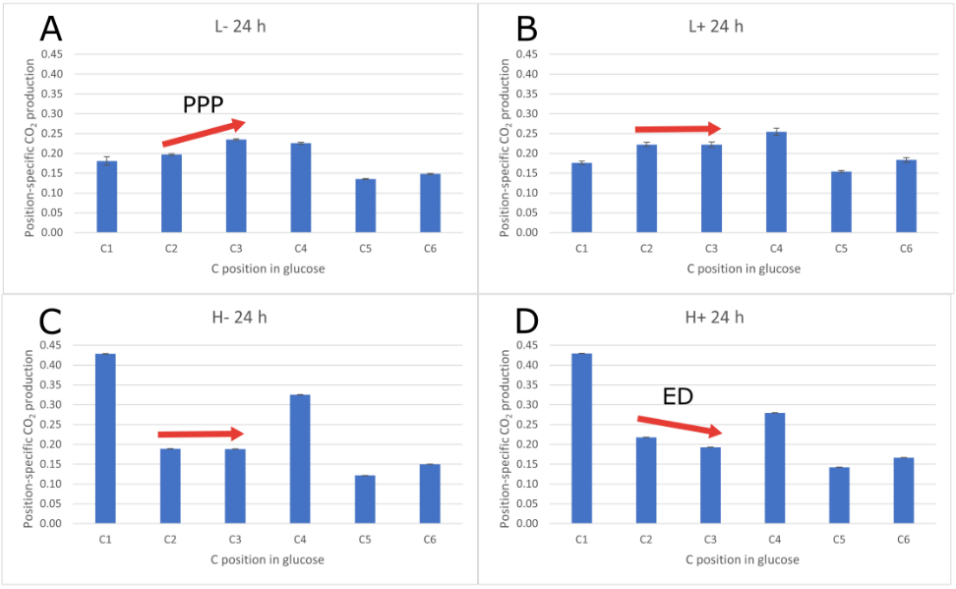

S3 Suppl. Fig.1: **Glucose position C2 and C3 comparison whether either pentose phosphate pathway (PPP) or Entner–Doudoroff pathway (ED) are active.** For the treatments of low glucose without nutrients (L-, **A**), low glucose with nutrients (L+, **B**), high glucose without nutrients (H-, **C**) and high glucose with nutrients (H+, **D**) after 24 h.

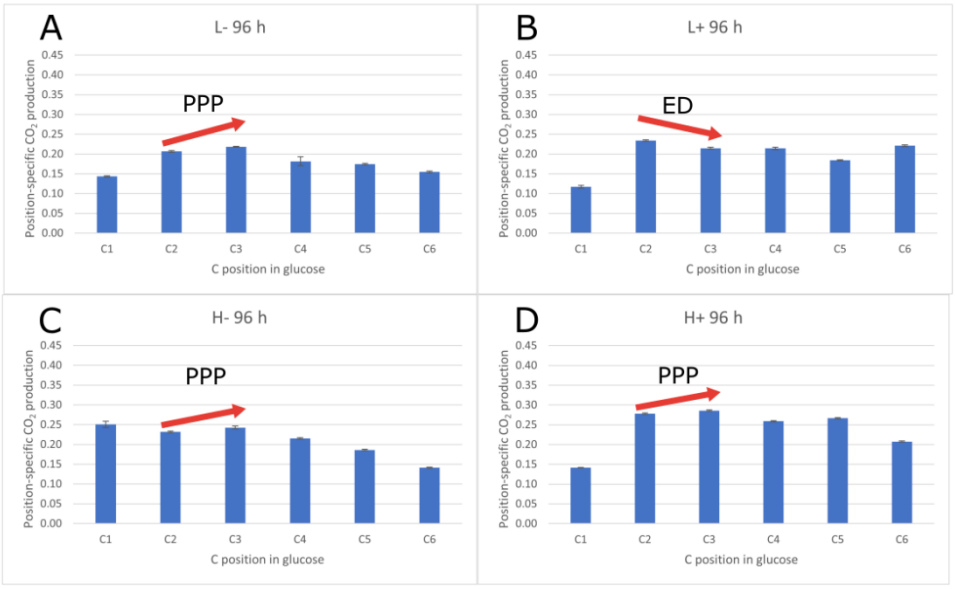

S3 Suppl. Fig.2: **Glucose position C2 and C3 comparison whether either pentose phosphate pathway (PPP) or Entner–Doudoroff pathway (ED) are active.** For the treatments of low glucose without nutrients (L-, **A**), low glucose with nutrients (L+, **B**), high glucose without nutrients (H-, **C**) and high glucose with nutrients (H+, **D**) after 96 h.

S3 Suppl. Table 1: **Model input combinations** of uniformly labelled and position-specific replicate F-values at the 24 h sampling point.

		F value							
Treatment	**U-replicate**	**U**	**C1**	**C2**	**C3**	**C4**	**C5**	**C6**	**combination**
Low None	a	0.403	0.183	0.185	0.231	0.227	0.134	0.143	baaddd
Low None	a	0.403	0.183	0.194	0.217	0.227	0.132	0.143	bbddad
Low None	a	0.403	0.113	0.194	0.231	0.213	0.129	0.149	cbaccb
Low None	a	0.403	0.189	0.200	0.230	0.226	0.133	0.149	dccabb
Low None	b	0.378	0.241	0.213	0.232	0.241	0.141	0.159	acddbb
Low None	b	0.378	0.120	0.197	0.246	0.241	0.143	0.147	cdadda
Low None	b	0.378	0.120	0.207	0.246	0.227	0.137	0.152	cbaccd
Low None	b	0.378	0.241	0.213	0.245	0.227	0.143	0.152	acccdd
Low None	c	0.394	0.232	0.205	0.235	0.232	0.135	0.141	accdaa
Low None	c	0.394	0.194	0.189	0.222	0.218	0.132	0.158	dadccc
Low None	c	0.394	0.187	0.205	0.236	0.218	0.136	0.146	bcacbd
Low None	c	0.394	0.187	0.198	0.236	0.232	0.137	0.153	bbaddb
Low None	d	0.402	0.113	0.194	0.242	0.228	0.134	0.143	cbbbdd
Low None	d	0.402	0.227	0.185	0.231	0.213	0.133	0.138	aaacba
Low None	d	0.402	0.183	0.185	0.230	0.227	0.132	0.155	bacdac
Low None	d	0.402	0.183	0.185	0.242	0.213	0.134	0.143	babcdd
Low N+P	a	0.411	0.161	0.214	0.192	0.222	0.148	0.176	adadba
Low N+P	a	0.411	0.158	0.203	0.206	0.222	0.148	0.154	ccddbb
Low N+P	a	0.411	0.167	0.203	0.203	0.236	0.150	0.154	dccccb
Low N+P	a	0.411	0.178	0.220	0.203	0.250	0.145	0.176	bacada
Low N+P	b	0.398	0.164	0.223	0.209	0.229	0.149	0.197	cbcdad
Low N+P	b	0.398	0.172	0.209	0.213	0.229	0.150	0.197	dcdddd
Low N+P	b	0.398	0.184	0.227	0.199	0.229	0.155	0.205	baadcc
Low N+P	b	0.398	0.184	0.209	0.199	0.267	0.149	0.197	bcabad
Low N+P	c	0.342	0.200	0.257	0.248	0.311	0.173	0.238	dddbac
Low N+P	c	0.342	0.214	0.244	0.292	0.311	0.174	0.212	bcbbda
Low N+P	c	0.342	0.193	0.259	0.248	0.311	0.180	0.185	abdbcb
Low N+P	c	0.342	0.193	0.259	0.231	0.311	0.174	0.185	ababdb
Low N+P	d	0.422	0.174	0.209	0.236	0.216	0.144	0.150	bdbdbb
Low N+P	d	0.422	0.157	0.209	0.236	0.252	0.140	0.186	adbbad
Low N+P	d	0.422	0.162	0.214	0.201	0.243	0.146	0.150	dadacb
Low N+P	d	0.422	0.154	0.197	0.236	0.230	0.141	0.172	ccbcda
High None	a	0.889	0.429	0.188	0.191	0.326	0.121	0.152	adcacd
High None	a	0.889	0.429	0.190	0.188	0.327	0.123	0.152	aabcad
High None	a	0.889	0.429	0.188	0.188	0.326	0.122	0.152	adbadd
High None	a	0.889	0.429	0.188	0.188	0.326	0.123	0.151	adbdac
High None	b	0.890	0.433	0.190	0.189	0.325	0.122	0.151	caabdc
High None	b	0.890	0.426	0.190	0.190	0.327	0.120	0.147	badcca
High None	b	0.890	0.426	0.190	0.190	0.325	0.123	0.152	bcdbad
High None	b	0.890	0.433	0.188	0.189	0.325	0.122	0.147	cdabba
High None	c	0.893	0.424	0.189	0.188	0.326	0.121	0.151	babcdd

High None	c	0.893	0.427	0.189	0.188	0.325	0.122	0.151	aaaaac
High None	c	0.893	0.431	0.189	0.188	0.326	0.120	0.151	caaccc
High None	c	0.893	0.427	0.189	0.188	0.324	0.120	0.149	aaadcb
High None	d	0.892	0.427	0.188	0.188	0.324	0.122	0.147	ababda
High None	d	0.892	0.431	0.188	0.188	0.324	0.122	0.147	dbabba
High None	d	0.892	0.431	0.187	0.188	0.324	0.122	0.151	ddabad
High None	d	0.892	0.425	0.189	0.188	0.325	0.122	0.151	babadc
High N+P	a	0.950	0.427	0.219	0.193	0.279	0.142	0.167	cdbbdb
High N+P	a	0.950	0.432	0.219	0.192	0.280	0.142	0.167	addcdd
High N+P	a	0.950	0.429	0.216	0.193	0.280	0.143	0.167	bcadcd
High N+P	a	0.950	0.432	0.218	0.193	0.280	0.142	0.166	abbdbc
High N+P	b	0.950	0.428	0.217	0.193	0.279	0.142	0.166	baabaa
High N+P	b	0.950	0.427	0.216	0.193	0.279	0.142	0.166	ccadad
High N+P	b	0.950	0.429	0.219	0.193	0.273	0.142	0.166	ddbadc
High N+P	b	0.950	0.427	0.217	0.192	0.279	0.142	0.167	cadbbb
High N+P	c	0.948	0.428	0.219	0.193	0.280	0.142	0.166	cbccac
High N+P	c	0.948	0.432	0.219	0.193	0.280	0.142	0.166	adabdc
High N+P	c	0.948	0.430	0.219	0.193	0.280	0.142	0.167	ddbdba
High N+P	c	0.948	0.428	0.216	0.193	0.280	0.144	0.167	ccbcca
High N+P	d	0.950	0.427	0.216	0.192	0.279	0.142	0.166	ccdcdc
High N+P	d	0.950	0.431	0.219	0.192	0.279	0.142	0.166	addcbd
High N+P	d	0.950	0.429	0.219	0.193	0.279	0.142	0.166	bdadac
High N+P	d	0.950	0.431	0.219	0.192	0.279	0.143	0.166	adcccd

S3 Suppl. Table 2: **T-test p-values** from the comparison of the model with and without storage adaptation for phi ratio, br1 and br5 for each treatment.

Flux	**Treatment**	**p**	**Significant**
br1	High None	1.0165E-11	significant
	High N+P	5.6195E-18	significant
	Low None	0.04801107	significant
	Low N+P	0.00036796	significant
br5	High None	5.6204E-29	significant
	High N+P	7.6701E-28	significant
	Low None	2.3181E-17	significant
	Low N+P	2.7095E-10	significant
phi	High None	1.3545E-15	significant
	High N+P	1.0324E-18	significant
	Low None	2.6331E-09	significant
	Low N+P	1.0965E-07	significant

3.1.4. Study 4: Intracellular carbon storage by microorganisms is an overlooked pathway of biomass growth

Supplement A: Supplementary figures

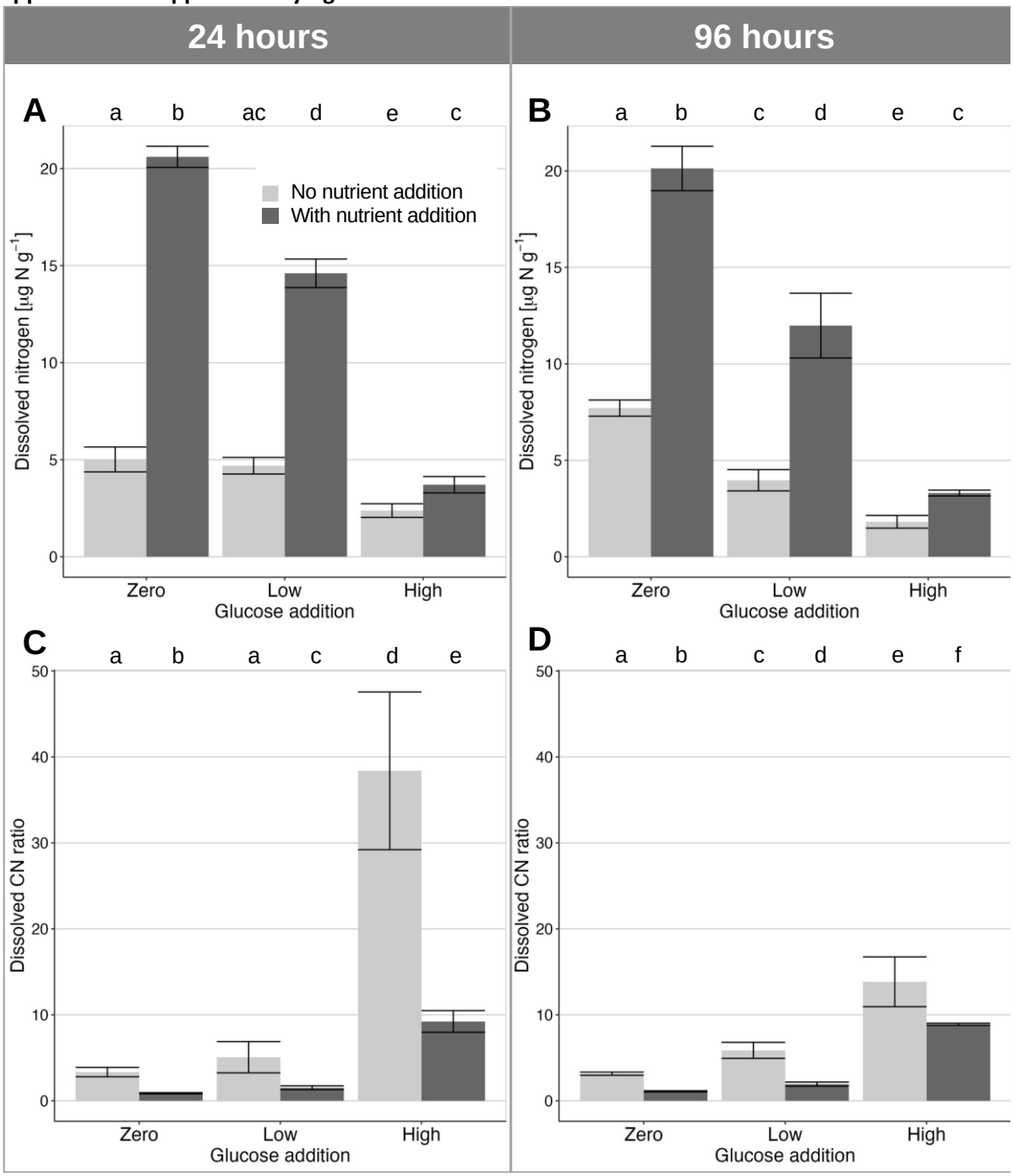

S4 Suppl. Fig. 1: **Dissolve nitrogen and C:N ratio.** Dissolved nitrogen after 24 h (**A**) and 96 h (**B**) following addition of glucose at 0, 90 and 400 µg C g^{-1} soil (Zero, Low, High) with or without mineral nutrient supply (N, P, K, S), and the corresponding dissolved C:N ratio (dissolved organic C to total dissolved N) at the corresponding timepoints (**C** and **D**). Error bars show mean ± standard deviation, with n = 4 independent soil microcosms. Different letters above the plots indicate significant differences with $p < 0.05$ (2-sided Tukey HSD test on log-transformed values, which adjusts for multiple comparisons).

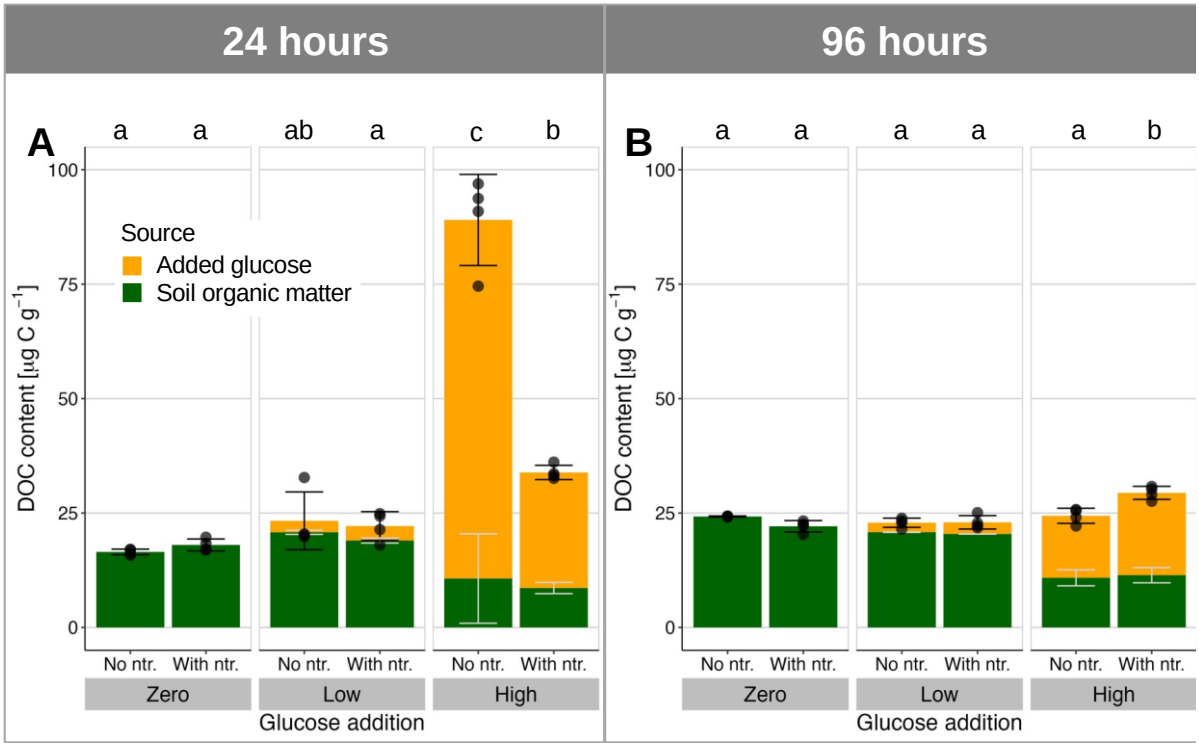

S4 Suppl. Fig. 2: **Dissolved organic carbon.** Organic carbon extractable into 0.5 M K_2SO_4 after 24 h (**A**) and 96 h (**B**) following addition of glucose at 0, 90 and 400 µg C g^{-1} soil (Zero, Low, High) with or without mineral nutrient supply (N, P, K, S). Contrasting colors reflect the source of the extractable biomass as determined by isotopic composition, with light gray error bars showing mean ± standard deviation of the relative composition. Black error bars show mean ± standard deviation of the total. Different letters above the plots indicate significant differences in total DOC with $p < 0.05$ (2-sided Tukey HSD test on log-transformed values, which adjusts for multiple comparisons), with n = 4 independent soil microcosms.

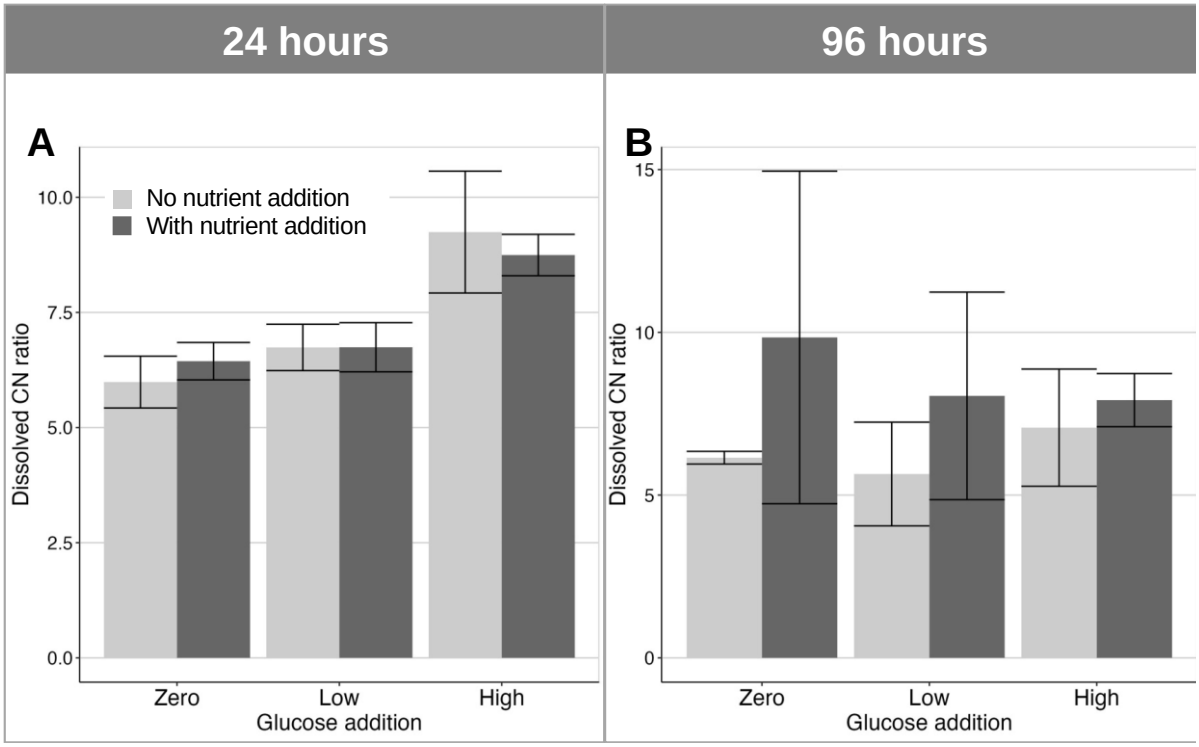

S4 Suppl. Fig. 3: **C:N ratio of extractable microbial biomass.** (**A**) 24 h and (**B**) 96 h after glucose and/or nutrient addition to soil microcosms. Error bars show mean ± standard deviation, with n = 4 independent soil microcosms, except for one treatment n = 3 (zero glucose, no nutrients at 96 h).

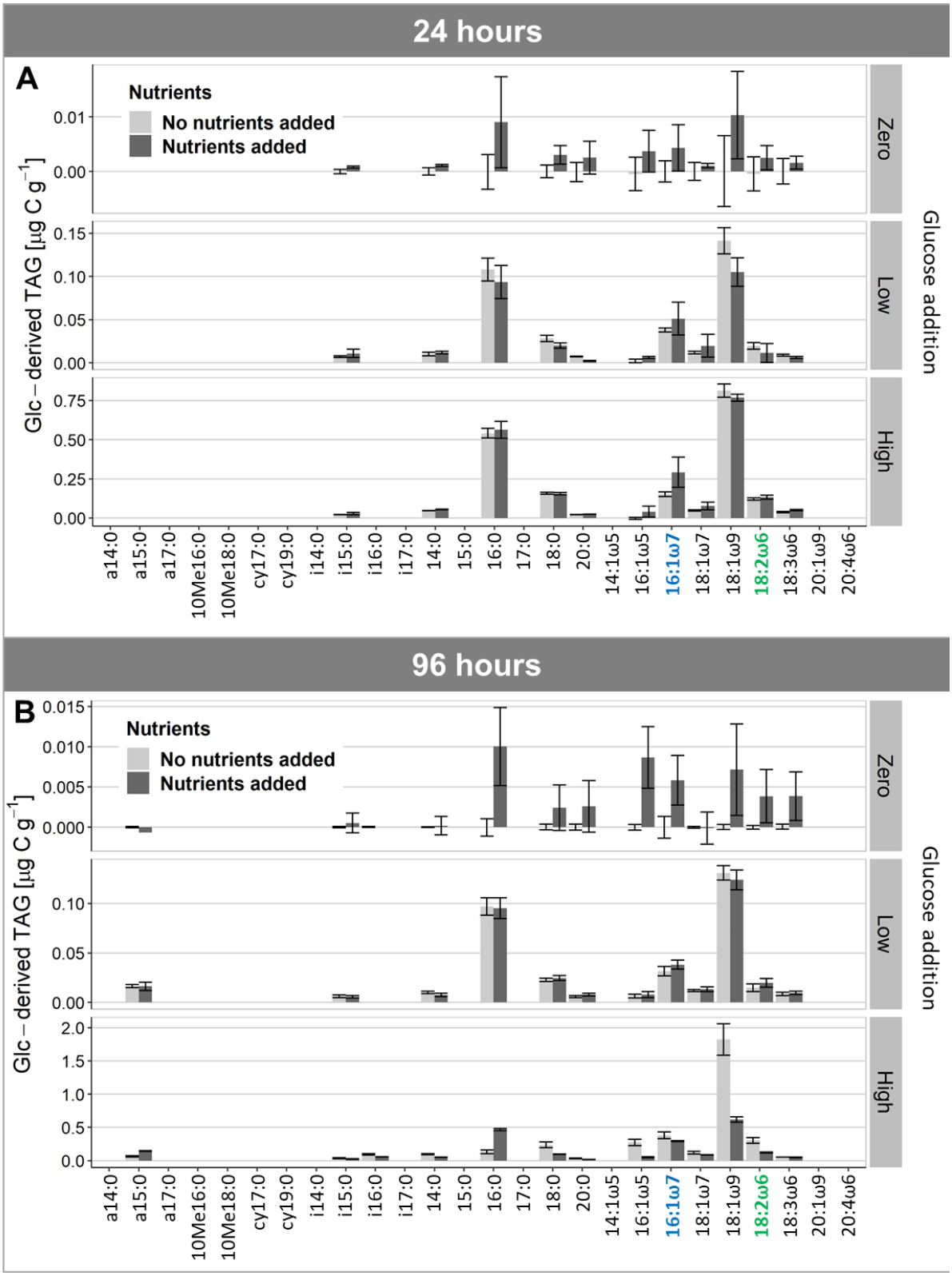

S4 Suppl. Fig. 4: **Fatty acid profile of glucose-derived TAGs.** (**A**) 24 h and (**B**) 96 h following addition of glucose at 0, 90 and 400 µg C g^{-1} soil (Zero, Low, High) with or without mineral nutrient supply (N, P, K, S). The diagnostic bacterial biomarker 16:1ω6 (highlighted blue on the horizontal axis) and fungal biomarker 18:2ω6 (highlighted in green) showed substantial incorporation of glucose-derived C. Error bars show mean ± standard deviation, with n = 4 independent soil microcosms. Note that the vertical axis scale varies between glucose treatments.

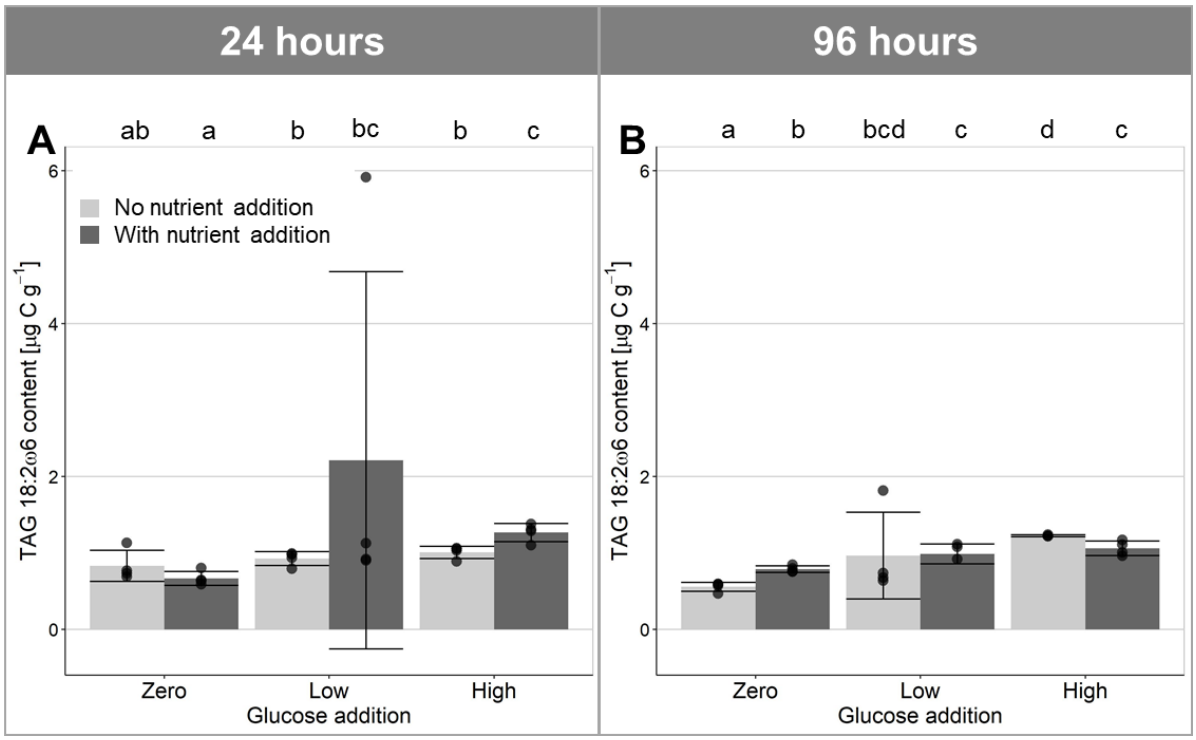

S4 Suppl. Fig. 5: **Total soil content of fungal biomarker TAG 18:2ω6.** (**A**) 24 h and (**B**) 96 h following addition of glucose at 0, 90 and 400 µg C g^{-1} soil (Zero, Low, High) with or without mineral nutrient supply (N, P, K and S). Error bars show mean ± standard deviation, with n = 4 independent soil microcosms. Lowercase letters above the plots show post-hoc differences with $p<0.05$ (2-sided pairwise comparison of medians with Benjamini-Hochberg adjustment for multiple comparisons).

Supplement B: Two-pool mixing model

The fraction of O atoms in DNA originating from the added $H_2{}^{18}O$ was calculated using a standard two-pool isotope mixing model (Mason-Jones et al., 2018), which is derived from mass-balance principles:

$$O_{add} = \frac{(atom\%_{tot} - atom\%_{nat})}{atom\%_{add} - atom\%_{nat}}$$

where

O_{add} is the fraction of O in DNA that originated from the added (^{18}O-labelled) water

$atom\%_{tot}$ is the isotopic abundance of ^{18}O in the total extracted DNA (in atom percent)

$atom\%_{add}$ is the $_{18}O$ isotopic abundance of soil water during the incubation (in atom percent)

$atom\%_{nat}$ is the $_{18}O$ isotopic abundance of DNA in the absence of $_{18}O$-labelled water (i.e. the natural ^{18}O abundance in DNA from the experimental soil prior to labelling)

Reference:

Mason-Jones, K., Schmucker, N. & Kuzyakov, Y. Contrasting effects of organic and mineral nitrogen challenge the N-Mining Hypothesis for soil organic matter priming. *Soil Biol. Biochem.* **124**, 38–46 (2018).

3.2.Contribution to the studies

Study 1: Tibet

Study design	Per-Marten Schleuß, Georg Guggenberger, Yakov Kuzyakov, Sandra Spielvogel
Field work	Sandra Spielvogel, Yakov Kuzyakov, Per Marten Schleuß, Georg Miehe, Elke Seeber, Xingliang Xu
Laboratory work	**Andreas Breidenbach,** Claudia Blaser, Per Marten Schleuß, Xingliang Xu, Jianchu Xu, Sandra Spielvogel
Literature study	Shibin Liu
Bioinformatics and statistics	**Andreas Breidenbach**, Dominik Schneider, Matthias Gube, Helge Norf, Jutta Meier, Tilman de la Haye, Felix Heitkamp, Yang Huanming, Jianchu Xu, Shibin Liu, Tsechoe Dorji, Kyle Mason-Jones
Manuscript writing	**Andreas Breidenbach**, Per Marten Schleuß, Sandra Spielvogel
Comments on the manuscript	All co-authors
Contribution Andreas Breidenbach	high

Study 2:

Study design	**Andreas Breidenbach**, Kyle Mason-Jones, Callum C. Banfield, Yakov Kuzyakov, Sandra Spielvogel, Nico Jehmlich, Steffen Kolb, Michaela A. Dippold
Experimental preparation	**Andreas Breidenbach**, Kyle Mason-Jones, Callum Banfield
Experimental execution and sampling	**Andreas Breidenbach**, Kyle Mason-Jones
Laboratory work and bioinformatics	**Andreas Breidenbach,** Sonja Wende, Nico Jehmlich
Manuscript writing	**Andreas Breidenbach**

Comments on the manuscript	All co-authors
Contribution Andreas Breidenbach	high

Study 3:

Study design	**Andreas Breidenbach**, Kyle Mason-Jones, Callum C. Banfield, Sandra Spielvogel, Michaela A. Dippold
Experimental preparation	**Andreas Breidenbach**, Kyle Mason-Jones, Callum C. Banfield
Experimental execution and sampling	**Andreas Breidenbach**, Kyle Mason-Jones
Laboratory work	**Andreas Breidenbach**, Kyle Mason-Jones
Manuscript writing	**Andreas Breidenbach**
Comments on the manuscript	All co-authors
Contribution Andreas Breidenbach	high

Study 4:

Study design	**Andreas Breidenbach**, Kyle Mason-Jones, Callum C. Banfield, Michaela A. Dippold
Experimental preparation	**Andreas Breidenbach**, Kyle Mason-Jones
Experimental execution and sampling	**Andreas Breidenbach**, Kyle Mason-Jones, Jens Dyckmans
Laboratory work	Kyle Mason-Jones**, Andreas Breidenbach**
Manuscript writing	Kyle Mason-Jones
Comments on the manuscript	All co-authors
Contribution Andreas Breidenbach	high - medium

3.3.Acknowledgements

I want to thank everyone who supported me scientifically or personally during my PhD and who contributed to my PhD thesis.

I am very thankful to Prof. Dr. Michaela A. Dippold, who gave me the opportunity to work in her group. Her guidance, passion and infinite knowledge brought me through even the darkest hours of accomplishing my PhD. I could count on her at any time when either developing the lab experiment, solving problems within the lab, helping me interpret the ton of data we measured, or helping me write this thesis. Her joy and optimism always sparked new hope and ideas when I felt stuck. I also want to thank Michaela for always finding a way to employ me after our multi-meta-omics proposal was not granted and I had to begin my lab experiments without funding.

I especially want to thank Prof. Dr. Sandra Spielvogel for laying the cornerstone for my PhD studies after my master thesis by believing in my scientific abilities and referring me to Michaela and Prof. Dr Yakov Kuzyakov. Without Sandra, I would have never continued further in my scientific career. I also want to thank her for employing me when contracts in Göttingen had ended during my PhD studies.

I want to thank Prof Dr. Rolf Daniel and Dr. Matthias Gube for being my supervisors who gave me valuable advice during our meetings. I especially like to thank Prof Dr. Rolf Daniel for stepping in as my supervisor for my thesis committee.

I also thank Stefan Scholten for being part of my defense committee in such short notice.

I am also thankful to Prof. Dr. Yakov Kuzyakov for giving me the opportunity to start my PhD studies with a scholarship under his and Michaela's supervision. Without his financial support, my PhD would not have been able to begin in the first place. I also valued his scientific advice and guidance during my first steps as PhD student.

A special thanks goes out to Kyle Mason-Jones with whom I conducted our enormous lab experiment. His insight in setting up an experiment and his knowledge is unmatched. I thank him for his patience while discussing results and explaining me his thoughts. Although the lab work sometimes took place in the late hours, we still had fun together in our desperation.

I want to thank Tilman de la Haye for every R session we had together tackling my never-ending special problems with my datasets. His patience in explaining, his inventiveness in creating a solution in R and his ability to digress towards any computer topic during our sessions will always be in my mind.

I want to thank my friends and colleagues who I met during my PhD and who became dear to me: Carolin Apostel and Joscha Becker for our coffee breaks and discussions will always have a place in my

heart. I'd like to thank Nina Hennings, Svenja Stock, Moritz Köster, Sara Loftus and Maire Holz for our "shut up and write sessions". Thank you for our Harry Potter movie nights and slightly oversized portions of food. Also, I want to thank Caro and Maire for reading and commenting my thesis. Peter Gernandt for our discussions about Lego and its alternatives and going on excursions together. Callum Banfield for digressing about cars and tools. I'd like to thank Lingling Shi for having a lot of fun during laboratory practical courses and conferences. A big thanks goes out to Thomas Zilla for his funny insights into LotR, Star Wars, Asterix and a lot of memes.

I am very thankful for our Hiwis Kali Middleby, Lydia Köbele, and Andrew Gall who helped us with performing our lab experiment and analyzing samples.

I also want to thank the technicians Karin Schmidt, Susann Enzmann and Irene Nalik measuring our samples, for helping us and supplying us with food during our lab experiment. I would like to thank Nico Jehmlich from the UFZ Leipzig and Steffen Kolb and Sonja Wende from the ZALF in Müncheberg for collaborating with us to analyze the metatranscriptome and metaproteome.

Finally, I am very thankful for my family, my parents Jürgen and Iris Breidenbach, who always encouraged my interests, and curiosity. Their unconditional love and support kept me going even through the rough patches of my career.

3.3.1. Declarations

1. I, hereby, declare that this Ph.D. dissertation has not been presented to any other examining body either in its present or a similar form.

Furthermore, I also affirm that I have not applied for a Ph.D. at any other higher school of education.

Göttingen,

.....

(Signature)

2. I, hereby, solemnly declare that this dissertation was undertaken independently and without any unauthorized aid.

Göttingen,

.....

(Signature)